REPUBLIC OF TURKEY

YILDIZ TECHNICAL UNIVERSITY

GRADUATE SCHOOL OF SCIENCE AND ENGINEERING

RESPONSE OF BLACK SEA COASTLINE TO CLIMATE CHANGE IMPACTS

Tunay ÇARPAR

DOCTOR OF PHILOSOPHY THESIS

Department of Civil Engineering

Hydraulics Program

Supervisor

Assoc. Prof. Dr. Berna AYAT AYDOĞAN

July, 2022

YILDIZ TECHNICAL UNIVERSITY

GRADUATE SCHOOL OF SCIENCE AND ENGINEERING

RESPONSE OF BLACK SEA COASTLINE TO CLIMATE CHANGE IMPACTS

A thesis submitted by Tunay ÇARPAR in partial fulfillment of the requirements for the degree of DOCTOR OF PHILOSOPHY is approved by the committee on 05.07.2022 in the Department of Civil Engineering, Hydraulics Program.

Assoc. Prof. Dr. Berna AYAT AYDOĞAN

Yıldız Technical University

Supervisor

Approved By the Examining Committee

Assoc. Prof. Dr. Berna AYAT AYDOĞAN, Supervisor
Yıldız Technical University _____

Prof. Dr. Hayrullah AĞAÇCIOĞLU, Member
Yıldız Technical University _____

Assis. Prof. Dr. Bilge TUTAK, Member
İstanbul Technical University _____

Prof. Dr. Güleda ENGİN, Member
Yıldız Technical University _____

Assoc. Prof. Dr. Emin ÇİFTÇİ, Member
Maltepe University _____

I hereby declare that I have obtained the required legal permissions during data collection and exploitation procedures, that I have made the in-text citations and cited the references properly, that I haven't falsified and/or fabricated research data and results of the study and that I have abided by the principles of the scientific research and ethics during my Thesis Study under the title of Response Of Black Sea Coastline To Climate Change Impacts supervised by my supervisor, Assoc. Prof. Dr. Berna AYAT AYDOĞAN. In the case of a discovery of false statement, I am to acknowledge any legal consequence.

Tunay ÇARPAR

This research was funded in frame of the BS-STEMA project (Changes in storminess and coastal erosion induced by climate variability along the Black Sea coasts. Management and adaptation) funded by the European Union through Era.Net RUS Plus initiative and TUBITAK Grant Agreement no. 116M061.

ACKNOWLEDGEMENTS

I would like to express my gratitude to all the people who in one way or another contributed to the development of this research.

Firstly, I would like to express my sincere appreciation to my supervisor Assoc. Prof. Dr. Berna AYAT AYDOĞAN; thank you for your valuable help in instructing, guiding, and supporting me throughout this thesis.

Also, I would like to thank the members of my thesis committee: Prof. Dr. Hayrullah AĞAÇCIOĞLU, Asst. Prof. Dr. Bilge TUTAK, Prof.Dr. Güleda ENGİN, Assoc. Prof. Dr. Emin ÇİFTÇİ for their knowledgeable and in-depth comments and advice.

I would like to thank Prof. Dr. Yalçın YÜKSEL and all the Hydraulics Division Researchers for their motivation and support throughout my PhD studies.

I also express my deep sense of gratitude to Assoc. Prof. Dr. Burak AYDOĞAN and Tahsin GÖRMÜŞ for their valuable advice and feedback during my study.

I am grateful for the guidance I received from the late Prof. Dr. Ahmet DOĞAN, whose advice I will always try to follow. His memory will always be with me.

Further, I would like to thank Istanbul Water and Sewerage Administration (İSKİ) and my colleagues for their support during my PhD.

I would also like to extend my deepest gratitude to my mother Sevdiye ÇARPAR and my father Ayhan Kamil ÇARPAR for their self-sacrifice and patience through my education.

I owe special gratitude to my true love Burcu KIRANLAR ÇARPAR for her endless support.

Finally, and above all, I also would like to thank my daughter Nisan ÇARPAR, who joined us when I was writing my dissertation, for giving me unlimited happiness and pleasure.

Tunay ÇARPAR

TABLE OF CONTENTS

LIST OF SYMBOLS viii

LIST OF ABBREVIATIONS ix

LIST OF FIGURES x

LIST OF TABLES xvi

ABSTRACT xix

ÖZET xxi

1 INTRODUCTION 1

1.1 Literature Review 1

1.2 Objective of the Thesis 19

1.3 Hypothesis 20

2 THE STUDY AREA 21

2.1 Climate 22

2.2 Topography 24

2.3 Geology 26

2.4 Land Use 26

2.5 Demography 29

2.6 Coastal Erosion and Its Reasons Along the Black Sea 31

3 DATA AND METHODOLOGY 32

3.1 Data 32

3.1.1 Wind Data 33

3.1.2 Mean Sea Level Pressure Data 34

3.1.3 Wave Data 34

3.1.4 Sea Surface Temperature Data 35

3.1.5 Precipitation and Evaporation Data 35

3.1.6 Shoreline Data 35

3.2 Methodology 37

3.2.1 Trend Analysis of Atmospheric Parameters 37

3.2.2 Analysis of Shoreline Changes 40

3.2.3 Pearson Correlation Coefficients 41

4 RESULTS AND DISCUSSION 43

4.1 Long-Term Changes in Atmospheric Forcing 43

4.1.1 Long-Term Variations of Wind Speeds over the Black Sea 43

4.1.2 Long-Term Variations of Significant Wave Heights over the Black Sea 68

4.1.3 Long-Term Variations of Sea Surface Temperatures over the Black Sea 81

4.1.4 Long-Term Variations of Precipitation over the Black Sea 84

4.2 Shoreline Changes along the Black Sea Coasts 91

4.2.1 Danube 96

4.2.2 Terkos 101

4.2.3 Cide 107

4.2.4 Sinop 111

4.2.5 Bafra 115

4.2.6 Çarşamba 119

4.2.7 Sochi 122

4.2.8 Long-Term Variations of Atmospheric Properties on the Selected Shoreline Regions 126

4.2.9 Relation of Shoreline Changes with Long-Term Variations of Atmospheric Parameters 128

4.3 Conclusion 145

REFERENCES **150**

PUBLICATIONS **164**

LIST OF SYMBOLS

°C	Celsius Degree
m	Meters
mm	Millimeters
%	Percent
s	Seconds

LIST OF ABBREVIATIONS

hr	hours
NSWH	Normalized Significant Wave Height
SST	Sea Surface Temperature
SWH	Significant Wave Height
U10	10 meters Wind Speeds
$U10_{95}$	95^{th} Percentile 10m Wind Speeds
$U10_{m}$	Mean 10 meters Wind Speeds
yr	year

LIST OF FIGURES

Figure 1.1 Global Temperatures and CO_2 Concentrations (Moore et al., 2021) 1

Figure 1.2 Sea level changes between the years 1880 and 2020 (NOAA Technical Report 53, 2021) 3

Figure 1.3 Coastal Erosion in the village of Withernsea on the East coasts of England (The Guardian, 2020).....4

Figure 1.4 San Clemente, Orange County, California (The Orange County Register, 2019).....4

Figure 1.5 SST Changes in the Global Ocean and the European Regional Seas (EC, 2021).....11

Figure 1.6 Five-year moving average filtered time series of basin-mean winter SST in the Black Sea based on GISST (bold solid line), MCSST (thin solid line), and NCEP (dotted line) data. The solid horizontal line indicates the climatological mean SST for 1950 – 2005 (Kazmin and Zatsepin, 2007) 12

Figure 1.7 Basin-averaged, winter (December–March) mean (squares) and annual mean SST distributions in the Black Sea from 1985 to 2001 (Oğuz et al., 2003). 13

Figure 2.1 The study area: the Black Sea Basin. 21

Figure 2.2 Circulation pattern of the surface layer of the Black Sea (Fach, 2014) 24

Figure 2.3 The bathymetry of the Black Sea (National Geophysical Data Center, NOAA.) 25

Figure 2.4 The watershed of the Black Sea (Koulov, 2012). 27

Figure 2.5 The expected land use for the Black Sea by 2050 (Lehmann et al., 2017) 28

Figure 2.6 Important ports near the Black Sea (Nicolae et al., 2018) 29

Figure 3.1 Selected erosion-prone coastal regions along the Black Sea coasts where the shoreline changes were calculated. 37

Figure 3.2 Graphs showing a correlation of -1, 0, and +1 (Cohen, 1988) ...42

Figure 4.1 Long-term averaged U10 considering 38 years period (1979–2016) over the Black Sea: a) ERA-I, b) CFSR. White dots indicate land and the black dots indicate sea points 43

Figure 4.2 The ratio of long-term average U10 values from the CFSR data to the ones from ERA-I 44

Figure 4.3 Long-term 95th percentile U10 considering 38 years period (1979–2016) over the Black Sea: a) ERA-I, b) CFSR. 45

Figure 4.4 Interannual variability of annual $U10_m$ and annual $U10_{95}$ at selected study sites (Figure 2.1), a) A, b) B, c) C, d) D, e) E, f) F, g) G, h) H, and I) I, j) J 46

Figure 4.5 Spatial variability of long-term trends of a) annual MSLP from ERA-I, b) annual MSLP from CFSR, c) ERA-I annual $U10_m$, d) CFSR annual $U10_m$, e) ERA-I annual U1095, f) CFSR annual U1095 for the study period (1979–2016) over the study area. Black dots indicate locations with statistically significant trends at the 95% or higher confidence level. Contours indicate the time-averaged MSLP (Pa) in a and b 50

Figure 4.6 Spatial variability of long-term trends in ERA-I MSLP on a monthly basis. Black dots indicate locations with statistically significant trends at the 95% or higher confidence level.....53

Figure 4.7 Spatial variability of long-term trends in CFSR MSLP on a monthly basis. Black dots indicate locations with statistically significant trends at the 95% or higher confidence level.....55

Figure 4.8 Spatial variability of long-term trends in ERA-I monthly $U10_m$ on a monthly basis. Black dots indicate locations with statistically significant trends at the 95% or higher confidence level.....56

Figure 4.9 Spatial variability of long-term trends in CFSR monthly $U10_m$ on a monthly basis. Black dots indicate locations with statistically significant trends at the 95% or higher confidence level.....57

Figure 4.10 Spatial variability of long-term trends in ERA-I monthly U1095 on a monthly basis. Black dots indicate locations with statistically significant trends at the 95% or higher confidence level.....58

Figure 4.11 Spatial variability of long-term trends in CFSR monthly U1095 on a monthly basis. Black dots indicate locations with statistically significant trends at the 95% or higher confidence level.....60

Figure 4.12 Correlation coefficients between teleconnection indices and the annual $U10_m$ over the Black Sea for both ERA-I and CFSR reanalysis data, a) [ERA-I]–[EA], b) [ERA-I]–[EA/WR], c) [ERA-I]–[NAO], d) [ERA-I]–[PNA], e) [ERA-I]–[POL], f) [ERA-I]–[SCA], g) [CFSR]–[EA], h) [CFSR]–[EA/WR], I) [CFSR]–[NAO], j) [CFSR]–[PNA], k) [CFSR]–[POL], l) [CFSR]–[SCA] 64

Figure 4.13 Correlation coefficients between teleconnection patterns and the $U10_{95}$ over the Black Sea for both ERA-I and CFSR reanalysis data. a) [ERAI]–[EA], b) [ERA-I]–[EA/WR], c) [ERA-I]–[NAO], d) [ERA-I]–[PNA], e) [ERA-I]– POL], f) [ERA-I]–[SCA], g) [CFSR]–[EA], h) [CFSR]–[EA/WR], I) [CFSR]–[NAO], j) [CFSR]–[PNA], k) [CFSR]–[POL], l) [CFSR]–[SCA] 66

Figure 4.14 Long-term averaged Annual SWHs considering 38 years period (1979–2016) over the Black Sea (ERA-Interim) 69

Figure 4.15 Spatial variability of long-term trends in averaged Annual SWH. Black dots indicate locations with statistically significant trends at the 90% or higher confidence level. 70

Figure 4.16 Long-term 95th percentile Annual SWHs considering 38 years period (1979–2016) over the Black Sea (ERA-Interim) 71

Figure 4.17 Long-term variations of 95th percentile Annual SWHs considering 38 years period (1979–2016) over the Black Sea (ERA-Interim). Black dots indicate locations with statistically significant trends at the 90% or higher confidence level. 71

Figure 4.18 a) Spatial distribution of the trends for annual NSWHs (%/year) based on the Theil-Sen method. b) The significance of the long-term trends in annual mean NSWHs based on the Mann-Kendall test for different confidence levels (Aydoğan and Ayat, 2018). ..72

Figure 4.19 a) Spatial distribution of the long-term trends for 95th percentile NSWHs (%/year) based on the Theil-Sen method. b) The significance of the long-term trends in the annual 95th percentile NSWHs based on the Mann-Kendall test for different confidence levels (Aydoğan and Ayat, 2018).....73

Figure 4.20 Spatial variability of long-term trends in mean NSWHs for each month (%/year) on a monthly basis (Aydoğan and Ayat, 2018). 75

Figure 4.21 Spatial distribution of the trend significance for mean NSWHs for each month at different confidence levels based on the Mann-Kendall test (Aydoğan and Ayat, 2018).....76

Figure 4.22 Spatial variability of long-term trends in 95th percentile NSWHs for each month (%/year) on a monthly basis (Aydoğan and Ayat, 2018). 78

Figure 4.23 Spatial distribution of the trend significance for 95th percentile NSWHs for each month at different confidence levels based on the Mann-Kendall test (Aydoğan and Ayat, 2018).....79

Figure 4.24 Correlations of Black Sea SWH and different oscillation patterns for mean and severe sea states (Aydoğan and Ayat, 2018).....80

Figure 4.25 Long-term averaged Annual SSTs considering 38 years period (1979–2016) over the Black Sea (ERA-Interim) 82

Figure 4.26 Spatial variability of long-term trends in averaged Annual SSTs. Black dots indicate locations with statistically significant trends at the 90% or higher confidence level. 82

Figure 4.27 Long-term annual 95th percentile Annual SSTs considering 38 years period (1979–2016) over the Black Sea (ERA-Interim) 83

Figure 4.28 Spatial variability of long-term trends in 95th percentile Annual SSTs. Black dots indicate locations with statistically significant trends at the 90% or higher confidence level.....84

Figure 4.29 Long-term average Annual Total Precipitation considering 38 years period (1979–2016) over the Black Sea (ERA-5).....85

Figure 4.30 Long-term variations of annual total precipitations considering 38 years period (1979–2016) over the Black Sea (ERA-5). Black dots indicate locations with statistically significant trends at the 90% or higher confidence level.....85

Figure 4.31 Long-term averaged annual number of days with precipitation considering 38 years period (1979–2016) over the Black Sea (ERA-5) precipitations in 38 years period (1979–2016). 87

Figure 4.32 Long-term variations of annual number of days with precipitation considering 38 years period (1979–2016) over the Black Sea (ERA-5). Black dots indicate locations with statistically significant trends at the 90% or higher confidence level. 88

Figure 4.33 a) Long-term average Annual Total Precipitations and b) Long-term average Annual Total Evaporations over the Black Sea Basin, considering 38 years period (1979–2016) over the Black Sea (ERA-5) 89

Figure 4.34 a) Annual differences of total precipitations and total evaporations b) with their long-term variations over the Black Sea Basin, considering 38 years period (1979–2016) over the Black Sea (ERA-5) 90

Figure 4.35 The locations and id numbers of shoreline zones along the Black Sea Coasts. To figure out the id numbers more clearly, the numbers were represented by fives starting from 1 to 271.....91

Figure 4.36 Selected study site in the Danube where the long-term variations of shoreline are explored. The id numbers of the points from south to north (Luijendijk et al., 2018). 97

Figure 4.37 Shoreline positions and trends for particular points in the study site in the Danube.....101

Figure 4.38 Selected study site in Terkos where the long-term variations of shoreline are explored. The id numbers of the points go from west to east (Luijendijk et al., 2018). 102

Figure 4.39 Shoreline positions and trends for particular points in the study site in Terkos 106

Figure 4.40 Selected study site in Cide where the long-term variations of shoreline are explored. The id numbers of the points go from west to east (Luijendijk et al., 2018). 107

Figure 4.41 Shoreline positions and trends for particular points in the study site in Cide.....111

Figure 4.42 Selected study site in Sinop where the long-term variations of shoreline are explored. The id numbers of the points go from west to east (Luijendijk, 2018). 112

Figure 4.43 Shoreline positions and trends for particular points in the study site in Sinop.....115

Figure 4.44 Selected study site in Bafra where the long-term variations of shoreline are explored (Luijendijk et al., 2018).....116

Figure 4.45 Shoreline positions and trends for particular points in Bafra. ...119

Figure 4.46 Selected study site in Çarşamba where the long-term variations of shoreline are explored (Luijendijk et al., 2018).....120

Figure 4.47 Shoreline positions and trends for particular points in Çarşamba. 122

Figure 4.48 Selected study site in Sochi where the long-term variations of shoreline are explored (Luijendijk et al., 2018).....123

Figure 4.49 Shoreline positions and trends for particular points in the study site in Sochi 126

Figure 4.50 Mean Annual Shoreline Changes vs Mean Annual Wind Speed Trends Scatter Graph in 130 Points where the trends are significant 129

Figure 4.51 Mean Annual Shoreline Changes vs 95th percentile Annual Wind Speed Trends Scatter Graph in 75 Points where the trends are at least 90% significant 130

Figure 4.52 Mean Annual Shoreline Changes vs Mean Annual SST Trends in 174 Points where the trends are at least 90% significant.....130

Figure 4.53 Mean Annual Shoreline Changes vs 95th percentile Annual SST Trends in 198 Points where the trends are at least 90% significant.....131

Figure 4.54 Mean Annual Shoreline Changes vs Mean Annual SWH Trends in 103 Points where the trends are at least 90% significant.....131

Figure 4.55 Mean Annual Shoreline Changes vs Mean Annual SWH Trends in 68 Points where the trends are at least 90% significant.....132

LIST OF TABLES

Table 2.1 Populations of the Black Sea Riparian Countries according to 2022 census (Worldometer.info) 30

Table 2.2 Most Populated Urban Areas along the Black Sea Coastline according to 2022 census (Worldometer.info, tuik.gov.tr) 30

Table 3.1 Properties of the reanalysis U10 data used in this study. 34

Table 3.2 Coastal regions near the Black Sea where the mean shoreline changes were calculated (Tatui et al., 2019) 36

Table 3.3 Strength of the correlations due to Pearson correlation coefficient.....42

Table 4.1 Interannual variability coefficients for the selected study sites and the basin averaged U10 48

Table 4.2 Percentage of grid points where statistically significant negative and positive trends exist in monthly/annual $U10_m$ and U1095 over the Black Sea. 61

Table 4.3 The total lengths and number of transection points for each shoreline zone. The red color scale indicates erosion whereas the green color scale indicates deposition. 92

Table 4.4 The ID numbers of the shoreline zones given in Figure 4.35 which constitute selected shorelines segments 96

Table 4.5 Long-term changes of the shorelines in the transactions in the Danube Delta. 90% statistically significant trends (p value<0.1) are shown with *. 99

Table 4.6 Long-term changes of the shorelines in the transactions in the Terkos. 90% statistically significant trends (p value<0.1) are shown with *. 104

Table 4.7 Long-term changes of the shorelines in the transactions in the Cide. 90% statistically significant trends (p value<0.1) are shown with *. 108

Table 4.8 Long-term changes of the shorelines in the transactions in the Sinop. 90% statistically significant trends (p value<0.1) are shown with *. 113

Table 4.9 Long-term changes of the shorelines in the transactions in the Bafra. 90% statistically significant trends (p value<0.1) are shown with *. 117

Table 4.10 Long-term changes of the shorelines in the transactions in the Çarşamba. 90% statistically significant trends (p value<0.1) are shown with *. 121

Table 4.11 Long-term changes of the shorelines in the transactions in the Sochi. 90% statistically significant trends (p value<0.1) are shown with *. 124

Table 4.12 Long-term annual averaged and 95th percentile wind speeds and their variations considering 38 years period (1979–2016) for selected regions along the Black Sea Coastline. 90% statistically significant trends (p value<0.1) are shown with *. 127

Table 4.13 Long-term averaged and 95th percentile SSTs and their variations considering 38 years period (1979–2016) for selected regions along the Black Sea Coastline. 90% statistically significant trends (p value<0.1) are shown with *. 127

Table 4.14 Long-term averaged and 95th percentile SWHs and their variations considering 38 years period (1979–2016) for selected regions along the Black Sea Coastline. 90% statistically significant trends (p value<0.1) are shown with *. 128

Table 4.15 Pearson correlation coefficients (r) between annual atmospheric parameters and shoreline positions for Danube. Green and yellow colors indicate strong and moderate correlations, respectively. 134

Table 4.16 Pearson correlation coefficients (r) between annual atmospheric parameters and shoreline positions for Terkos. Green and yellow colors indicate strong and moderate correlations, respectively. 135

Table 4.17 Pearson correlation coefficients (r) between annual atmospheric parameters and shoreline positions for Cide. Green and yellow colors indicate strong and moderate correlations, respectively .137

Table 4.18 Pearson correlation coefficients (r) between annual atmospheric parameters and shoreline positions for Sinop. Green and yellow colors indicate strong and moderate correlations, respectively. 139

Table 4.19 Pearson correlation coefficients (r) between annual atmospheric parameters and shoreline positions for Bafra. Green and yellow colors indicate strong and moderate correlations, respectively. 140

Table 4.20 Pearson correlation coefficients (r) between annual atmospheric parameters and shoreline positions for Çarşamba. Green and yellow colors indicate strong and moderate correlations, respectively. 141

Table 4.21 Pearson correlation coefficients (r) between annual atmospheric parameters and shoreline positions for Sochi. Green and yellow colors indicate strong and moderate correlations, respectively. 143

ABSTRACT

Response of Black Sea Coastline to Climate Change Impacts

Tunay ÇARPAR

Department of Civil Engineering

Doctor of Philosophy Thesis

Supervisor: Assoc. Prof. Dr. Berna AYAT AYDOĞAN

This thesis presents an investigation of the long-term variations of climate parameters and shoreline changes in the Black Sea. Long-term trends of mean and 95th percentile wind speeds, significant wave heights, sea surface temperatures, and precipitation for the term between 1979 and 2016 were calculated. Besides, the shoreline changes in the last decades along the Black Sea were examined. To define the possible relations between climate parameters and shoreline changes, statistical analyses were conducted. The analysis for climate parameters were done by using two different data: European Centre for Medium-Range Weather Forecasts-ERA-Interim and U.S. National Centers for Environmental Prediction-Climate Forecast System Reanalysis (CFSR). The time series of shoreline positions for transaction points at 271 shoreline segments along the Black Sea coasts were gained from Deltares' Aqua-Monitor Database. The Mann-Kendall and Sen's Slope methods are used to determine all the trends and statistical significances. For climate parameters, significant trends show spatial variability over the study area. Similarly, the shoreline changes exhibit significant trends in the same period.

While sea surface temperatures showed significant increasing trends in almost all of the Black Sea, wind speeds and wave heights were found to show significant increasing trends in the eastern Black Sea. It was also determined that precipitation intensity in the Black Sea region tend to increase. On the 49% of 271 shoreline segments along the Black Sea, there is erosion between 0.01 m/year and 6.76 m/year. 51% of these shoreline segments, there is deposition between 0.02 m/year and 9.29 m/year. Local shoreline erosion values in the Danube, Kızılırmak, and Yeşilırmak Deltas, reached the order of 8.7, 21.81, and 23.33 m/year, respectively. The correlations between the time series of climate parameters and the shoreline positions indicate significant relationships with spatial variations. In this study, sea surface temperatures provided the strongest statistical relationship with the shoreline changes.

Key Words: Climate change, winds, waves, shoreline, Black Sea

ÖZET

Karadeniz Kiyilarinin İklim Değişikliği Etkilerine Tepkisi

Tunay ÇARPAR

İnşaat Mühendisliği Bölümü

Doktora Tezi

Danışman: Doç. Dr. Berna AYAT AYDOĞAN

Bu çalışmada iklim değişikliğinin Karadeniz kıyı çizgisi üzerindeki etkisi incelenmiştir. Bu amaçla rüzgâr hızları, belirgin dalga yükseklikleri, deniz suyu sıcaklıkları ve yağış olarak seçilen iklim parametrelerinde 1979 ve 2016 yılları arasındaki uzun dönemli değişimler belirlenmiştir. Yine aynı dönemde Karadeniz kıyı çizgisindeki değişimler belirlenmiş ve dikkate alınan iklim parametreleri ile Karadeniz kıyıları boyunca meydana gelen kıyı çizgisi değişimleri arasındaki olası ilişkilerin ortaya konulabilmesi amacıyla istatistiksel analizler gerçekleştirilmiştir. Çalışmada kullanılan veriler Avrupa Orta Vadeli Hava Tahminleri Merkezi'nden ERA-Interim ve ERA-5 ve ABD Ulusal Çevresel Tahmin Merkezi'nden CFSR yeniden analiz veri setlerinden temin edilmiştir. Karadeniz kıyıları boyunca 271 sektöre ait kıyı çizgisi konumlarına ilişkin zaman serileri Deltares tarafından sağlanan Aqua-Monitor veri tabanından elde edilmiştir. Değişim eğilimlerinin ve bu eğilimlerin belirginliklerinin tespiti için parametrik olmayan Mann-Kendall ve Sen's Slope yöntemleri kullanılmıştır. Seçilen iklim parametrelerinin tamamı için çalışma alanında uzamsal olarak farklılık gösteren istatistiksel olarak anlamlı

değişim eğilimleri elde edilmiştir. Benzer şekilde aynı dönemde kıyı çizgisi değişimleri de istatistiksel olarak anlamlı değişimler sergilemektedir. Deniz suyu sıcaklıkları neredeyse tüm Karadeniz'de istatistiksel olarak anlamlı artış eğilimleri sergilerken, rüzgâr hızları ve dalga yüksekliklerinin Karadeniz'in doğusunda istatistiksel olarak anlamlı artış eğilimleri göstermektedir. Yıllık toplam yağış ve yıllık yağışlı gün sayısındaki değişimler tüm Karadeniz'de yağış şiddetinin arttığını göstermektedir. Güneydoğu kıyılarında ise toplam yıllık yağış miktarını artmaktadır. Kıyı çizgisi değişimi analizlerinde dikkate alınan 271 kıyı sektörünün %49'unda 0,01 m/yıl ile 6,76 m/yıl arasında erozyon ve %51'i için ise 0,02 m/yıl ile 9,29 m/yıl arasında yığılma eğilimleri belirlenmiştir. En yüksek kıyı çizgisi değişimine maruz kalan Tuna, Kızılırmak ve Yeşilırmak Deltalarında yerel kıyı çizgisi erozyonu değerlerinin sırasıyla 8,7; 21,8 ve 23,3 m/yıl mertebelerine ulaştığı belirlenmiştir. İklim parametreleri zaman serileri ile kıyı çizgisi konumu zaman serileri arasındaki korelasyonlar uzamsal olarak farklılık gösteren, istatistiksel olarak anlamlı ilişkilere işaret etmektedir. Bu çalışmanın sonuçları kıyı çizgisi değişimleri ile deniz suyu sıcaklıkları arasında belirgin istatistiksel ilişkilerin dikkate alınan diğer iklim parametrelerine göre daha fazla olduğunu göstermektedir.

Anahtar Kelimeler: İklim değişikliği, rüzgâr, dalga, kıyı çizgisi, Karadeniz

1

INTRODUCTION

1.1 Literature Review

The prevalent use of fossil fuels for energy especially after the industrial revolution has resulted in emissions of vast amounts of carbon dioxide and other greenhouse gases into the atmosphere. This situation induced global warming which has severe impacts on the Earth. Figure 1.1 declares that; since 1880, the mean global temperatures have increased by around 1.2° Celsius along with increasing carbon dioxide concentrations in the atmosphere. Especially, the oceans have been highly vulnerable to climate change effects, in the last century. To sum up, we face severe impacts of global climate change on marine ecosystems like coastal areas, fisheries, coral islands, etc. where we stand now.

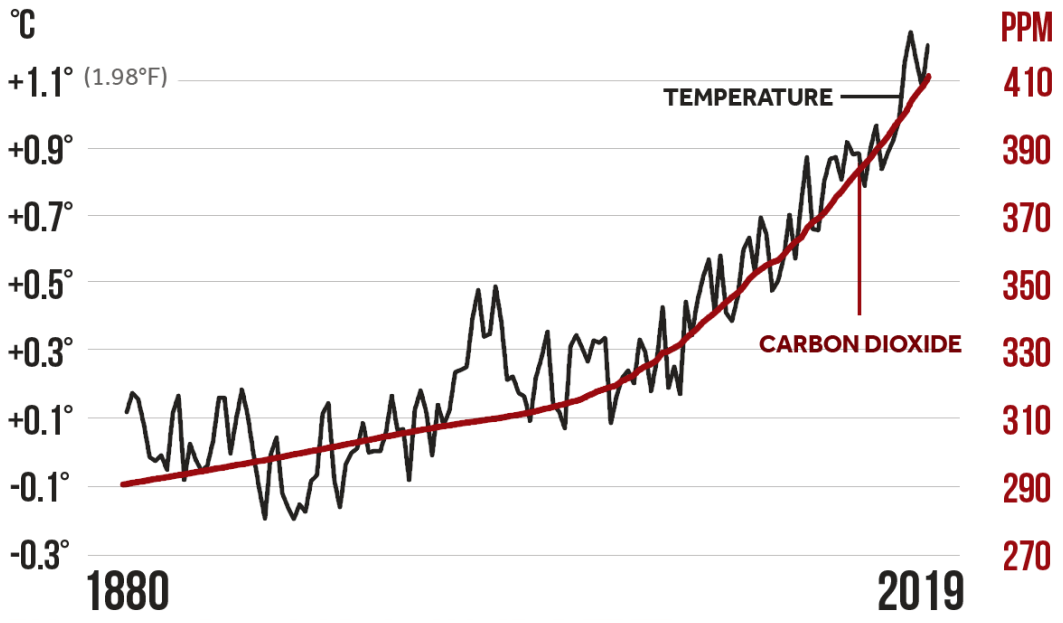


Figure 1.1 Global temperatures and CO_2 concentrations (Moore et al., 2021)

The integrity of coastal areas, where significant anthropogenic and natural processes occur, has been under the effect of several environmental stressors and this is widespread, especially in the last decades. A common example of these stressors can be counted as the variations of atmospheric parameters like wind speed, sea surface temperature (SST), and precipitation, all of which lead to distinct changes in the frequency and strength of extreme storms along with warmer or cooler weather conditions for coastal regions.

The interaction between the oceans and the atmosphere can be seen via several mechanisms such as the exchange of heat, water, and momentum from one to another. For example, wind over an ocean surface transfers its energy to the water surface layers to generate waves and oceanic currents. That's why; to have a better understanding of the future impacts of these climatic changes on coastal environments, it is necessary to predict how these climatic variations occur in the future.

Global climate change, which is commonly known as global warming, has significant effects on coastal systems. Sea level rise is one of the major consequences of global climate change which threatens coastal areas. Sea level rise occurs due to the melting of glaciers and ice sheets. Also, expanding volume of Earth's oceans due to increasing water temperatures contribute to sea-level rise. Since 1880; it is known that the total sea rise in the global mean sea levels reached up to 24 centimeters. Besides, the rate of sea-level change has increased from a mean value of 1.4 mm/yr to 3.6 mm/yr in the last decades. Just for the United States, it is stated that high tide floods are more frequent than usual, between 3 and 9 times. Figure 1.2 shows global sea-level changes between the years 1880 and 2020 (FEMA, 2008).

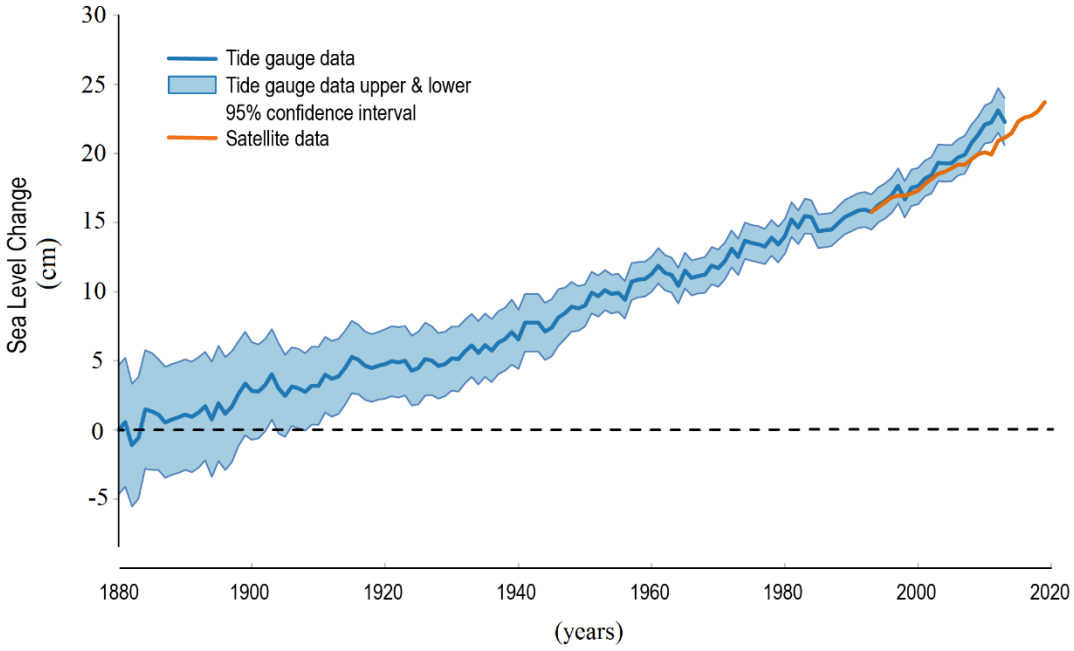


Figure 1.2 Sea level changes between the years 1880 and 2020 (NOAA Technical Report 53, 2021)

Besides Sea level rise, global climate change has some other consequences which affect coastal regions. The change in the intensity and frequency of storminess, changes in precipitation patterns, rising temperatures, and acidity of ocean waters are the main examples of the processes, which can be destructive to vulnerable coastal areas and marine ecosystems. Especially, coastal erosions, coastal floods, and salt water intrusion into the groundwater are some of the undesired results seen in these regions (Figure 1.3-4). By taking into consideration that, most of the world's population live in coastal areas, the tangible and intangible losses of these process would be far beyond our imagination (FEMA, 2008).



Figure 1.3 Coastal erosion in the village of Withernsea on the east coasts of England (The Guardian, 2020)



Figure 1.4 San Clemente, Orange County, California (The Orange County Register, 2019)

The major reason for coastal erosion and coastal flooding is wave action and waves are shaped by wind forcing over the water surface. That is why it is possible to say that wind is the former trigger for coastal erosion or flooding. Additionally, winds have a direct contribution to these processes. Hereby, the necessity to explore the changes in wind speeds due to global change is a key input for the investigation of coastal vulnerability (Healy, 2018).

As mentioned above, wind speed is the direct and indirect forcing for many natural processes such as storms (Zainescu et al., 2017), coastal erosion (Healy, 2018), ventilation of the water in the marine environment, coastal circulation (Shepherd et al., 2017), wind-wave generation (Rusu et al., 2014; Aydoğan and Ayat, 2018), etc. Wind speed also affects marine activities such as seakeeping safety, stabilities of the offshore structures (Wang and Hwang, 2001), marine transportation (Rusu et al., 2018), port operations (Athanasatos et al., 2014), tourism (Georgopoulou et al., 2018), fisheries (Masuda et al., 2014), renewable energy generation (Ganea et al., 2018; Aydoğan, 2017), etc. Long-term changes in wind speed in coastal and offshore regions have great importance on the sustainability of natural processes and marine activities.

Long-term trends in 10 m-wind speeds (U10) have been studied at local (Li, 2011), regional (Troccoli et al., 2012; Jiang et al., 2010), and global scales (Young et al., 2011). For the evaluation of the U10 variations at a local scale, local measurement data is sufficient (Tuller, 2004). Regional and global scale evaluations require homogeneous time series that cover the study area with proper temporal and spatial details (Weisse and Gunther, 2007). Zheng et al. (2016) presented spatial and seasonal variations of annual mean U10 ($U10_m$) for the period between 1988 and 2011, focusing on a study area covering all the global oceanic sea surfaces. The researchers reported that the $U10_m$ increased at a significant overall rate of 3.35 cm/s/yr for the period 1988–2011 over the global oceanic sea surface and the long-term trend values showed noticeable regional inhomogeneity.

Sterl and Caires (2005) also studied spatiotemporal variations in U10 over the global ocean and reported an increasing trend reaching up to the rate of 6 cm/s/yr for $U10_m$ between 1971 and 2000 based on ERA40 reanalysis provided by the European Center for Medium-Range Weather Forecasts (ECMWF). Authors found that 99^{th} percentile U10 increases at even a higher rate of 12 cm/s/yr over some specific regions.

Long-term changes in U10 over the Black Sea have also been studied intensively due to the need for both sustainable marine activities in riparian countries and the preservation of its unique natural environment. Cakiroglu et al. (2017) analyzed measured wind data at seven coastal stations for the period between 1970 and 2010 and reported that the $U10_m$ changes at statistically significant rates of 2 cm/s/yr and -3 cm/s/yr over the southwestern Black Sea and the southeastern Black Sea, respectively. Aydoğan (2017) presented the offshore wind power atlas of the Black Sea. The author used the ECMWF ERA-Interim reanalysis (ERA-I) to evaluate offshore wind energy potential within the basin for the 38 years between 1979 and 2016. The author compared the ERA-I data with the in-situ measurements from two coastal stations in the southwestern Black Sea and concluded that ERA-I data well matched the observations. Comparison of U.S. National Centers for Environmental Prediction (NCEP) of National Oceanic and Atmospheric Administration (NOAA), Climate Forecast System Reanalysis (CFSR) reanalysis wind data with the in-situ measurements at Gloria platform conducted by Rusu et al. (2018) reporting that the CFSR reanalysis data give slightly higher wind speeds than the measured ones at that location.

Ganea et al. (2019) studied the temporal variations in U10 at six nearshore locations along the Black Sea coastline based on ERA-I data for the term 1983-2017 in the frame of “Assessment of the Climate Change Effects on the Wave Conditions in the Black Sea (ACCWA)” project. The authors reported a statistically significant decreasing trend with a rate of 1 cm/s/decade in $U10_m$ for the northwestern Black Sea.

Akpinar and Bingolbali (2016) analyzed the long-term variations of wind conditions in 33 coastal locations along the Black Sea coastline, excluding the offshore. Researchers used the CFSR wind fields for the term between 1979 and 2009. They reported that $U10_m$ have statistically significant increasing trends in the ranges of 0.398 cm/s/yr - 0.813 cm/s/yr and 0.902 cm/s/yr - 1.337 cm/s/yr, for the southeastern coasts of the Black Sea and around the Crimean Peninsula, respectively. Zainescu et al. (2017) studied storminess along the Danube Delta Coast since 1949 by analyzing wind data.

Authors also revealed the relation of teleconnection patterns with the regional variability of sea storms and concluded that the North Atlantic Oscillation (NAO) has the highest correlation with the storminess of the Danube Delta Coast, however, for the last 10 years, the East Atlantic (EA) pattern and the East Atlantic/West Russia (EA/WR) pattern becomes more notable. Valchev et al. (2012) aimed to explore the trends for storminess in the western Black Sea for the years between 1948 and 2010. The authors conducted a temporal analysis of the variations of storminess and concluded that there is no statistically significant increasing or decreasing trend in the storminess over the western Black Sea.

Wind fields over the Black Sea basin are influenced by large-scale atmospheric circulations controlled by the Siberian anticyclone, Mediterranean cyclonic activity, Azores anticyclone, and Island cyclone. The influence of the Siberian anticyclone manifests itself, especially in winter. In the eastern basin, dominated large-scale atmospheric circulation is caused by the Azores anticyclone with an increasing impact during summer (Kubryakov et al., 2019). Another important cyclonic airflow is the Island cyclone which affects the wind climate in the Black Sea throughout the year (Efimov and Anisimov, 2011; Rusu et al., 2014). Different heights of mountainous ridges, the North Anatolian Mountains along the southern coasts, the Caucasus Mountains along the eastern coasts, and the Crimean Mountains induce an important impact on the windiness of the Black Sea since they interrupt the winds from the arc from south to east (Arkhiphin et al., 2014).

Lowlands between the mountains and the narrow valleys cause high-velocity winds such as Novorossiyskaya Bora, occasionally (Rusu et al., 2014).

Özsoy and Ünlüata (1997) reported two primary pathways for winter winds; one is moving northeastward direction over the Sea of Marmara originating from the Mediterranean Sea and the other one in eastward and southeastwards directions from Romania. The detailed atmospheric setting of the Black Sea basin can be found in Özsoy and Ünlüata (1997), Surkova et al. (2013), Zecchetto and de Biasio (2007), and Kostianoy and Kosarev (2008).

Difficulties arise in the comparison and synthesis of the results due to the different data sources analyzed and different temporal coverages considered in the studies so far. Comparative studies for the long-term trends of wind speeds over the Black Sea become important in this regard. This kind of comparative analysis of wind speeds was conducted by Rusu et al. (2018) along the shipping routes in the Black Sea. Authors evaluated the wind conditions for the term between 1 January 1987 and 31 December 2009 based on the CFSR reanalysis data and the hindcast results provided by a Regional Climate Model (RCM) that were retrieved from European Domain-Coordinated Regional Climate Downscaling Experiment (EURO-CORDEX). The authors reported a good agreement between two data sources for the offshore sites and nearshore sites except for the southern part of the Black Sea. Rusu et al. (2018) evaluated the long-term trends in 95th percentile U10 ($U10_{95}$) as well as the $U10_m$ and concluded that no statistically significant trend exists for both time series within the study period at the selected location.

The variations of the wind speeds over the sea surfaces represent perceptible seasonal differences, which point out the necessity of seasonal analysis of wind speeds (Zheng et al., 2016). Seasonal variations of the wind speeds were also analyzed in recent studies (Rusu et al., 2018; Aydoğan, 2017; Akpinar and Bingolbali, 2016) indicating higher wind speeds during the winter months and lower wind activity during the summer months. Based on this finding, Velea et al. (2014) analyzed the frequency of extreme winds over the Black Sea surface by focusing on January for the period 2001 to 2009. The entire Black Sea basin was

studied, and western and northern areas were found to have moderate and strong winds between 2001 and 2009. Although the wind climate and the storminess in the Black Sea have been studied widely for different parts of the basin or some specific locations, the spatial variability of the long-term trends of wind speeds, their spatiotemporal variability on a monthly basis, correlations to the teleconnection indices has not been examined sufficiently.

Besides wind speeds, which is a ruling parameter affecting storminess, SST is also a key natural process to shape storminess. Here, SST becomes another important phenomenon that regulates how the oceans and atmosphere interact with each other. Warmer air conditions evaporate water more rapidly while wind fastens this. Evaporation of water from oceans cools water by absorbing heat energy from it and then the vapor gives this energy to the atmosphere during condensation. This system can be evaluated as one of the leading mechanisms through which the atmosphere gains energy. Condensed water vapor forms clouds in the atmosphere and these clouds determine the amount of reflected incoming and outgoing radiation from the Sun. It tunes the warming of the sea surfaces and generates a two-way feedback thermal mechanism. Also, water has more specific heat, the heat capacity of it is higher than air, that's why it needs more time to warm or cool water regarding air. This leads to a usual temperature difference between seas and air, besides a heat flux from one to another. That's why SST is an important variable to understand the nature of a climate system.

Additively, sea-level rise is directly related to sea water temperatures. Sea level rise occurs due to the melting of glaciers and ice sheets. Also, expanding volume of Earth's oceans due to increasing water temperatures contribute to sea-level rise. SSTs are representative of mean water temperatures in large reservoirs. As SSTs have an important contribution to storminess and sea-level rise, investigating the change of SSTs becomes very important to have an understanding of coastal evolutions (Aral and Guan, 2016; Potter et al., 2019).

Besides, the dissolved salt concentration of seas, which is a very important parameter for marine ecosystems, is also affected by evaporation. Evaporating or

freezing water increases the salt concentration whereas precipitation decreases. The strong wind also results in the dispersion of salty droplets into the atmosphere and the forming of salty rains in inland areas. Along with saltiness, the acidity of sea water is also affected by sea water temperatures. As known, acidity has a great impact on marine ecosystems, especially coral reefs (Foo and Asner, 2020).

Oceans cover more than 70% of the Earth's surface and regulate the climate of the planet, effectively. Global warming due to the rapid increase of atmospheric greenhouse gas levels also affects the oceans deeply and the ocean temperatures tend to rise. The Intergovernmental Panel on Climate Change (IPCC) states that global SSTs are predicted to increase by approximately 0.4 – 1.1°C by 2025 (IPCC Report). Research also explored that the mean SSTs of the oceans increased by nearly 0.06°C per decade from 1901 until 2012 and this is 0.095°C per decade for the years between 1979 and 2012 (Hartmann et al., 2013).

Deser et al. (2010) revealed that most of the oceans have become warmer in the years between 1900 and 2008 with some small exceptions, despite some inconsistency among some data sets. It is thought to be a result of a lack of proper observed data on some areas.

Knutson et al (2013) also stated that there is an agreement between the variations in the SSTs changes due to ensemble mean SSTs from climate models within the Coupled Model Intercomparison Project (CMIP3, Meehl, et al., 2007, and CMIP5, Taylor, et al., 2012) with ones due to the observed data over more than 70 percent of the global oceans.

Long-term variations of SST have also been studied at regional seas. It is important to understand the fate of the regional marine ecosystems. For example, SST in the coastal seas of the United Kingdom and the Northeast Atlantic waters increased by between 0.1 and 0.5 °C per decade after the year 1980 (Dye et al., 2013). Additionally, the European Commission declared SST changes in major European Seas, and the changes were presented in Figure 1.5.

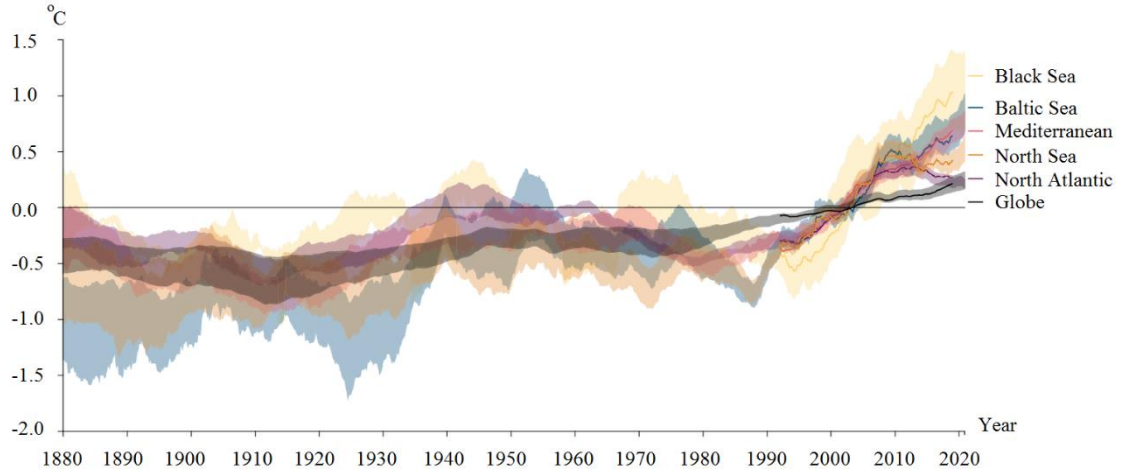


Figure 1.5 SST Changes in the global ocean and the European regional seas (EC, 2021)

In this context, the Black Sea has also been the focus of several studies about SST changes up to now. Various factors affect the SSTs over the Black Sea. Firstly, it is an enclosed sea and there is a limited amount of water flux between the Mediterranean Sea and the Sea of Azov. Besides, as a result of distinct stratification, no significant vertical mixing in the water column is observed. This leads to the fact that the temperature of the upper water layers and SST variability are characterized deeply by atmospheric conditions. This is not the only mechanism to determine the thermal regime of the Black Sea, we can also count heat advection due to precipitations, currents, waves, river discharges, and suspended matter near major river mouths as other contributors (Nardelli et al., 2010).

One study which investigated the variability of SST over the Black Sea was conducted by Ginzburg et al. (2004). In this research, inter-annual variability of SST over the Black Sea during the time was explored between November 1981 and December 2000 by using the data which is nighttime weekly multichannel SST data set from National Oceanic and Atmospheric Administration (NOAA) Advanced Very High-Resolution Radiometer measurements. The spatial resolution was 18 km whereas temperature increments were set as 0.1 °C.

The results showed an increasing inter-annual variation for mean SST over the Black Sea about 0.09 ºC per year. This increase was seen as about 0.09 ºC per year in the western regions of the Sea whereas it is 0.11 ºC per year in the eastern regions.

Kazmin and Zatsepin (2007) also explored the long-term variabilities of the basin mean winter SST over the Black Sea for the period between the years 1950 and 2005 and its correlation with the North Atlantic Oscillation (NAO), which can be defined as one of the major large scale atmospheric teleconnection indices. It is found that basin-mean winter SST in the Black Sea showed both increasing and decreasing trends in the sub-periods of the study period. For the analysis data from monthly-mean SST on 1° latitude by 1° longitude grid from Global Sea-Ice and SST Version 2.2 (GISST 2.2), National Center for Atmospheric Research (NCEP/ NCAR) Reanalysis Project and Weekly-mean multi-channel SST (MCSST) at an approximately 18-km resolution based on the Advanced Very High-Resolution Radiometer (AVHRR) nighttime measurements were used. The results can be seen in Figure 1.6.

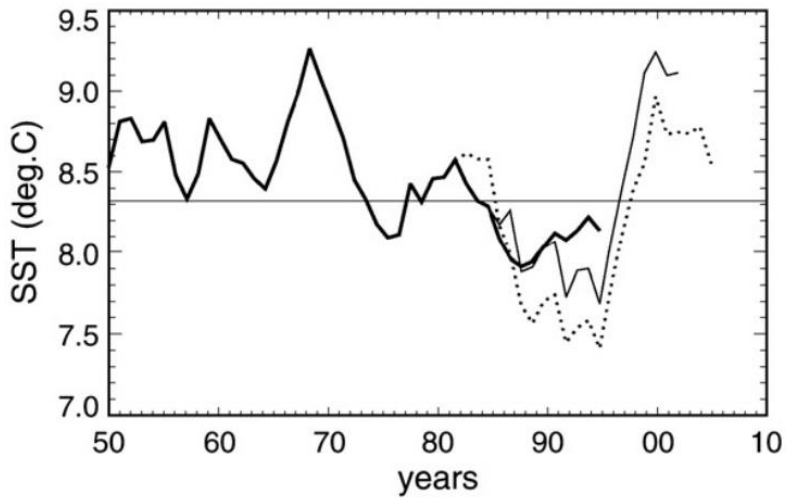


Figure 1.6 Five-year moving average filtered time series of basin-mean winter SST in the Black Sea based on GISST (bold solid line), MCSST (thin solid line), and NCEP (dotted line) data. The solid horizontal line indicates the climatological mean SST for 1950 – 2005 (Kazmin and Zatsepin, 2007)

Another study about the SST variations over the Black Sea is the one conducted by Oğuz et al. (2003). In this study, variations of winter and annual mean SSTs were evaluated for the period between 1985 and 2001 and their expected results on the ecological regime of the sea. In the study, it is stated that a gradual increase is experienced after 1993 for the basin-averaged winter-mean (December–March) and annual-mean SST variations for the deep basin of the Black Sea except for the shelf areas which are shallower than 200 m. The authors used the SST (SST) data, derived from a 9-km monthly, gridded NOAA / NASA AVHRR Oceans Pathfinder data set. The SST variations for the study period are presented in Figure 1.7.

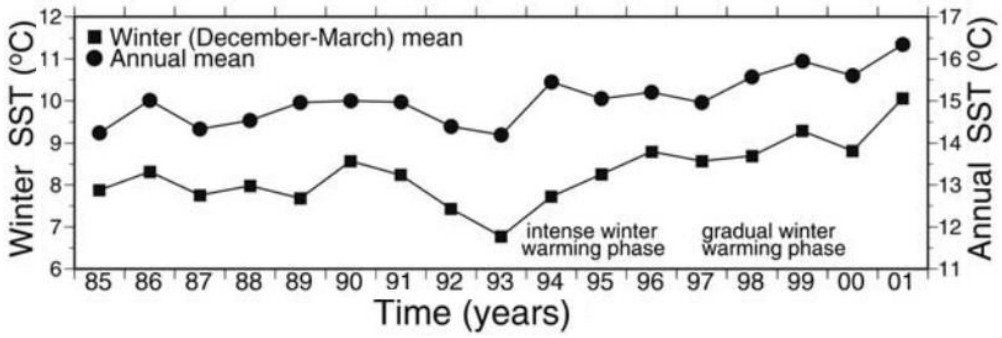


Figure 1.7 Basin-averaged, winter (December–March) mean (squares) and annual mean SST distributions in the Black Sea from 1985 to 2001 (Oğuz et al., 2003)

Besides winds and SST, one other important phenomenon which regulates how the oceans and atmosphere interact with each other is precipitation. Precipitation has a serious influence on spatial and temporal patterns of water availability for a particular region and it makes precipitation one of the most noteworthy climatic parameters for the climate. Defining long-term variations in precipitation patterns is essential for water resources management, agriculture, and other activities. Revealing trends in precipitation patterns are also very important indicators to point out climate change effects. IPCC (2019) stated that in the regions between latitudes between 0° and 55° of the southern hemisphere, mean annual precipitation has increased by 2% in the last century, whereas this increase is between 7% and 12% for areas between 30° and 85° latitudes of the northern hemisphere. However, global historical climate observations or predictions can be considered less helpful for planning at local scales. That is why local or regional

analysis of historical and future trends becomes important (Hadi and Tombul, 2018).

The regional studies focused on the long-term variations of precipitation over the Black Sea Basin are limited. One study that is conducted by Croitoru (2013) is about changes in precipitation extremes on the Black Sea Western Coasts including Bulgarian, Romanian, and partially Ukrainian coastlines. The study evaluated the trends of daily extreme precipitation indices in these regions for 48 years between 1961 and 2008. Daily precipitation data that were used for analysis were recorded in 13 weather stations distributed on Bulgarian, Romanian, and partially Ukrainian coastlines. The results were evaluated as consistent with the outputs of global and European continental-scale research. There are increasing trends for almost all stations however among the detected slopes less than 30% of them are statistically significant at a 95% significance level. Also, the orientation of positive and negative trends in the study area was found to be irregular and the trends in Northern stations came out more significant compared to the ones for Southern stations.

Besides atmospheric parameters of the Black Sea, Wave height is also an important key point for coastal engineering and maritime activities. Long-term wave data including wave heights can be gained by spectral wave models. After proper calibration and validation with measured data, these models provide a highly accurate wave database for the research area to enable a relevant evaluation for long-term variations of wave properties to provide a better understanding of the future wave climate (Aydoğan and Ayat, 2018). For example, Divinsky and Kosyan (2015) investigated the spatiotemporal variability of the wave climate of the Black Sea. The authors examined the Black Sea by dividing it into three particular regions representing western, central, and eastern areas. In the study, storminess was defined as the waves with a wave power over a threshold value of 20kw/m. It is concluded that an obvious spatial and temporal inhomogeneity exists in the redistribution of wave energy concerning the propagating directions of the waves.

One major study which aims to estimate the spatial variability of the long-term trends of Significant Wave Height (SWH) in the Black Sea is the one covered by Aydoğan and Ayat (2018). In the study, SWHs for 38 years between 1979 and 2016 were estimated by a spectral wave model using ECMWF ERA-Interim wind fields as input. Spatial maps were used by the authors to show the spatial variability of long-term trends of mean and 95th percentile normalized SWH data for each month separately. Here, 95th percentile normalized SWH was evaluated to reflect the trends of the severe sea states. Besides, a basin-averaged analysis was used to find out the overall leaning of SWHs in the Black Sea. The significance tests for the trends were conducted by using the Mann-Kendall test. As a result, in the study, it is declared that the annual mean SWH has an increasing trend up to 1.6 %/yr in the eastern part of the Black Sea. On the other hand, there is a decreasing trend down to -1.2 %/yr in the western part. Also, long-term trends of the 95th percentile SWHs showed steeper slopes and higher statistical significance concerning the mean SWH trends. This situation revealed that storm SWHs have a higher tendency to change than the mean ones.

We can consider all of the parameters like wind, temperature, precipitation, and waves as a component of the storminess of the particular marine environment. Storminess, as an important natural process, plays a key role in the forming of shorelines. That's why, all these climatic processes (wind, temperature, precipitation, and waves) mentioned above have significant effects on the morphology of the shorelines of particular seas under changing climates. Here, understanding the variations of these parameters due to climate change is very essential to determine shoreline vulnerabilities to different hazards, such as storms, sea-level rise, or flooding. In the last decades, increasing magnitudes and frequencies of these climatic processes as a result of climate changes increased the pressure on the coastal areas and represented significant impacts on human activities like tourism, marine transport, urbanization, etc. (Torresan et al., 2012).

Shoreline changes often result in hazards in coastal environments. We can count coastal storms, erosion, or flooding among these hazards, which have obvious threats to the physical, economic, and social environments of coastal regions. We can define the phenomena which determine how people or places are affected by the disturbances of shoreline changes as coastal vulnerability.

If one seeks a brief definition of vulnerability, firstly he/she should look at the notion of risk. Risk is the possibility of harmful results or probable losses like loss of lives, injuries, disruption in economic activities, environmental damages, or losing residential areas. Vulnerability can be comprehended as the degree to which the systems are affected by a disaster or a hazard and are unable to cope with the adverse effects of the situation. In other words, the notion of vulnerability can come out as "*The probability to be wounded*" (Adger, 2006).

Understanding the amount of vulnerability, a particular region has against any threat is very essential due to several reasons. Most people and cities on The Planet have faced so many disasters since the beginning of humanity. The disasters may have resulted from both natural and social incidents. The destruction of civilizations due to earthquakes or volcanic eruptions; Hurricanes that destroy cities and so many catastrophes are seen in the history of men. People used to believe disasters to be the punishments sent from gods; however, in the modern world, the perspectives of people have changed. Today, disasters in The World are considered a consequence of development that does not take into account hazards related to natural or social phenomena accurately and sufficiently. Unfortunately, the ascending losses of developing countries due to disasters show that such a development process is far from sustainable (Füssel, 2006).

In developed countries, we see numerous sustainable systems that constitute harmony between nature and civilization. In developing countries, the main objective in the field of disaster reduction should be changing the understanding of people to make them recognize disasters as an outcome of development processes that generate vulnerabilities and risks.

It is easy to say that establishing this perception through people is also another development. This should be seen as human development which has great importance besides industrial and economic development (Leon, 2006).

From this point of view, it is possible to define coastal vulnerability due to natural processes and hazards in several ways. These can be categorized under index-based methods, Indicator-based approach (with GIS applications), GIS-based Decision Support Systems, or dynamic computer methods (Ramieri et al., 2011).

One pioneer scheme for index-based methods is the one developed by Gornitz and Seeber (1990). The study focused on the vulnerability of the East Coast of the United States against sea-level rise. It is possible to find different studies on coastal vulnerability due to varied hazards that depend on index-based formulations.

The parameters which are used to estimate coastal vulnerabilities of different areas can simply include coastal land formations, shoreline change, sea-level rise, wave height, and the tidal range. Also, the determination of processes like longshore or cross-shore sediment transport and wave run-up contributes to the coastal vulnerability indices (Abuodha and Woodroffe, 2010; Mclaughlin and Cooper, 2010, Paola et al., 2011, Alexandrakis and Poulos, 2015). In the end, the purpose of all studies on coastal vulnerability is to designate the critical regions that are vulnerable to several coastal hazards and to make a foundation for proper planning to decrease the possible impacts of these hazards.

As it is known, coastal zones of the world are the most densely populated and developed regions. Although there are lots of economic and social activities around coastal regions, there is not sufficient evaluation of long-term variations of shoreline changes. One major study to investigate global shoreline changes is the one by Luijendijk et al. (2018). The authors used cost-free sources to get optical satellite images for the period between 1984 and 2016 and adapted advanced image analysis methods including pixel-based supervised classification to explore the worldwide distribution of sandy beaches and rates of shoreline changes. In the study, it is concluded that 31% of the Earth's ice-free shorelines and 24% of these sandy beaches are facing erosion with rates beyond 0.5 meters

per year while 28% of them are accreting. 48% of the Earth's sandy beaches seem stable. The authors indicated that the majority of the sandy shorelines in protected marine areas suffer from erosion and this situation needs to be evaluated much more seriously.

Regional studies focusing on shoreline changes can give a more detailed picture of how coastal zones are being affected due to climate change impacts. The results of these regional studies for particular marine ecosystems are very important to determine more detailed regional policies on coastal management plans. One essential step to reaching a proper understanding of the coastal vulnerability of a region is a comprehensive inventory of the coastal properties of the accentuated sea. For instance, the study by Allenbach et al. (2014) represented a database for the Black Sea Beaches. The authors declared that there are 1228 beaches with a total coastline length of 2042 km and an area of 224 km^2. Also, it is stated that most of the Black Sea beaches (61%) are evaluated as having short widths (shorter than 50m). It is also reported by the authors that 47% of the Black Sea beaches are under several coastal protection plans, which is evidence of serious beach erosion problems for the Black Sea coasts.

Allenbach et al. (2014) also investigated the risk of the erosion of the Black Sea coasts due to sea-level rise by a combined numerical morphodynamic model. The analysis explored that sea-level rise would have distinct effects on the Black Sea beaches. For example, due to a 0.5 m sea-level rise, 56% of all beaches are estimated to lose 50% of their maximum width. Also, to the high IPCC estimate for the period 2081–2100, a 0.82 m sea-level rise is expected to lead 41% of the Black Sea beaches to lose their entire maximum width. In the worst scenario, 51% of all Black Sea beaches will be drowned or shifted landward by their maximum width after a sea-level rise of 1m. In the end, the researchers concluded that the risk of beach erosion is an actual environmental problem for the Black Sea coasts and urgent coastal management plans must be considered immediately.

Another important study that deals with the erosion hazards along the Black Sea coasts are completed by Tatui et al. (2019). The authors used a comprehensive

database of multiple sources and computed a Coastal Sensitivity Index (CSI) with a 1 km spatial resolution including more than 4000 sectors along the Black Sea coasts. They considered the physical and geological properties of each sector and determined several parameters which are coastal lithology and slope, shoreline changes in the last 33 years, wave characteristics, and sea-level rise. The results showed that nearly 19% of the Black Sea coasts are at serious risk of erosion, which is usually threatening the coastlines of Romania (37%), Ukraine (29%), and Georgia (26%). It was also stated that the deltaic coastlines of the main deltas of the Black Sea with relatively high storm waves and incidence angles are the most sensitive regions. Danube, Kızılırmak, Yeşilırmak, Sakarya, Rioni, Enguri, Kodori, and Chorokh deltas were given as prominent examples.

In addition, the low-lying areas along the lagoon lakes, harbors, coastal barriers, and spits are at risk. (Kalamitsky, Odesa and Karkinitsky Bays, Chornomorske – Yevpatoriya areas in Crimea, Taman – Anapa regions in Russia, and Karasu – Karaburun in Turkey and the rocky areas Gelendzhik – Tuapse in Russia, Sevastopol – Cape Meganom in Crimea and Inebolu – Eregli in Turkey.

To sum up; it has been detected that, a quantification study for the relationship between long-term variations of atmospheric parameters and shoreline changes along the Black Sea coasts comes out as a necessity, because of the lack of such investigations.

1.2 Objective of the Thesis

The objective of this thesis is to analyze the response of the Black Sea coastline to climate change impacts. The study objectives are:

- To explore the long-term variations of atmospheric properties (temperature, wind, and precipitation) due to climate in the last decades.
- To examine extreme - unusual climate and sea states.
- To define the changes in the Black Sea shorelines in the last decades.
- To explore a relationship between variations of atmospheric properties along with sea states and shoreline morphology.

1.3 Hypothesis

The natural cycle of global climate warming, which is mainly characterized by the greenhouse effect, has been notably intensified especially since the middle 20th century, and has already had observable effects on the environment. These effects can be direct or indirect and particularly can be observed in the systems of oceans and inland seas. We can evaluate long-term variations of atmospheric conditions among direct effects of the climate change in a region, whereas changes in an ecosystem or morphologic changes (shoreline changes, erosion, landslides, etc.) due to newly adapted atmospheric conditions can be regarded as indirect effects of the climate change. Here, it is expected that there should be apparent long-term variations in the Black Sea climate and response of its coastlines due to climate change impacts.

2

THE STUDY AREA

The study area is delimited by latitudes 40-48°N and longitudes 26-42°E and covers the Black Sea basin and the Sea of Azov as shown in Figure 2.1. The Black Sea: which is a recognized inland sea; is surrounded by Ukraine from the north, Russia from the northeast, Georgia from the east, Turkey from the south, and Bulgaria and Romania from the west. Its surface area is 411540 km^2 and its volume is 555000 km^3 whereas the mean and maximum depths are 1315 m and 2258 m, respectively. The total length of the Black Sea coastline is ~4400 km. The Black Sea is an enclosed basin connected to the Mediterranean through the Turkish Sea Strait System consisting of the Strait of Istanbul, the Sea of Marmara and the Dardanelles, and the Sea of Azov via the Strait of Kerch. The Black Sea basin has intensive shipping activities between the important harbors of Europe, Asia, and Africa (Onea and Rusu, 2014).

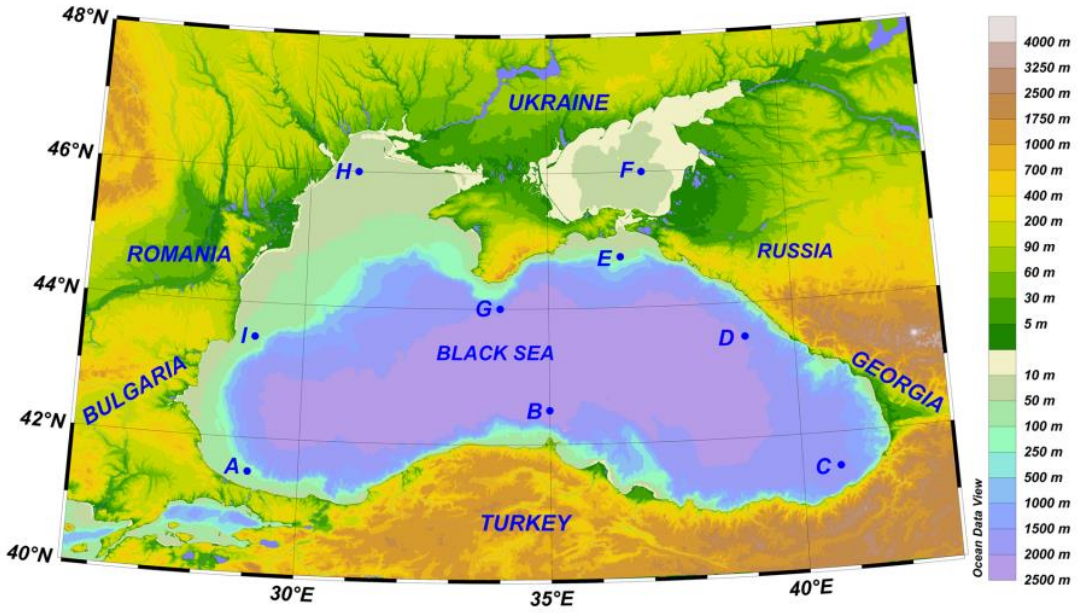


Figure 2.1 The study area: the Black Sea Basin

2.1 Climate

The Black Sea is one of the most isolated divisions of the world ocean system and as a result of wind activity over the sea, heavy waves are observed (Onea and Rusu, 2014). Black Sea basin is under the influence of air masses which come and pass over in various directions, because of its geographical location. As a consequence of its position, The Black Sea can be regarded as a component of the Mediterranean and the North Atlantic climate systems, and the Black Sea climate is affected by continental, polar, and marine tropical air fluxes from several directions. The marine tropical air mass flow results from southwest winds from the Mediterranean basin and in the winter, polar air masses coming from the north and northeast lead to low temperatures and frequent storms over the Black Sea (Valchev et al., 2010).

The climate and weather conditions of the Black Sea are also determined by the coastal topography which shows several discrepancies, especially between the north and south coastlines. The northwestern coasts are bottom land and the effect of northerly weather qualified by the steppe climate, which consists of cold winters and dry summers, can enter the Black Sea Basin easily. On the other hand, there is a chain of mountains along the southeastern coasts of the sea. This situation prevents the subtropical climate with high moisture, hot summer, and mild winter from entering the sea basin (Özsoy and Ünlüata, 1997).

Expectedly, air temperatures show an increasing behavior from north to south. In the northern regions, the annual mean air temperature is 8.96 °C, which is more than the average air temperature over the oceans and lower than the one of the adjacent Mediterranean Sea. Besides, the average SST is evaluated as 14.87 °C (Ivanov and Belokopytov, 2013).

Most of the annual precipitation over the Black Sea Basin (nearly 70%) occurs in the period between November and March; besides there is a distinct difference in precipitation amounts between the west and east regions. The minimum precipitation is seen on the northwestern coasts with an amount of between 400–450 mm. On the other hand, on the southern and southeastern coasts (Anatolian

and Caucasian Coasts) of the sea annual average rainfalls exceed 1000 mm. On the coasts from Trabzon to Poti, the mean value for annual precipitations is over 2000 mm. The maximum annual average air temperature (14.6° C) and precipitation (2750 mm) were observed on the coast of Georgia in Batumi. Annual variations of rainfall on the Anatolian, the Caucasian coast, and the southern coasts of Crimea, which are formed by higher values in autumn and winter, represent a Mediterranean climate characteristic. In the other coastal regions, a weak dominance of precipitation is observed in summer, and this is related to continental climate characteristics. (Avşar, 2019, Ivanov and Belokopytov, 2013).

When we consider the pressure fields over the Black Sea Basin, it is observed that there are high-pressure fields in the northern regions whereas low-pressure fields locate in the southern parts. This circumstance results in winds from north to south, especially in winter. It is also known that relatively higher wind speeds are seen in autumn and winter over the Back Sea. In addition, in the western and northwestern regions relatively higher wind speeds are observed in the southern and southeastern regions (Ivanov and Belokopytov, 2013).

Another phenomenon regarding the Black Sea is the concept of its general circulation pattern which has been given as a cyclonic motion with two large gyres since the late 19th century. Various research gave the cyclonic wind rotation over the sea and the river runoff as the main reasons for the cyclonic circulation of the sea. All known schemes suggest the following main features of general circulation: the Main Black Sea current, located over the continental slope, and two large-scale cyclonic gyres in the eastern and western parts of the sea; quasi-stationary anticyclonic eddies in the coastal zone, such as Batumi, Sevastopol, Caucasian, Sakarya, Sinop, etc. The circulation pattern of the surface layer of the Black Sea given by Fach et al. (2014) is presented in Figure 2.2.

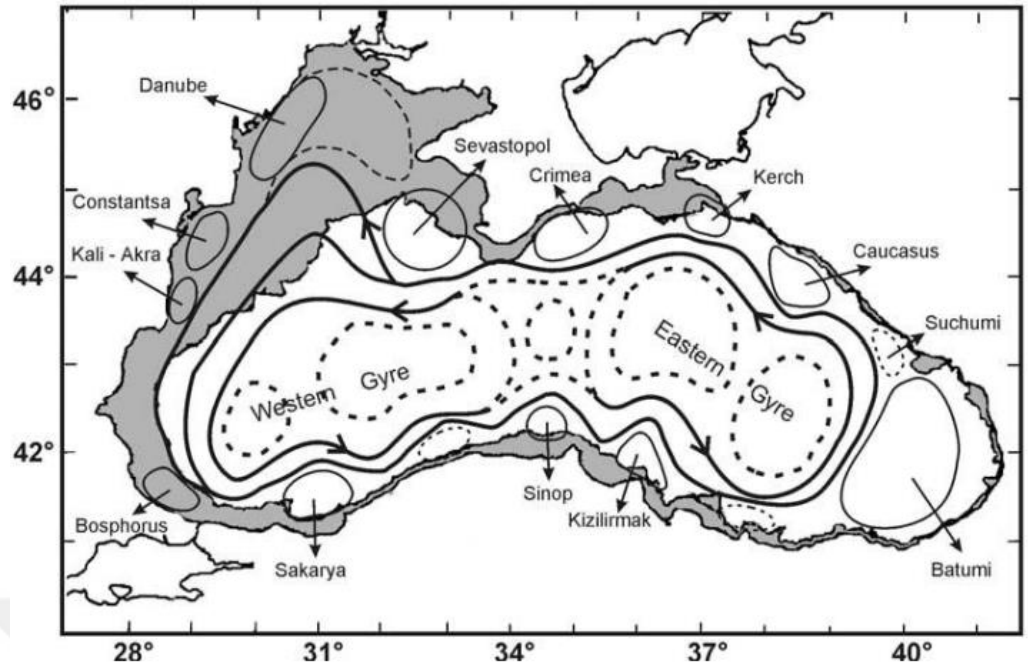


Figure 2.2 Circulation pattern of the surface layer of the Black Sea (Fach, 2014)

2.2 Topography

The Black Sea is an inland sea whose connection to the nearest Ocean (Atlantic Ocean) is through Bosporus and Dardanelles Straits, the Marmara Sea, The Aegean Sea, and the Mediterranean. This situation makes the Black Sea one of the furthest inland seas from the oceans. The Bosporus, which is the first door for the Black Sea opening to oceans, is very narrow and shallow. The width of The Bosporus varies from 760m to 3600m, whereas its deepest point is 110m. There are two layers of currents in the Bosporus, and they flow in reverse directions. The upper one is from north to south and carries the excess water of the Black Sea to the Marmara Sea. The bottom current directs from south to north and carries relatively more saline water from the Marmara Sea to the Black Sea. In addition, The Black Sea is connected to the Sea of Azov, which is a shallow inland sea with a maximum depth of 14m, through Kerch Strait (Gunnerson and Özturgut, 1974; Oğuz et al., 2006).

It would be possible to detect; the bottom topography of the Black Sea; shelves (0-200m), continental slopes (200-2000m), and abyssal plains (2000m and deeper). Here, the Black Sea is considered a deep sea with steep slopes and a bottom plain. Shelves, which are seen at the depths between 0 and 200m, occupy nearly 25% of the total seabed of the Black Sea; while continental slopes, where underwater valleys and canyons exist, corresponding to approximately 40% of the seabed area. The bottom plain with a gradual slope towards the center of the bottom accounts for roughly 35% of the total seabed surface of the Black Sea. The mean depth of the Black Sea basin is 1315 m while the maximum depth is 2258 m (Gunnerson and Özturgut, 1974; Özsoy and Ünlüata, 1997). The bathymetry of the Black Sea is shown in Figure 2.3.

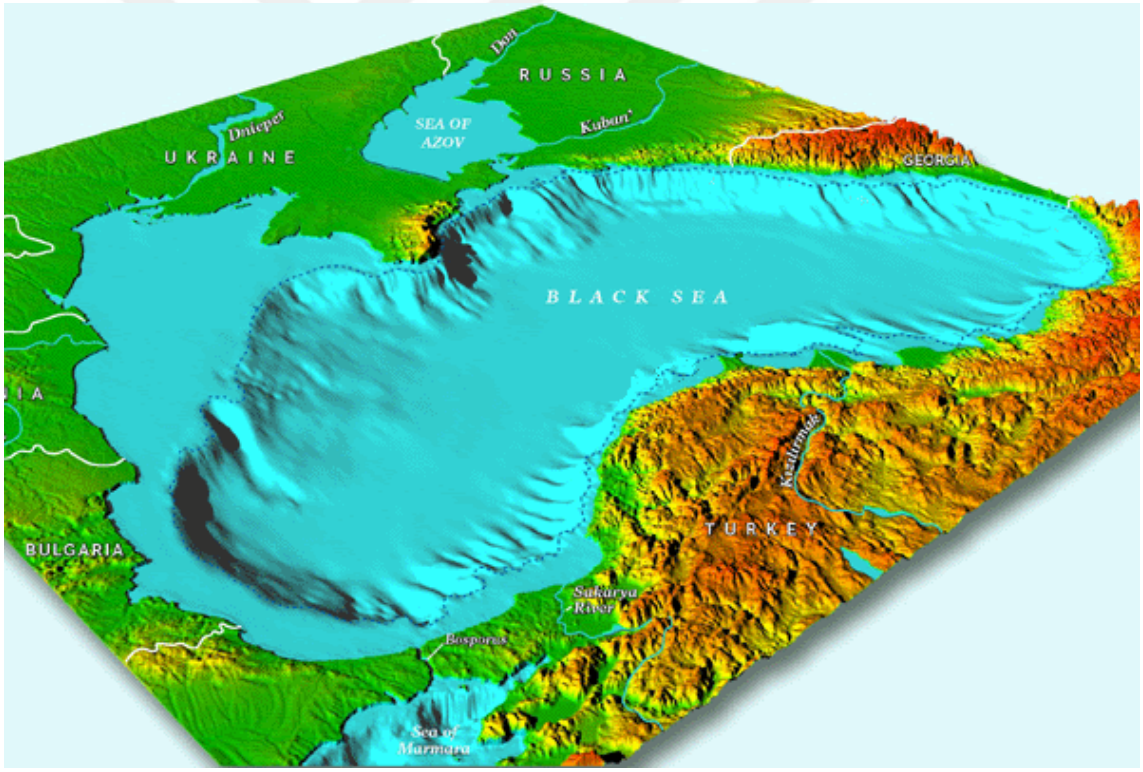


Figure 2.3 The bathymetry of the Black Sea (National Geophysical Data Center, NOAA)

2.3 Geology

The Black Sea has developed both on the continental crust and on the oceanic crust (abyssal plain). Besides, it is surrounded by young mountains in the south, the east, and the northeast, while there are ancient platforms and tectonic basins in the north and the west. Also, there are large deltas along the Black Sea coastline. One is the Danube Delta which is the second largest river delta with a 5142 km^2 surface area in Europe. In addition, Kızılırmak and Yeşilırmak Deltas are two major deltas which are located on the southern coasts. The surfaces of these deltas are 560 km^2 and 1042 km^2 respectively (Vespremeanu and Golumbeanu, 2018).

It is the general idea that the Black Sea, whose history reaches the Cretaceous, was in a form of a freshwater lake below. Besides, approximately 11.000 years ago, the global sea levels rose nearly 100 m after the ice age; and rising waters of the Mediterranean entered the Black Sea through the Bosporus. Different studies argue that the submergence of the Black Sea is considered to happen rapidly or in thousands of years instead of catastrophic flooding. In either case, saline water entering the Blacks Sea from the Mediterranean had a higher density and did not mix with the freshwater. This led to density stratification and formed a different water layer at the bottom of the Back Sea. The sub halocline water body of the Black Sea is life free due to its anoxic characteristics and formed at depths more than 150-200 m (Ross and Degens, 1974).

2.4 Land Use

The watershed of the Black Sea is shown in Figure 2.4, with an area of roughly two million square kilometers, and involves a much larger area consisting of lands of 17 countries. This area is also much larger than the total area of 6 coastal countries of the Black Sea. This situation results in the necessity for a collaboration of all the countries in the watershed to eliminate the man-induced environmental problems (Koulov, 2012).



Figure 2.4 The watershed of the Black Sea (Koulov, 2012)

To evaluate the anthropogenic pressure of the Black Sea, it is very important to understand the land use in the watershed of the sea. Lehmann et al. (2017) explored the expected land-use maps of the Black Sea by 2050. The study consists of a set of nine raster maps representing the land use classification derived from Nasa's MODIS in 2010 at a 500 m pixel resolution, and predictions were done with Metronamica until 2050 according to the four different land-use change scenarios (BS-HOT, BS-ALONE, BS-COOP, and BS-COOL). The expected land use for the Black Sea by 2050 is presented in Figure 2.5.

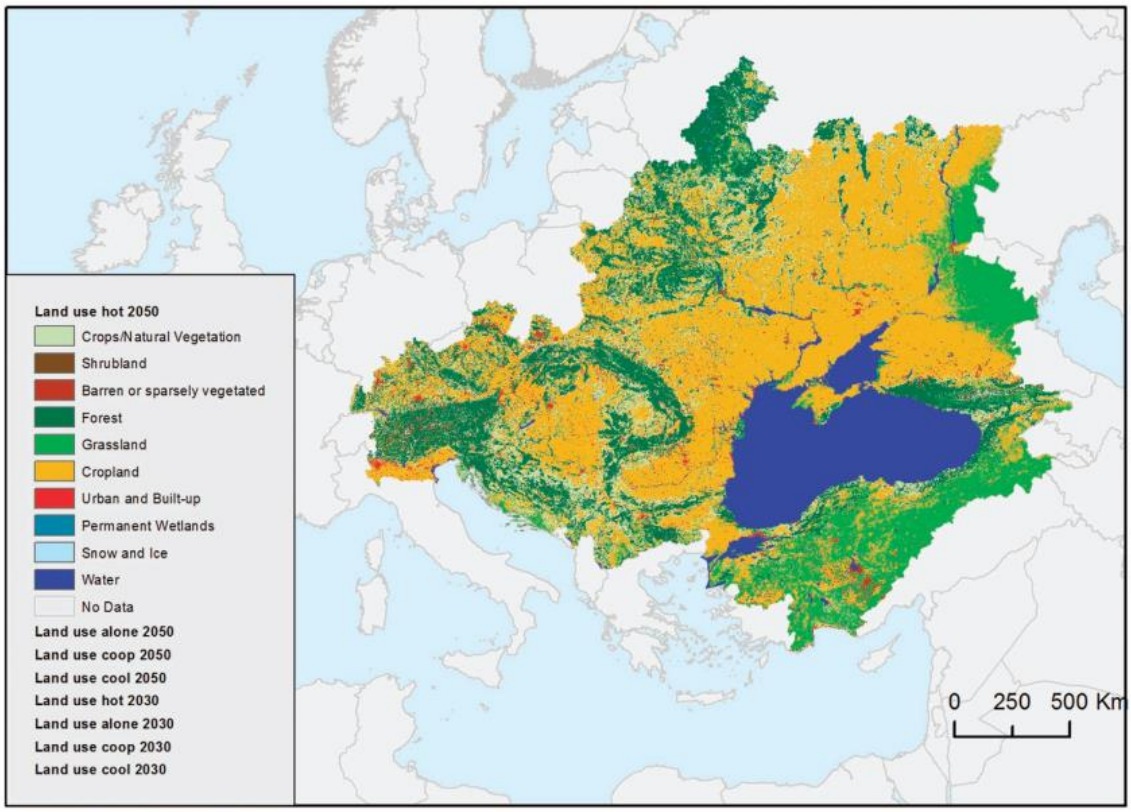


Figure 2.5 The expected land use for the Black Sea by 2050 (Lehmann et al., 2017)

In addition, in the coastal zones of the Black Sea, a high degree of urbanization is detected. Nevertheless, the coastal population of the Black Sea is distributed along the coastline unevenly. We can count among the important coastal cities along the Black Sea; Istanbul, Ordu, Samsun, Trabzon, and Zonguldak (Turkey), Burgas and Varna (Bulgaria), Batumi and Poti (Georgia), Constanta (Romania), Novorossiysk, Sochi, and Tuapse (Russia), Odesa and Sevastopol (Ukraine). Here, Istanbul, Odessa, and Varna are famous touristic cities with also large economic activities. Also, in the Danube, Kızılırmak, and Yeşilırmak deltas; a vast amount of agricultural activity is seen. The total coastline length of the Black Sea (including the Sea of Azov) is 5800 km.

The Black Sea has a great contribution to the regional and global economy, especially for the riparian countries with the existence of vast sea transport, oil/gas pipelines, productive fisheries, wood products, tourism, etc. Lastly, as water transport is one of the essential elements of the Black Sea environment, there are various important ports located on its coastlines (Nicolae et al., 2018). The important ports near the Black Sea are shown in Figure 2.6.



Figure 2.6 Important ports near the Black Sea (Nicolae et al., 2018)

2.5 Demography

The Black Sea has been a very important area for thousands of years and has a very key role in global transportation, economics, and politics. As a result of the existence of diverse natural sources and strategic geopolitical locations, so many different civilizations have been developed near its coastlines of it. Now, there are six riparian countries around the Black Sea, and they are Turkey, Russia, Bulgaria, Ukraine, Georgia, and Romania. The populations of these countries are presented in Table 2.1 according to the 2022 census.

Table 2.1 Populations of the Black Sea riparian countries according to 2022 census (Worldometer.info)

Populations of the Black Sea Riparian Countries		
#	Country	Population (Millions)
1	Russia	145.9
2	Turkey	84.4
3	Ukraine	43.7
4	Romania	19.2
5	Bulgaria	7.0
6	Georgia	4.0

It is evaluated that, the permanent population on the coastlines of the Black Sea is around 17 million and there are important cities along the sea's coastlines. The most populated urban areas along the Black Sea coastline are listed in Table 2.2. (Vespremeanu and Golumbeanu, 2018)

Table 2.2 Most populated urban areas along the Black Sea coastline according to 2022 census (Worldometer.info, tuik.gov.tr)

#	City	Population (urban)
1	Istanbul	14,804,116
2	Odessa	1,001,558
3	Samsun	535,401
5	Varna	312,770
4	Constanta	303,399
6	Sevastopol	416,263
7	Sochi	327,608
8	Trabzon	305,231
9	Novorossiysk	241,952
10	Burgas	195,966
11	Ordu	217,640
12	Batumi	121,806

2.6 Coastal Erosion and Its Reasons Along the Black Sea

Up to now, various researchers explored that shoreline of the Black Sea have been facing morphological changes due to anthropogenic factors like regulation of rivers, sediment removal, new marine structures, coastal urbanization, and insufficient engineering solutions. Changing climate conditions also increased the intensity and frequency of storms and floods. All of these conditions lead to the fact that erosions have become one of the most serious problems of the Black Sea coastline. It is reported that the Black Sea lost many of its natural coastlines in the last century. The results showed that nearly 19% of the Black Sea coasts are at serious risk of erosion, which is usually threatening the coastlines of Romania (37%), Ukraine (29%), and Georgia (26%). It was also stated that the deltaic coastlines of the main deltas of the Black Sea with relatively high storm waves and incidence angles are the most sensitive regions. Danube, Kızılırmak, Yesilirmak, Sakarya, Rioni, Enguri, Kodori, and Chorokh deltas were given as prominent examples. In the next decades, these processes will go on rapidly and the protection of the ecosystems of the Black Sea will be essential (Görmüş et. al, 2021, Allenbach et al., 2014, Tatui et al., 2019).

3

DATA AND METHODOLOGY

3.1 Data

In this study, it is aimed to investigate the impact of long-term variations of atmospheric properties, wind climate, wave climate, SST, and precipitation, on the shoreline morphology. For this purpose, atmospheric data (temperature, wind, and precipitation), wave data, and shoreline change data in a proper temporal and spatial resolution are used.

As it is difficult to have absolute atmospheric data from observations or historical recordings, reanalysis data sets become very convenient to get the needed atmospheric data for large study areas covering long historical study periods. To have a brief understanding of the variations of selected atmospheric properties in the last decades, wind, precipitation, and temperature data covering the last decades were gathered from reanalysis data sets, which are ERA-I (Dee et al., 2011) and CFSR (Saha et al., 2010, Saha et al., 2014).

Both ERA-I and CFSR assimilate different data from various sources such as scatterometers, altimeters, satellite measurements, in situ meteorological observations, etc. with 12 hr of analysis periods. Historical information about the various climate parameters including wind velocities at different pressure levels, precipitation, evaporation, cloud cover, snowfall, temperature, spectral wave parameters, mean sea level, and many others can be obtained for the global atmosphere, land, and ocean.

3.1.1 Wind Data

In this study, a comparative analysis for the long-term trends in 10 m wind speeds (U10) due to ERA-I and CFSR is aimed, so both reanalysis data over the Black Sea are processed for the same period between 01 January 1979 and 31 December 2016.

ERA-I data is provided by the ECMWF for the period starting from 01 January 1979 to the present and the project will be terminated on 31 August 2019. ERA-I is generated by 4D variational assimilation of data from various sources. ERA-I uses the stability function of the bulk algorithm to compute air-sea fluxes given by Holtslag and de Bruin (1988) and Dyer (1974). The roughness length for momentum is computed from the coupled ocean wave model (Zhang et al., 2016). The near-surface u and v components of wind velocity at 10 m height are obtained from ERA-I with a spatial resolution of 0.7°x0.7° (∼80 km) from the native T255 spectral grid and a temporal resolution of 6 hr for this study.

CFSR reanalysis data covers the term from 01 January 1979 to the present. CFSR data is derived from 3D-Var assimilation of the various data based on a coupled atmosphere-ocean-land data assimilation system. The air-sea fluxes in the CFSR are derived from the model, which uses the roughness lengths given by Zeng and Dickinson (1998) for heat and moisture (Zhang et al., 2016). CFSR reanalysis data has a spatial resolution of 0.312°×0.312° (∼38 km) from the native T382 spectral grid and near-surface u and v wind velocity components are obtained with a temporal resolution of 6 hr for this study.

U10 data is constructed by using the wind velocity components from reanalysis data. Spatial resolutions and temporal coverages of the reanalysis data used in this study are presented in Table 3.1.

Table 3.1 Properties of the reanalysis U10 data used in this study

Reanalysis	Start Date	End Date	Temporal resolution	Original spatial resolution	The spatial resolution used in this study
ERA-I	01/01/1979	31/12/2016	6 hr	0.7° × 0.7° (~80 km)	0.25° × 0.25° (~27 km)
CFSR	01/01/1979	31/12/2016	6 hr	0.312°×0.312° (~38 km)	0.25° × 0.25° (~27 km)

To have a comparable homogeneous spatial analysis of long-term changes in the U10 data, both reanalysis data are interpolated onto the study area with a resolution of 0.25° x 0.25°. The interpolated value at any grid point is based on linear interpolation of the values at neighboring grid points in each respective dimension. The number of the grid points analyzed in this study is 2048 over the study area for both reanalysis data.

3.1.2 Mean Sea Level Pressure Data

Mean Sea Level Pressure (MSLP) data was gained from both ERA-Interim and SCFSR datasets. Spatial resolutions and temporal coverages of the reanalysis data used in this study are presented in Table 3.1. The data covers the period between 01 January 1979 and 31 December 2016 with a temporal resolution of 6 hr.

3.1.3 Wave Data

SWH data was also gained from the ERA-Interim dataset, which is a global reanalysis dataset prepared by the ECMWF. The original spatial resolution of the data is 0.7° x 0.7° (~80 km) and the spatial resolution used in this study is 0.25° x 0.25° (~27 km). The data covers the period between 01 January 1979 and 31 December 2016 with a temporal resolution of 6 hr (Dee et. al, 2011).

3.1.4 Sea Surface Temperature Data

SST data was also gained from the ERA-Interim dataset, which is a global reanalysis dataset prepared by the ECMWF. The original spatial resolution of the data is 0.7° × 0.7° (~80 km) and the spatial resolution used in this study is 0.25° × 0.25° (~27 km). The data covers the period between 01 January 1979 and 31 December 2016 with a temporal resolution of 6 hr (Dee et al., 2011).

3.1.5 Precipitation and Evaporation Data

Precipitation data was gained from the ERA5 dataset (Hersbach et al., 2020), which is also a global reanalysis dataset prepared by the ECMWF. Era-Interim was not chosen as a precipitation data resource because, it was reported that precipitation data from Era-Interim represented biases between other precipitation data resources, whereas ERA5 did not (Nogueira, 2020). The original spatial resolution of the data is 0.7° × 0.7° (~80 km) and the spatial resolution used in this study is 0.25° × 0.25° (~27 km). The data covers the period between 01 January 1979 and 31 December 2016 with a temporal resolution of 1 hr (Copernicus Climate Change Service Website). Evaporation data was also taken from the ERA5 database with the same temporal and spatial resolutions.

3.1.6 Shoreline Data

One of the favorable resources to gain global shoreline data is the output of the study is the one by Luijendijk et al. (2018). They provided a comprehensive database which is offered by a free internet website for all shorelines of our planet. By using this database, it is possible to detect worldwide shoreline change rates for the 33-year period between 1984 and 2016. The database gives the changes in shoreline points with 500 m distance between each along worldwide ice-free shorelines, which is determined in this study as 1.11 million km. Thus, it becomes accomplishable to investigate and evaluate the coastal changes for a particular shoreline in a particular study period.

To provide a proper global analysis and visualization proses, the researchers defined the pre-mentioned 500 m spaced transections perpendicular to the global shoreline from the OpenStreetMap45 (OSM) dataset of 2016.

To represent a focus on the shoreline changes in the Black Sea coasts, seven coastal regions near the Black Sea were chosen and the mean shoreline changes were calculated along each beach by analyzing the database given by Luijendijk et al. (2018). These seven study locations were chosen to represent each shoreline geomorphology (Tatui et al., 2019), which are represented in Table 3.2 and Figure 3.1. In addition, long-term variations in atmospheric parameters observed in these regions along these Black Sea coasts are investigated, to provide an understanding of the effects of climate change on atmospheric forcing on these coastal regions:

Table 3.2 Coastal regions near the Black Sea where the mean shoreline changes were calculated (Tatui et al., 2019)

#	Selected Coastlines	Morphology	Geological Formation
1	Sinop	Minimally	Very hard rocks, Coastal
2	Cide	Weakly Abraded	Ancient metamorphic
3	Terkos	Moderately	Moldy rocks, cemented
4	Sochi	Intensively	Clays, sandstones, clay loam,
5	Bafra (Kızılırmak Delta)	Extremely Abraded	Sands, sand with pebble, sandy-aleuritic
6	Çarşamba (Yeşilırmak Delta)		
7	Danube Delta		

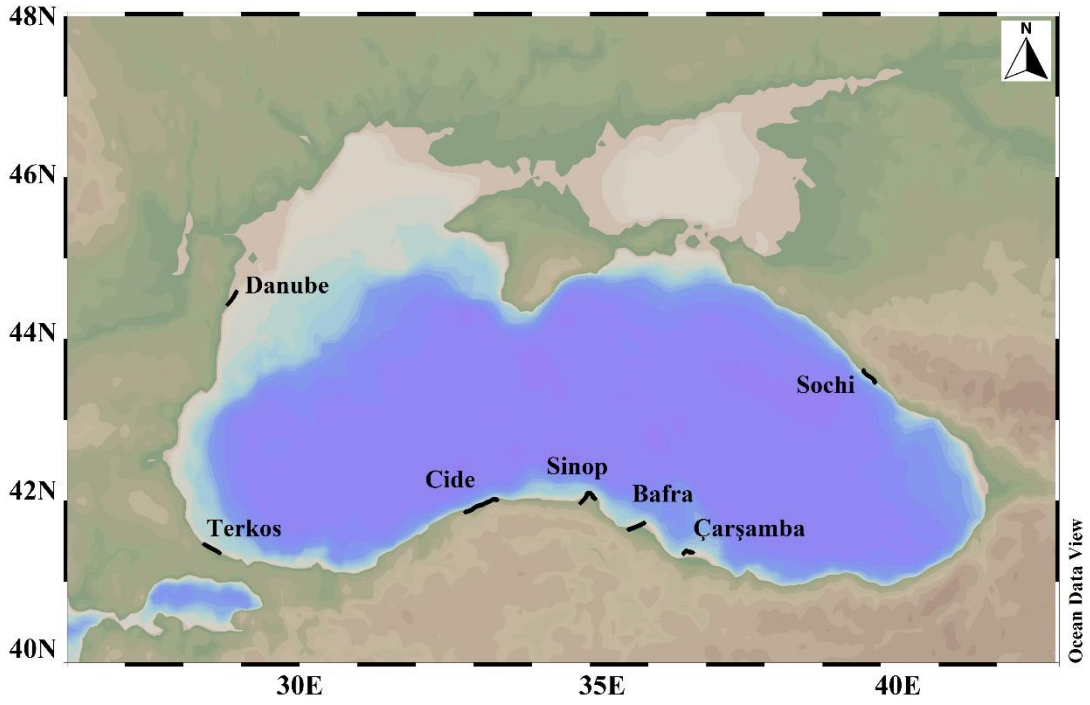


Figure 3.1 Selected erosion-prone coastal regions along the Black Sea coasts where the shoreline changes were calculated

3.2 Methodology

3.2.1 Trend Analysis of Atmospheric Parameters

To reveal the long-term trends of atmospheric conditions over the study area, time series each consisting of a particular amount of data between 1979 and 2016 are constructed for both mean and 95th percentile values. The seasonality of atmospheric parameters of the Black Sea is analyzed by detecting spatiotemporal variations for each month separately, as well as the annual variations. Hence, for wind data, we constructed 26-time series (12 monthly time series and one annual time series for both $U10_m$ and $U10_{95}$) each including 38 values at each grid point for ERA-I and CFSR data and conducted trend analysis. We analyzed 53248 (2048x26) time series for each analysis in total. Trend analysis results are presented in means of percentages rather than the exact rates of change in the atmospheric parameter in focus. Mean values, such as U10, are normalized by

each gird's mean value to get the relative trend in each time series as shown in Equation 3.1,

$$U10^{*}_{k,t} = U10_{k,t}/\overline{U}_{k} \tag{3.1}$$

Where $U10^{*}_{k,t}$ is the normalized $U10$, $\overline{U}$ is the mean of the $U10$ series being calculated, k is the grid number and t is the time step.

In addition, precipitation, SST, and SWH data were also investigated similarly. Data for each parameter from the ERA-I database were tabulated and the long-term variations of each parameter were calculated on an annual basis. The trends of annual mean values and 95th percentile values were examined and presented spatially over the study area.

For each time series at each grid point, trends are estimated by using Theil-Sen's estimator and Mann-Kendall test to detect the variations of the time-series data generated from the mean and 95th percentile values of a particular atmospheric parameter. The Mann-Kendall test, introduced by Kendall (1938, 1970) and Mann (1945), is a non-parametric test that does not require the data to be normally distributed and has low sensitivity to outliers in the time series. The Mann-Kendall test is often combined with the Theil–Sen estimator, which is used to fit a line through the sample points in the coordinate system (simple linear regression) by calculating the median of the slopes of all lines along with the pairs of the data points (Sen, 1968).

Mann-Kendall test (Kendall, 1938; Mann, 1945) is an instrument used to test whether a randomly distributed time series has a monotonic (increasing or decreasing) trend or not. No trend case is defined as a null hypothesis against the alternative hypothesis which means that there is a monotonic trend. The test evaluates the data values and orders time series and compares each data value with all subsequent ones. If a data value is smaller than a later one, a statistic S is increased by one; on the contrary, S is decreased by one if a data value is larger than the one at a later period. After evaluating all data values, S comes out with

a final value (Shahid, 2011). If the final value of S is positive, this refers to the existence of an increasing trend; a negative value of S refers to a negative trend. S is calculated using Equation 3.2;

$$sgn(x_j - x_k) = \begin{cases} +1 \; if \; x_j - x_k > 0 \\ 0 \; if \; x_j - x_k = 0 \\ -1 \; if \; x_j - x_k < 0 \end{cases} \tag{3.2}$$

$$S = \sum_{k=1}^{n-1} \sum_{j=k+1}^{n} sgn(x_j - x_k)$$

Where x_j and x_k are the data values in time j and k, respectively *(j>k)*, (Gilbert, 1987).

To evaluate a trend whether it is significant at α level or not, statistic *p*-value is used. The null hypothesis is rejected if the $|p| > p_{1\text{-}\alpha/2}$, where $p_{1\text{-}\alpha/2}$ is obtained from standard normal cumulative distribution tables (Salmi et al., 2002). For instance, to state a significance level of more than 90%, a p-value smaller than 0.1 should be calculated. *P-value* is calculated using Equation 3.3;

$$p = \begin{cases} \dfrac{S-1}{\sqrt{VAR(S)}} \; if \; S > 0 \\ 0 \quad if \; S = 0 \\ \dfrac{S+1}{\sqrt{VAR(S)}} \; if \; S < 0 \end{cases} \tag{3.3}$$

$$VAR(S) = \frac{1}{18}\left[n(n-1)(2n+5) - \sum_{m=1}^{q} t_m \, (t_m - 1)(2t_m + 5)\right]$$

Where q is the number of tied groups and t_p is the number of data values in the m^{th} group (Salmi et al., 2002).

In the case of the existence of a linear trend for a time series, a true slope that defines the change per unit of time can be evaluated by using Sen's slope estimator (Sen, 1968). In Sen's slope nonparametric procedure, the linear model is described in Equation 3.4;

$$f(t) = Q_t + B \tag{3.4}$$

Where Q is the slope and B is a constant.

Q is determined by using each slope of the lines across all data pairs, Q_i (Equation 3.5). There are $N = n\ (n\text{-}1)/2$ slope estimates, Q_i, for a time series with n values. The Sen's slope is found to be the median of these N values as shown in Equation 3.6 (Drapela and Drapelova, 2011),

$$Q_i = \frac{x_j - x_k}{j-k}, i = 1,2,3,\dots,N,\ j > k \tag{3.5}$$

$$\begin{cases} Q_{\frac{N+1}{2}} & if\ N\ is\ odd \\ \frac{1}{2}\left(Q_{\frac{N}{2}} + Q_{\frac{N+2}{2}}\right) & if\ N\ is\ even \end{cases} \tag{3.6}$$

The calculations for the trend analysis of the time series data are done by using in-house code via the MATLAB© Environment. The results including Sen's Slope and their significance at 90% or higher confidence level are explored and represented by color contours on spatial maps.

3.2.2 Analysis of Shoreline Changes

The output data of the study is the one by Luijendijk et al. (2018), which has been received via a spreadsheet from the author of the study. The data consists of numerous time series for shoreline positions for 75769 transaction points for all coastlines of the Black Sea and the Sea of Azov, along with all estuaries, lagoons, harbors, etc. The distance between these transection points is 500 m and the period is between 1984 and 2016.

Data sets were classified due to country borders and geographic conditions. The shoreline position time series were taken out from the data for each seven study areas (Danube, Terkos, Cide, Sinop, Bafra, Çarşamba, and Sochi) and the long-term variations of the shoreline positions at each transection point were calculated. For each time series at each grid point, trends are estimated by using Theil-Sen's estimator and Mann-Kendall test to detect the variations of the time-series data gathered from the dataset taken from Luijendijk et al. (2018). Here, positive trends in the shoreline position declares deposition, whereas negative trends declare erosion for the particular transaction point in a shoreline.

3.2.3 Pearson Correlation Coefficients

For the years between 1984 and 2016, we constructed time series for annual mean and annual 95th percentile wind speeds, SWHs, and SSTs along with shoreline positions. Each time series consists of 33 annual mean or 95th percentile values. After this, the Pearson correlation coefficients were calculated between each atmospheric parameter time series and the annual shoreline position time series.

The correlation coefficient values change from -1 to +1, and it evaluates if there is any relationship between two data series in terms of their magnitude and direction (Figure 3.2). The sign of the coefficient value defines the correlation between two series is positive or negative. Positive correlation coefficients mean that two variables are increasing or decreasing together, whereas negative ones state that one variable tends to increase while the other one is decreasing.

Besides, the magnitude of the correlation coefficient indicates the strength of the correlation. The correlation coefficient which is closer to 1 or -1 declares that there is a strong relationship between the variables. A result around zero indicates there is no relationship at all (Edwards, 1976).

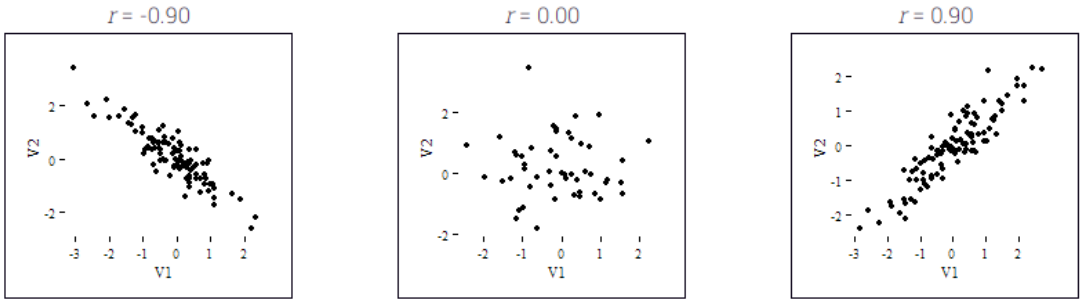


Figure 3.2 Graphs showing a correlation of -1, 0, and +1 (Cohen, 1988)

In most of the disciplines, the strength of the correlation due to the Pearson correlation coefficient can be categorized in Table 3.3;

Table 3.3 Strength of the correlations due to Pearson correlation coefficient (Dancey and Reidy, 2004)

Pearson Coefficient Value	Strength
$0.1 < \mid r \mid < 0.3$	small / weak
$0.3 < \mid r \mid < 0.5$	medium / moderate correlation
$0.5 < \mid r \mid < 1.0$	large / strong correlation

The formula which gives the correlation coefficient between two variables x and y, which is r or r_{xy}, is given as equation 3.7 (Cohen,1988)

$$r_{xy} = \frac{cov(x,y)}{\sqrt{var(x)}\sqrt{var(y)}} \tag{3.7}$$

4

RESULTS AND DISCUSSION

4.1 Long-Term Changes in Atmospheric Forcing

4.1.1 Long-Term Variations of Wind Speeds over the Black Sea

Determination of long-term changes in wind speeds over the Black Sea Basin is important to understand the climate change conditions for the study area. For this purpose, both CFSR and ERA-I reanalysis U10 data are used to provide an understanding of the long-term variations of U10. Two major datasets were evaluated here to have comparative results and to gather more reliable answers to define the trends for U10. Long-term averages of U10 over 38 years (1979-2016) are mapped for both ERA-I and CFSR in Figure 4.1. Only the magnitudes are considered, and wind directions are not analyzed. Grid points based on the native spatial resolution are indicated with dots on spatial maps in Figure 4.1. Land/Sea mask data are obtained from ERA-I and CFSR for corresponding reanalysis data and are depicted in Figure 4.1. Additionally, in Figure 4.1, the land area is indicated by white dots whereas the sea points are indicated by black dots.

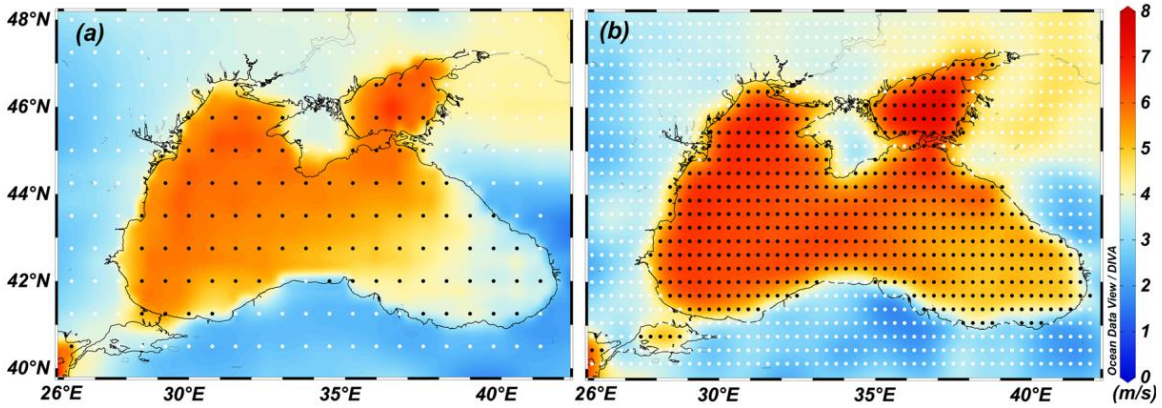


Figure 4.1 Long-term averaged U10 considering 38 years period (1979–2016) over the Black Sea: a) ERA-I, b) CFSR. White dots indicate land and the black dots indicate sea points

Figure 4.1 shows that the spatial distribution of long-term averaged of U10 from two reanalysis data over the Black Sea Basin presents a similar pattern. Higher long-term averaged U10 values occur in the center of the Sea of Azov and offshore northwestern Black Sea. Where the lowest long-term averaged U10 values exist in the eastern part of the basin. For the land area, the northern part of the Black Sea has higher long-term averaged U10 values than the south. Generally, CFSR gives higher long-term averaged U10 values in the sea. The Sea of Marmara exhibits much higher long-term averaged U10 in CFSR data since it is accepted as an open sea whereas it is accepted as a land area in ERA-I data. A clear magnitude difference between the two data is revealed. The long-term averaged U10 from ERA-I varies between 1.63 m/s and 6.63 m/s with an average value of 4.04 m/s (Figure 4.1a). CFSR data varies between 1.74 m/s and 7.35 m/s with an average value of 4.42 m/s (Figure 4.1b). To quantify the magnitude difference from both reanalysis data the ratio of CFSR long-term averaged U10 to ERA-I long-term averaged U10 is computed spatially as illustrated in Figure 4.2.

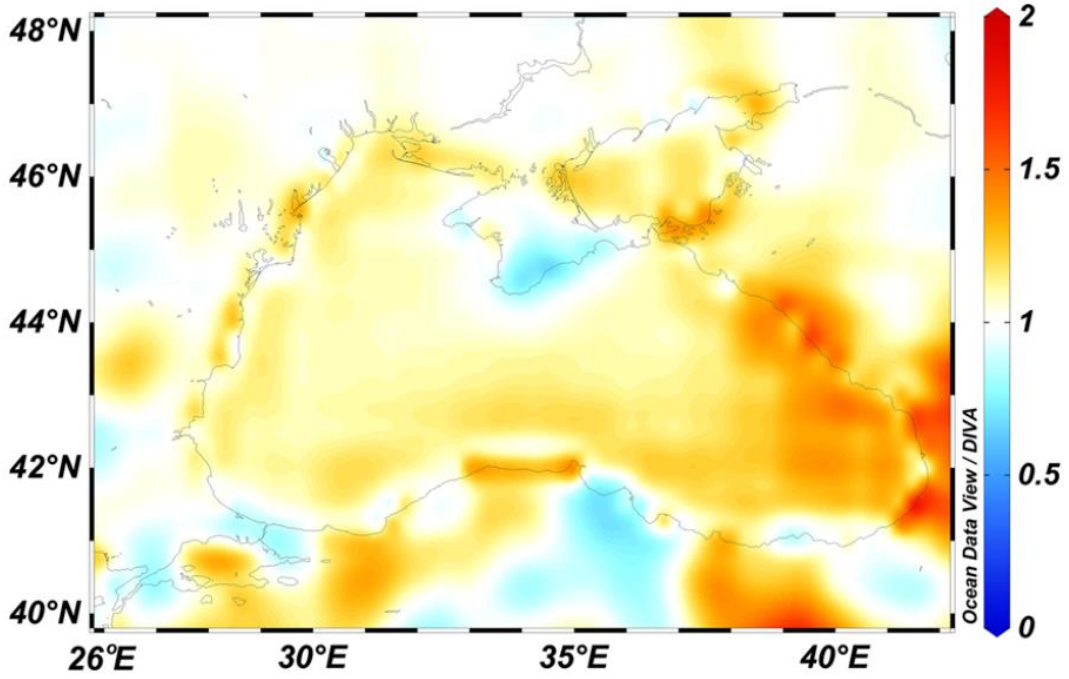


Figure 4.2 The ratio of long-term average U10 values from the CFSR data to the ones from ERA-I

Figure 4.2 presents that, the magnitude of the difference between long-term averaged U10s from two data is inhomogeneous throughout the study area. The ratio of long-term averaged U10 from CFSR to long-term averaged U10 from ERA-I varies between 0.66 and 1.8 with a basin average value of 1.10. CFSR gives higher long-term averaged U10 values in most of the study areas where the only exceptions are coastlines along the Crimean Peninsula, and the southern coasts of the Black Sea basin. Ratios smaller than one occur along the shoreline of the Crimean Peninsula, Strait of Istanbul, and Dardanelles. The highest ratios exist along the eastern coasts of the Black Sea, westernmost and southern coasts of the Sea of Azov, and along the eastern Black Sea coastlines. On the land area, the highest rates of ratio occur in the eastern part of the study area.

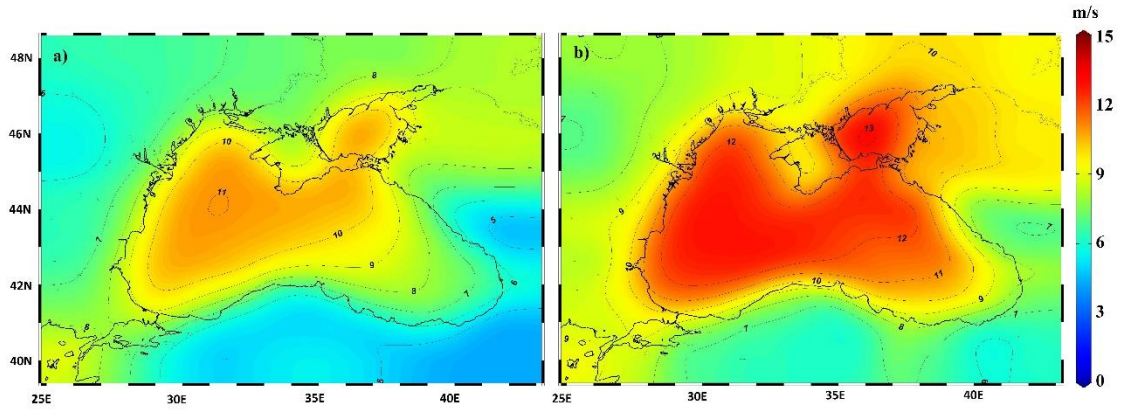


Figure 4.3 Long-term 95th percentile U10 considering 38 years period (1979–2016) over the Black Sea: a) ERA-I, b) CFSR

Figure 4.3 shows that the spatial distribution of the long-term 95th percentile of U10 from two reanalysis data over the Black Sea Basin presents a similar pattern. Higher long-term 95th percentile U10 values occur in the center of the Sea of Azov and offshore northwestern Black Sea. Where the lowest long-term 95th percentile U10 values exist in the eastern part of the basin. For the land area, the northern part of the Black Sea has higher long-term 95th percentile U10 values than the south. Generally, CFSR gives higher long-term 95th percentile U10 values in the sea. The Sea of Marmara exhibits a much higher long-term 95th percentile U10 in CFSR data since it is considered an open sea whereas it is considered a land area

in ERA-I data. A clear magnitude difference between the two data is revealed. The long-term 95th percentile U10 from ERA-I varies between 3.33 m/s and 12.49 m/s with an average value of 7.87 m/s (Figure 4.3a). CFSR data varies between 4.73 m/s and 14.63 m/s with an average value of 9.75 m/s (Figure 4.3b).

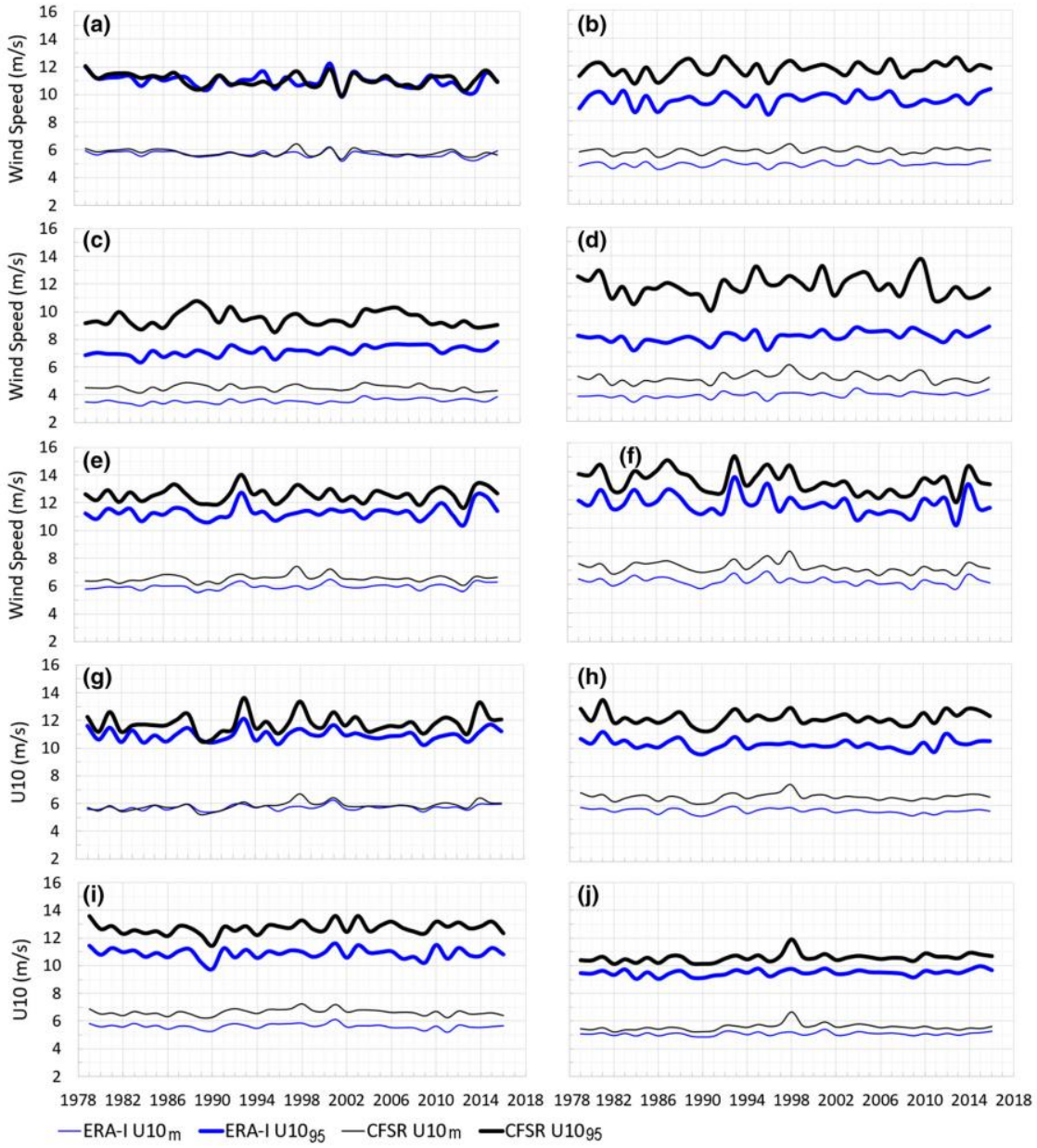


Figure 4.4 Interannual variability of annual $U10_m$ and annual $U10_{95}$ at selected study sites (Figure 2.1), a) A, b) B, c) C, d) D, e) E, f) F, g) G, h) H, and I) I, j) J

Long-term variations of the U10 are analyzed for both ERA-I and CFSR reanalysis data, comparatively. We evaluated the annual $U10_m$ and $U10_{95}$ time series for each corresponding grid point during the study period covering 38 years between 1979-2016. In Figure 4.4, the time series from the selected study sites (Figure 2.1) is shown to present the interannual variability in both annual $U10_m$ and $U10_{95}$ over different parts of the Black Sea.

Figure 4.4 indicates different interannual patterns in the temporal long-term evaluations of moderate and severe U10 values over the Black Sea. Both reanalysis data present similar interannual variability for almost all the study sites for both annual $U10_m$ and annual $U10_{95}$. Although the interannual variability looks similar, CFSR data gives higher annual U10s at almost all study sites. Higher time-averaged differences between ERA-I and CFSR exist for the annual $U10_{95}$ than the annual $U10_m$ reaching up to 3 m/s in B, D, and H. Interannual Variability (IV) is calculated at the selected study sites for both reanalysis data and both the annual $U10_m$ and annual $U10_{95}$ as shown in Equation 4.1,

$$IV = \frac{U10_{max} - U10_{min}}{U10_{mean}} \tag{4.1}$$

IV of Differences (IVD) is computed for the temporal evolution of the differences between ERA-I and CFSR data as shown in Equation 4.2,

$$IVD = \frac{(U10_{CFSR} - U10_{ERA-I})_{max} - (U10_{NCEP} - U10_{ERA-I})_{min}}{(U10_{ERA-I})_{mean}} \tag{4.2}$$

Computed IV and IVD values are shown in Table 4.1.

Table 4.1 Interannual variability coefficients for the selected study sites and the basin averaged U10

Study Site	IV				IVD	
	ERA-I		CFSR			
	$U10_m$	$U10_{95}$	$U10_m$	$U10_{95}$	$U10_m$	$U10_{95}$
A	0.17	0.22	0.19	0.20	0.15	0.16
B	0.15	0.19	0.16	0.17	0.14	0.16
C	0.20	0.21	0.16	0.24	0.28	0.33
D	0.26	0.21	0.30	0.31	0.35	0.32
E	0.16	0.21	0.21	0.19	0.19	0.11
F	0.20	0.29	0.24	0.24	0.20	0.10
G	0.15	0.17	0.25	0.26	0.20	0.20
H	0.13	0.16	0.21	0.18	0.16	0.11
I	0.16	0.17	0.15	0.17	0.12	0.09
Basin-averaged U10	0.11	0.10	0.26	0.17	0.24	0.15

Table 4.1 shows that the interannual variability of the annual U10 is slightly smaller than the interannual variability of the annual $U10_{95}$ based on the ERA-I data, while they are higher based on the CFSR data. The highest IV was computed in D from both reanalysis data. Whereas the smallest variability was computed in H from the ERA-I data, and in I from the CFSR data. These highest and lowest IV patterns are found to be consistent with annual $U10_m$ and $U10_{95}$ data, but they are inconsistent between two considered reanalysis data. Basin-averaged IV is much smaller than the IVs for the considered study sites for the ERA-I data. It is relatively smaller for the CFSR data as well. IVD presents a wider range of variability for both annual $U10_m$ and annual $U10_{95}$ over the Black Sea coastline. The highest and lowest IVD for annual $U10_m$ is computed at D and I, respectively. It is also revealed that the variability of differences between the two reanalysis data is much higher for the annual $U10_m$ than the annual $U10_{95}$.

4.1.1.1 Spatial Variations of Long-Term Trends in Annual Mean Sea Level Pressure, Annual Mean and 95th Percentile Surface Wind Speeds

As it is seen from the interannual variability analysis of U10 over 38 years at selected sites, long-term variability is inhomogeneous over the study area. To study the long-term trends and their spatial variability, trends of 38 year-long time series of both annual $U10_m$ and annual $U10_{95}$ are computed at each grid point over the study area at 0.25° × 0.25° resolution. 12288 (2048x6) time series in total are analyzed and the results are presented as maps in this section. Considering that the atmospheric pressures are the forcing causing wind, we analyzed the long-term trends in Mean Sea Level Pressure (MSLP) from both reanalysis data over the same period (1979-2016) and the same study area. Long-term trends in MSLP, annual $U10_m$, and annual $U10_{95}$ are shown in Figure 4.5. Locations with statistically significant trends at 95% or higher confidence levels are depicted by black dots. Time-averaged MSLP over 38 years is also shown as contour maps in Figure 4.5(a) and Figure 4.5(b). All trend estimates are computed and presented as (%/yr).

Figure 4.5 shows that two reanalysis present different rates of change in pressure fields over the study area. ERA-I indicates a decreasing trend in the MSLP values as shown in Figure 4.5(a). Especially the changes in eastern and northeastern parts were statistically significant at 95% or higher confidence level. No statistically significant increasing trends have been found regarding the ERA-I data. The most important difference between the two reanalysis data manifested itself over the Anatolian Peninsula where CFSR data shows statistically significant increasing trends in Figure 4.5(b) while ERA-I shows no significant trend. Since this increase occurs over land, it can be said that no significant trend exists over the sea grids for CFSR data. Long-term mean values of MSLP are consistent between two reanalysis data.

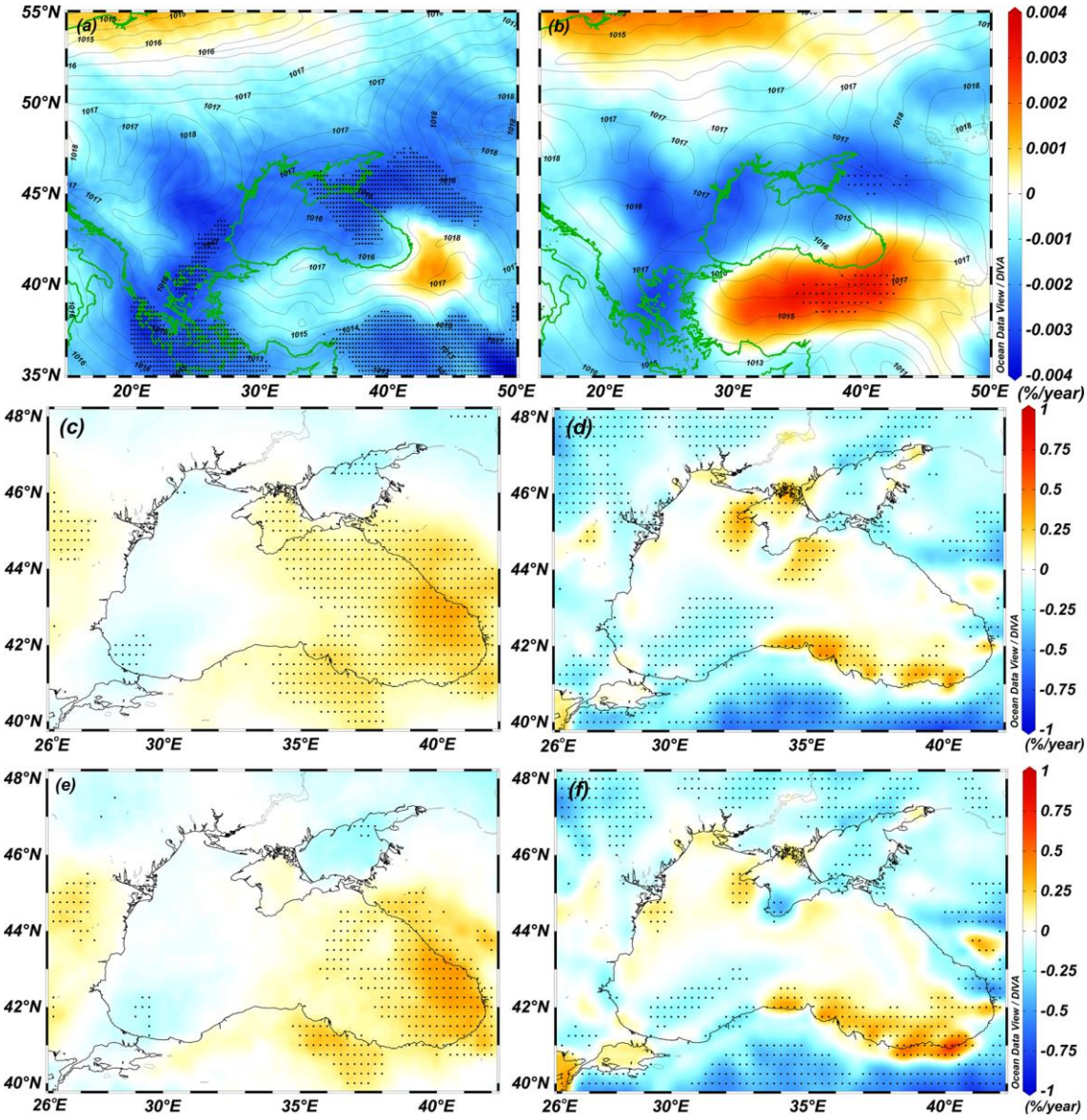


Figure 4.5 Spatial variability of long-term trends of a) annual MSLP from ERA-I, b) annual MSLP from CFSR, c) ERA-I annual $U10_m$, d) CFSR annual $U10_m$, e) ERA-I annual U1095, f) CFSR annual U1095 for the study period (1979–2016) over the study area. Black dots indicate locations with statistically significant trends at the 95% or higher confidence level. Contours indicate the time-averaged MSLP (Pa) in a and b

In Figure 4.5(c) and Figure 4.5(e), ERA-I data shows statistically significant increasing trends in the eastern part of the Black Sea and along the coastline of Kızılırmak and Yeşilırmak Deltas for both $U10_m$ and $U10_{95}$. These increasing trends reach the highest rates (0.35 %/yr) along the Georgia coastline. Statistically significant decreasing trends are computed at the Odessa coastline, southwestern coasts, and the Sea of Azov reaching down to -0.17 %/yr for annual $U10_m$ from ERA-I. The spatial variation of changes in annual $U10_{95}$ in Figure 4.5(e) presents statistically significant trends varying between -0.23 %/yr and 0.38 %/yr in the Black Sea basin. The highest and lowest trends are computed along the nearshore Georgia, and the northern coasts of the Sea of Azov, respectively. A comparison of trend rates of annual mean and annual $U10_{95}$ from ERA-I reveals that changes in severe wind states occur at higher rates than the moderate wind states.

Long-term trends computed based on CFSR data are slightly higher than the ERA-I for both annual $U10_m$ and annual $U10_{95}$. Trends in annual $U10_m$ vary between -0.28 %/yr and 0.41 %/yr, spatially as depicted by Figure 4.5(d). Statistically significant decreasing trends exist only in the offshore parts of the southwestern Black Sea with rates down to -0.21 %/yr. Significant increasing trends occur mostly in the sea area along the Danube Delta coastal zone, the southern and southeastern coastal strip of the Black Sea basin, and along the nearshore and offshore zones of the Crimean Peninsula. Statistically significant decreasing trends are computed in the central and northern parts of the Sea of Azov. The highest decreasing trends in annual $U10_m$ were computed on the land area, especially in the eastern and southern parts of the study area (Figure 4.5(d)).

Figure 4.5(f) presents a similar pattern of spatial variability of long-term trends in annual U1095 to the one presented in Figure 4.5(d). Statistically significant increasing trends manifest themselves over a wider sea area, whereas statistically significant decreasing trends cover a narrower area. An important difference between Figure 4.5(d) and Figure 4.5(f) exists along the northwestern coasts of the basin where statistically significant increasing trends occur in annual $U10_{95}$. Trends presented in Figure 4.5(f) vary between -0.41 %/yr and 0.66 %/yr, indicating the highest rates of change in a statistically significant increasing trend.

The highest trend rate for the increasing $U10_{95}$ is computed to be along the southeastern Turkish coasts of the Black Sea. The highest decreasing trend in Figure 4.5(f) is computed over the continental shelf of Georgia. Figure 4.5(f) also indicated statistically significant decreasing trends in the Sea of Azov.

4.1.1.2 Spatio-Seasonal Variations of Long-Term Trends in Monthly Mean Sea Level Pressure, Monthly mean and 95th Percentile Surface Wind Speeds

Seasonal variations are expected in the Black Sea. To illustrate the seasonality in the data, we constructed a time series of mean MSLP, $U10_m$, and U1095 on a monthly basis from both reanalysis data. The same temporal coverage of 38 years (1979-2016) is considered for the analysis. Monthly spatial variations of long-term trends in annual MSLP are shown in Figure 4.5 for the ERA-I reanalysis data.

It is clear that the spatial variability of mean MSLP and the long-term trends in MSLP is inhomogeneous and vary seasonally. The influence of the Siberian Anticyclone is seen over the eastern basin during winter according to 38-year means. Results indicate that its influence has a significant increasing trend for December. Statistically significant increasing trend rates reach up to 0.01%/yr over the terrestrial part of the easternmost study area. The southeastern part of the study area presents decreasing trends for summer low-pressure systems. These statistically significant decreasing trends are computed to be -0.01%/yr. This effect is found for the term from April to September except for August where no significant trend exists. The influence of the Mediterranean cyclonic activity is visible for July, August, and September and exhibits statistically significant decreasing trends reaching down to -0.01%/yr.

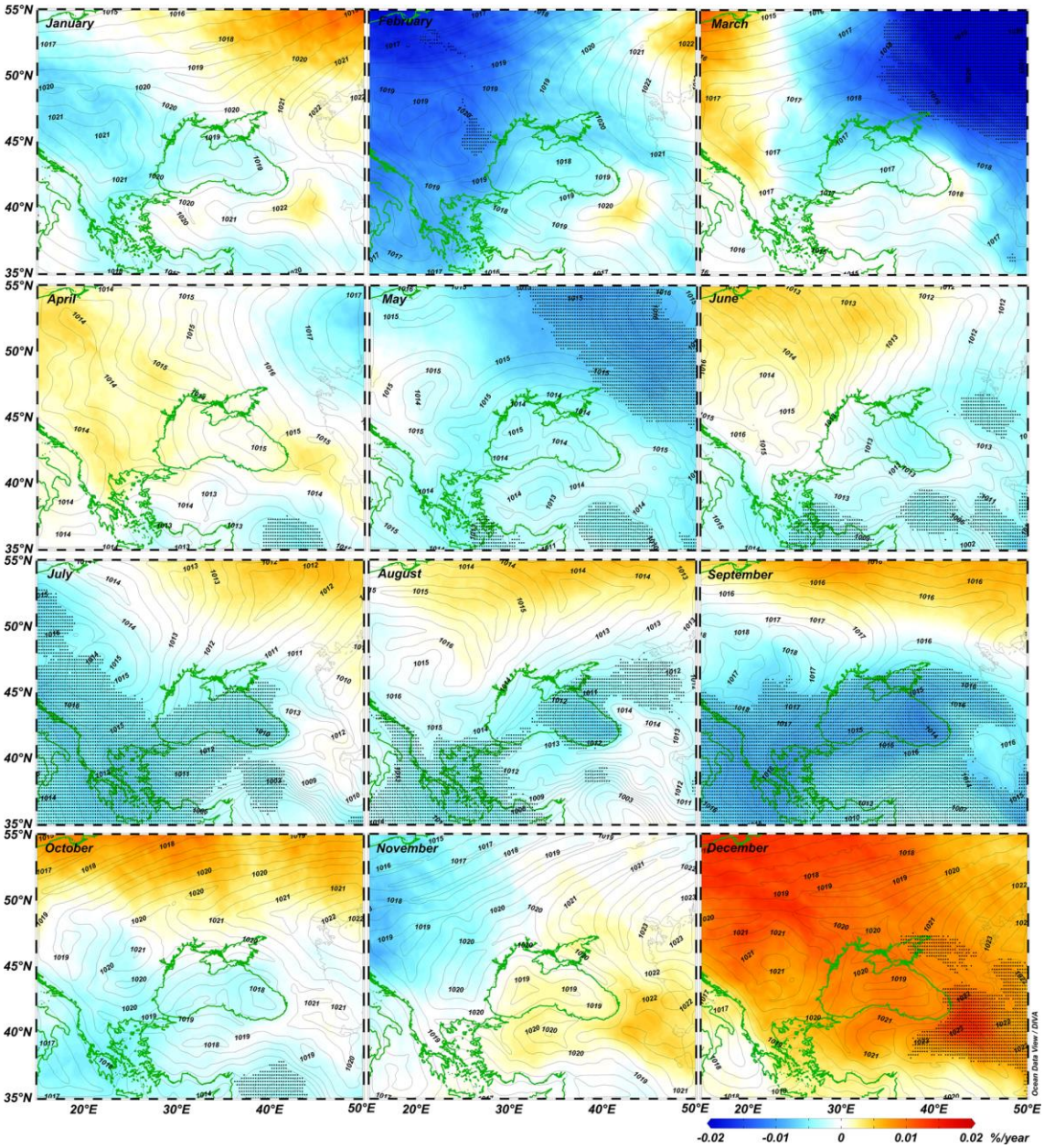


Figure 4.6 Spatial variability of long-term trends in ERA-I MSLP on a monthly basis. Black dots indicate locations with statistically significant trends at the 95% or higher confidence level

Monthly spatial variations of long-term trends in annual MSLP are shown in Figure 4.7 for the CFSR reanalysis data. Figure 4.7 showed that 38-year long-term means of MSLP are consistent from both reanalysis for almost all months. Statistically significant decreasing trends in Mediterranean cyclonic activity have also been captured by the CFSR reanalysis data whereas the influence of summer low pressure in the southern part of the study area presents no significant trends.

The activity of the Siberian anti-cyclone and increasing trends in its influence have also been captured by CFSR at almost the same rates as that of the ERA-I for December.

Monthly spatial variations of long-term trends in annual $U10_m$ are shown in Figure 4.8 for the ERA-I reanalysis data. Figure 4.8 illustrates that the Black Sea manifests clear seasonality in means of long-term trends of monthly $U10_m$ based on ERA-I data. The rates of trends are found to be between -0.56 %/yr (in the Sea of Azov for January) and 0.96 %/yr (on the eastern coasts of the Black Sea for March) over the study area in January and March, respectively. The highest positive trends are computed in February and March along the eastern part of the basin including both the terrestrial and aquatic parts of the coastal zone. January, April, June, October, and December also present statistically significant increasing trends in the eastern part of the basin with lower trend rates. The Sea of Azov manifests significantly increasing trends in September and in August partly, where the statistically significant decreasing trends are estimated for January, March, November, and December. Other statistically significant decreasing trends are computed along the eastern, western, and southwestern coasts of the basin for July, November, and December, respectively. No statistically significant decreasing trend is revealed in the Crimean Peninsula coastal area while increasing trends are estimated for April, August, and September. No significant increasing or decreasing trend is found for May except for decreasing trends at the central-western part of the basin.

By generally saying, $U10_m$ values are found to be increasing at all seasons in the eastern Black Sea, and decreasing trends exist during the transition from summer to autumn (for the months August and September) in the western part. In September most of the basin together with the Sea of Azov presents a statistically significant increasing trend reaching up to 0.59 %/yr at the Kızılırmak Delta coastline.

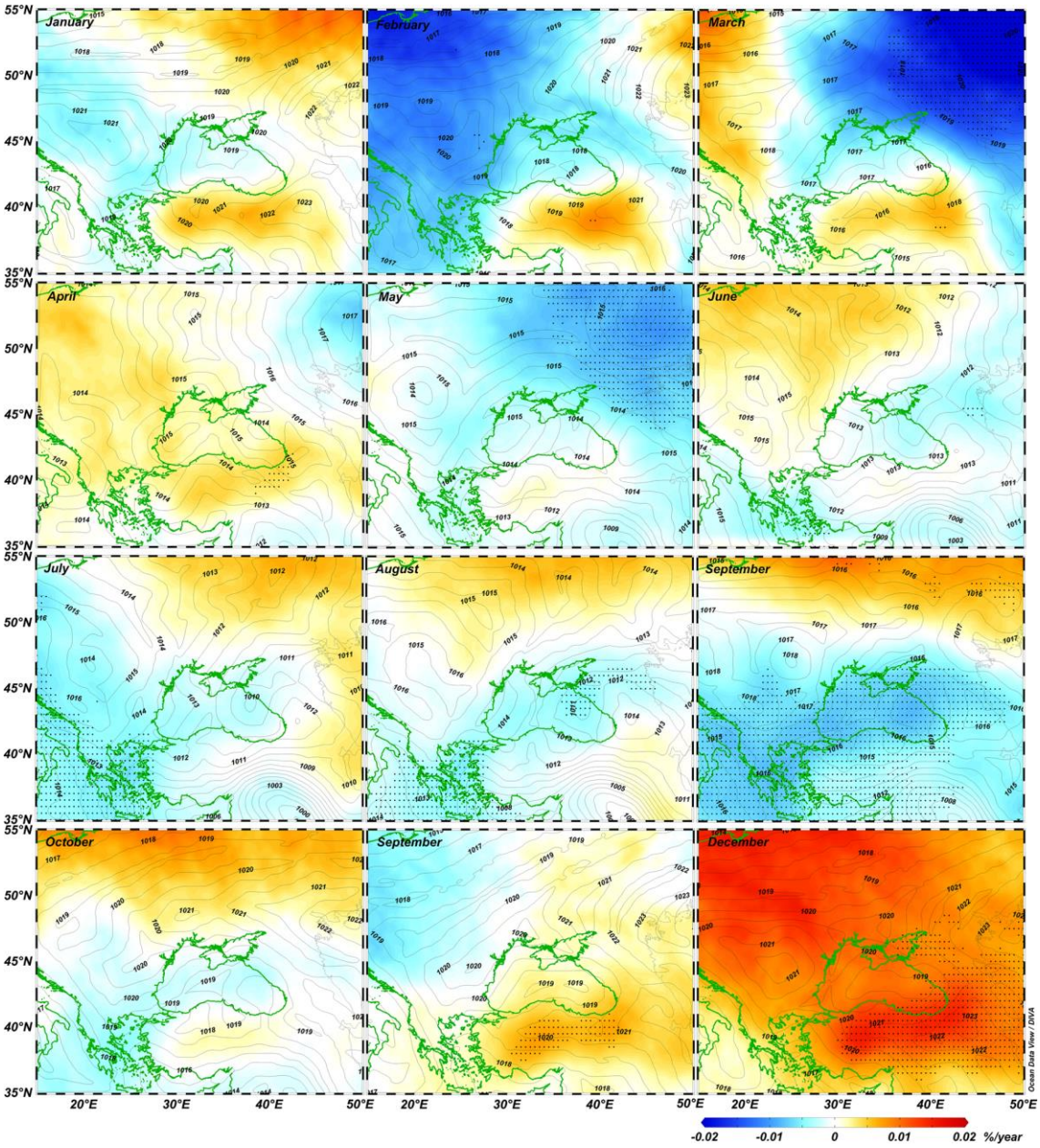


Figure 4.7 Spatial variability of long-term trends in CFSR MSLP on a monthly basis. Black dots indicate locations with statistically significant trends at the 95% or higher confidence level

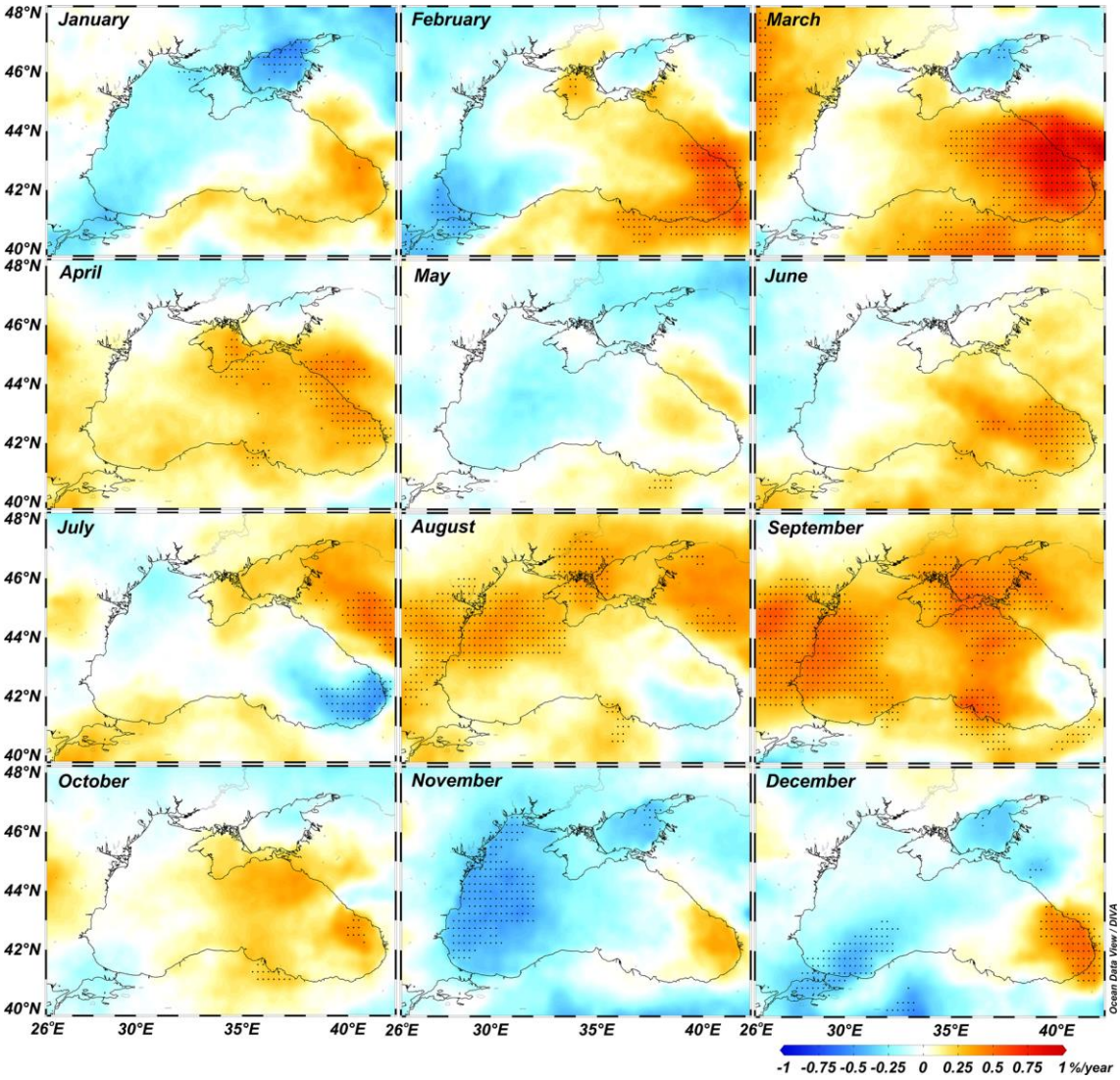


Figure 4.8 Spatial variability of long-term trends in ERA-I monthly $U10_m$ on a monthly basis. Black dots indicate locations with statistically significant trends at the 95% or higher confidence level

Spatial distributions of trends in annual $U10_m$ from CFSR reanalysis data are mapped and presented in Figure 4.9. Figure 4.9 presents the different spatial distribution of trends in annual $U10_m$ from CFSR reanalysis data. Generally, both decreasing and increasing trends have greater rates than the ERA-I reanalysis data, varying between -0.62 %/yr (at the southeastern part of the basin for November) and 1.16 %/yr (at the southeastern coasts of the Black Sea for March). Generally increasing trends are covering wider areas that existed at greater rates than the statistically significant decreasing trends. Statistically significant increasing trends are computed along the southeastern coasts of the basin for March, June, and

September. Dramatically varying trends in the terrestrial and aquatic region manifested themselves along the central and southeastern coasts of the Black Sea for all the months. Around the Crimean Peninsula, consistent statistically significant increasing trends are revealed for March, April, June, July, August, September, and October. Statistically significant decreasing trends are computed for January, May, November, and December in the Sea of Azov where the statistically significant increasing trends are found at a transition from summer to autumn for August and September.

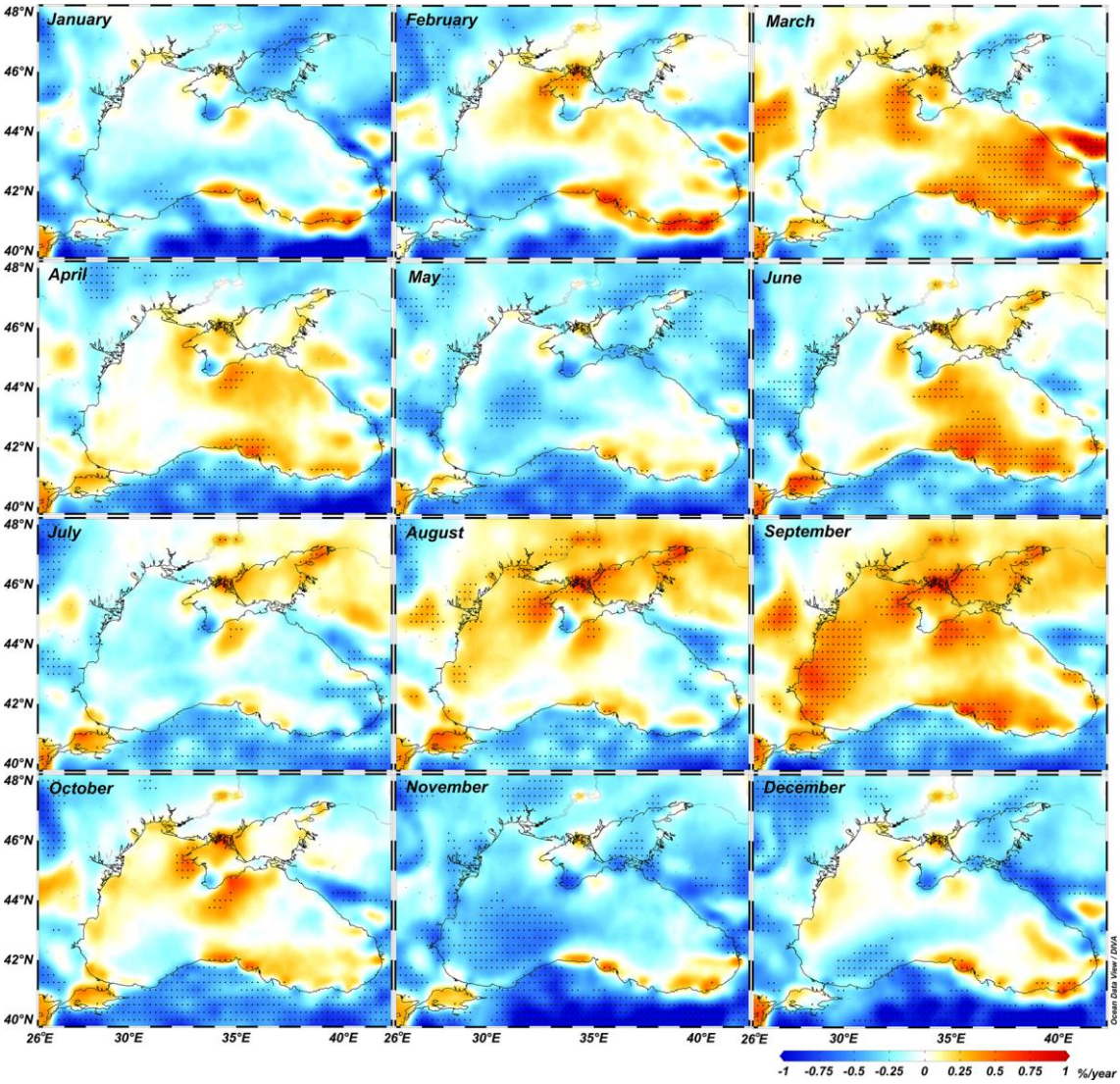


Figure 4.9 Spatial variability of long-term trends in CFSR monthly $U10_m$ on a monthly basis. Black dots indicate locations with statistically significant trends at the 95% or higher confidence level

Understanding the long-term variability in severe U10s is also important to evaluate the climate change impacts on the storminess of the Black Sea. Long-term trends in monthly $U10_{95}$ are analyzed on a monthly basis for this purpose. The results are presented in Figure 4.10 for the ERA-I reanalysis data.

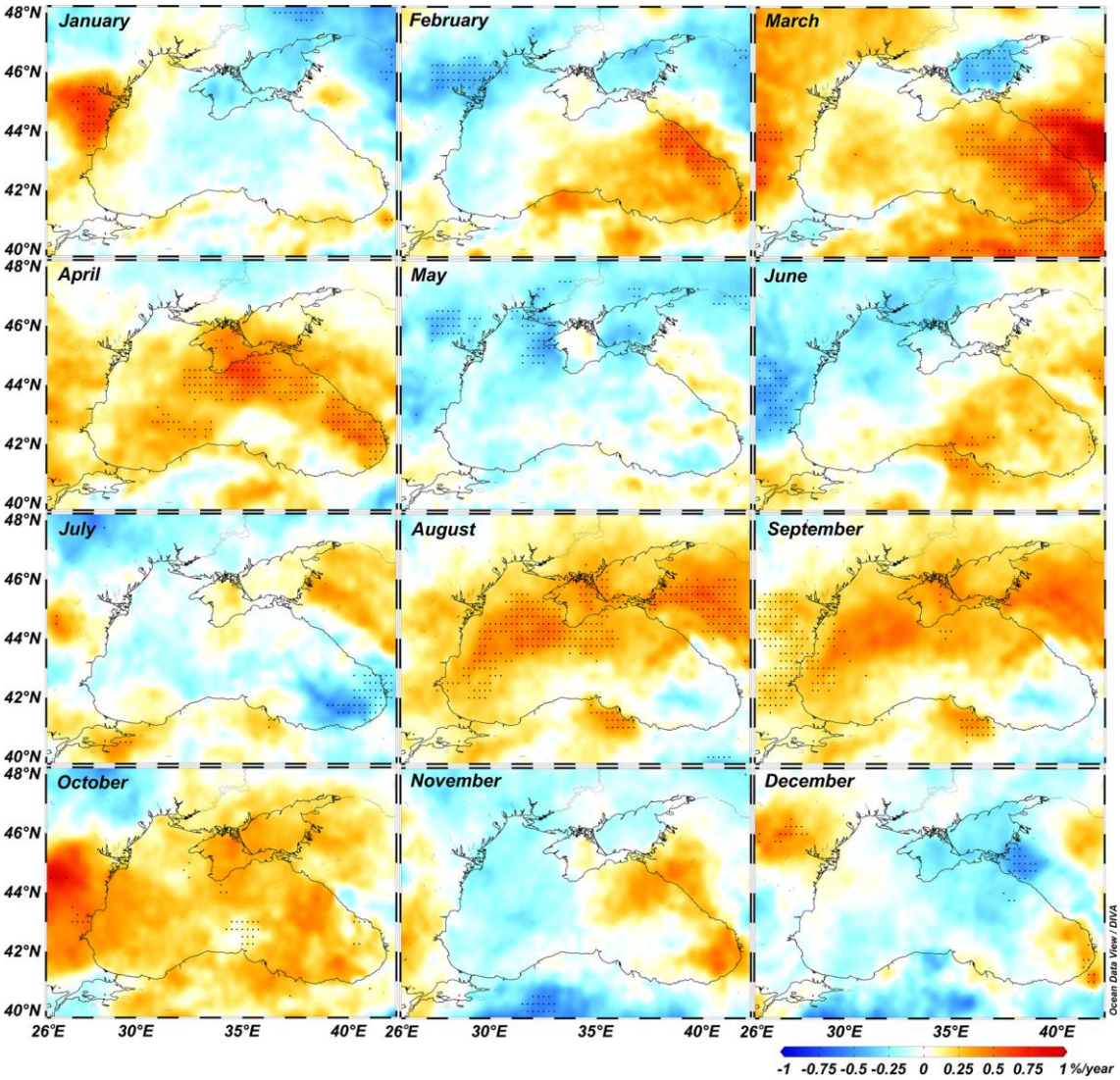


Figure 4.10 Spatial variability of long-term trends in ERA-I monthly $U10_{95}$ on a monthly basis. Black dots indicate locations with statistically significant trends at the 95% or higher confidence level

In Figure 4.10, statistically significant decreasing and increasing trends vary between -0.57%/yr and 0.81 %/yr within the basin for July and March, respectively. On the land area, the highest increasing trend is computed at the northeastern coasts at a rate of 1.27 %/yr. Decreasing trends are found for February on northwestern coasts, for March in the Sea of Azov, for May on both sides of the Crimean Peninsula, for July along southeastern coasts, and for December in the northeastern part. Statistically significant increasing trends are computed for all months except May and July. The highest statistically significant increasing trends are computed for March, April, and August, along with the eastern, northern, and western parts of the basin, respectively. $U10_{95}$ from the ERA-I data are found to be increasing in most of the Black Sea for March, April, and August.

Decreasing trends in the annual $U10_{95}$ in Figure 4.10, cover a slightly wider area than that of $U10_{m}$ in Figure 4.8. The coverage of increasing trends is wider for January, October, and November and narrower for others. While increasing trends manifest themselves in a very limited area in the east with relatively lower rates for January, increasing trends at higher rates exist in the west at the terrestrial zone just behind the coastline.

Spatial distributions of long-term trends in monthly $U10_{95}$ regarding CFSR data are presented in Figure 4.11 to provide a comparison between two reanalysis data. Figure 4.11 shows statistically significant decreasing and increasing trends varying between -1.50 %/yr and 1.10 %/yr over the study area. Severe winds (represented by monthly $U10_{95}$) present higher increasing/decreasing trend rates concerning moderate winds (represented by monthly $U10_{m}$) for each month. Especially the south to southeast coast arc has the highest increasing trend rates followed by the highest decreasing trends behind the coast in the mountainous terrestrial area. This sharp transition between increasing and decreasing trends does not exist in ERA-I data.

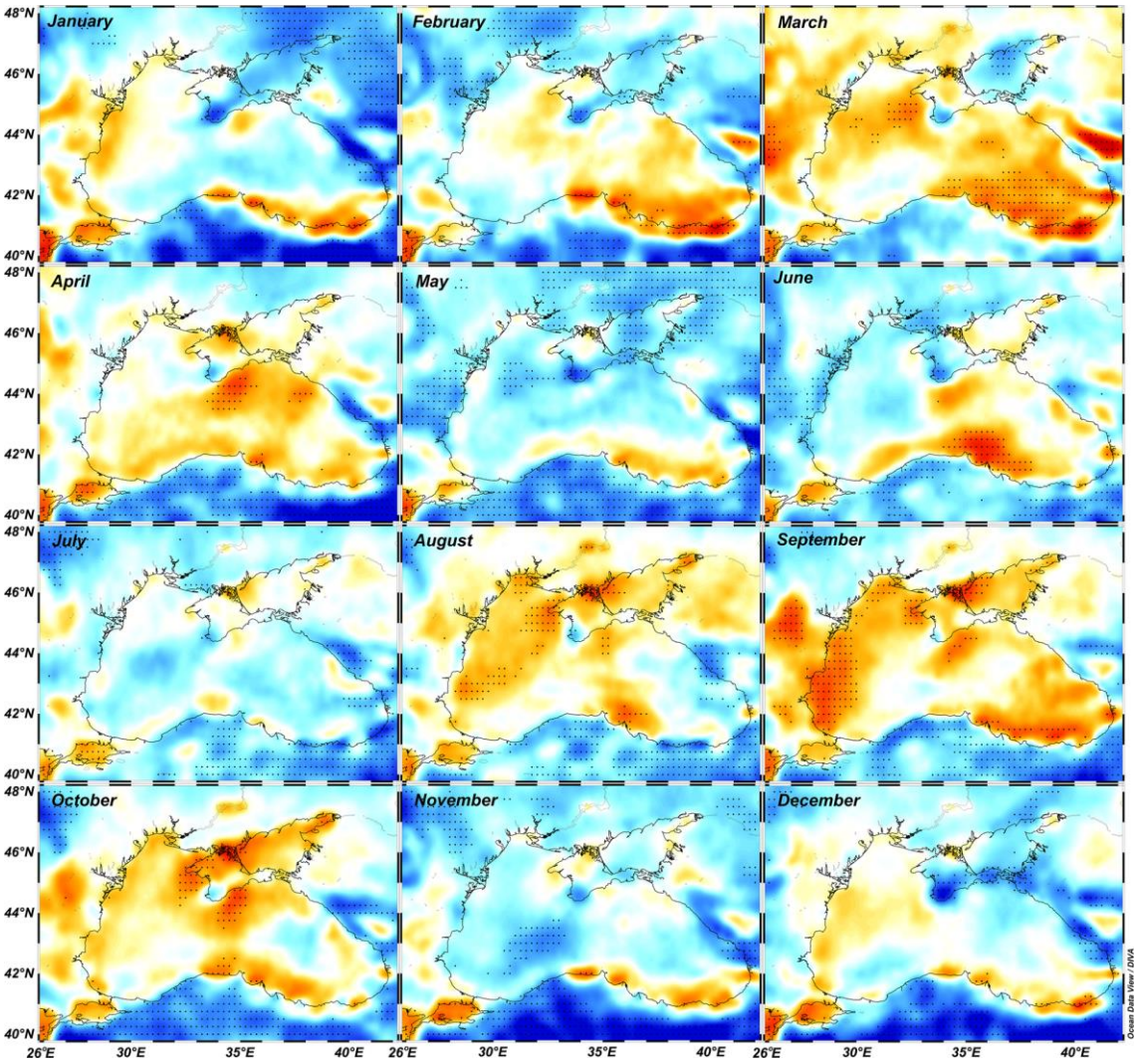


Figure 4.11 Spatial variability of long-term trends in CFSR monthly $U10_{95}$ on a monthly basis. Black dots indicate locations with statistically significant trends at the 95% or higher confidence level

Another hot location is the Crimean Peninsula characterized by relatively high increasing trends. A comparison of severe (Figure 4.11) and moderate (Figure 4.9) winds reveals that increasing trends along the south and southeastern coasts are higher for the severe winds than that for the moderate winds while increasing trends for severe winds are lower than that for moderate winds around the Crimean Peninsula for all months except October.

4.1.1.3 Statistics of the Spatial Distribution of Trends

To study the size of the area having increasing or decreasing trends for both monthly $U10_m$ and monthly $U10_{95}$ are analyzed statistically for both reanalysis data. Results are presented in Table 4.2. Only sea points with significant trends are considered.

Table 4.2 Percentage of grid points where statistically significant negative and positive trends exist in monthly/annual $U10_m$ and $U10_{95}$ over the Black Sea

	ERA-I	CFSR						
	(-) Trends in $U10_m$	(+) Trends in $U10_m$	(-) Trends in $U10_{95}$	(+) Trends in $U10_{95}$	(-) Trends in $U10_m$	(+) Trends in $U10_m$	(-) Trends in $U10_{95}$	(+) Trends in $U10_{95}$
January	4.86	0.12	0	0	4.50	1.20	2.14	2.37
February	0	10.79	7.00	0.59	3.60	2.73	0.24	2.49
March	0.59	29.18	3.91	22.18	0.50	26.3	1.90	18.86
April	0	11.63	0	25.15	0	4.74	1.07	4.74
May	0	0	4.39	0	8.10	0.80	7.24	0.47
June	0	11.63	0	1.30	0	15.54	1.42	6.52
July	7.47	0	4.98	0	3.80	1.07	3.32	0
August	0	0	0	7.47	2.80	8.78	3.44	13.88
September	0	0	0	5.46	0	27.60	0	19.34
October	0	0	0	3.68	0	3.70	0	7.59
November	21.47	0	0	0	23.30	0.50	6.64	0.47
December	9.13	6.64	0.47	0.59	7.10	1.80	4.03	1.30
Annual	3.91	36.42	1.78	28.00	15	12.5	8.90	14.47

Table 4.2 indicates that both $U10_m$ and $U10_{95}$ tend to increase over ~36% and ~28% of the Black Sea surface area considering annual distribution, respectively. Annual decreasing trends cover a much smaller surface area between ~4% and ~2% of the Black Sea surface area based on ERA-I reanalysis data. The surface area covered by significant trends (decreasing or increasing) is larger for ERA-I than that of CFSR for annual $U10_m$. The area covered by significant decreasing or increasing annual trends for CFSR is narrower concerning ERA-I for both $U10_m$ and $U10_{95}$. Regarding the ERA-I, almost no decreasing trend in $U10_{95}$ is visible for almost all months and annual computations. In general, increasing trends cover wider surfaces are for $U10_m$ than $U10_{95}$ if they exist. But significantly increasing trends exist for only six months for $U10_m$ whereas they exist for eight months for $U10_{95}$ based on ERA-I data. Statistically significant decreasing trends exist over less coverage area than the statistically significant increasing trends.

Overall, the spatial variability of the long-term trends for both $U10_m$ and $U10_{95}$ in the CFSR data is found to be greater concerning ERA-I data during the analysis, especially along the coastlines. We analyzed time-series data for inspecting the reason for the results. Our analysis indicated that the change in the model land/sea mask data during the transition from CFSR version 1 to version 2 created some disturbances in the wind speeds. This effect can be seen in Figure 4.4(c) and Figure 4.4(d) where the wind speeds present a sudden change after 2011 which is the transition year between the two versions of the models. The clearest effect is visible over the Crimean Peninsula where data indicated a decreasing trend at the center of increasing trends. Although general consistency between ERA-I and CFSR wind reanalysis data is found in means of the spatial variability of the increasing and decreasing trends, this possible effect of transition from CFSR version 1 and CFSR version 2 must be considered for the significance of the trends and the rates of trends.

It has also been a common fact that the wind climate at any location on the earth is related to the wind climate at other locations far away. The distances between these two locations are generally huge and sometimes halfway around the Earth. The linkage between the variations in dynamic climate variables in a region and the fluctuations of a climate variable such as wind at a remote location is described as teleconnection. Teleconnection patterns link weather patterns over large distances across the globe. Atmospheric teleconnections may influence mean and extreme climate parameters (temperature, precipitation, or wind) on the global or regional scales and have been used in previous research, widely (Hasanean, 2005). The prominent teleconnection patterns over the North Atlantic and their affected regions are NAO, EA, EA/WR, West Pacific (WP), East Pacific/ North Pacific (EP/NP), Pacific/ North American (PNA), Scandinavia (SCA), Tropical/ Northern Hemisphere (TNH), Polar/ Eurasia (POL), Pacific Transition (PT).

In this study, the relationship between long-term variations of U10 over the Black Sea and teleconnection patterns are also studied. To understand the most influencing teleconnection pattern on the temporal variation of the wind fields of the Black Sea, correlation coefficients between each corresponding teleconnection with the $U10_m$ and U1095 are computed for EA (Wallace and Gutzler, 1981), EA/WR (Barnston and Livezey, 1987), NAO (Barnston and Livezey, 1987), PNA (Barnston and Livezey, 1987), POL (CPC, 2011), and SCA (Barnston and Livezey, 1987). Only the simultaneous correlations with no lags are studied. The spatial distribution of the Pearson's correlation coefficients (r) between the considered teleconnection patterns and the annual $U10_m$ and annual $U10_{95}$ time series during the study period of 38 years (1979-2016) is presented in Figure 4.12. For the 38 years-long time series threshold value of r is 0.304 at a 95% confidence level. Only r values greater than $|\pm 0.304|$ are presented since they are statistically significant in this analysis.

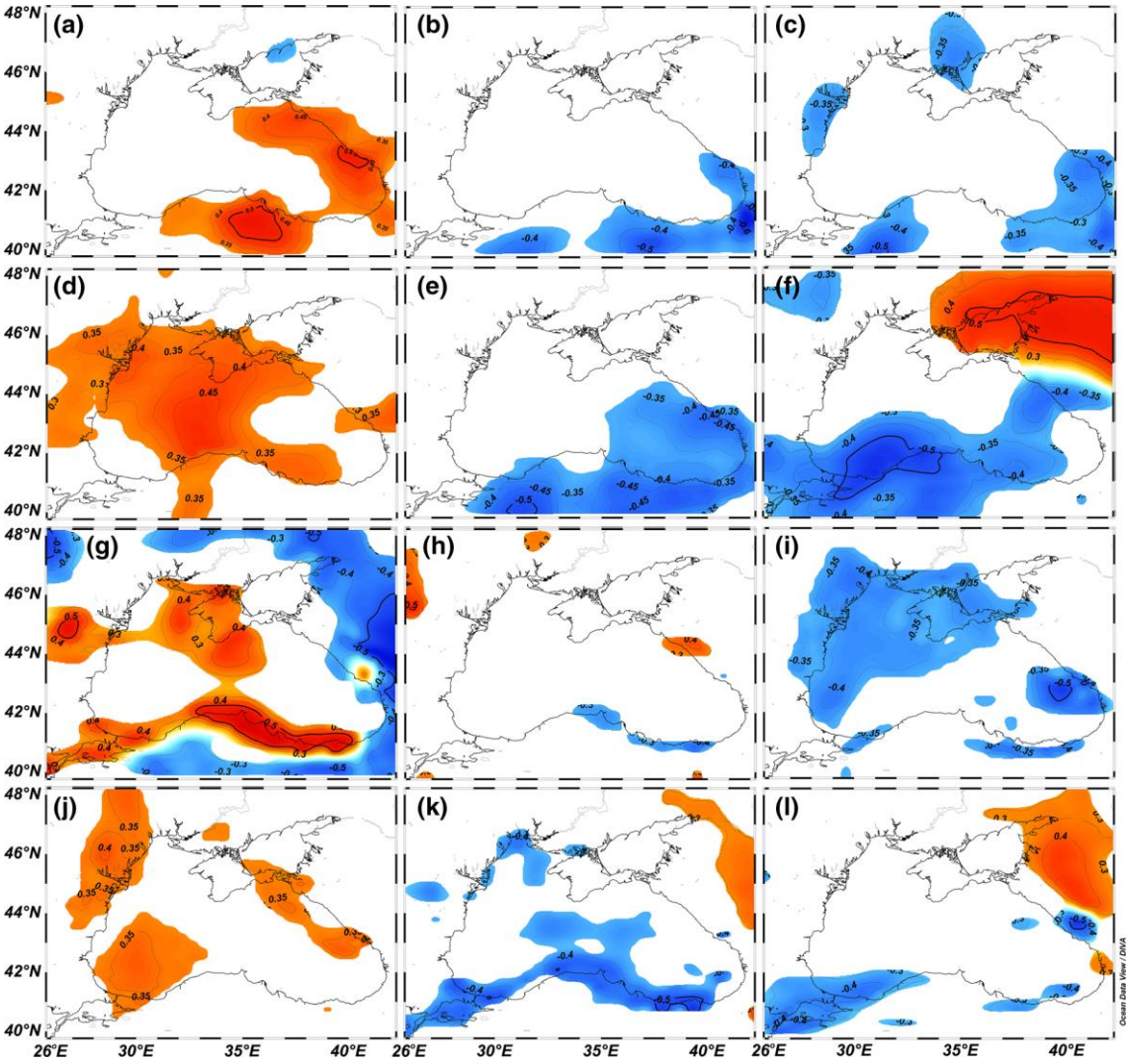


Figure 4.12 Correlation coefficients between teleconnection indices and the annual $U10_m$ over the Black Sea for both ERA-I and CFSR reanalysis data, a) [ERA-I]–[EA], b) [ERA-I]–[EA/WR], c) [ERA-I]–[NAO], d) [ERA-I]–[PNA], e) [ERA-I]–[POL], f) [ERA-I]–[SCA], g) [CFSR]–[EA], h) [CFSR]–[EA/WR], I) [CFSR]–[NAO], j) [CFSR]–[PNA], k) [CFSR]–[POL], l) [CFSR]–[SCA]

Figure 4.12 shows that fluctuations in $U10_m$ correlate with all the considered teleconnection patterns more or less. PNA correlates with the $U10_m$ from ERA-I positively over the whole basin with r values over 0.4. EA/WR, NAO, and POL are inversely correlated with the $U10_m$ based on ERA-I along southern, and southeastern coasts, and nearby the Crimean Peninsula with r values over 0.5. In the Sea of Azov, dominating teleconnection pattern is SCA for both reanalysis data with r values reaching up to 0.5 for both ERA-I and CFSR data. CFSR data shows that the least influencing teleconnection pattern is EA/WR and its influence exists

only along the south to southeastern coasts inversely with r values reaching 0.3. POL also influences the southern part of the basin with inverse r values up to 0.5 and 0.4 for CFSR and ERA-I, respectively. The highest r values are reached over 0.6 along the south to southeastern coast by the EA based on the CFSR data. NAO manifests its influence over a wide surface area covering north and northwestern parts of the basin with r values over 0.4 for the CFSR data. In general, CFSR and ERA-I reanalysis data provide consistent spatial distribution patterns and rates of r values over the Black Sea indicating the influence of different teleconnection indices.

It is expected that the severe wind speeds represented by $U10_{95}$ may present different distribution. Spatial variability of the r values between corresponding teleconnection indices and the $U10_{95}$ is presented in Figure 4.13 for both ERA-I and CFSR reanalysis data.

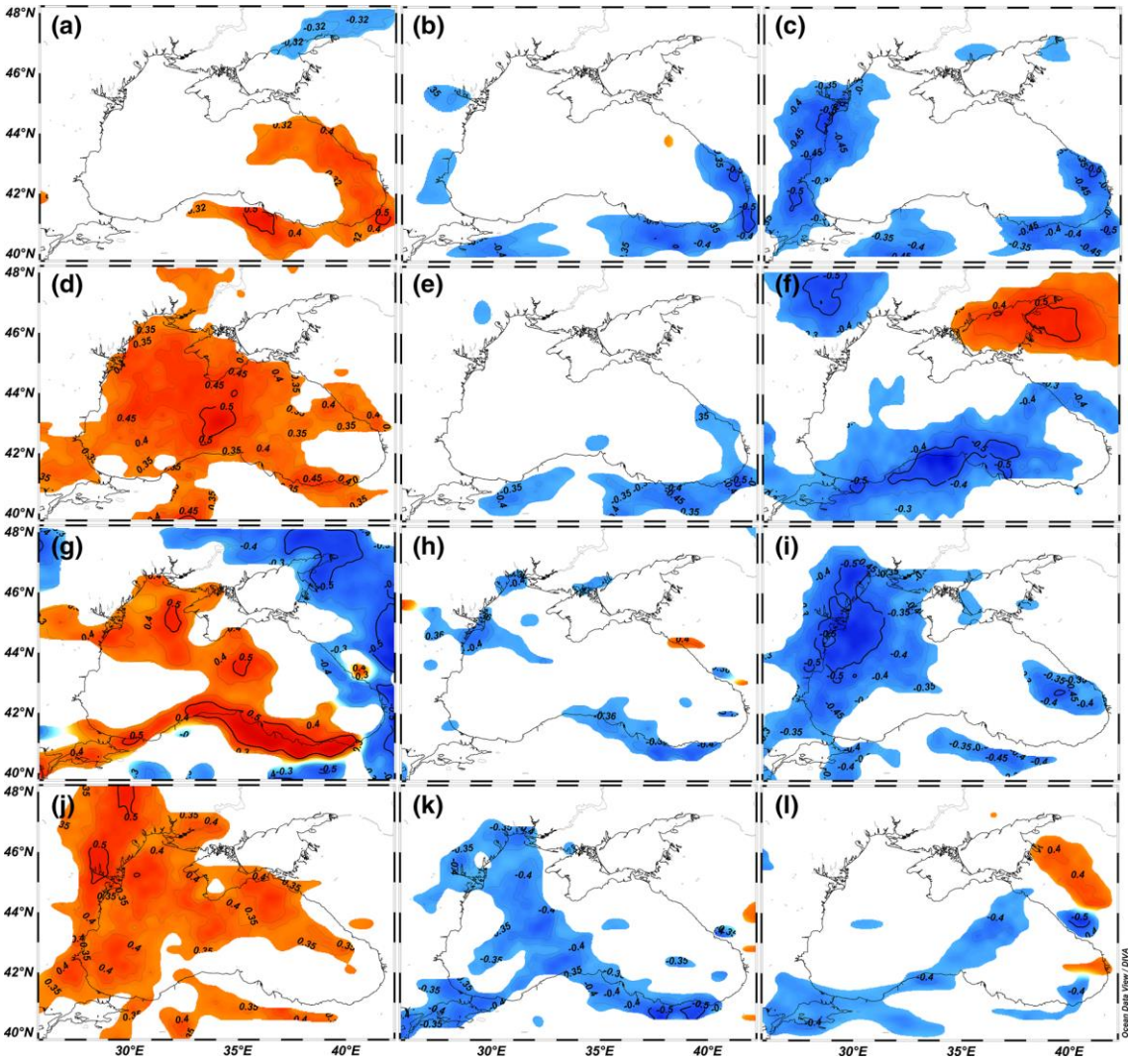


Figure 4.13 Correlation coefficients between teleconnection patterns and the $U10_{95}$ over the Black Sea for both ERA-I and CFSR reanalysis data. a) [ERAI]–[EA], b) [ERA-I]–[EA/WR], c) [ERA-I]–[NAO], d) [ERA-I]–[PNA], e) [ERA-I]–POL], f) [ERA-I]–[SCA], g) [CFSR]–[EA], h) [CFSR]–[EA/WR], I) [CFSR]–[NAO], j) [CFSR]–[PNA], k) [CFSR]–[POL], l) [CFSR]–[SCA]

Studying the long-term trends in $U10_m$ and $U10_{95}$ over the Black Sea by using both ERA-I and CFSR data enhanced the understanding of how these two major reanalysis data differ from each other. The inter-comparison of two reanalysis data is also the focus of some other researchers. Stopa and Cheung (2014) compared wind speeds from ERA-I and CFSR by using the same set of buoy observations from several locations over the global oceans. They concluded that both data provide a reasonably good match with the buoy and altimetry observations. But ERA-I slightly underestimates and the CFSR slightly overestimates the

measurements. Although no observational wind data were used in this study, our findings confirmed Stopa and Cheung (2014) for the Black Sea by showing that CFSR gives approximately 10% higher long-term average wind speeds than ERA-I over the Black Sea.

Results of the analysis of the long-term averaged U10 over the Black Sea from CFSR indicated that the highest values exist in the Sea of Azov and the northwestern offshore parts of the basin. This finding is found to be consistent with the results presented by Rusu et al. (2018). The magnitude of the highest long-term U10 is estimated as 7.35 m/s in this study whereas it is reported to be 7.29 m/s in Rusu et al. (2018). Slight differences are caused by the analysis of different terms. Rusu et al. (2018) studied 23-year data (1987-2009) whereas it is extended to 38 years (1979-2016) in the present study. Ganea et al. (2019) reported a statistically significant decreasing trend with a rate of -0.01 cm/decade for annual $U10_m$ at the offshore western Black Sea by analyzing ERA-I reanalysis data between 1983 and 2017 whereas our findings indicate no significant trend.

The findings presented in this study are in line with the long-term variations of annual U10 at selected locations over the Black Sea presented by Akpinar and Bingolbali (2016) based on CFSR reanalysis data for 31 years between 1979 and 2009. It is explored that the annual $U10_m$ over the coasts of the Crimean Peninsula represents a significant increasing trend of 1.33 cm/s/yr in the study period (Akpinar and Bingolbali, 2016). In the present study, U10 in the same location shows a significant increasing trend of 1.41 cm/s/yr for the term between 1979 and 2016. Besides the authors reported an increasing trend of 0.71 cm/s/yr for the south-eastern coasts of the Black Sea, where it is on par with the ones illustrated in the present study as 0.74 cm/s/yr. Severe wind states represented by annual maximum wind speeds were also investigated by Akpinar and Bingolbali (2016), however, it is not possible to make a direct comparison between them and the results of the present study in which the U1095 are evaluated.

Zainescu et al. (2017) studied the storm variability along the north-western coasts of the Black Sea since 1949 and evaluated the influence of different teleconnection indices. The authors reported a statistically significant correlation of -0.76 between the NAO and the storm variability at the Danube Delta coast which is confirmed by our findings in this study for the partly different period between 1979-2016 giving r values of -0.6.

Although the findings of this study are well in line with the previous studies, some slight differences exist due to the different temporal coverages of the studies and consideration of different representative variables ($U10_{max}$, $U10_{95,}$ or some specific definition of sea storms combining wind and wave properties).

4.1.2 Long-Term Variations of Significant Wave Heights over the Black Sea

Wave height is a very important parameter for coastal engineers, in designing new offshore structures and planning maritime activities. Also, the wave climate affects coastal areas like deltas, beaches, and low-level zones. That's why it is very important to explore the changes in wave climate due to climate change effects. To understand the long-term variations of atmospheric forcing over the Black Sea Basin, the Annual mean and 95^{th} percentile SWH were investigated and their trend between 1979 and 2016 was clarified.

4.1.2.1 Spatial Variations of Long-Term trends in Annual Significant Wave Heights

The spatial distribution of averaged SWHs over the Black Sea Basin was presented in Figure 4.14, which says that higher annual mean SWHs are seen on the Sea of Azov and offshore northwestern Black Sea. On the other hand, the smallest mean SWH comes out in the eastern regions of the Black Sea. Over the Black Sea Basin, by considering annual mean values; the minimum SWH is 0.43 m, the mean SWH is 0.73 m and the maximum SWH is 0.93 m.

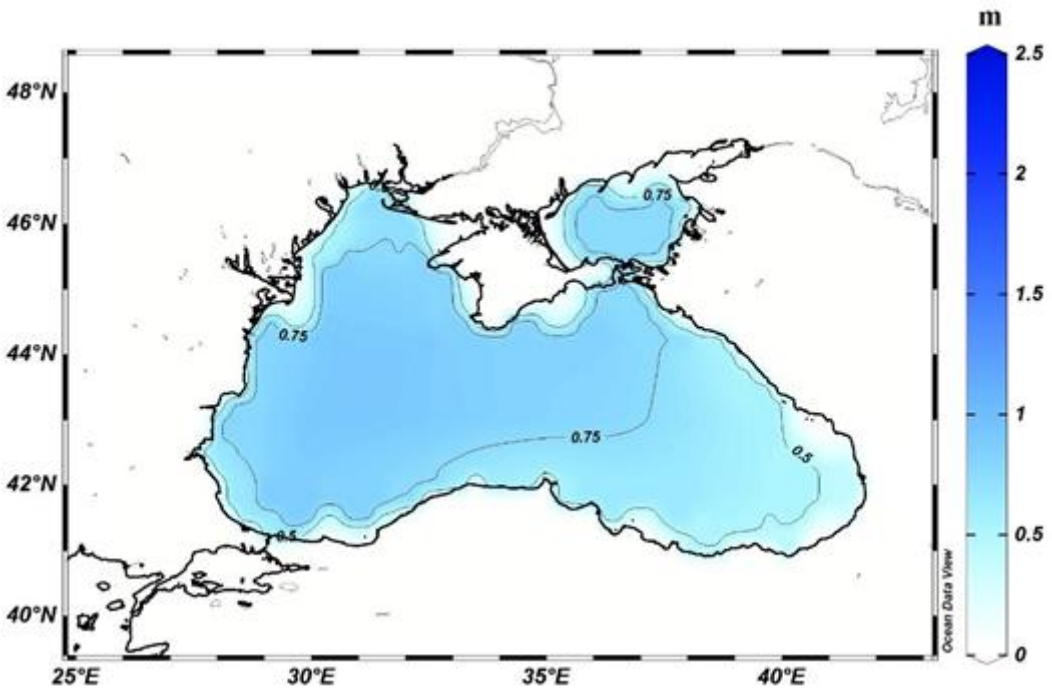


Figure 4.14 Long-term averaged Annual SWHs considering 38 years period (1979–2016) over the Black Sea (ERA-Interim)

Long-term variations of annual mean SWHs over the Black Sea Basin were presented spatially in Figure 4.15. There are decreasing trends only on the Sea of Azov for SWH up to 0.002 m/y. On the Basin of Black Sea, we see just an increasing annual mean SWH. In the eastern regions, increasing trends are relatively high and the values reach up to 0.004 m/yr. On the basin of the Black Sea, the mean increasing trend in SWH is 0.002 m/yr.

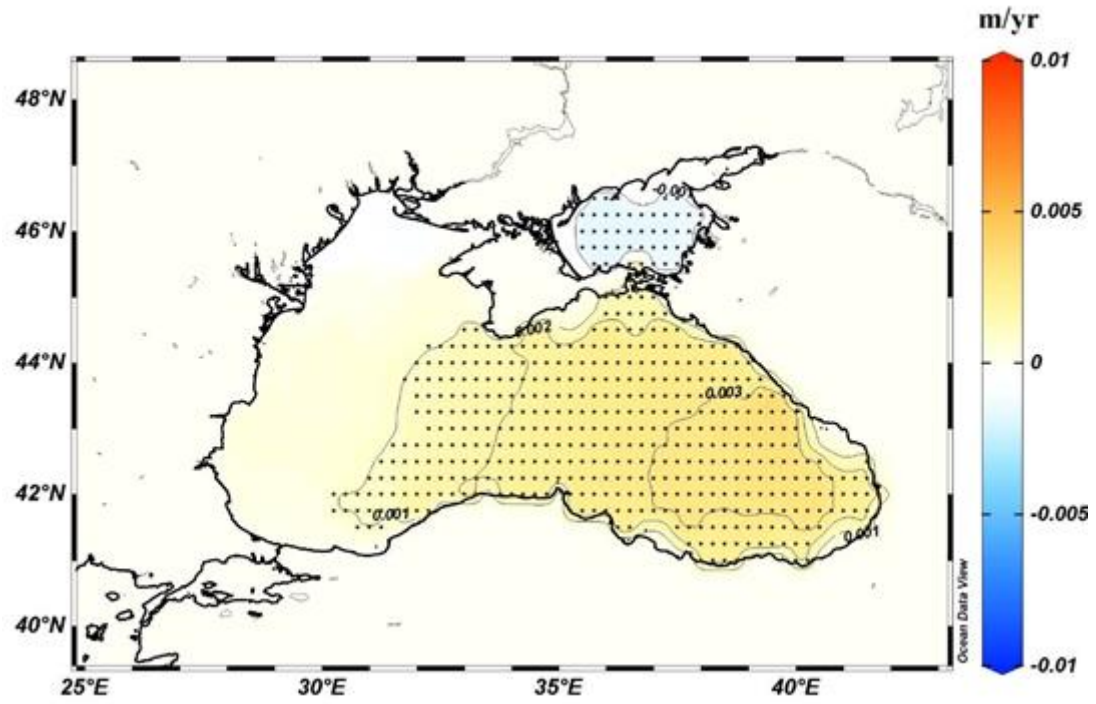


Figure 4.15 Spatial variability of long-term trends in averaged Annual SWH. Black dots indicate locations with statistically significant trends at the 90% or higher confidence level

The spatial distribution of 95th percentile SWH over the Black Sea Basin was presented in Figure 4.16. From the figure, we can figure out that higher annual 95th percentile wave heights are seen on the Sea of Azov and offshore western Black Sea. On the other hand, in the southeastern regions of the Black Sea, relatively smaller annual 95th percentile wave heights are detected. Over the Black Sea Basin, by considering annual 95th percentile wave heights; the minimum 95P wave height is 1.03 m, the mean 95th percentile wave height is 1.78 m, and the maximum 95P wave height is 2.29 m.

Long-term variations of annual 95th percentile SWHs over the Black Sea Basin were presented spatially in Figure 4.17. There are decreasing trends on the Sea of Azov for an annual 95 P SWH up to 0.007 m/yr. In addition, we see decreasing trends in the southwestern regions reaching 0.004 m/yr. In the eastern regions of the Black Sea Basin, there are increasing trends and they are relatively high, the values can reach up to 0.007 m/yr.

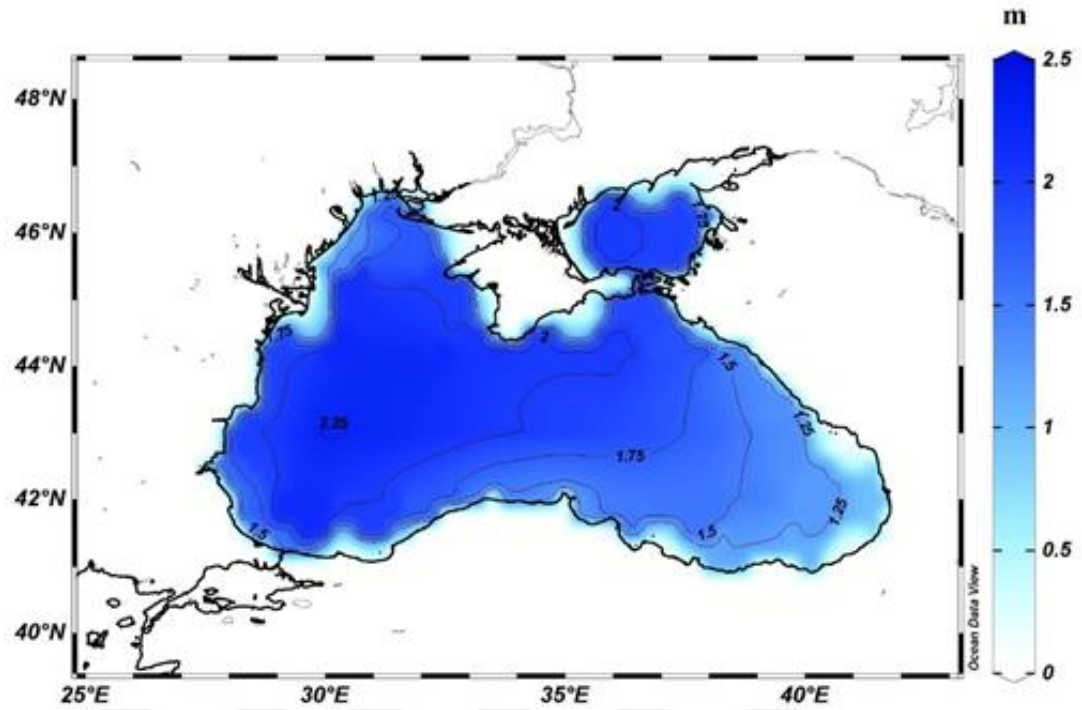


Figure 4.16 Long-term 95th percentile Annual SWHs considering 38 years period (1979–2016) over the Black Sea (ERA-Interim)

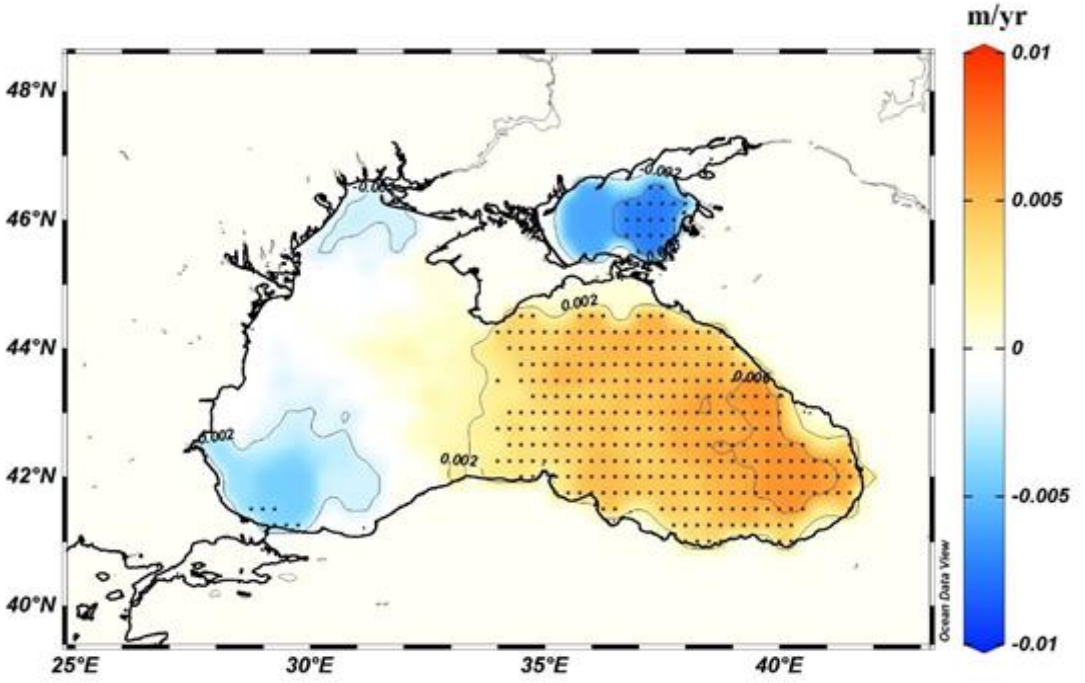


Figure 4.17 Long-term variations of 95th percentile Annual SWHs considering 38 years period (1979–2016) over the Black Sea (ERA-Interim). Black dots indicate locations with statistically significant trends at the 90% or higher confidence level

The Spatial variability of long-term trends in averaged and 95th percentile Annual SWHs over the Black Sea Basin is also consistent with the study conducted by Aydoğan and Ayat (2018). In this study, the trend values and their significances were also calculated by the Theil-Sen estimator and Mann Kendall Tests. Wave fields were generated by using a third-generation spectral wave model, which is DHI's MIKE 21 SW Model. The model used 38 years of wind field data between the years 1979 and 2016 from ERA-Interim. SWH values from the spectral wave model were normalized with the mean value at each data point. For trend calculations, Normalized Significant Wave Heights (NSWH) were used (Aydoğan and Ayat, 2018).

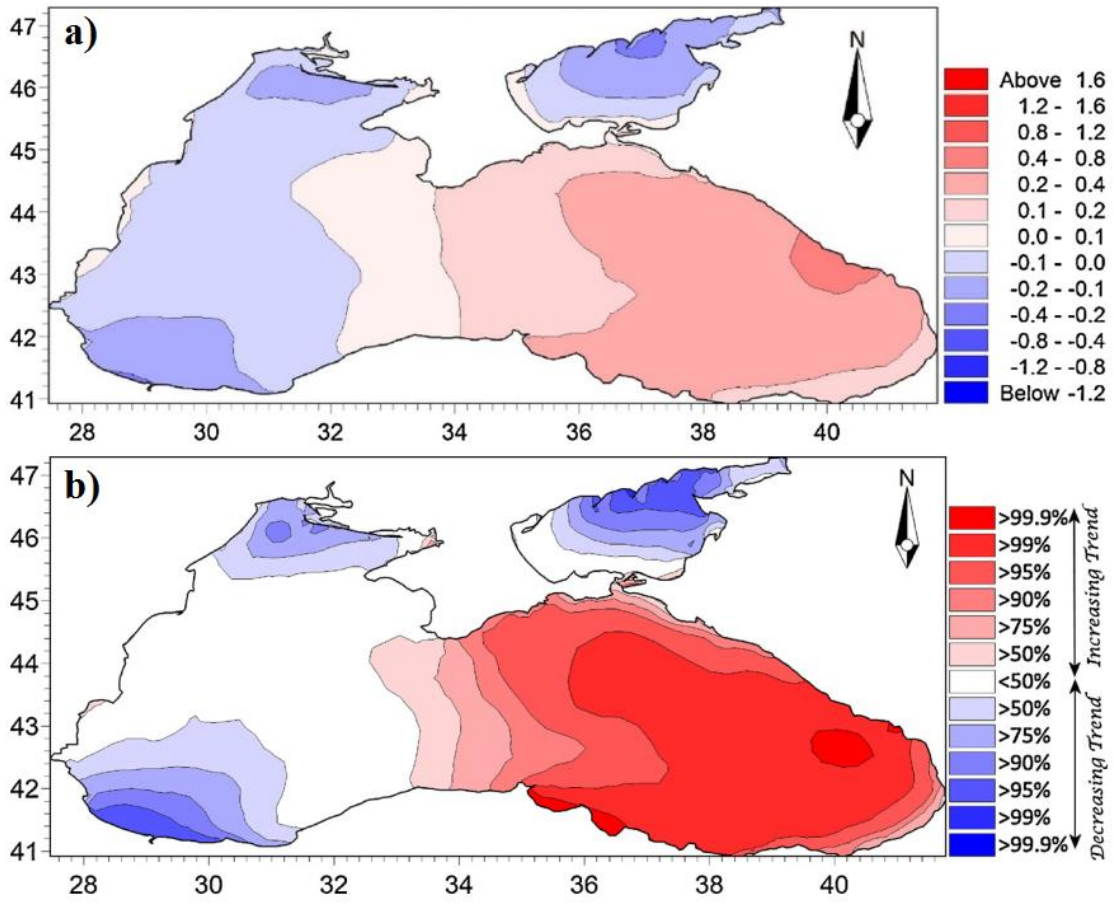


Figure 4.18 a) Spatial distribution of the trends for annual NSWHs (%/year) based on the Theil-Sen method. b) The significance of the long-term trends in annual mean NSWHs based on the Mann-Kendall test for different confidence levels (Aydoğan and Ayat, 2018)

Figure 4.18 shows the spatial distribution of the long-term trends of the mean percentile NSWHs and their significance. In the western regions of the Black Sea and the Sea of Azov, there are significant negative trends for NSWHs. The trend values can reach down to -0.4%/yr. On the other hand, there are significant positive trends on the eastern side of the basin and here, the trend values can be seen up to 0.85%/yr (Aydoğan and Ayat, 2018).

Additionally, Figure 4.19 represents the spatial distribution of the long-term trends of the 95th percentile NSWHs and their significance. In some northern regions and the Sea of Azov, there are significant negative trends for NSWHs. The trend values can reach down to -0.2%/yr. On the other hand, there are significant positive trends on the northeastern side of the basin and here, the trend values can be seen up to 0.4%/yr (Aydoğan and Ayat, 2018).

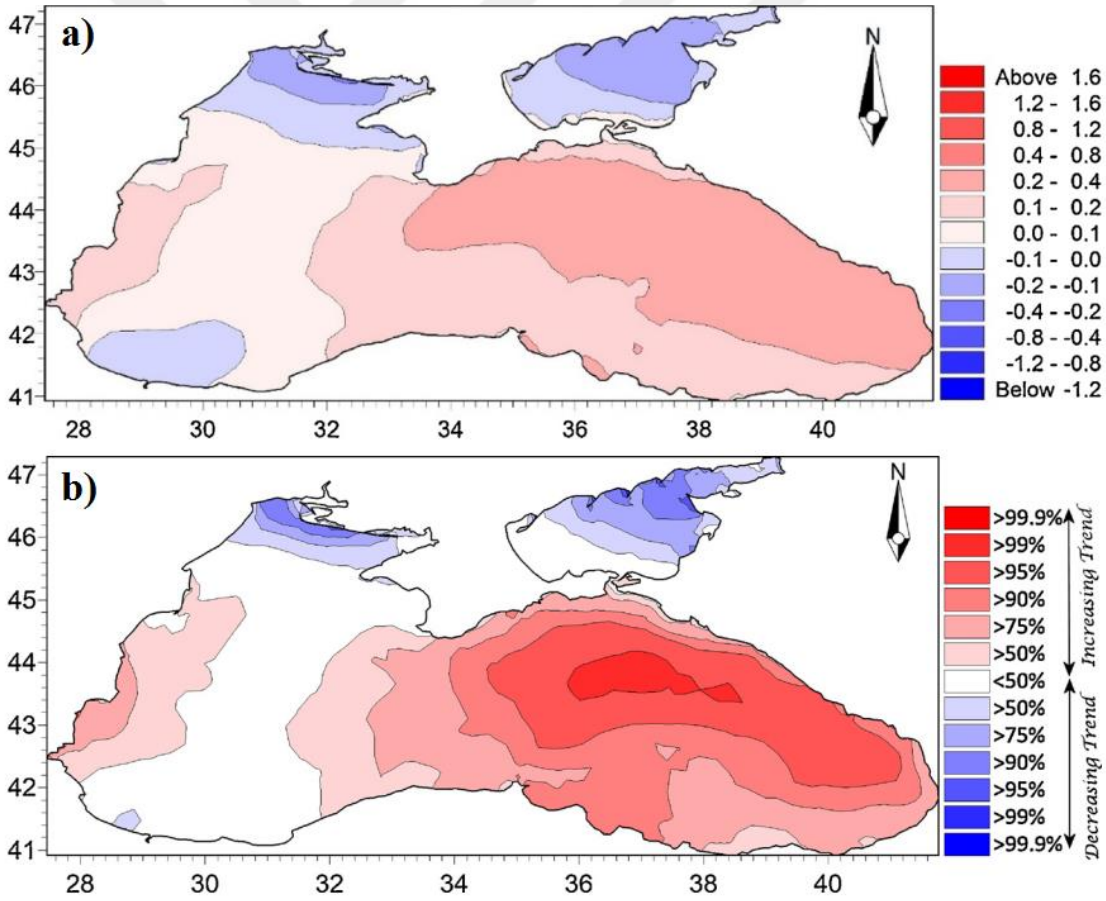


Figure 4.19 a) Spatial distribution of the long-term trends for 95th percentile NSWHs (%/year) based on the Theil-Sen method. b) The significance of the long-term trends in the annual 95th percentile NSWHs based on the Mann-Kendall test for different confidence levels (Aydoğan and Ayat, 2018)

4.1.2.2 Spatial Variations of Long-Term Trends in Monthly Significant Wave Heights

An important study to determine the variations of long-term trends in monthly SWH on monthly basis to define seasonal variations is conducted by Aydoğan et al. (2018). In the study, the trend values and their significances were also calculated by the Theil-Sen estimator and Mann Kendall Tests. Wave fields were generated by using a third-generation spectral wave model, which is DHI's MIKE 21 SW Model. The model used 38 years of wind field data between the years 1979 and 2016 from ERA-Interim. SWH values from the spectral wave model were normalized with the mean value at each data point. In the trend calculations Normalized, Significant Wave Heights (NSWH) were used.

The trend values for monthly mean values of NSWHs are presented spatially in Figure 4.20 to present seasonal variations. The significance of these trends were also shown in Figure 4.21. In Figure 4.20, it is seen that the steepest positive trends are located in the northeastern Black Sea. In these regions which correspond to Georgia and Russian Coasts, the positive trend values reach up to 1.6 %/yr in September. For the western regions of the Black Sea, which is near Bulgaria and Romania, the positive trends up to 1.2 %/yr are also seen in September. On the other hand, decreasing trends that reach down to -1.2 %/yr were evaluated near the coasts of Istanbul in the winter months. For the whole basin, positive trends are steeper than negative ones. Positive trends are more prevalent than negative trends in April, August, September, and October, whereas negative trends are more common in May and December (Aydoğan and Ayat, 2018).

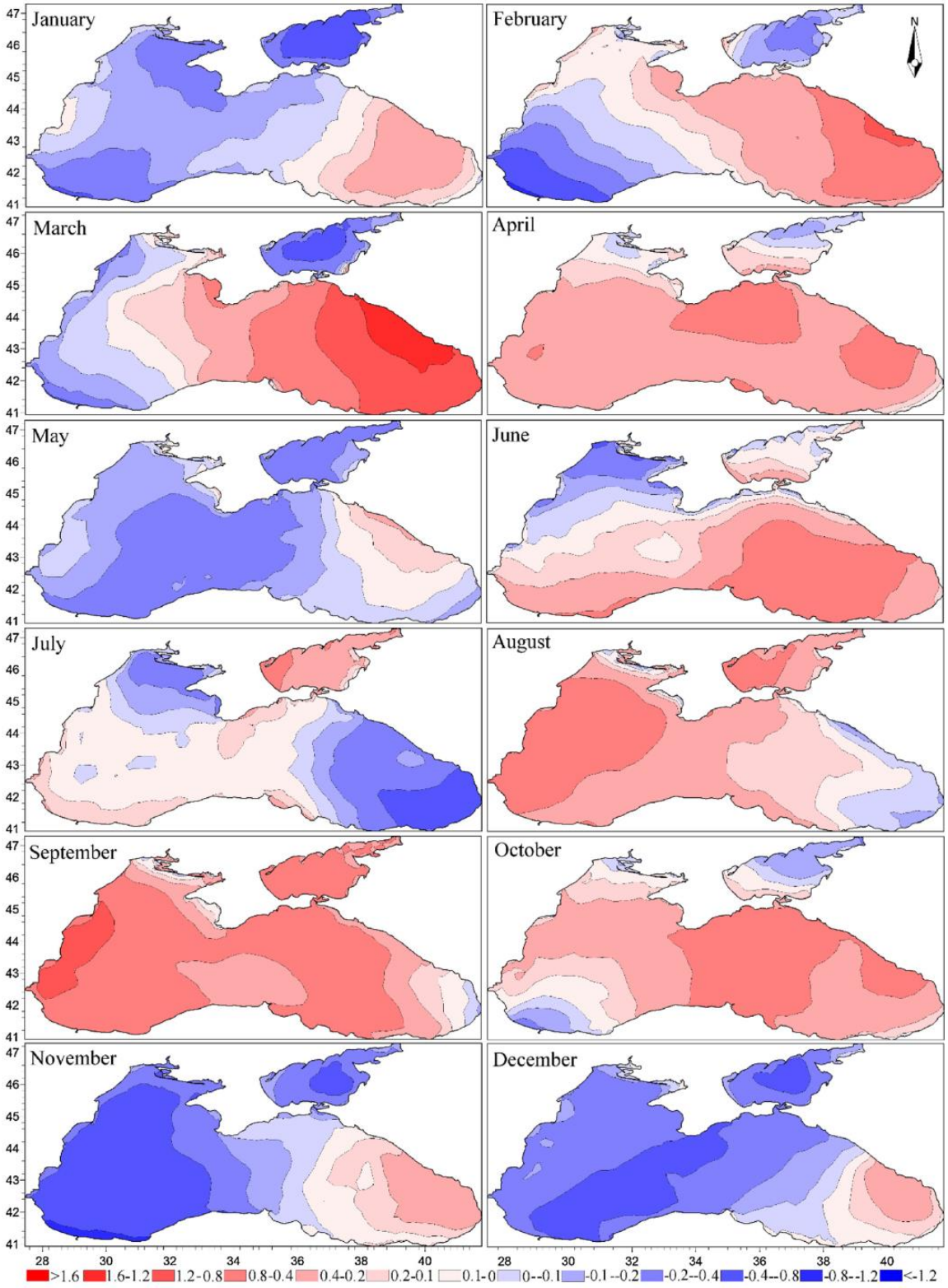


Figure 4.20 Spatial variability of long-term trends in mean NSWHs for each month (%/year) on a monthly basis (Aydoğan and Ayat, 2018)

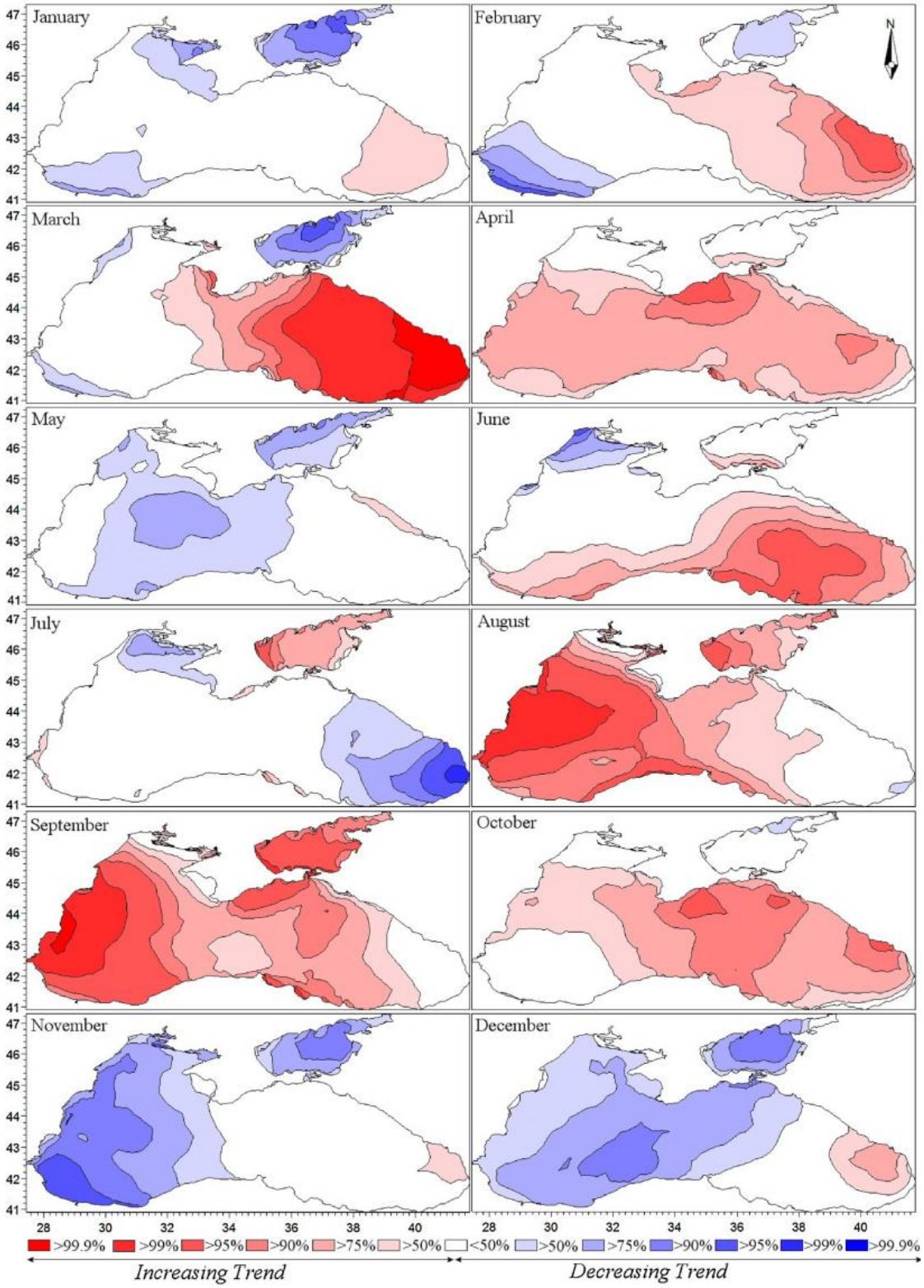


Figure 4.21 Spatial distribution of the trend significance for mean NSWHs for each month at different confidence levels based on the Mann-Kendall test (Aydoğan and Ayat, 2018)

Aydoğan and Ayat (2018) also explored the long-term trends for 95th percentile NSWHs over the Black Sea Basin and the results are represented in Figure 4.22. The existence of positive values for long-term trends during August and September is more common whereas more negative trends are seen during February, March, May, and December. It was declared that 95th percentile NSWHs have more significant trends than mean NSWHs have for April, August, and October. We see significant increasing trends up to 1.2 %/yr at various parts of the Black Sea in March, April, August, September, and October. For the northeastern Black Sea, it is also possible to define positive trends around 1.6 %/yr in May. On the other hand, In the northern regions of the Black Sea; the value of negative significant rends for 95th percentile NSWHs reach down to -0.8 %/year in January, February, March, May, June, and December (Aydoğan and Ayat, 2018).

To find out the relation of the long-term variations of NSWHs with climate indices, Aydoğan and Ayat (2018) also conducted several analyses. Main oscillation patterns North Atlantic Oscillation (NAO), Arctic Oscillation (AO), Antarctic Oscillation (AAO), Atlantic Multi-decadal Oscillation (AMO), Pacific North American (PNA), East Atlantic (EA), East Atlantic/West Russia (EA/WR), Scandinavia (SCAND), and Niño3 indices were analyzed to find their correlations with long-term variations of both mean and 95th percentile NSWHs. The Pearson correlation values greater than 0.3 were regarded as significant and the results were presented in Figure 4.24.

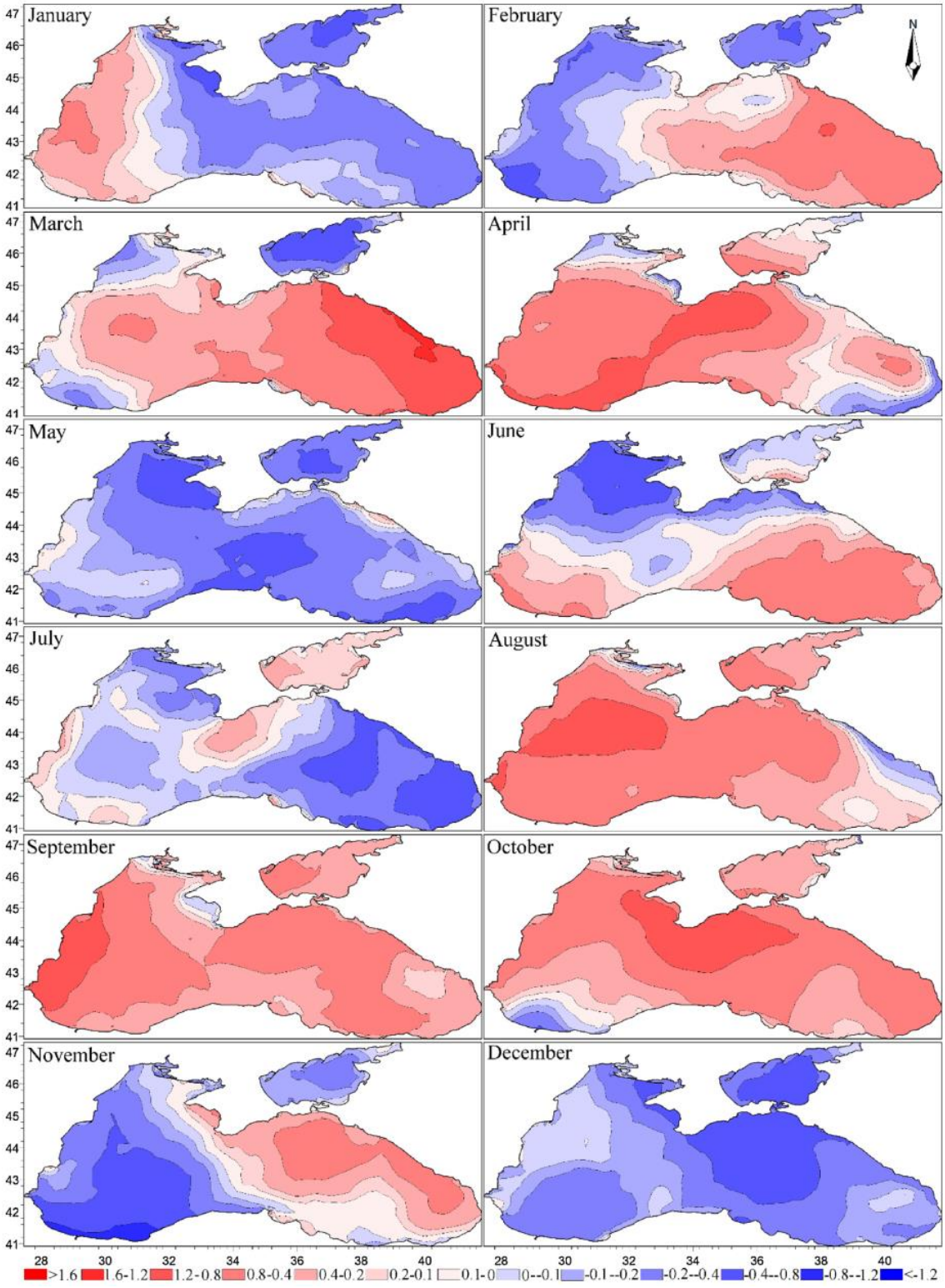


Figure 4.22 Spatial variability of long-term trends in 95th percentile NSWHs for each month (%/year) on a monthly basis (Aydoğan and Ayat, 2018)

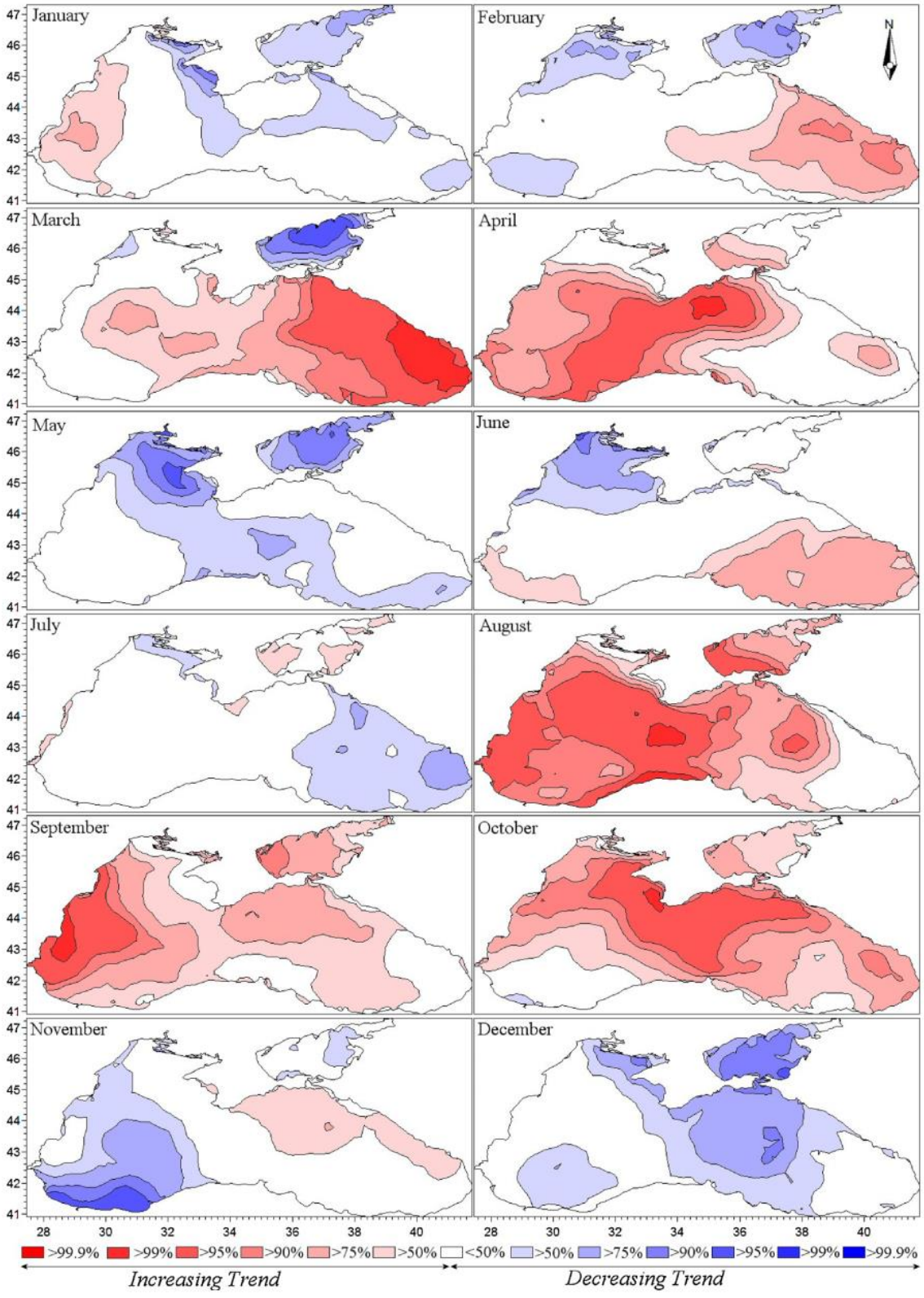


Figure 4.23 Spatial distribution of the trend significance for 95th percentile NSWHs for each month at different confidence levels based on the Mann-Kendall test (Aydoğan and Ayat, 2018)

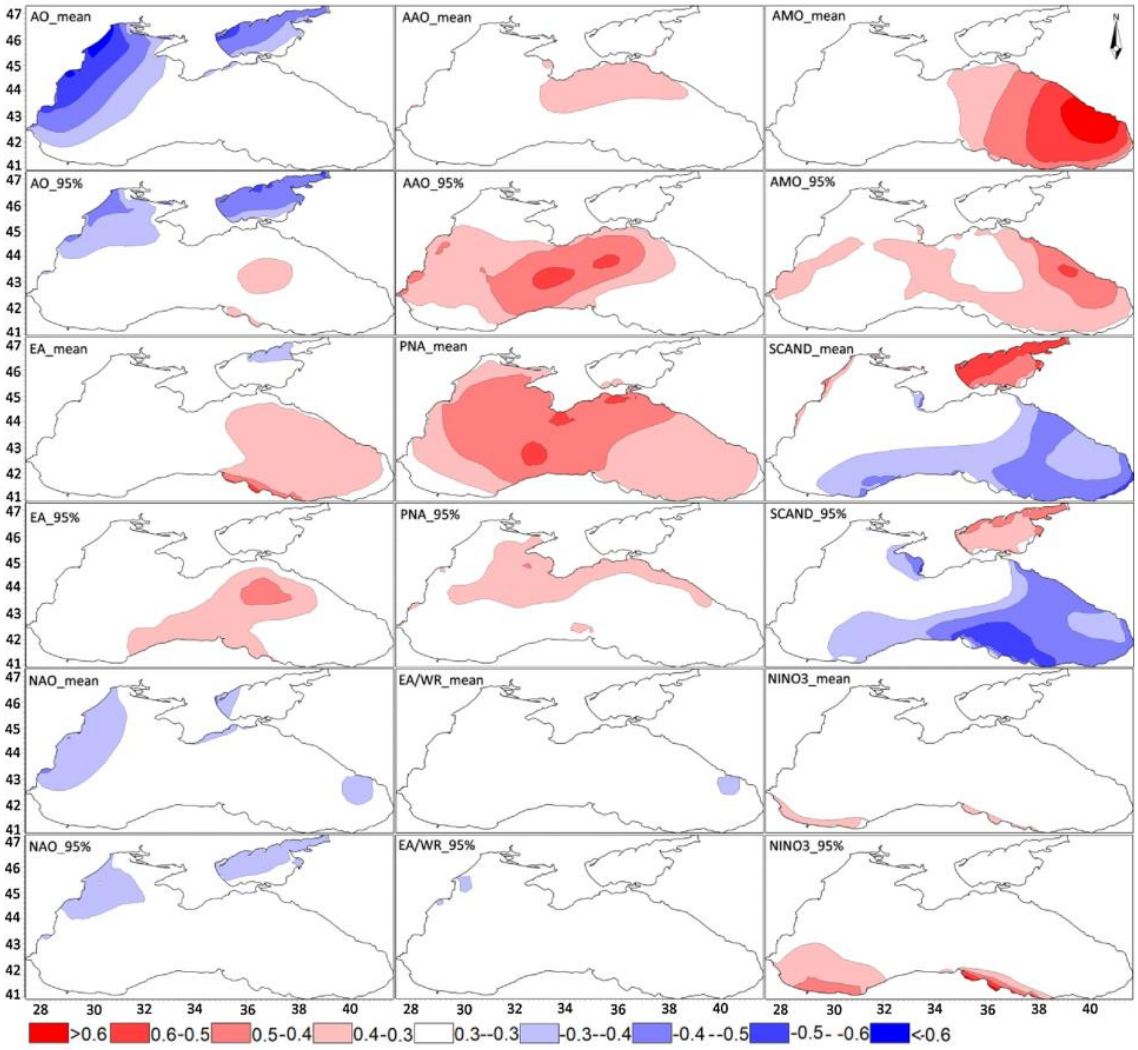


Figure 4.24 Correlations of Black Sea SWH and different oscillation patterns for mean and severe sea states (Aydoğan and Ayat, 2018)

From Figure 4.24, both mean and 95th percentile SWHs on the northwestern Black Sea represent negatively correlated relations with AO and NAO. Especially, AO has correlation values of more than 0.6 with mean SWHs. Besides, AAO reaches positive correlation values up to 0.6 with 95th percentile SWHs over the central areas of the Basin. AMO and EA both have an influence on mean SWH with a positive correlation value reaching 0.6 in Eastern Regions of the Black Sea. Severe sea conditions are highly correlated with AMO in eastern areas where the maximum values are around 0.6. When considering PNA, there are positive correlation values over the central Black Sea for mean SWHs up to 0.6, whereas there are limited correlations between severe conditions. For mean, SWHs SCAND represented positive correlations with negative ones together. Over the Sea of

Azov, there are positive correlations up to 0.6, while in southeastern regions, negative correlations down to 0.5 were detected. SCAND and 95th percentile SWHs also have similar patterns but lower correlation values. EA/WR has slight correlations for both mean and severe sea states. Lastly, Nino3 represents powerful positive coalitions up to 0.6 with both mean and severe sea conditions near the southern coastlines of the Black Sea.

4.1.3 Long-Term Variations of Sea Surface Temperatures over the Black Sea

To understand the long-term variations of atmospheric forcing over the Black Sea Basin, the Annual mean and 95th percentile SST were investigated, and their trend between 1979 and 2016 was clarified. The spatial distribution of averaged SSTs over the Black Sea Basin were presented in Figure 4.25. As seen in Figure 4.25, the bigger mean SST is seen in the southeastern regions of the Basin. On the other hand, in the northwestern waters of the Basin and on the Sea of Azov, the SST is relatively smaller. Over the Black Sea Basin, by considering annual mean values; the minimum SST is 12.4 °C, the mean SST is 15.2 °C and the maximum SST is 16.9 °C.

Long-term variations of annual mean SSTs over the Black Sea Basin were presented spatially in Figure 4.26. There are decreasing trends only on the Sea of Azov for SST down to -0.02 °C/yr. On the Basin of Black Sea, we see just increasing annual mean SSTs. In the eastern regions, increasing trends are relatively high and the values reach up to 0.07 °C/yr. On the basin of the Black Sea, the mean increasing trend in SST is 0.036 °C/yr.

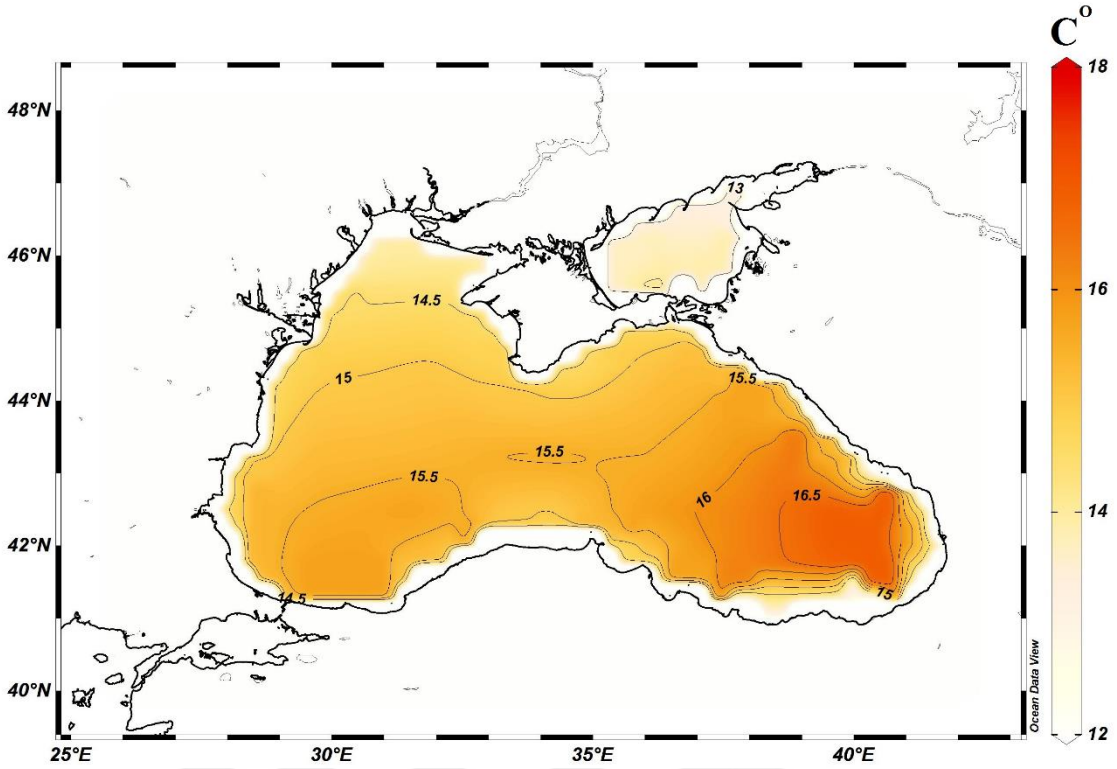


Figure 4.25 Long-term averaged Annual SSTs considering 38 years period (1979–2016) over the Black Sea (ERA-Interim)

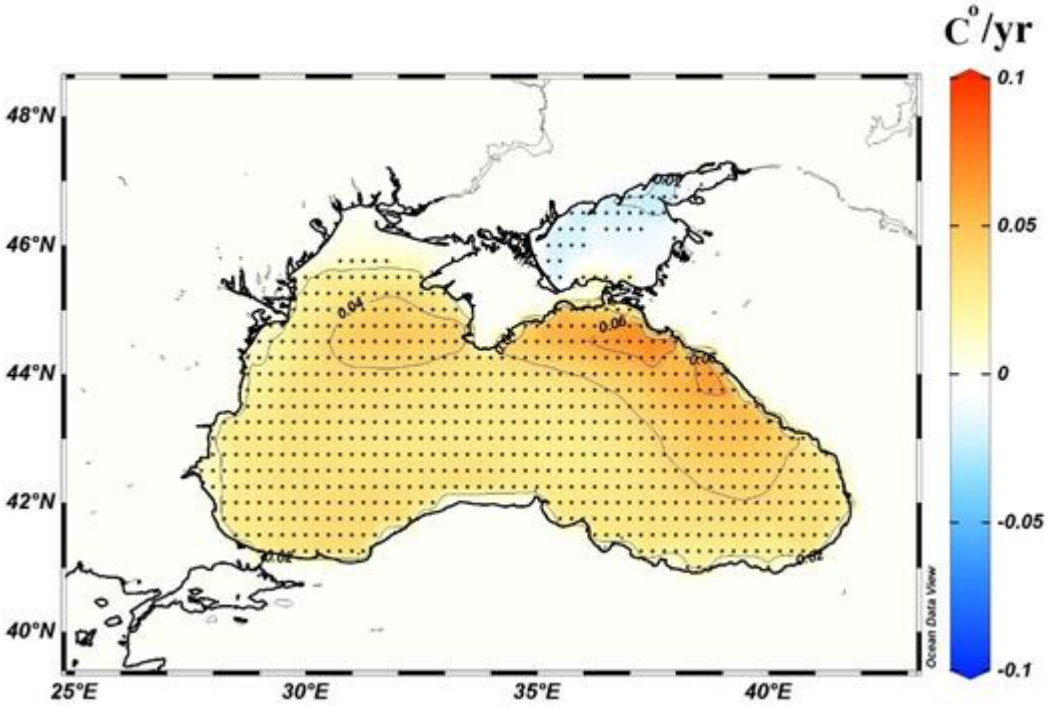


Figure 4.26 Spatial variability of long-term trends in averaged Annual SSTs. Black dots indicate locations with statistically significant trends at the 90% or higher confidence level

To understand the extreme SST and their variations, annual 95th percentile SST were investigated and their trends between 1979 and 2016 were clarified and the results were presented in Figure 4.27. As seen in Figure 4.27, the bigger annual 95th percentile SST is also seen in the south-eastern regions of the Basin. On the other hand, in the north-western waters of the Basin and on the Sea of Azov, the annual 95th percentile SST are relatively smaller. Over the Black Sea Basin, the minimum SST is 21.9 °C, the mean SST is 25.0°C and the maximum SST is 26.4 °C. The spatial distribution of extreme SST is similar to one of the mean SST values.

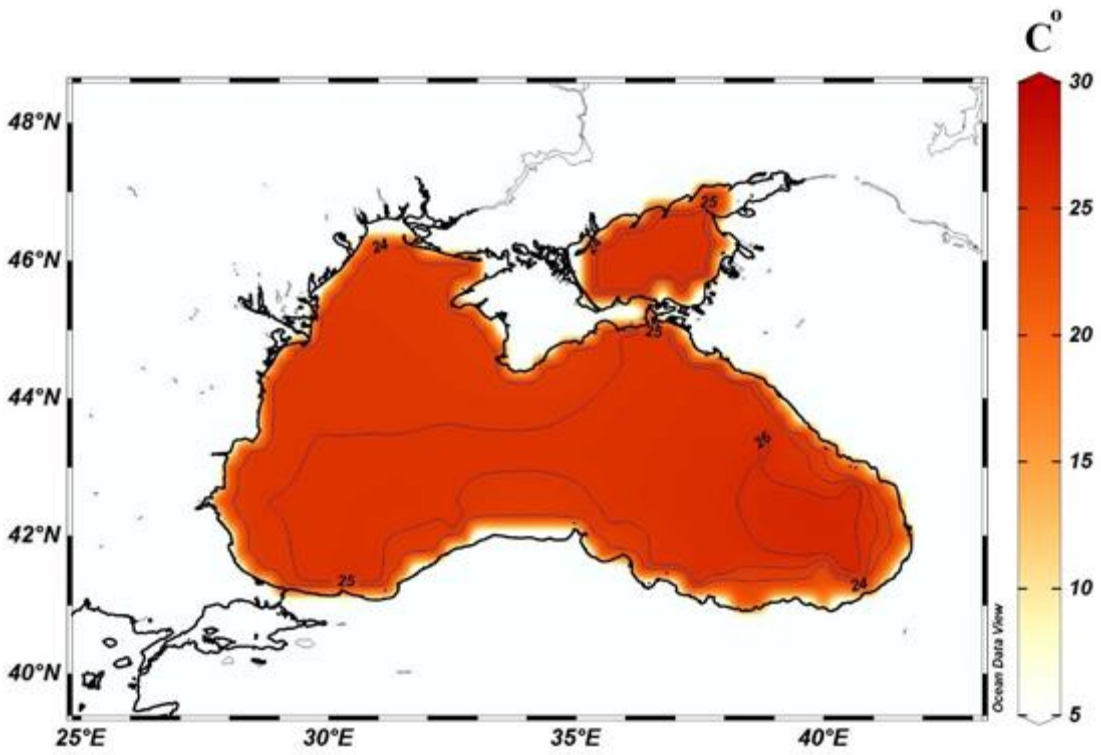


Figure 4.27 Long-term annual 95th percentile Annual SSTs considering 38 years period (1979–2016) over the Black Sea (ERA-Interim)

Long-term trends of annual 95th percentile SSTs over the Black Sea Basin were presented spatially in Figure 4.27. There are increasing trends all over the Basin of the Black Sea and the Sea of Azov. The minimum increasing trend of 95th percentile SST is 0.05 °C/yr, and the mean increasing trend of 95th percentile SST

is 0.08°C/yr. On the basin of the Black Sea, the maximum increasing trend in 95P SST is detected as 0.11 °C/yr.

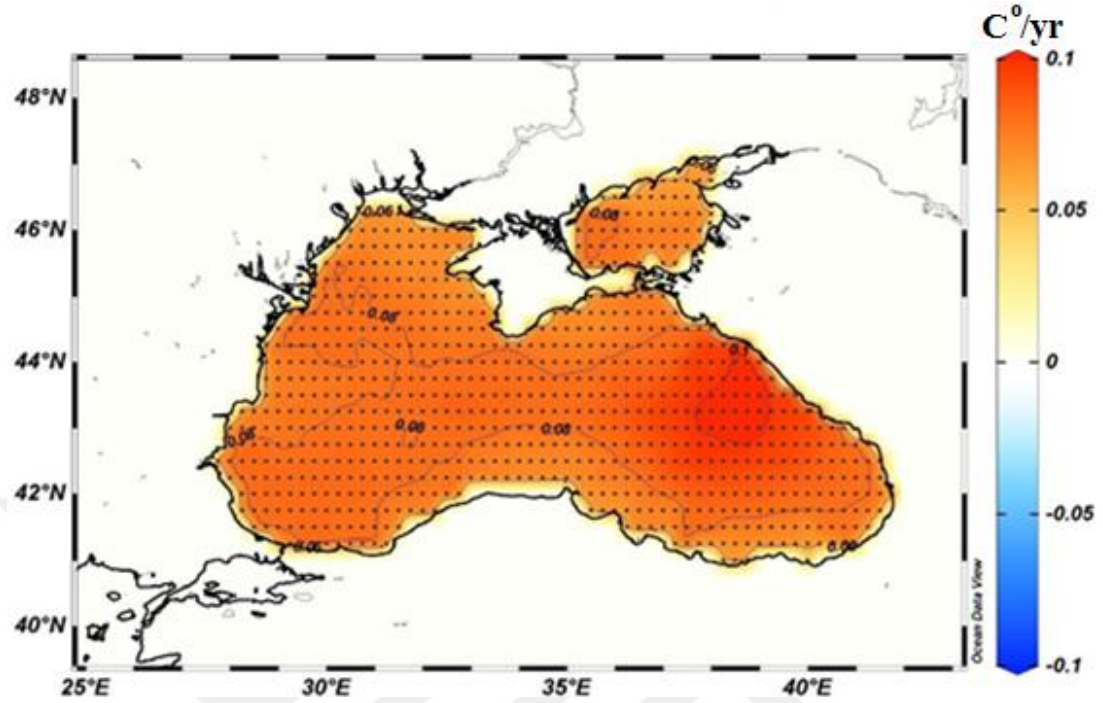


Figure 4.28 Spatial variability of long-term trends in 95th percentile Annual SSTs. Black dots indicate locations with statistically significant trends at the 90% or higher confidence level

4.1.4 Long-Term Variations of Precipitation over the Black Sea

As an important atmospheric parameter, it is also very important to understand the long-term variations of precipitation over the Black Sea Basin. Here, to explore the precipitation climate over the Black Sea Basin, annual total precipitation and the annual number of days with precipitation were investigated. Annually averaged values and their trend were found to figure out the situation for the years between 1979 and 2016. The spatial distribution of average annual total precipitation considering 38 years period (1979–2016) over the Black Sea is presented in Figure 4.29 The least amount of annual total precipitation is seen in the northern regions of the Black Sea Basin, with a value set down to 338 mm. In addition, the most amount of annual total precipitation is detected over the southeastern regions of the study area. Here, the maximum annual total precipitation is 2475 mm. The mean amount of annual total precipitation over the Black Sea Basin can be concluded as 680 mm.

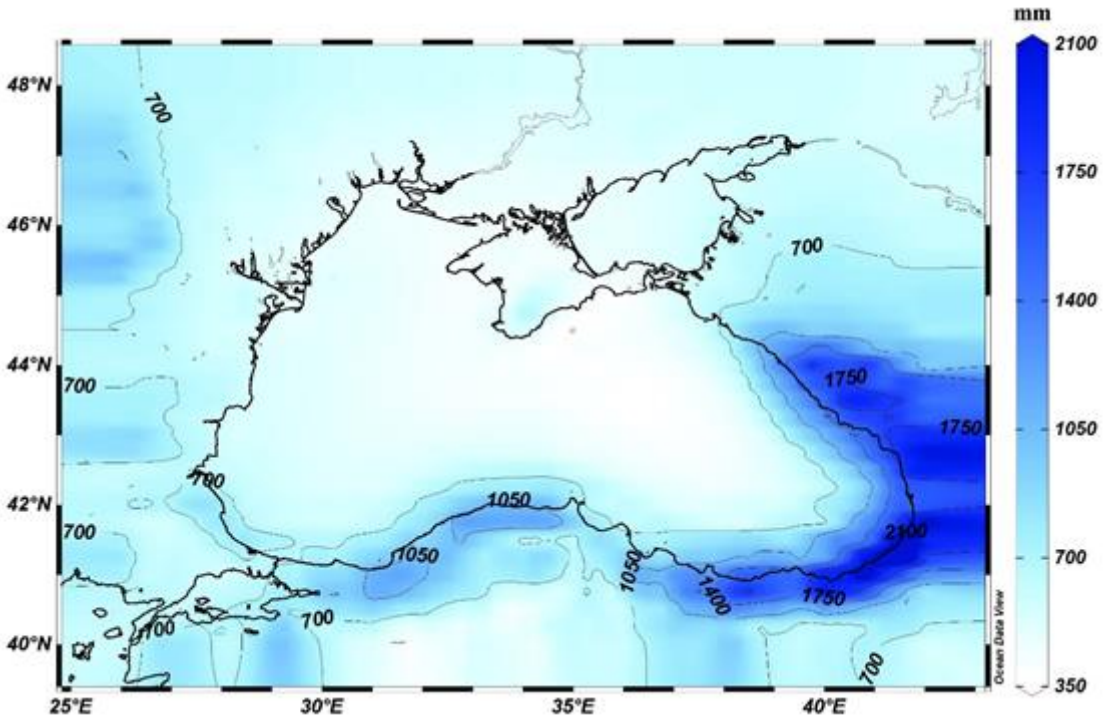


Figure 4.29 Long-term average Annual Total Precipitation considering 38 years period (1979–2016) over the Black Sea (ERA-5)

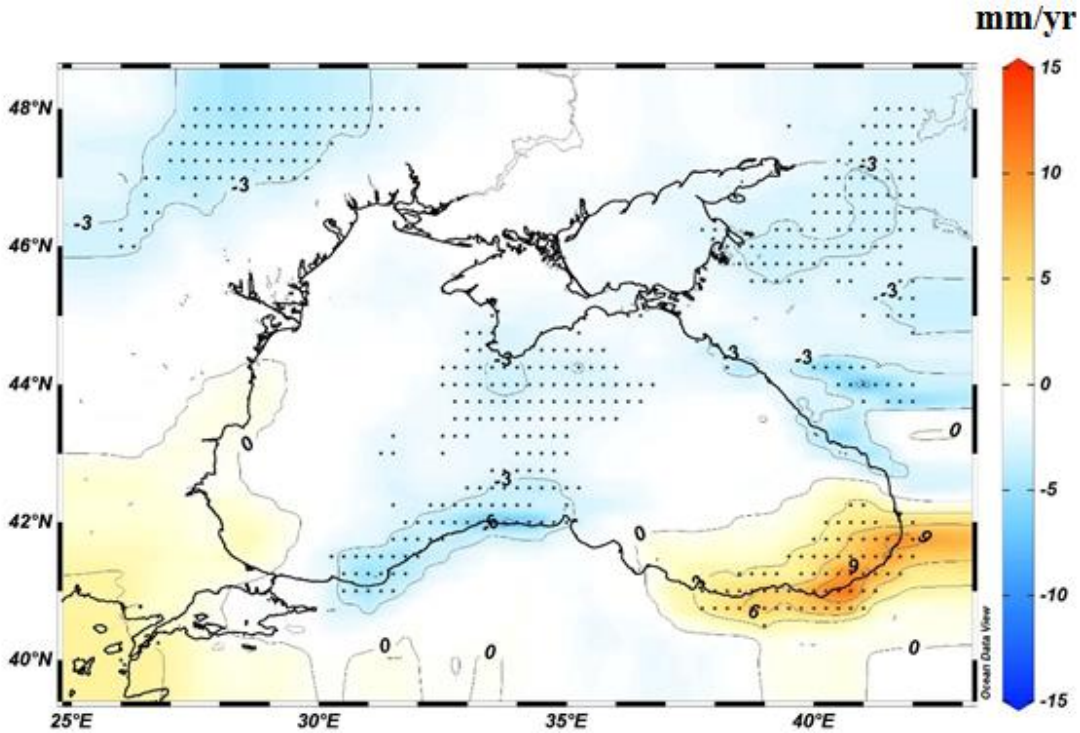


Figure 4.30 Long-term variations of annual total precipitations considering 38 years period (1979–2016) over the Black Sea (ERA-5). Black dots indicate locations with statistically significant trends at the 90% or higher confidence level

Long-term variations of annual total precipitations considering 38 years period (1979–2016) over the Black Sea were investigated and the results were presented in Figure 4.30. On the Sea of Azov, on the central offshore of the Black Sea, south-western coasts and south-eastern coasts represent decreasing trends in annual total precipitations. Over the western coasts and eastern coasts, we see increasing trends.

The minimum decreasing trends are seen on the southeastern coasts and the values reach down to -6.6 mm/yr, on the other hand, the maximum increase in annual total precipitation reaches 2.6 mm/yr on the western coasts. If we consider the mean annual total precipitation over the study area as 261 mm, the trends can be evaluated as small. Even in some areas, the trends are around zero and insignificant. From this point of view, it is possible to conclude that; annual total precipitations did not represent significant changes in 38 years period (1979–2016).

The spatial distribution of average annual numbers of days with precipitation considering 38 years period (1979–2016) over the Black Sea is presented in Figure 4.31. The least annual number of days with precipitation is seen in the north-western regions of the Black Sea Basin, with a value down to 110 days. On the other hand, the annual number of days with precipitation is highest over the southeastern regions of the study area. Here, the maximum annual number of days with precipitation is 253 days. The mean annual number of days with precipitation over the Black Sea Basin can be concluded as 163.

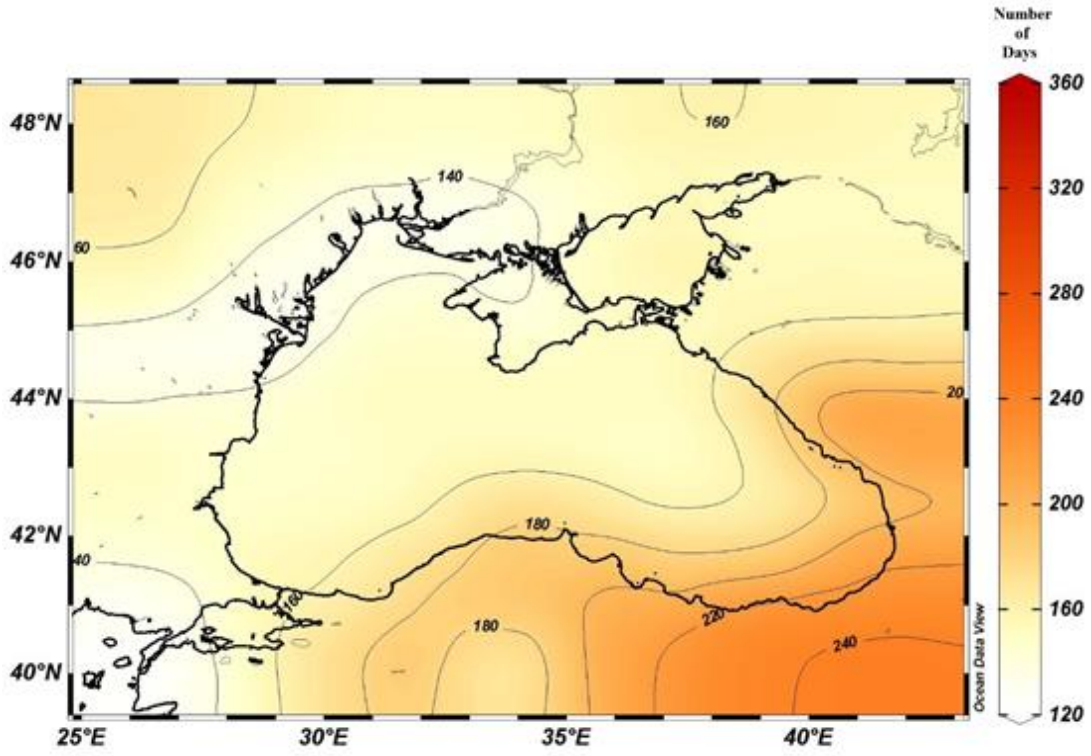


Figure 4.31 Long-term averaged annual number of days with precipitation considering 38 years period (1979–2016) over the Black Sea (ERA-5) precipitations in 38 years period (1979–2016)

Long-term variations of the annual number of days with precipitation considering 38 years period (1979–2016) over the Black Sea were investigated and the results were presented in Figure 4.32. Prominently, the trends are negative nearly all over the Black Sea Basin. The trend values can reach up to -1 day/yr. If we consider small Long-term variations of annual total precipitations and the negative trends in the annual number of days with precipitations together; it is possible to state that, in the study period, the amount of precipitation over the Black Sea did not change however the days which these precipitations occurred decreased. In other words, the same amount of precipitation started to be seen in less time over the Black Sea Basin. Besides, on the southeastern coasts, it was detected that the total annual precipitation has increased.

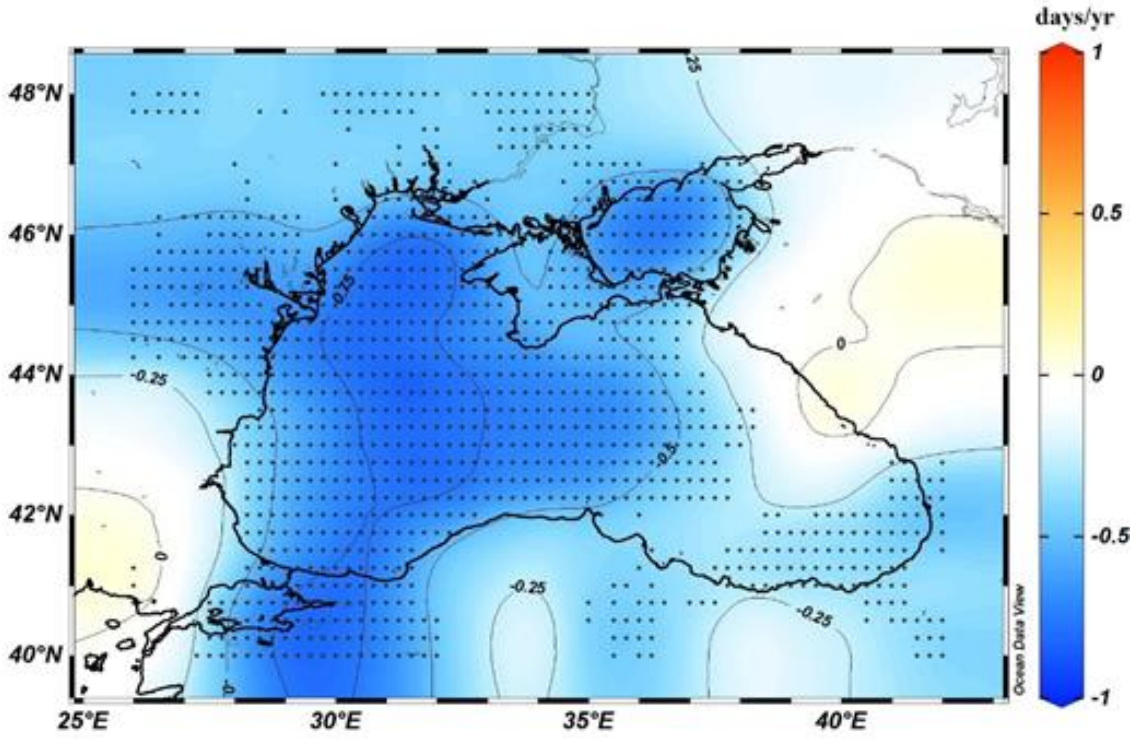


Figure 4.32 Long-term variations of annual number of days with precipitation considering 38 years period (1979–2016) over the Black Sea (ERA-5). Black dots indicate locations with statistically significant trends at the 90% or higher confidence level

In addition, have an understanding of freshwater flux into the Black Sea, evaporation over the Black Sea is also explored in Figure 4.33. Long term averaged annual total precipitations and long term averaged annual total precipitations were found for each point and the differences were represented in Figure 4.34 to define the net freshwater flux between the Black Sea and the atmosphere. Total evaporations are relatively higher in the northern regions of the Black Sea, and here the total evaporation in a year reaches up to 990 mm. If we consider that; these regions are the places where fewer precipitations occur, the total evaporation becomes greater than total precipitation in a year. This difference can be 506 mm per year. Over the Black Sea Basin, only on the south-eastern coasts we distinctly see that precipitation values are higher than evaporation. This difference reaches up to 1390 mm per year. If we take the total area of the Black Sea including The Sea of Azov as 461.000 km^2; the total precipitation over the whole basin in a year is 275 km^3/yr whereas the total evaporation is 384 km^3/yr.

The difference between these two values also comes out as 110 km^3/yr. These values are also consistent with the previous studies using different data resources (Efimov et al., 2012).

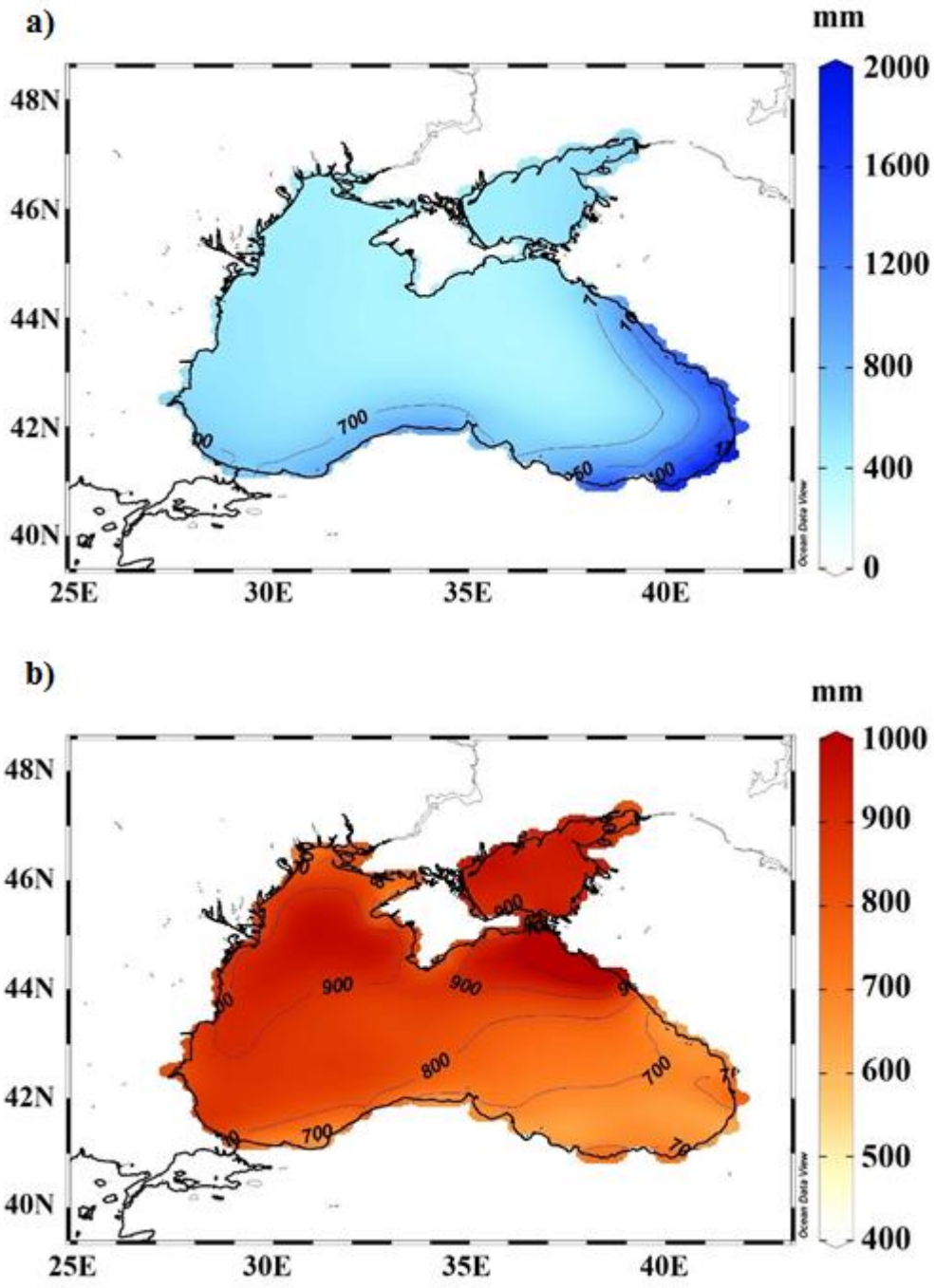


Figure 4.33 a) Long-term average annual total precipitations and b) Long-term average annual total evaporations over the Black Sea Basin, considering 38 years period (1979–2016) over the Black Sea (ERA-5)

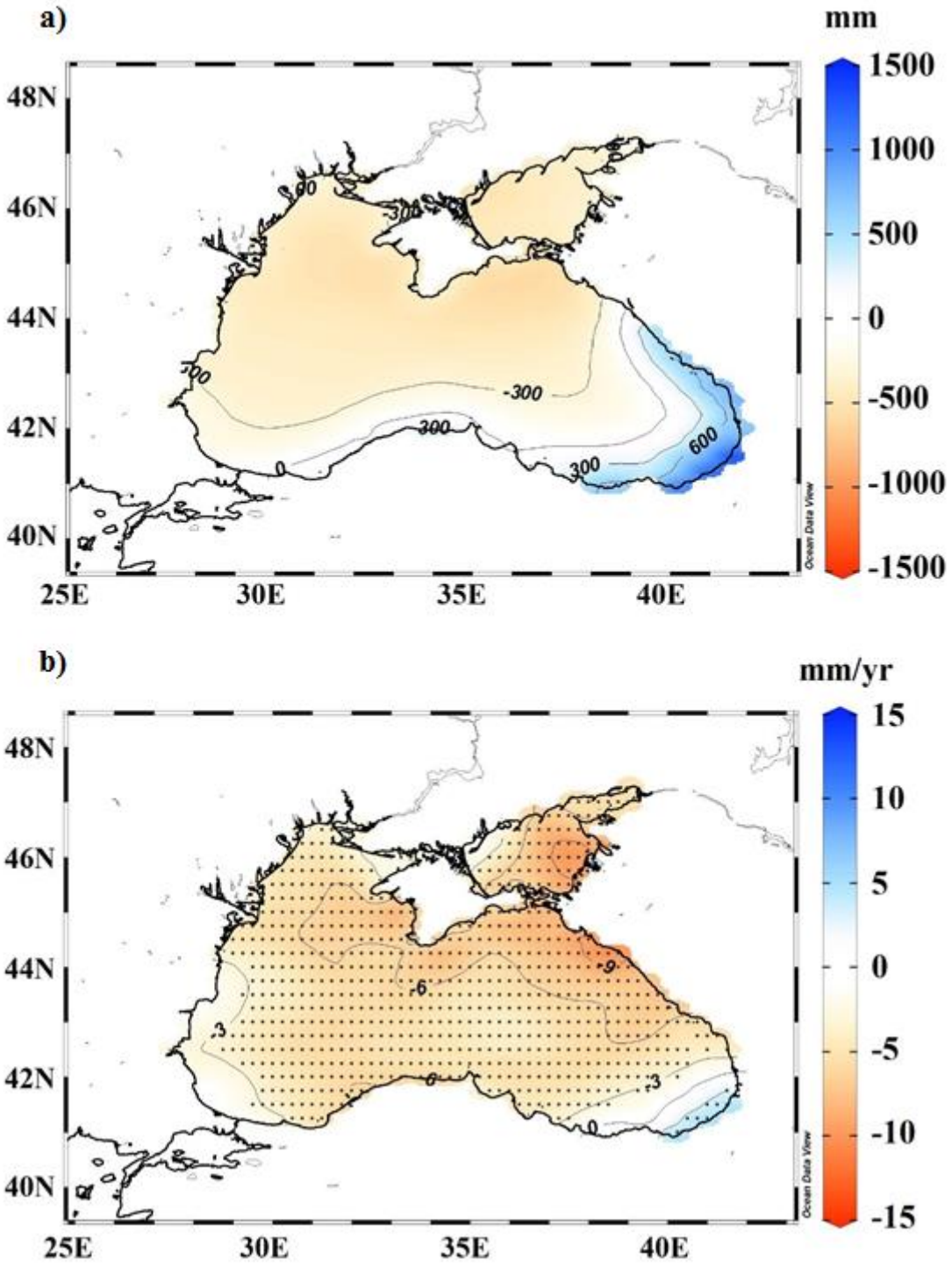


Figure 4.34 a) Annual differences of total precipitations and total evaporations b) with their long-term variations over the Black Sea Basin, considering 38 years period (1979–2016) over the Black Sea (ERA-5)

4.2 Shoreline Changes along the Black Sea Coasts

To explore the annual changes in shoreline morphology along the Black Sea Coasts, all coastlines were split into 271 shoreline zones and the annual shoreline changes were investigated for each zone. The locations of these shoreline zones were shown in Figure 4.35. Each shoreline zone consists of transection points that are 500 m apart from each other. The total lengths and number of transection points for each shoreline zone were represented in Table 4.3.

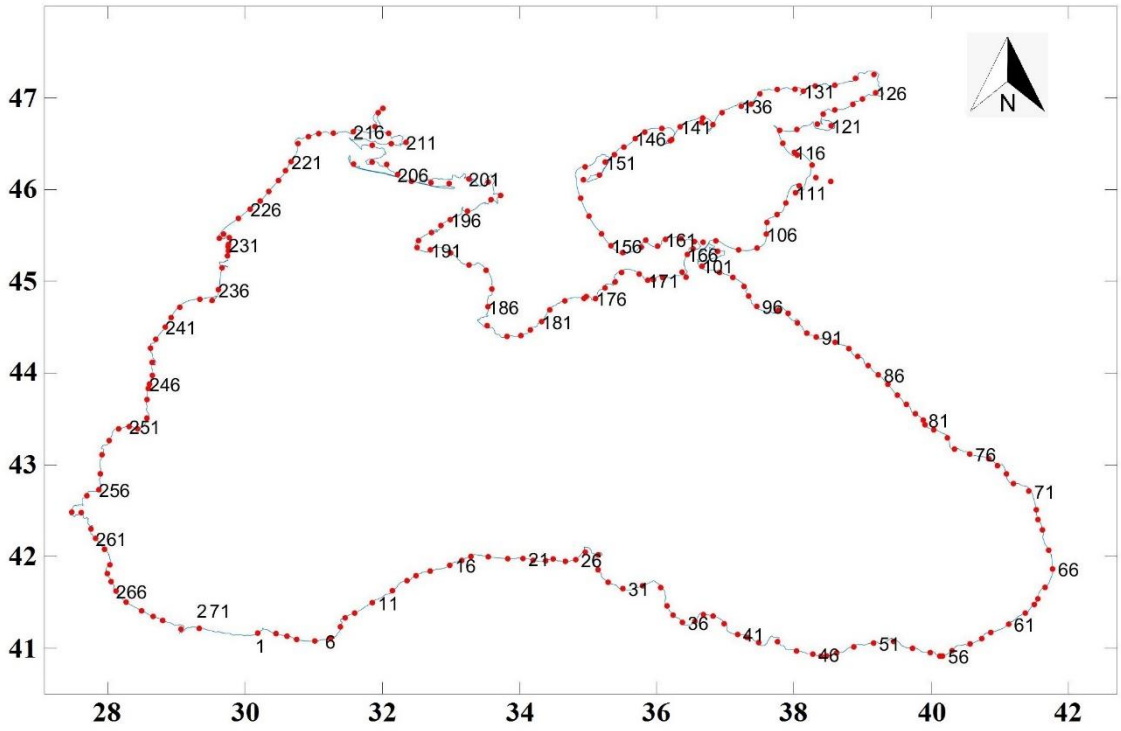


Figure 4.35 The locations and id numbers of shoreline zones along the Black Sea Coasts. To figure out the id numbers more clearly, the numbers were represented by fives starting from 1 to 271

Table 4.3 The total lengths and number of transection points for each shoreline zone. The red color scale indicates erosion whereas the green color scale indicates deposition

Shoreline id	Number of transections	Length (km)	Mean shoreline change trend (m/yr)	Shoreline id	Number of transections	Length (km)	Mean shoreline change trend (m/yr)	Shoreline id	Number of transections	Length (km)	Mean shoreline change trend (m/yr)
1	63	31.5	0.10	46	42	21	2.34	91	62	31	-0.10
2	78	39	-0.06	47	18	9	-5.86	92	7	3.5	0.07
3	65	32.5	0.00	48	4	2	1.40	93	103	51.5	-0.08
4	5	2.5	-4.87	49	61	30.5	0.94	94	20	10	0.15
5	56	28	-0.27	50	68	34	1.90	95	94	47	0.71
6	62	31	0.07	51	67	33.5	2.54	96	81	40.5	-0.10
7	37	18.5	-0.07	52	75	37.5	1.59	97	9	4.5	3.86
8	75	37.5	2.10	53	69	34.5	4.87	98	72	36	-0.87
9	9	4.5	0.90	54	57	28.5	2.25	99	26	13	-0.44
10	60	30	-0.78	55	7	3.5	0.83	100	64	32	-0.90
11	72	36	1.43	56	9	4.5	2.10	101	77	38.5	-0.38
12	82	41	0.84	57	61	30.5	3.59	102	189	94.5	-0.12
13	39	19.5	0.71	58	66	33	4.53	103	41	20.5	0.22
14	34	17	0.12	59	18	9	1.19	104	63	31.5	0.25
15	65	32.5	-1.63	60	55	27.5	2.58	105	64	32	1.73
16	68	34	-1.25	61	75	37.5	2.74	106	62	31	0.15
17	14	7	-1.89	62	52	26	3.67	107	15	7.5	-4.93
18	51	25.5	-0.74	63	32	16	-1.76	108	76	38	0.17
19	62	31	-3.36	64	8	4	0.04	109	26	13	-2.83
20	62	31	-0.47	65	71	35.5	0.98	110	82	41	5.77
21	37	18.5	-2.09	66	62	31	-0.25	111	82	41	4.27
22	23	11.5	-1.78	67	63	31.5	-0.12	112	124	62	-0.37
23	59	29.5	-0.69	68	63	31.5	2.49	113	80	40	3.83
24	4	2	0.82	69	11	5.5	-0.76	114	78	39	-0.64
25	62	31	-1.00	70	49	24.5	-1.41	115	48	24	0.81
26	4	2	1.79	71	89	44.5	-0.40	116	40	20	-1.08
27	89	44.5	-0.23	72	15	7.5	0.77	117	57	28.5	-2.62
28	62	31	0.10	73	88	44	-0.26	118	70	35	-0.45
29	67	33.5	0.38	74	11	5.5	-0.62	119	67	33.5	-1.54
30	40	20	-2.11	75	63	31.5	-0.08	120	137	68.5	0.85
31	66	33	0.72	76	70	35	-0.09	121	79	39.5	1.70
32	66	33	-0.27	77	45	22.5	-0.29	122	28	14	-0.83
33	76	38	0.02	78	57	28.5	-0.53	123	66	33	0.15
34	55	27.5	2.40	79	51	25.5	0.10	124	64	32	0.08
35	18	9	0.33	80	16	8	-0.67	125	14	7	-0.13
36	62	31	3.11	81	18	9	-0.29	126	103	51.5	0.21
37	36	18	0.22	82	49	24.5	0.15	127	83	41.5	0.92
38	44	22	-3.31	83	38	19	-0.19	128	89	44.5	0.15
39	20	10	-0.36	84	48	24	0.05	129	80	40	0.16
40	70	35	1.60	85	46	23	-0.20	130	67	33.5	-0.85
41	57	28.5	-0.09	86	42	21	0.07	131	35	17.5	1.48
42	10	5	-1.63	87	47	23.5	-0.01	132	57	28.5	-0.92
43	77	38.5	0.62	88	47	23.5	0.06	133	64	32	-0.73
44	95	47.5	0.28	89	34	17	-0.25	134	60	30	1.40
45	63	31.5	0.65	90	65	32.5	-0.02	135	31	15.5	0.15

Table 4.3 The total lengths and number of transection points for each shoreline zone. The red color scale indicates erosion whereas the green color scale indicates deposition (Continued)

Shoreline id	Number of transections	Length (km)	Mean shoreline change trend (m/yr)	Number of transections	Length (km)	Mean shoreline change trend (m/yr)	Shoreline id	Number of transections	Length (km)	Mean shoreline change trend (m/yr)
136	102	51	0.31	54	27	0.14	226	22	11	0.83
137	53	26.5	-0.30	50	25	0.29	227	74	37	-0.28
138	74	37	0.46	25	12.5	0.15	228	20	10	2.53
139	7	3.5	7.85	67	33.5	0.16	229	88	44	1.84
140	57	28.5	0.26	95	47.5	0.09	230	23	11.5	-6.76
141	83	41.5	-0.57	63	31.5	-0.33	231	9	4.5	0.62
142	7	3.5	0.10	68	34	-0.75	232	4	2	7.48
143	11	5.5	-0.76	70	35	-0.44	233	17	8.5	4.93
144	63	31.5	-1.22	73	36.5	-0.32	234	34	17	7.14
145	51	25.5	-0.18	76	38	-0.28	235	102	51	1.19
146	26	13	-1.22	67	33.5	-0.32	236	72	36	-3.78
147	71	35.5	0.94	41	20.5	-0.31	237	58	29	2.34
148	9	4.5	9.29	20	10	-0.12	238	67	33.5	-0.53
149	123	61.5	0.04	83	41.5	-0.10	239	78	39	2.48
150	76	38	-0.31	5	2.5	-0.07	240	12	6	-2.48
151	168	84	-0.02	65	32.5	-0.12	241	60	30	-2.15
152	65	32.5	-0.17	80	40	-1.21	242	44	22	4.62
153	64	32	0.28	124	62	-0.51	243	28	14	0.42
154	69	34.5	-0.05	36	18	1.33	244	33	16.5	0.85
155	76	38	-1.21	157	78.5	-0.20	245	29	14.5	0.14
156	24	12	-5.34	145	72.5	0.04	246	26	13	0.26
157	72	36	0.23	124	62	-0.09	247	6	3	-3.38
158	64	32	-0.01	184	92	0.09	248	57	28.5	0.21
159	47	23.5	-0.03	66	33	-1.04	249	71	35.5	0.16
160	38	19	0.14	147	73.5	-0.02	250	44	22	-0.25
161	39	19.5	-0.10	51	25.5	-0.62	251	13	6.5	-0.11
162	68	34	0.17	62	31	-0.91	252	53	26.5	0.22
163	29	14.5	0.15	179	89.5	-0.23	253	55	27.5	0.07
164	7	3.5	0.59	148	74	-0.30	254	67	33.5	-0.02
165	16	8	0.10	124	62	0.03	255	63	31.5	0.05
166	55	27.5	0.43	241	121	0.22	256	52	26	-0.05
167	160	80	0.48	39	19.5	-0.43	257	62	31	-0.74
168	100	50	-0.14	84	42	1.34	258	53	26.5	1.65
169	55	27.5	-0.16	10	5	0.06	259	118	59	0.12
170	8	4	-0.12	139	69.5	-0.12	260	76	38	0.76
171	29	14.5	-0.32	70	35	-0.01	261	18	9	0.10
172	48	24	-0.49	60	30	-0.31	262	78	39	0.28
173	80	40	0.03	37	18.5	-0.14	263	43	21.5	0.22
174	20	10	0.15	21	10.5	-0.50	264	38	19	0.41
175	100	50	-0.10	83	41.5	0.15	265	20	10	-0.02
176	9	4.5	-0.08	63	31.5	0.24	266	56	28	0.11
177	30	15	-0.21	4	2	0.31	267	42	21	-0.10
178	38	19	-0.26	77	38.5	0.94	268	69	34.5	0.37
179	68	34	-0.13	21	10.5	-0.03	269	13	6.5	-0.86
180	50	25	0.24	64	32	-0.73	270	52	26	2.53
							271	129	64.5	0.73

After considering the mean shoreline change rates for the 33 years between 1984 and 2016 over the 271 shoreline zones along the Black Sea Coasts, it is possible to make some conclusions. Firstly, to make it clear, negative values of mean shoreline change rates state that there is erosion in the particular coastal zone, whereas positive values dictate deposition. The number of shoreline zones where there is erosion is 132 and the values range from 0.01 m/yr to 6.76 m/yr. On the other hand, the number of shoreline zones where there is deposition is 139 and the values range from 0.02 m/yr to 9.29 m/yr.

The distribution of shoreline zones with erosion or the ones with deposition does show a slightly significant relation considering successive zones. Some successive shoreline zones represent similar characteristics. For example, in the region between zones 34 and 62, which corresponds eastern half of the Turkish coasts along the Black Sea, we see an apparent density of zones with depositions. In these regions, the deposition values can reach up to 4.87 m/yr.

Here there are some exceptions, which are the areas that represent erosion. These are zone 32 and zone 38. These zones are Bafra and Çarşamba Deltas, which are very important agricultural plains of Turkey. On the other hand, in the regions on the western side of the Sinop Peninsula, which can be considered the midpoint of the Turkish Blacks Sea coastline, we see significant erosion in the years between 1984 and 2016. Here, the shoreline zones 15-25, represent shoreline change trends between 0.47 m/yr and 3.55 m/yr.

In the region between zones 180 and 185, there is a deposition and the mean deposition values for one shoreline zone range from 0.1 m/yr and 0.29 m/yr. The regions are located in the southern part of the Crimean Peninsula. Next to these regions, in western regions of the Crimean Peninsula, Shoreline zones with erosion are located. This area is between zones 186 and 196. The erosion amount is detected between 0.1 m/yr and 0.75 m/yr.

Additionally, on the shorelines of the northern Danube Delta, which are represented by the region between the zones 231 and 235, positive shoreline change trends up to 7.45 m/yr are seen. This means there has been deposition here; whereas in the southern regions of the delta between the shoreline zones 236 and 241, there has been erosion reaching 3.78m/yr between the years 1984 and 2016.

Besides, the coastal regions between the zones 69 and 93, we see negative shoreline trends which means erosion for the years between 1984 and 2016. These regions are the western coasts of the Back Sea and the erosion for particular shoreline zones reaches up to 0.67 m/yr.

The shoreline changes in seven important coastal areas near the Black Sea were also investigated in a more detailed way. The selected shoreline is in the regions of Danube Delta, Terkos Lake, Cide, Sinop Peninsula, Bafra Delta, Çarşamba Delta, and Sochi. These regions were selected due to their economic or strategic importance for human activities along with their vulnerability to shoreline change. Danube Delta, Bafra Delta, and Çarşamba Delta are the important Delta Plains of the Back Sea and they have been regarded as vulnerable to sea-level rise and coastal erosion (Süzen and Özhan, 2003; Stanica et al., 2011; Öztürk and Sesli, 2015; Görmüş et al., 2021). Also, Terkos Lake is the most important water resource in Istanbul, which is the most populated city in Turkey. As it is located just near the Black Sea, the coastal barrier between the sea and the lake is very narrow and is sensitive to coastal erosion (Kaya et al., 2019). Furthermore, Sochi is a very important coastal city located on the eastern coast of the Black Sea and is known to have serious coastal erosion problems (Kosyan et al., 2012). Lastly, the Cide Region of Turkey, which is located near the southern coastal coasts of Turkey, has been facing charges in its coastal morphology (Tatui et al., 2019, Allenbach et al., 2014). The locations of these coastal areas are shown in Figure 4.35 and the id numbers of the shoreline zones which constitute the selected segments from Figure 4.35 are shown in Table 4.4.

The variations in these seven shoreline profiles were detected again by the determination of the trends in the lengths of transactions, orthogonal to the shoreline, with their significance. The results are presented in Tables 4.5-12, where the negative trends declare erosion and positive trends mean deposition in the particular shoreline point. As a reminder, the distance between each transaction orthogonal to the shoreline is 500m.

Table 4.4 The ID numbers of the shoreline zones given in Figure 4.35 which constitute selected shorelines segments

Coastal Area	The ID of the shorelines	Total Number of Transections	Total Length of the Shoreline (km)
Danube	241	60	30
Terkos	268	69	34.5
Cide	16, 17, 18	133	66.5
Sinop	27	89	44.5
Bafra	32	66	33
Çarşamba	38	44	22
Sochi	80, 81 ,82	82	41

4.2.1 Danube

The selected shoreline in the Danube Region is 30 km long, consists of 60 transaction points, and is shown in Figure 4.36. The region is in the Danube delta and is expected to be sensitive to erosion. The Danube shoreline is sandy and represents an abraded morphology. In addition, sediment loads of the Danube River mostly drive the hydrodynamic processes of the Danube Delta. In Table 4.5, it can be evaluated that the trends are significant at 59 points out of 60. In addition, 11 of the significant trends are positive and declare deposition on the shoreline. The minimum deposition rate is 0.15 m/yr and the maximum deposition rate is 3.83 m/yr. Here, the mean deposition is calculated as 2.33 m/yr. On the other hand, as expected, 48 of the trends are negative, which means erosion. The minimum erosion rate is -0.19 m/yr and the maximum erosion rate is -8.7 m/yr. Here, the mean erosion is calculated as -3.2 m/yr.



Figure 4.36 Selected study site in the Danube where the long-term variations of shoreline are explored. The id numbers of the points from south to north (Luijendijk et al., 2018)

The results are consistent with previous studies as well. Vespremeanu-Store et al. (2017) stated that 55% of the Danube Delta coastline has been eroding in the last 150 years. Also, Görmüş et al. (2021) observed severe erosion patterns in Danube Delta Coastline with an average rate of -1.7 m/yr. Especially, for the southern part of the Danube Delta, where locates near the transection points given in Table 4.5, coastline erosion rates down to -5.26 m/yr were evaluated.

As the reason for erosion seen in the Danube Delta, Vespremeanu-Stroe et al. (2017) pointed to the reduction in the sediment discharge from the Danube River. It was dictated that the Danube River is now carrying one-third of the sediments it used to carry in the previous century. This situation has come out because of anthropogenic activities along the Danube River and its tributaries. Vespremeanu-Stroe et al. (2017) also added that the entrapment of sediments by several dams over the Danube River shaped the coastline erosion, mostly after 1950. In

addition, Aydoğan and Ayat (2018) and Görmüş et al. (2021) stated that highly eroded regions of the Danube Delta are located in the highly energetic regions of the Black Sea, where relatively more severe storm conditions are observed.

In addition, the construction of jetties at the Sulina mouth of the Danube River after 1950 affected the coastal morphology. Today, two parallel jetties, which are nine km long, interrupt the longshore drifts and sediment transports. This situation leads to the release of river sediments in deeper regions where they cannot be deposited on the shoreline by hydrodynamic processes (Görmüş et al., 2021). To sum up, it can be accepted that all these conditions together resulted in severe erosion of the coastline Danube Delta.

Table 4.5 Long-term changes of the shorelines in the transactions in the Danube Delta. 90% statistically significant trends (p value<0.1) are shown with *

Point No	Long.	Lat.	Trend (m/yr)	p-value
1	28.76	44.43	3.83	0.000*
2	28.77	44.43	2.85	0.000*
3	28.77	44.43	2.27	0.000*
4	28.77	44.43	2.94	0.000*
5	28.78	44.44	3.12	0.000*
6	28.78	44.44	3.03	0.000*
7	28.78	44.44	2.76	0.000*
8	28.78	44.44	2.08	0.000*
9	28.79	44.45	1.54	0.000*
10	28.79	44.45	1.06	0.000*
11	28.79	44.45	0.15	0.092*
12	28.80	44.45	-0.13	0.107
13	28.80	44.46	-0.57	0.008*
14	28.80	44.46	-0.52	0.016*
15	28.80	44.46	-0.61	0.009*
16	28.81	44.46	-0.41	0.059*
17	28.81	44.47	-0.19	0.058*
18	28.81	44.47	-0.75	0.001*
19	28.82	44.47	-1.46	0.000*
20	28.82	44.47	-1.92	0.000*
21	28.82	44.48	-2.85	0.000*
22	28.82	44.48	-2.76	0.000*
23	28.83	44.48	-2.73	0.000*
24	28.83	44.48	-2.80	0.000*
25	28.83	44.49	-3.02	0.000*
26	28.84	44.49	-3.31	0.000*
27	28.84	44.49	-3.42	0.000*
28	28.84	44.49	-3.78	0.000*
29	28.84	44.50	-3.79	0.000*
30	28.85	44.50	-3.82	0.000*

Table 4.5 Long-term changes of the shorelines in the transactions in the Danube Delta. 90% statistically significant trends (p value<0.1) are shown with * (Continued)

Point No	Long.	Lat.	Trend (m/yr)	p-value
31	28.85	44.50	-3.87	0.000*
32	28.85	44.50	-3.76	0.000*
33	28.85	44.51	-3.85	0.000*
34	28.86	44.51	-3.39	0.000*
35	28.86	44.51	-3.63	0.000*
36	28.86	44.52	-3.37	0.000*
37	28.86	44.52	-3.40	0.000*
38	28.86	44.52	-3.31	0.000*
39	28.87	44.52	-3.31	0.000*
40	28.87	44.53	-2.91	0.000*
41	28.87	44.53	-2.66	0.000*
42	28.87	44.53	-2.80	0.000*
43	28.88	44.53	-3.23	0.000*
44	28.88	44.54	-4.07	0.000*
45	28.88	44.54	-4.23	0.000*
46	28.88	44.54	-4.78	0.000*
47	28.88	44.55	-4.84	0.000*
48	28.89	44.55	-5.08	0.000*
49	28.89	44.55	-5.60	0.000*
50	28.89	44.55	-5.32	0.000*
51	28.89	44.56	-5.21	0.000*
52	28.89	44.56	-5.00	0.000*
53	28.90	44.56	-4.90	0.000*
54	28.90	44.57	-5.08	0.000*
55	28.90	44.57	-3.57	0.000*
56	28.90	44.57	-3.57	0.000*
57	28.90	44.57	-0.60	0.000*
58	28.91	44.58	-1.24	0.000*
59	28.91	44.58	-8.67	0.000*
60	28.91	44.58	-0.45	0.087*

To give an idea of the shoreline position changes in transaction points in the Danube, four shoreline position-time graphs were presented in Figure 4.37 as an example.

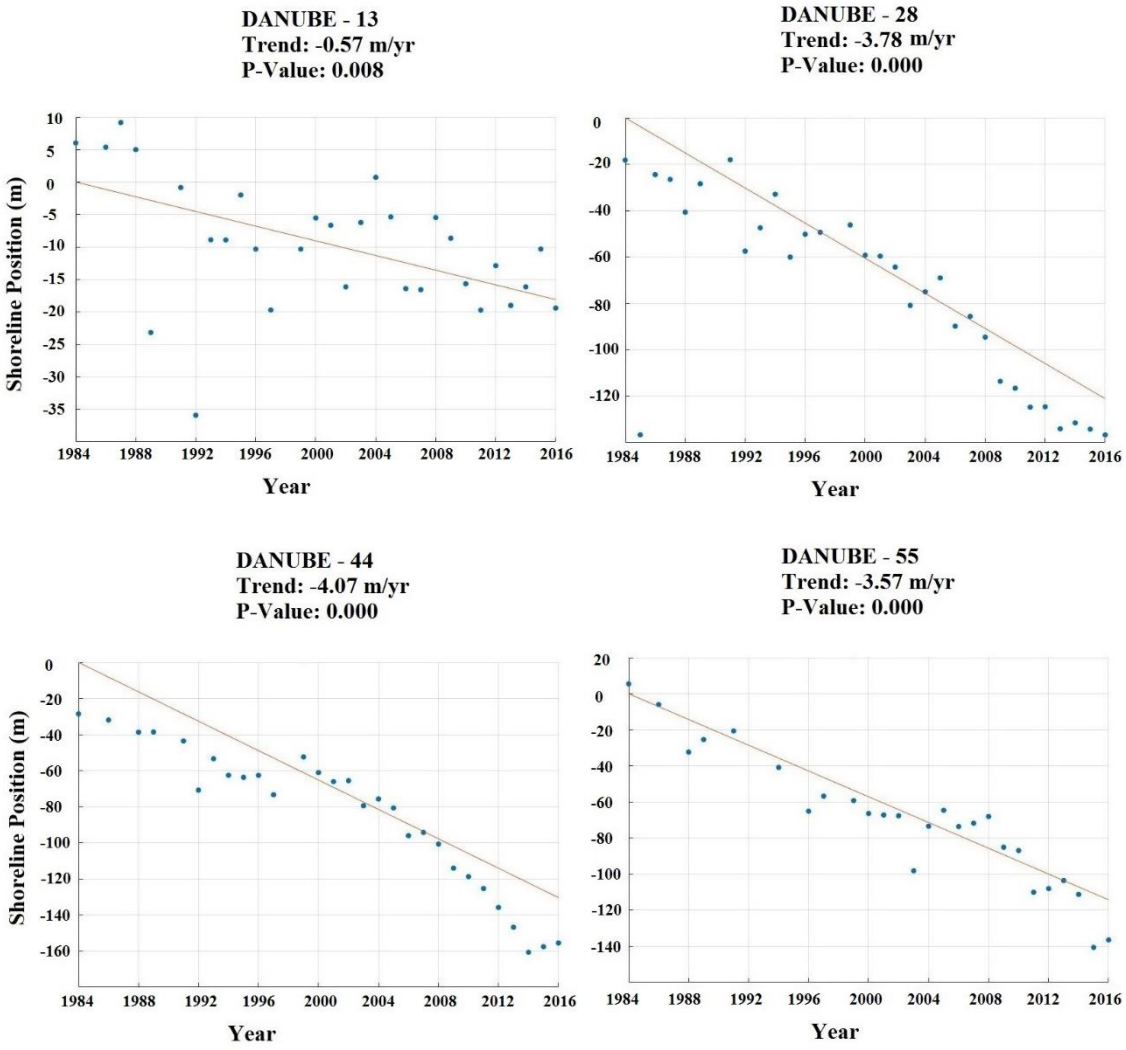


Figure 4.37 Shoreline positions and trends for particular points in the study site in the Danube

4.2.2 Terkos

The selected shoreline in the Terkos is 34 km long, consists of 69 transection points, and is shown in Figure 4.38. The region is between Terkos Lake and the Black Sea. Terkos Lake is a very important freshwater resource for Istanbul and is expected to be sensitive to erosion due to seawater intrusion into the lake. The shoreline is sandy and represents a moderately abraded morphology. In Table 4.6, it can be evaluated that the trends are significant at 45 points out of 69. In addition, 34 of the significant trends are positive and state deposition on the shoreline. The minimum deposition rate is 0.5 m/yr and the maximum deposition rate is 1.62 m/yr. Here, the mean deposition is calculated as 0.98 m/yr. On the

other hand, 11 of the trends are negative, which means erosion. The minimum erosion rate is -0.16 m/yr and the maximum erosion rate is -1.35 m/yr. Here, the mean erosion is calculated as -0.67 m/yr.

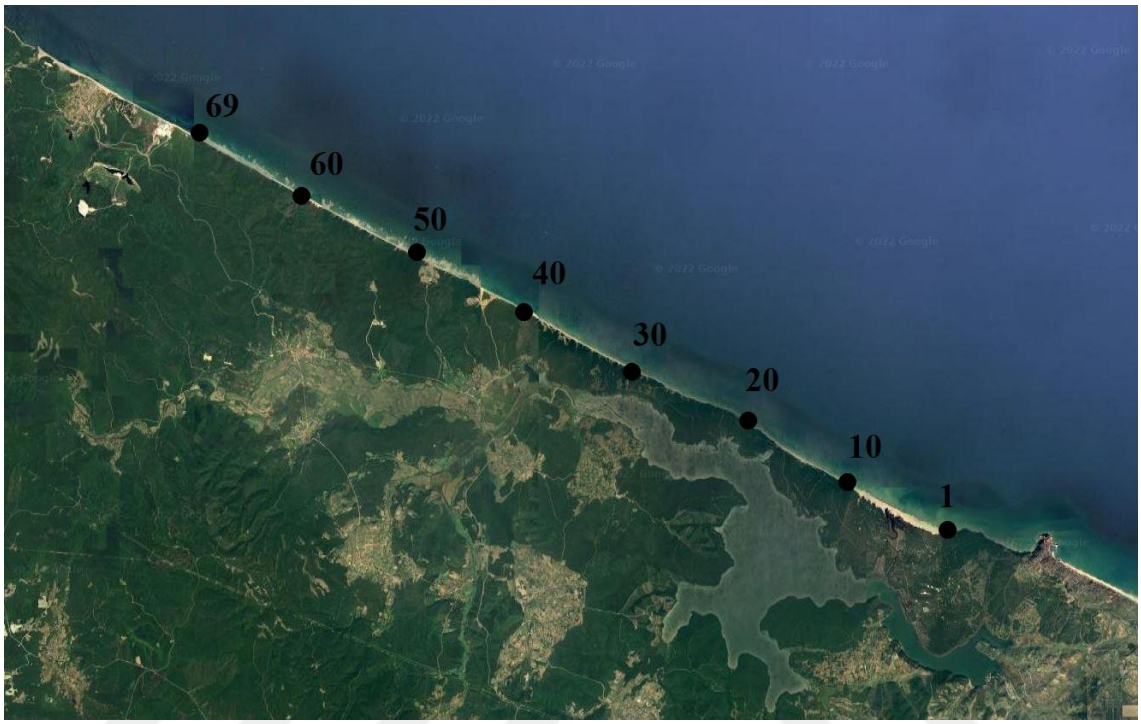


Figure 4.38 Selected study site in Terkos where the long-term variations of shoreline are explored. The id numbers of the points go from west to east (Luijendijk et al., 2018)

Terkos Lake is one of the most important freshwater resources of Istanbul and is located in northern Istanbul near the Black Sea coast. Between the lake and the sea, there is a thin barrier separating the two water bodies. This barrier is very essential to prevent the entrance of salt water into the lake. The barrier consists of mostly sandy beaches and forests. The vegetation on the barrier was formed by people at the beginning of the twentieth century to increase the resistance of land barriers against severe sea conditions. This became successful and the Terkos Lake has not connected to the Black Sea and become a lagoon. However, in the last decades, the natural barrier has been losing its width due to some anthropogenic activities. Maktav et al. (2002) stated that the width of the narrowest part of the

natural barrier has decreased from 430 m to 230 m in 14 years between 1984 and 1998. This situation, which corresponds to an erosion rate of around 14 m/yr, is explained by the uncontrolled offshore sand excavation near the natural barrier in the relevant period. In addition, severe northern winds and waves can be evaluated as another factor for erosion in the barrier (Maktav et al., 2002).

In Table 4.6, the narrow part of the natural barrier between the Terkos Lake and the Black Sea faced erosion between the years 1984 and 2016. The erosion rate at the narrowest point of the barrier is 1 m/yr. The erosion rate showed a significant decrease from the previous period. This reduction in the erosion rate occurred due to the regulations of offshore sand excavations along with strengthening the barrier by planting new trees, and construction of hedges and landfills after 2000 (Baylan and Karadeniz, 2006). Nevertheless, erosion is still going on threatening the natural barrier between the Terkos Lake and the Black Sea, the more efficient protection strategies should be held urgently.

Table 4.6 Long-term changes of the shorelines in the transactions in the Terkos. 90% statistically significant trends (p value<0.1) are shown with *

Point No	Long.	Lat.	Trend (m/yr)	p-value
1	28.63	41.35	-0.86	0.034*
2	28.62	41.36	-0.22	0.311
3	28.62	41.36	-0.08	0.624
4	28.62	41.36	-0.29	0.146
5	28.61	41.36	0.08	0.659
6	28.61	41.36	-0.32	0.201
7	28.60	41.36	-0.67	0.009*
8	28.60	41.37	-0.13	0.597
9	28.60	41.37	-0.05	0.826
10	28.59	41.37	0.30	0.315
11	28.59	41.37	0.18	0.414
12	28.59	41.37	-0.40	0.071*
13	28.58	41.37	-0.59	0.011*
14	28.58	41.38	-1.00	0.011*
15	28.57	41.38	-0.21	0.597
16	28.57	41.38	-0.04	0.624
17	28.57	41.38	-0.15	0.262
18	28.56	41.38	0.06	0.823
19	28.56	41.38	-0.26	0.528
20	28.55	41.39	-0.06	0.712
21	28.55	41.39	-0.16	0.097*
22	28.55	41.39	-0.28	0.053*
23	28.54	41.39	-0.07	0.657
24	28.54	41.39	-0.84	0.000*
25	28.53	41.39	-0.81	0.000*
26	28.53	41.39	-0.46	0.000*
27	28.53	41.40	0.50	0.002*
28	28.52	41.40	1.19	0.000*
29	28.52	41.40	1.62	0.000*
30	28.51	41.40	1.26	0.000*
31	28.51	41.40	1.09	0.000*
32	28.51	41.40	0.30	0.400
33	28.50	41.40	0.12	0.252
34	28.50	41.41	0.15	0.747
35	28.49	41.41	1.18	0.000*

Table 4.6 Long-term changes of the shorelines in the transactions in the Terkos. 90% statistically significant trends (p value<0.1) are shown with * (Continued)

Point No	Long.	Lat.	Trend (m/yr)	p-value
36	28.49	41.41	0.81	0.000
37	28.49	41.41	1.08	0.000
38	28.48	41.41	0.82	0.000
39	28.48	41.41	1.12	0.000
40	28.47	41.42	1.02	0.000
41	28.47	41.42	-0.13	0.591
42	28.47	41.42	-1.35	0.001
43	28.46	41.42	-0.25	0.201
44	28.46	41.42	0.60	0.103
45	28.45	41.42	1.12	0.000
46	28.45	41.42	0.72	0.008
47	28.45	41.43	1.37	0.000
48	28.44	41.43	1.24	0.000
49	28.44	41.43	0.80	0.002
50	28.43	41.43	1.41	0.000
51	28.43	41.43	0.86	0.004
52	28.43	41.43	1.09	0.000
53	28.42	41.44	1.08	0.001
54	28.42	41.44	1.00	0.000
55	28.41	41.44	1.33	0.000
56	28.41	41.44	0.64	0.000
57	28.41	41.44	0.75	0.001
58	28.40	41.44	0.96	0.000
59	28.40	41.45	0.58	0.002
60	28.39	41.45	-0.10	0.930
61	28.39	41.45	0.60	0.004
62	28.39	41.45	1.08	0.000
63	28.38	41.45	-0.10	0.528
64	28.38	41.45	0.51	0.003
65	28.37	41.45	0.72	0.003
66	28.37	41.46	0.63	0.006
67	28.37	41.46	1.02	0.000
68	28.36	41.46	1.00	0.000
69	28.36	41.46	1.22	0.000

To give an idea of the shoreline position changes in transaction points in the Terkos, four shoreline position-time graphs were presented in Figure 4.39 as an example.

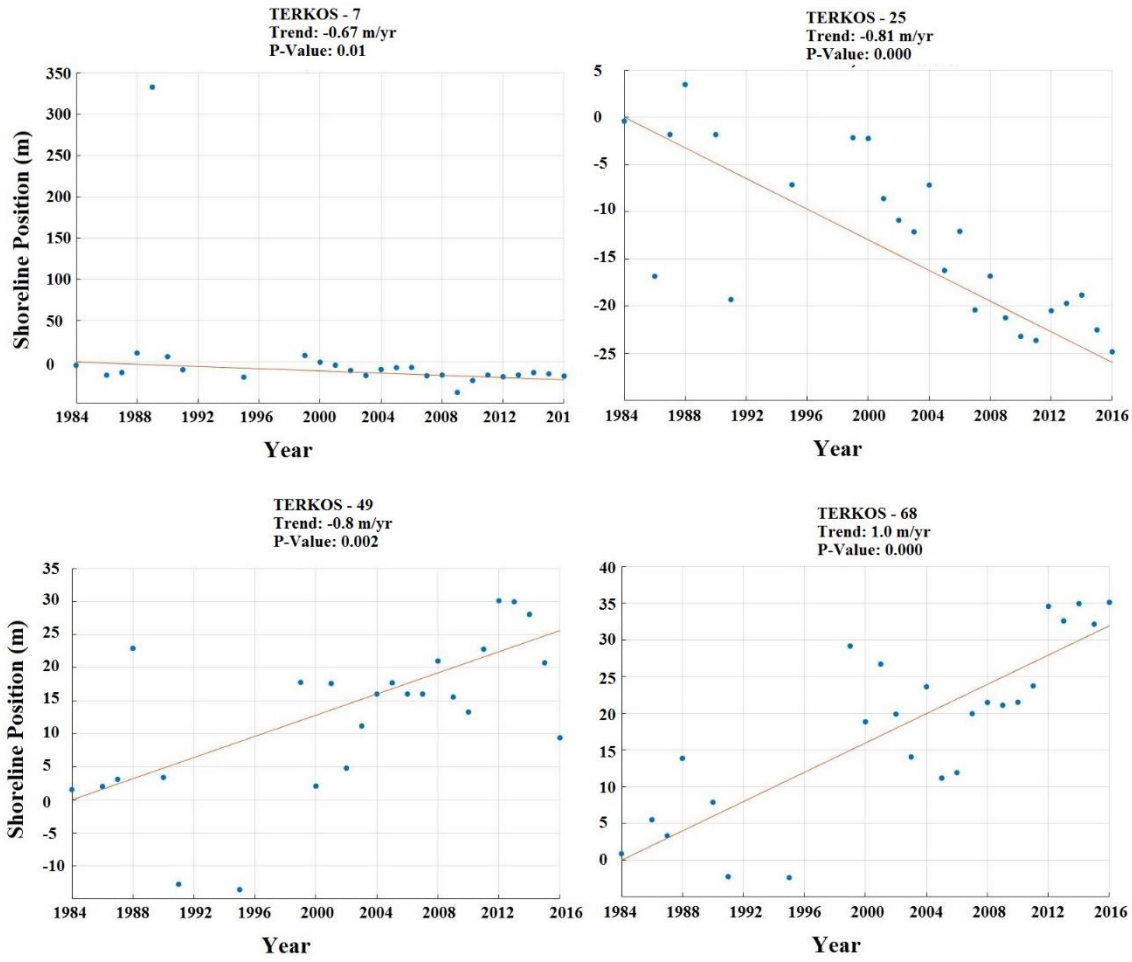


Figure 4.39 Shoreline positions and trends for particular points in the study site in Terkos

4.2.3 Cide

The selected shoreline in the Cide is 66 km long and consisted of 133 transection points, as shown in Figure 4.40. The region is in the Cide district of the Kastamonu Province in the Black Sea region of Turkey. The shoreline is mostly rocky and represents a moderately abraded morphology. In Figure 4.40, it can be evaluated that the trends are significant at 68 points out of 133. In addition, 4 of the significant trends are positive and state deposition in the shoreline. The minimum deposition rate is 1.21 m/yr and the maximum deposition value is 3.4 m/yr. Here, the mean deposition is calculated as 2.04 m/yr. On the other hand, 64 of the trends are negative, which means erosion. The minimum erosion rate is -0.21 m/yr and the maximum erosion rate is -7.25 m/yr. Here, the mean erosion is calculated as -1.79 m/yr. Cide can be evaluated as a mountainous area that has strong cliffs, which are resistant to erosion. Here, the shoreline change rates vary from -1 m/yr to +1 m/yr, which can be regarded as stable.

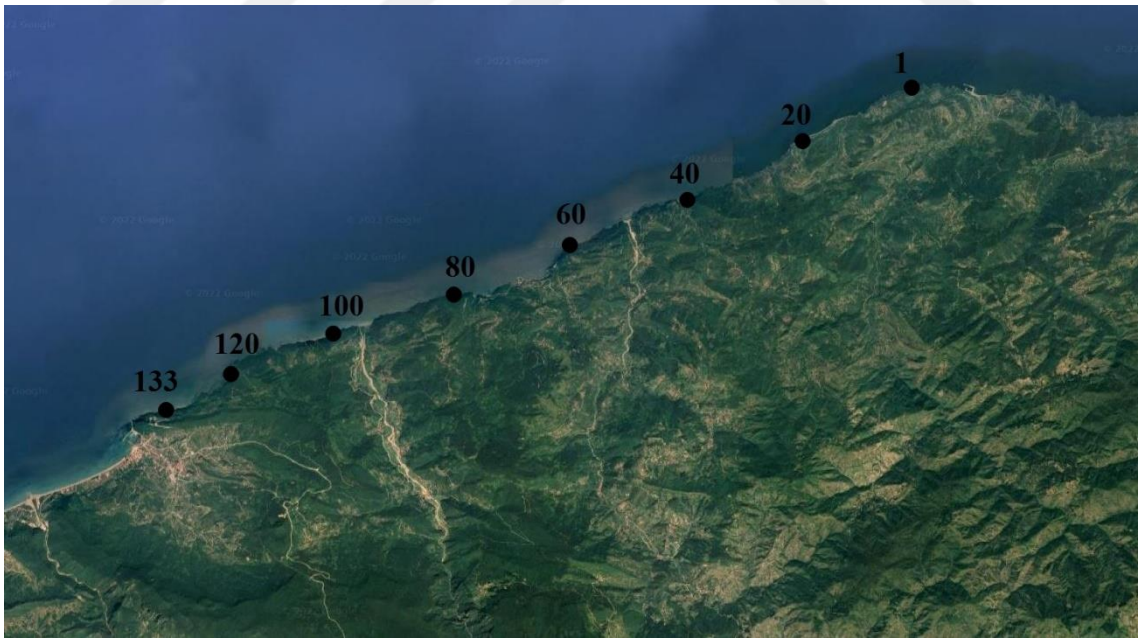


Figure 4.40 Selected study site in Cide where the long-term variations of shoreline are explored. The id numbers of the points go from west to east (Luijendijk et al., 2018)

Table 4.7 Long-term changes of the shorelines in the transactions in the Cide. 90% statistically significant trends (p value<0.1) are shown with *

Point No	Long.	Lat.	Trend (m/yr)	p-value
1	33.40	42.01	-0.10	0.319
2	33.40	42.01	0.01	0.981
3	33.39	42.01	0.13	0.761
4	33.39	42.01	-0.26	0.234
5	33.38	42.01	-0.68	0.401
6	33.38	42.02	0.01	0.303
7	33.37	42.02	-0.21	0.567
8	33.37	42.02	0.16	0.454
9	33.37	42.02	1.21	0.038*
10	33.36	42.02	3.39	0.002*
11	33.36	42.02	1.61	0.002*
12	33.35	42.02	0.33	0.201
13	33.35	42.02	-0.08	0.284
14	33.34	42.02	-0.34	0.349
15	33.34	42.02	0.78	0.378
16	33.33	42.02	-1.57	0.139
17	33.33	42.02	-1.33	0.063*
18	33.33	42.02	-1.34	0.398
19	33.32	42.01	-2.02	0.012*
20	33.32	42.01	-0.52	0.004*
21	33.31	42.01	-0.21	0.021*
22	33.31	42.01	-1.10	0.154
23	33.31	42.01	-1.00	0.143
24	33.30	42.01	-0.69	0.454
25	33.30	42.01	-0.40	0.003*
26	33.29	42.00	-0.62	0.080*
27	33.29	42.00	-1.19	0.037*
28	33.29	42.00	-1.35	0.102
29	33.28	42.00	-1.15	0.041*
30	33.28	42.00	-0.78	0.018*
31	33.27	42.00	-1.18	0.027*
32	33.27	41.99	-0.99	0.021*
33	33.27	41.99	-1.75	0.129
34	33.26	41.99	-0.99	0.230
35	33.26	41.99	-0.59	0.003*
36	33.25	41.99	-0.78	0.037*
37	33.25	41.99	-0.85	0.091*
38	33.25	41.99	-2.48	0.014*
39	33.24	41.98	-0.92	0.205
40	33.24	41.98	-1.59	0.004*
41	33.23	41.98	-0.53	0.427
42	33.23	41.98	-0.16	0.378
43	33.22	41.98	-0.22	0.034*
44	33.22	41.98	-2.00	0.217

Table 4.7 Long-term changes of the shorelines in the transactions in the Cide. 90% statistically significant trends (p value<0.1) are shown with * (Continued)

Point No	Long.	Lat.	Trend (m/yr)	p-value
45	33.22	41.98	-2.41	0.027*
46	33.21	41.98	-2.58	0.012*
47	33.21	41.98	-1.24	0.000*
48	33.20	41.97	-0.45	0.034*
49	33.20	41.97	-1.74	0.078*
50	33.20	41.97	-4.09	0.019*
51	33.19	41.97	-0.74	0.348
52	33.18	41.97	-7.25	0.010*
53	33.18	41.96	-6.04	0.141
54	33.18	41.96	-0.96	0.797
55	33.17	41.96	-0.20	0.624
56	33.17	41.96	0.14	0.726
57	33.17	41.96	-0.89	0.168
58	33.16	41.96	-0.39	0.244
59	33.16	41.95	-0.56	0.189
60	33.15	41.95	-4.91	0.035*
61	33.15	41.95	-0.73	0.264
62	33.14	41.95	-1.12	0.008*
63	33.14	41.95	-2.30	0.064*
64	33.14	41.95	0.18	0.659
65	33.13	41.95	-1.47	0.355
66	33.12	41.95	-1.46	0.107
67	33.12	41.95	-4.99	0.078*
68	33.11	41.95	-3.33	0.071*
69	33.11	41.95	-3.14	0.217
70	33.10	41.94	-1.10	0.047*
71	33.10	41.94	-4.88	0.107
72	33.09	41.94	-1.40	0.087*
73	33.09	41.94	-0.32	0.039*
74	33.09	41.94	-0.54	0.503
75	33.08	41.94	0.37	0.290
76	33.08	41.94	-1.41	0.089*
77	33.07	41.94	-2.68	0.031*
78	33.07	41.94	-4.20	0.011*
79	33.06	41.94	-1.73	0.007*
80	33.06	41.93	-1.73	0.071*
81	33.06	41.93	-2.21	0.097*
82	33.05	41.93	-1.83	0.252
83	33.05	41.93	-1.47	0.123
84	33.04	41.93	-1.65	0.051*
85	33.04	41.93	-2.89	0.000*
86	33.04	41.93	-2.50	0.007*
87	33.03	41.93	-1.58	0.021*
88	33.028	41.923	-1.01	0.094*

Table 4.7 Long-term changes of the shorelines in the transactions in the Cide. 90% statistically significant trends (p value<0.1) are shown with * (Continued)

Poınt No	Long.	Lat.	Trend (m/yr)	p-value
89	33.02	41.92	-2.15	0.038*
90	33.02	41.92	-1.62	0.047*
91	33.02	41.92	-1.62	0.041*
92	33.01	41.92	-0.30	0.503
93	33.01	41.91	-2.60	0.003*
94	33.00	41.91	-2.07	0.096*
95	33.00	41.91	-1.09	0.034*
96	33.00	41.91	-2.29	0.146
97	32.99	41.91	-1.29	0.015*
98	32.99	41.91	-2.24	0.047*
99	32.98	41.91	0.17	0.239
100	32.98	41.90	0.03	0.692
101	32.98	41.90	0.73	0.198
102	32.98	41.90	0.67	0.113
103	32.98	41.89	0.19	0.355
104	32.97	41.89	0.19	0.350
105	32.97	41.89	-0.59	0.378
106	32.97	41.89	-0.77	0.217
107	32.96	41.89	-0.67	0.028*
108	32.96	41.89	-0.69	0.003*
109	32.95	41.89	-0.62	0.003*
110	32.95	41.88	-0.78	0.025*
111	32.94	41.88	-1.22	0.003*
112	32.94	41.88	1.94	0.034*
113	32.94	41.88	2.04	0.118
114	32.93	41.88	-0.71	0.012*
115	32.93	41.88	-7.15	0.007*
116	32.92	41.88	-1.59	0.017*
117	32.92	41.88	-0.59	0.012*
118	32.92	41.87	-0.29	0.129
119	32.91	41.87	-0.28	0.063*
120	32.91	41.87	-0.12	0.597
121	32.90	41.87	-0.09	0.508
122	32.90	41.87	-0.26	0.168
123	32.89	41.87	-0.29	0.113
124	32.89	41.87	-0.24	0.290
125	32.88	41.87	-0.56	0.118
126	32.88	41.87	-0.51	0.139
127	32.88	41.87	0.19	0.363
128	32.87	41.87	-0.89	0.143
129	32.87	41.86	-1.69	0.064*
130	32.86	41.86	-0.46	0.158
131	32.86	41.86	-3.13	0.038*
132	32.86	41.86	-0.13	0.256
133	32.85	41.86	-1.21	0.087*

To give an idea of the shoreline position changes in transaction points in the Cide, four shoreline position-time graphs were presented in Figure 4.41 as an example.

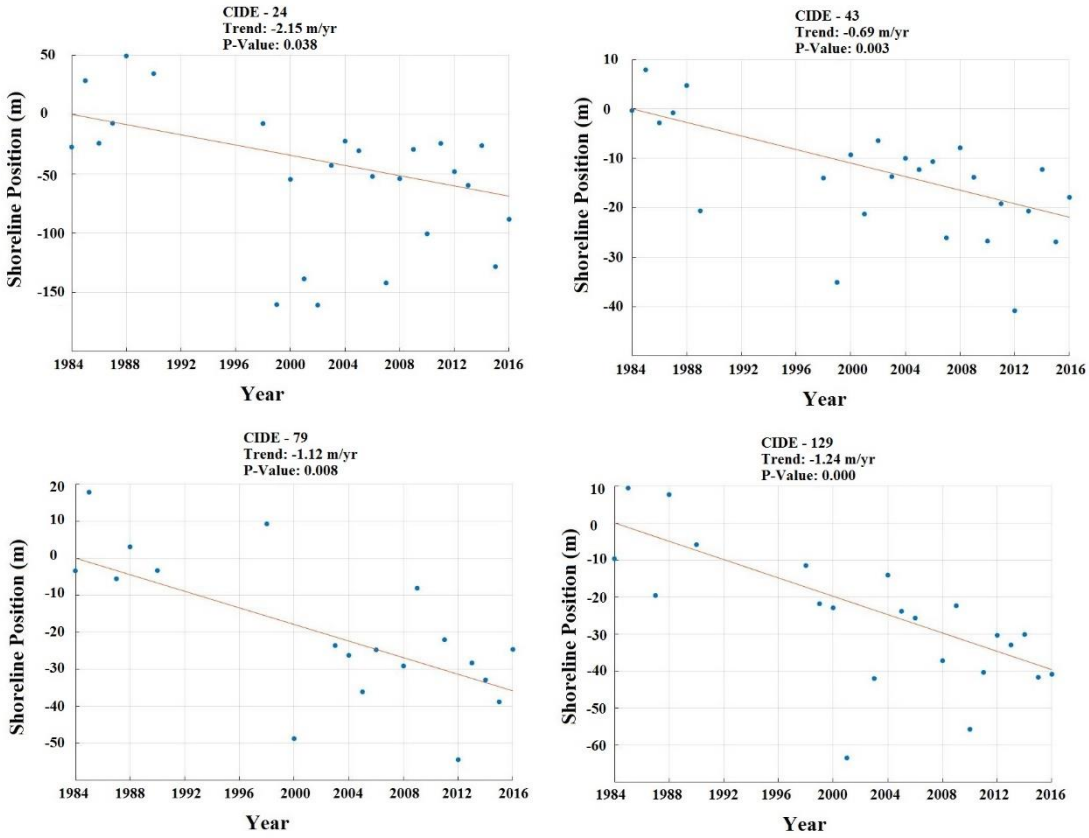


Figure 4.41 Shoreline positions and trends for particular points in the study site in Cide

4.2.4 Sinop

The selected shoreline in the Sinop is 44 km long. It consisted of 89 transection points and is shown in Figure 4.42. Sinop is an important peninsula of Turkey, which is located near the Black Sea. The shoreline is mostly rocky and represents a moderately abraded morphology. In Figure 4.42 it can be evaluated that the trends are significant at 34 points out of 89. Only, 1 of the significant trends is positive and state deposition in the shoreline, which is 0.55 m/yr. On the other hand, 33 of the significant trends are negative, which means erosion. The minimum erosion rate is -0.17 m/yr and the maximum erosion rate is -1.20 m/yr. Here, the mean erosion is calculated as -0.60 m/yr. Alike Cide, Sinop is also a mountainous area. On the shoreline, there are strong cliffs, which are resistant to

erosion. Here, the shoreline change rates vary from -1 m/yr to +1 m/yr, which can be regarded as stable.



Figure 4.42 Selected study site in Sinop where the long-term variations of shoreline are explored. The id numbers of the points go from west to east (Luijendijk et al., 2018)

Table 4.8 Long-term changes of the shorelines in the transactions in the Sinop. 90% statistically significant trends (p value<0.1) are shown with *

Point No	Long.	Lat.	Trend (m/yr)	p-value
1	35.09	42.03	0.21	0.338
2	35.08	42.03	-0.03	0.870
3	35.08	42.03	-0.35	0.088*
4	35.07	42.03	-0.55	0.018*
5	35.07	42.03	-0.42	0.130
6	35.06	42.03	-0.22	0.159
7	35.06	42.03	0.28	0.559
8	35.06	42.03	-0.13	0.710
9	35.05	42.04	-0.09	0.655
10	35.05	42.04	0.18	0.330
11	35.05	42.04	-0.22	0.150
12	35.04	42.04	-0.56	0.088*
13	35.04	42.05	0.13	0.347
14	35.04	42.05	-0.86	0.027*
15	35.05	42.05	-0.01	0.833
16	35.05	42.06	0.12	0.388
17	35.05	42.06	-0.44	0.252
18	35.04	42.06	0.00	0.944
19	35.04	42.07	-0.34	0.170
20	35.04	42.07	0.44	0.168
21	35.04	42.07	0.08	0.907
22	35.03	42.07	0.03	0.747
23	35.03	42.08	0.11	0.528
24	35.03	42.08	0.01	0.907
25	35.02	42.08	0.27	0.161
26	35.02	42.08	0.64	0.272
27	35.02	42.09	0.67	0.216
28	35.02	42.09	0.55	0.065*
29	35.01	42.09	-0.10	0.901
30	35.01	42.09	0.04	0.761
31	35.00	42.09	0.24	0.252
32	35.00	42.09	0.49	0.388
33	34.99	42.09	0.34	0.234
34	34.99	42.09	-0.10	0.761
35	34.98	42.09	0.34	0.624
36	34.98	42.09	0.00	0.981
37	34.98	42.09	0.40	0.252
38	34.97	42.09	0.24	0.498
39	34.97	42.10	-0.06	0.823
40	34.96	42.10	-0.75	0.072*
41	34.96	42.10	-0.15	0.691
42	34.95	42.09	-0.18	0.184
43	34.95	42.09	0.90	0.216
44	34.95	42.09	-0.55	0.000*
45	34.95	42.09	-0.46	0.045*

Table 4.8 Long-term changes of the shorelines in the transactions in the Sinop. 90% statistically significant trends (p value<0.1) are shown with * (Continued)

Point No	Long.	Lat.	Trend (m/yr)	p-value
46	34.95	42.08	-0.14	0.112
47	34.95	42.08	-0.54	0.150
48	34.95	42.08	-0.76	0.040*
49	34.95	42.07	-0.44	0.012*
50	34.94	42.07	-0.34	0.236
51	34.94	42.07	-0.80	0.130
52	34.94	42.06	-0.07	0.568
53	34.94	42.06	-0.42	0.224
54	34.94	42.06	-0.26	0.359
55	34.93	42.06	-0.21	0.398
56	34.93	42.05	0.54	0.498
57	34.93	42.05	-0.55	0.000*
58	34.93	42.05	0.24	0.528
59	34.92	42.04	-0.37	0.000*
60	34.92	42.04	-0.41	0.107
61	34.92	42.04	0.08	0.944
62	34.92	42.04	-0.58	0.024*
63	34.91	42.03	0.20	0.823
64	34.91	42.03	-0.46	0.015*
65	34.91	42.03	-0.57	0.006*
66	34.91	42.03	-0.83	0.001*
67	34.90	42.02	-0.56	0.002*
68	34.90	42.02	-0.59	0.000*
69	34.90	42.02	-0.57	0.002*
70	34.90	42.01	-0.93	0.004*
71	34.89	42.01	-0.59	0.007*
72	34.89	42.01	-0.74	0.002*
73	34.89	42.01	-0.81	0.004*
74	34.88	42.01	-1.20	0.001*
75	34.88	42.00	-0.19	0.040*
76	34.88	42.00	-0.54	0.003*
77	34.87	42.00	-0.17	0.076*
78	34.87	42.00	-0.59	0.009*
79	34.87	41.99	-0.18	0.014*
80	34.86	41.99	-0.10	0.272
81	34.86	41.99	-0.71	0.000*
82	34.86	41.99	-0.84	0.018*
83	34.85	41.98	-0.62	0.003*
84	34.85	41.98	-0.40	0.078*
85	34.85	41.98	-0.52	0.199
86	34.84	41.98	-0.54	0.002*
87	34.84	41.98	-0.61	0.002*
88	34.84	41.97	-0.98	0.035*
89	34.83	41.97	-0.68	0.359

To give an idea of the shoreline position changes in transaction points in the Sinop, four shoreline position-time graphs were presented in Figure 4.43 as an example.

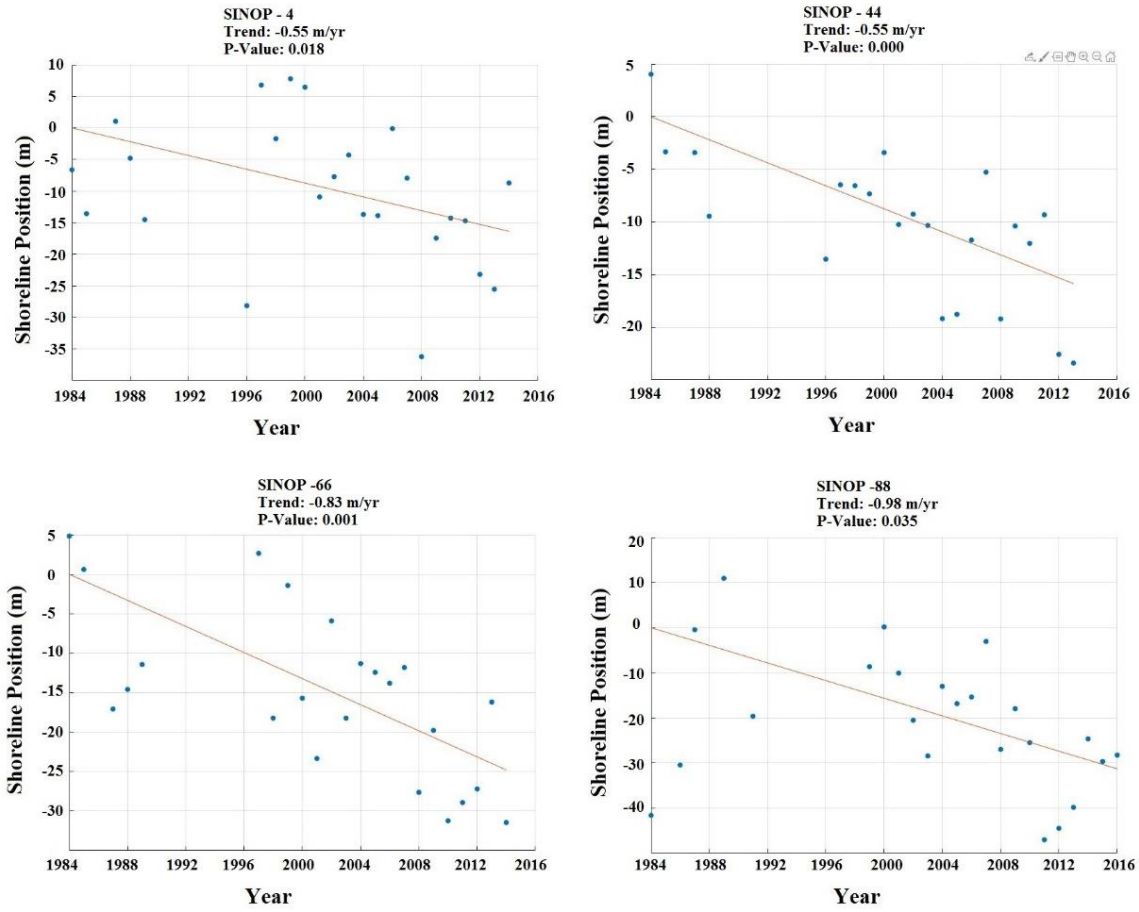


Figure 4.43 Shoreline positions and trends for particular points in the study site in Sinop

4.2.5 Bafra

The selected shoreline in the Bafra is 33 km long. It consisted of 74 transection points and is shown in Figure 4.44. The region is in the Kızılımak delta and is expected to be sensitive to erosion due to its low-lying coastal characteristics. It is one of the most important agricultural zones of Turkey with its fertile lands. The shoreline is sandy and represents an abraded morphology.

In Table 4.9, it can be evaluated that the trends are significant at 44 points out of 74. In addition, 12 of the significant trends are positive and declare deposition on

the shoreline. The minimum deposition rate is 0.10 m/yr and the maximum deposition rate is 0.73 m/yr. Here, the mean deposition is calculated as 0.42 m/yr. On the other hand, 29 of the trends are negative, which means erosion. The minimum erosion rate is -0.19 m/yr and the maximum erosion rate is 21.81 m/yr. Here, the mean erosion is calculated as -3.44 m/yr.

Kızılırmak Delta, which is shaped by the sediment fluxes from the Kızılırmak River, has been facing erosion since the 1960s. This situation occurred due to the construction of nine dams over the Kızılırmak River between the years 1959 and 2012 (Ataol, 2019). In addition, recent growths in the wind and wave impacts due to climate change contributed to erosion processes in the Kızılırmak Delta (Öztürk and Sesli, 2015). Görmüş et al. (2021) declared that the erosion rate at the river mouth is -17.8 m/yr between the years 1974 and 2017, which is also coherent with the results of this study.



Figure 4.44 Selected study site in Bafra where the long-term variations of shoreline are explored (Luijendijk et al., 2018)

Table 4.9 Long-term changes of the shorelines in the transactions in the Bafra. 90% statistically significant trends (p value<0.1) are shown with *

Point No	Long.	Lat.	Trend (m/yr)	p-value
1	35.96	41.73	-7.20	0.095*
2	35.97	41.73	-15.90	0.297*
3	35.98	41.73	-21.20	0.011*
4	35.99	41.73	-17.40	0.064*
5	36.00	41.73	-15.20	0.011*
6	36.00	41.73	-21.80	0.182*
7	36.01	41.72	-17.10	0.000*
8	36.02	41.72	-13.20	0.588*
9	35.93	41.72	-0.20	0.095*
10	35.92	41.72	-0.14	0.297
11	35.92	41.72	-0.56	0.011*
12	35.92	41.72	-0.29	0.064*
13	35.91	41.72	-0.45	0.011*
14	35.91	41.72	-0.26	0.182
15	35.90	41.72	-0.47	0.000*
16	35.90	41.71	-0.09	0.588
17	35.90	41.71	-0.19	0.073*
18	35.89	41.71	-0.35	0.026*
19	35.89	41.71	-0.09	0.343
20	35.88	41.71	0.10	0.057*
21	35.88	41.71	0.41	0.055*
22	35.88	41.71	0.46	0.001*
23	35.87	41.70	-0.08	0.367
24	35.87	41.70	0.49	0.038*
25	35.86	41.70	0.51	0.002*
26	35.86	41.70	0.72	0.010*
27	35.85	41.70	0.29	0.278
28	35.85	41.70	0.11	0.498
29	35.85	41.70	0.33	0.123
30	35.84	41.69	0.10	0.454
31	35.84	41.69	-0.04	0.835
32	35.83	41.69	-0.16	0.381
33	35.83	41.69	0.02	0.826
34	35.83	41.69	0.18	0.168
35	35.82	41.69	0.23	0.063*
36	35.82	41.69	0.29	0.086*
37	35.81	41.68	0.33	0.003*

Table 4.9 Long-term changes of the shorelines in the transactions in the Bafra. 90% statistically significant trends (p value<0.1) are shown with * (Continued)

Point No	Long.	Lat.	Trend (m/yr)	p-value
38	35.81	41.68	0.53	0.003*
39	35.81	41.68	-2.38	0.010*
40	35.80	41.68	-1.29	0.003*
41	35.80	41.68	-5.71	0.001*
42	35.79	41.68	0.73	0.008*
43	35.79	41.68	-0.85	0.620
44	35.78	41.68	0.41	0.279
45	35.78	41.67	0.13	0.484
46	35.78	41.67	0.44	0.378
47	35.77	41.67	0.24	0.080*
48	35.77	41.67	-0.13	0.359
49	35.76	41.67	-0.23	0.113
50	35.76	41.67	-0.08	0.602
51	35.75	41.67	-0.05	0.792
52	35.75	41.67	0.14	0.427
53	35.75	41.67	-0.15	0.612
54	35.74	41.66	-0.11	0.487
55	35.74	41.66	-0.16	0.333
56	35.73	41.66	-0.16	0.216
57	35.73	41.66	-0.13	0.252
58	35.73	41.66	-0.21	0.097*
59	35.72	41.66	-0.45	0.001*
60	35.72	41.66	-0.49	0.002*
61	35.71	41.66	-0.69	0.000*
62	35.71	41.66	-0.38	0.001*
63	35.70	41.65	-0.59	0.006*
64	35.70	41.65	-0.97	0.001*
65	35.70	41.65	-0.67	0.030*
66	35.69	41.65	-0.70	0.003*
67	35.69	41.65	-0.63	0.002*
68	35.68	41.65	-0.65	0.000*
69	35.68	41.65	-0.33	0.035*
70	35.67	41.65	0.13	0.758
71	35.67	41.65	-0.38	0.183
72	35.67	41.65	0.19	0.454
73	35.66	41.64	-1.53	0.000*
74	35.66	41.64	-1.31	0.000*

To give an idea of the shoreline position changes in transaction points in the Bafra coastline, four shoreline position-time graphs were presented in Figure 4.45 as an example.

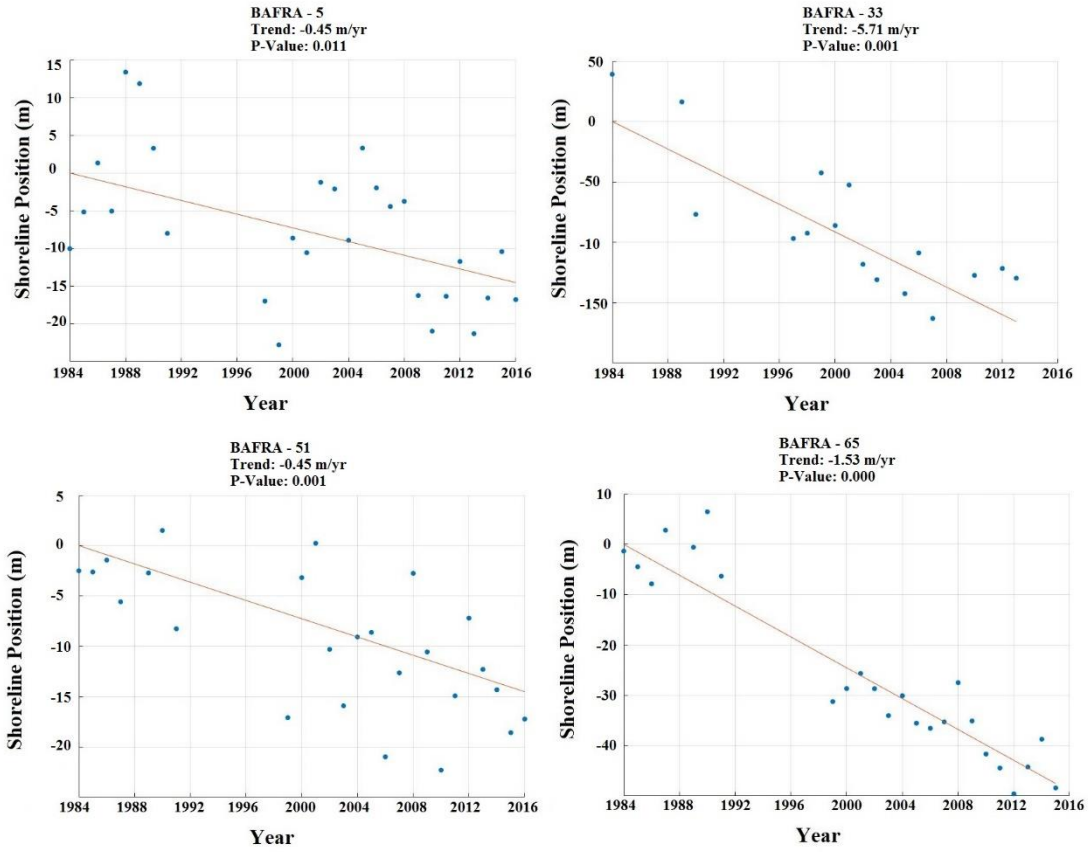


Figure 4.45 Shoreline positions and trends for particular points in Bafra

4.2.6 Çarşamba

The selected shoreline in the Çarşamba is 22 km long. It consisted of 44 transection points and is shown in Figure 4.46. The region is in the Yeşilırmak delta and is expected to be sensitive to erosion. It is one of the most important agricultural zones of Turkey with its fertile lands. The shoreline is sandy and represents an abraded morphology. In Table 4.10, it can be evaluated that the trends are significant at 33 points out of 44. In addition, nine of the significant

trends are positive and declare deposition on the shoreline. The minimum deposition rate is 1.07 m/yr and the maximum deposition rate is 16.92 m/yr.

Here, the mean deposition is calculated as 3.86 m/yr. On the other hand, 24 of the trends are negative, which means erosion. The minimum erosion rate is -0.39 m/yr and the maximum erosion rate is -23.33 m/yr. Here, the mean erosion is calculated as -7.32 m/yr.

Görmüş et al. (2021) also stated that there are erosion trends from -4.27 m/yr to -4.92 m/yr at the eastern regions of the Yeşilırmak month. Besides, on the western side, there are also erosional trends. The results seem consistent with the ones in this study. The continuous erosional characteristics of the Yeşilırmak Delta are evaluated as the consequence of the construction of 29 dams in the Yeşilırmak watershed (Kale et al., 2016).



Figure 4.46 Selected study site in Çarşamba where the long-term variations of shoreline are explored (Luijendijk et al., 2018)

Table 4.10 Long-term changes of the shorelines in the transactions in the Çarşamba. 90% statistically significant trends (p value<0.1) are shown with *

Point No	Longitude	Latitude	Trend (m/yr)	p-value
1	36.77	41.36	0.85	0.206
2	36.77	41.36	-0.85	0.003*
3	36.76	41.36	-1.38	0.000*
4	36.76	41.36	-1.21	0.000*
5	36.75	41.36	-1.25	0.000*
6	36.75	41.36	-0.95	0.001*
7	36.74	41.36	-0.39	0.087*
8	36.74	41.36	-0.12	0.747
9	36.73	41.36	0.48	0.206
10	36.73	41.36	1.07	0.004*
11	36.73	41.36	1.10	0.000*
12	36.72	41.37	2.33	0.000*
13	36.72	41.37	3.06	0.000*
14	36.71	41.37	1.40	0.008*
15	36.71	41.37	0.49	0.176
16	36.70	41.37	1.51	0.070*
17	36.70	41.37	1.49	0.535
18	36.69	41.37	-0.27	0.901
19	36.69	41.37	-4.48	0.107
20	36.69	41.37	-9.04	0.000*
21	36.68	41.37	-12.42	0.000*
22	36.68	41.37	-7.10	0.021*
23	36.67	41.37	-0.09	0.976
24	36.67	41.38	3.76	0.001*
25	36.67	41.38	-1.59	0.235
26	36.66	41.38	-2.27	0.785
27	36.66	41.38	16.92	0.000*
28	36.65	41.38	-12.67	0.000*
29	36.65	41.38	-23.32	0.000*
30	36.64	41.38	-18.70	0.000*
31	36.64	41.38	-12.82	0.000*
32	36.64	41.38	-10.53	0.000*
33	36.63	41.37	-8.22	0.000*
34	36.63	41.37	-7.38	0.000*
35	36.63	41.37	-6.50	0.000*
36	36.62	41.37	-6.24	0.000*
37	36.62	41.36	-6.48	0.000*
38	36.62	41.36	-7.33	0.000*
39	36.62	41.36	-6.76	0.000*
40	36.61	41.36	-5.53	0.006*
41	36.61	41.35	-4.63	0.000*
42	36.61	41.35	-3.88	0.040*
43	36.61	41.35	0.81	0.442
44	36.61	41.34	3.57	0.001*

To give an idea of the shoreline position changes in transaction points in the Çarşamba, four shoreline position-time graphs were presented in Figure 4.47 as an example.

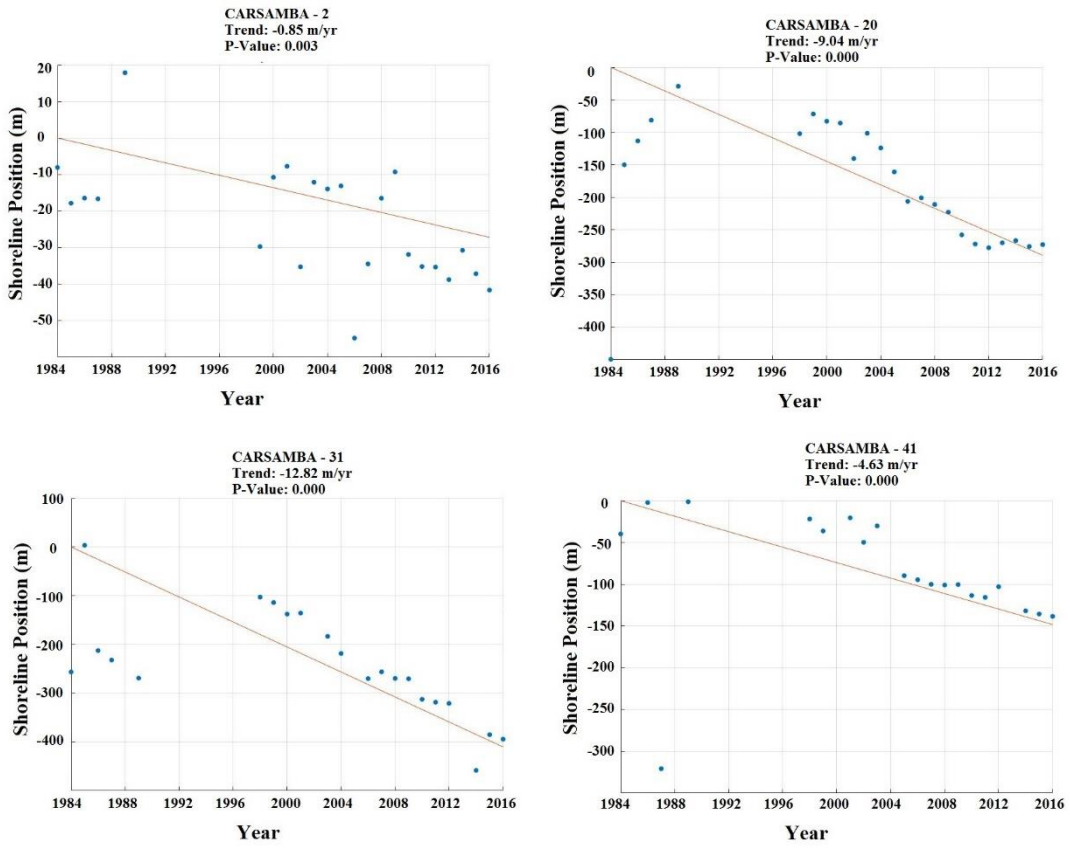


Figure 4.47 Shoreline positions and trends for particular points in Çarşamba

4.2.7 Sochi

The selected shoreline in the Sochi is 33 km long and it consisted of 67 transection points as shown in Figure 4.48. Sochi is an important coastal city in Russia, which is located near the Black Sea. The shoreline is mostly sandy and represents a moderately abraded weakly morphology. In Table 4.11, it can be evaluated that the trends are significant at 29 points out of 67. Here, 13 of the significant trends are positive and declare deposition on the shoreline. The minimum deposition rate is 0.17 m/yr and the maximum deposition rate is 5.24 m/yr. Here, the mean deposition is calculated as 0.85 m/yr. On the other hand, 16 of the trends are negative, which means erosion. The minimum erosion rate is -0.24 m/yr and the

maximum erosion rate is -0.75 m/yr. Here, the mean erosion is calculated as -0.39m/yr. Görmüş et al. (2021) also reported erosion rates with an average value of -0.62 m/yr, which also attracts attention to erosion for the Sochi Shoreline.

Anthropogenic activities are a strong forcing factor for coastal regions to shape their morphology. One prominent example of these activities is the construction of hard coastal protection structures. Especially, in the regions where severe erosion is observed, people try to prevent erosion by establishing these structures along the shorelines. Along the Russian coastline in the eastern Black Sea, it is very common to see hard coastal protection structures such as groynes, sea walls, revetments or breakwaters, etc. Nevertheless, in Sochi, despite the existence of hard coastal protection structures, erosion is going on (Kosyan et al., 2012).



Figure 4.48 Selected study site in Sochi where the long-term variations of shoreline are explored (Luijendijk et al., 2018)

Table 4.11 Long-term changes of the shorelines in the transactions in the Sochi. 90% statistically significant trends (p value<0.1) are shown with *

Point No	Long.	Lat.	Trend (m/yr)	p-value
1	39.70	43.61	-0.33	0.012*
2	39.70	43.61	-0.26	0.061*
3	39.70	43.61	-0.12	0.381
4	39.70	43.60	-0.26	0.123
5	39.71	43.60	-0.26	0.227
6	39.71	43.60	-0.18	0.317
7	39.71	43.59	0.70	0.002*
8	39.71	43.59	0.89	0.004*
9	39.71	43.59	0.76	0.008*
10	39.71	43.58	5.24	0.000*
11	39.72	43.58	0.14	0.532
12	39.72	43.58	0.02	0.802
13	39.72	43.58	-0.03	0.592
14	39.73	43.57	-0.09	0.167
15	39.73	43.57	-0.05	0.404
16	39.73	43.57	-0.07	0.491
17	39.74	43.57	0.35	0.019*
18	39.74	43.57	-0.04	0.323
19	39.74	43.56	0.24	0.091*
20	39.75	43.56	0.19	0.196
21	39.75	43.56	0.53	0.014*
22	39.75	43.56	0.51	0.030*
23	39.76	43.56	-0.29	0.118
24	39.76	43.56	-0.02	0.900
25	39.77	43.55	0.00	0.422
26	39.77	43.55	-0.01	0.741
27	39.77	43.55	-0.12	0.381
28	39.78	43.55	0.24	0.169
29	39.78	43.55	-0.07	0.602
30	39.78	43.55	-0.24	0.066*
31	39.79	43.54	-0.36	0.100*
32	39.79	43.54	-0.13	0.275
33	39.80	43.54	-0.20	0.104
34	39.80	43.54	0.16	0.381

Table 4.11 Long-term changes of the shorelines in the transactions in the Sochi. 90% statistically significant trends (p value<0.1) are shown with * (Continued)

Point No	Long.	Lat.	Trend (m/yr)	p-value
35	39.80	43.54	0.21	0.026*
36	39.81	43.54	-0.31	0.035*
37	39.81	43.53	-0.06	0.677
38	39.82	43.53	0.12	0.428
39	39.82	43.53	0.01	0.723
40	39.82	43.53	-0.15	0.178
41	39.83	43.53	-0.28	0.211
42	39.83	43.53	-0.10	0.393
43	39.83	43.52	-0.17	0.196
44	39.84	43.52	0.01	0.631
45	39.84	43.52	-0.14	0.478
46	39.85	43.52	-0.02	0.770
47	39.85	43.52	0.74	0.003*
48	39.85	43.51	0.38	0.003*
49	39.86	43.51	0.17	0.000*
50	39.86	43.51	0.30	0.037*
51	39.87	43.51	-0.10	0.707
52	39.87	43.51	-0.17	0.199
53	39.87	43.50	-0.24	0.178
54	39.88	43.50	-0.02	0.130
55	39.88	43.50	-0.37	0.001*
56	39.88	43.49	-0.30	0.039*
57	39.88	43.49	-0.16	0.114
58	39.89	43.49	-0.31	0.084*
59	39.89	43.49	-0.31	0.027*
60	39.89	43.48	-0.46	0.014*
61	39.89	43.48	-0.50	0.005*
62	39.89	43.48	-0.49	0.006*
63	39.89	43.47	-0.28	0.158
64	39.89	43.47	-0.31	0.045*
65	39.89	43.47	-0.40	0.006*
66	39.90	43.46	-0.75	0.005*
67	39.90	43.46	-0.56	0.019*

To give an idea of the shoreline position changes in transaction points in the Sochi, 4 shoreline position-time graphs were presented in Figure 4.49 as an example.

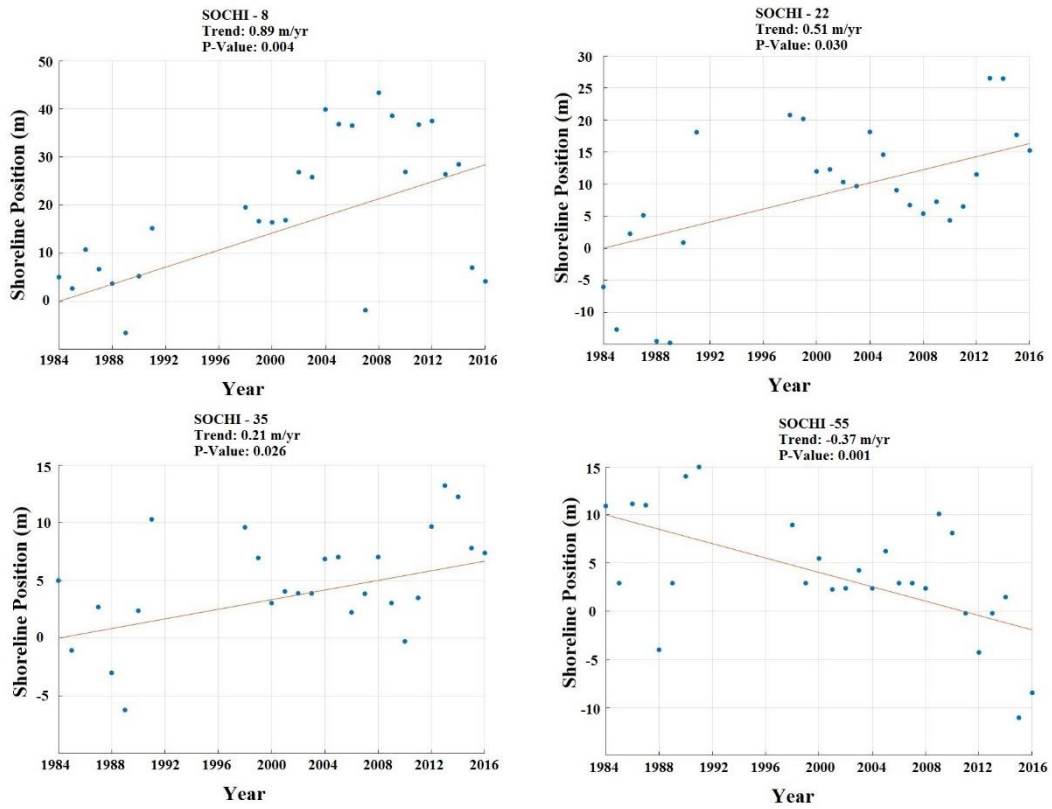


Figure 4.49 Shoreline positions and trends for particular points in the study site in Sochi

4.2.8 Long-Term Variations of Atmospheric Properties on the Selected Shoreline Regions

For seven shoreline regions (Danube Delta, Terkos Lake, Cide, Sinop Peninsula, Bafra Delta, Çarşamba Delta, and Sochi) which were investigated for their shoreline change trends, Long-Term Variations of Atmospheric Properties were also investigated. Firstly, Long-term annual averaged and 95th percentile wind speeds and their variations considering 38 years period (1979–2016) for selected regions along the Black Sea Coastline were shown in Table 4.12. Here, it is clear that on Terkos, Sinop, Bafra, Çarşamba, and Sochi, we see significant trends for the Long-term annual averaged wind speeds. Similarly, 95th percentile wind speeds represent significant trends in only Terkos, Çarşamba, and Sochi.

Table 4.12 Long-term annual averaged and 95th percentile wind speeds and their variations considering 38 years period (1979–2016) for selected regions along the Black Sea Coastline. 90% statistically significant trends (p value<0.1) are shown with *

SHORELINE	Annual Mean Wind Speed (m/s)	Trend of Annual Mean Wind Speed (ms^{-1}/yr)	Annual 95P Wind Speed (m/s)	Trend of Annual 95P Wind Speed (ms^{-1}/yr)
Danube	5.41	-0.05	10.16	-0.003
Terkos	5.74	-0.13*	11.09	-0.013*
Cide	3.53	0.08	6.66	-0.003
Sinop	4.71	0.12*	9.17	0.006
Bafra	4.06	0.2*	7.78	0.007
Çarşamba	3.98	0.19*	7.83	0.01*
Sochi	3.46	0.32*	7.21	0.024*

Besides; long-term annual average and 95th percentile SSTs and their variations considering 38 years period (1979–2016) for selected regions along the Black Sea Coastline were shown in the Table 4.13 Here; it is clear that in all of the regions, we see significant trends for both averaged and 95th percentile values.

Table 4.13 Long-term averaged and 95th percentile SSTs and their variations considering 38 years period (1979–2016) for selected regions along the Black Sea Coastline. 90% statistically significant trends (p value<0.1) are shown with *

Shoreline	Annual Mean SST (C^o)	Trend of Annual Mean SST (C^o/yr)	Annual 95th Percentile SST (C^o)	Trend of Annual Mean SST (C^o/yr)
Danube	14.68	0.01*	24.86	0.08*
Terkos	15.38	0.03*	24.42	0.07*
Cide	15.57	0.03*	25.11	0.08*
Sinop	15.38	0.03*	24.84	0.07*
Bafra	14.82	0.03*	24.22	0.07*
Çarşamba	15.76	0.03*	25.21	0.07*
Sochi	15.48	0.05*	25.00	0.01*

Likewise, the long-term annual average and 95th percentile SWHs and their variations considering 38 years period (1979–2016) for selected regions along the Black Sea Coastline were shown in Table 4.14. Here, it is clear that on Cide, Sinop, Bafra, Çarşamba, and Sochi, we see significant trends for the Long-term annual averaged wind speeds. In the same vein, for the long-term variations of annual 95th percentile SWHs, significant trends are shown on Terkos, Sinop, Bafra, Çarşamba, and Sochi.

Table 4.14 Long-term averaged and 95th percentile SWHs and their variations considering 38 years period (1979–2016) for selected regions along the Black Sea Coastline. 90% statistically significant trends (p value<0.1) are shown with *

Shoreline	Annual Mean SWH (m)	Trend of Annual Mean SWH (m/yr)	Annual 95th percentile SWH (SWH) (m)	Trend of Annual Mean SWH (m/yr)
Danube	0.8	0.0005	1.97	-0.0007
Terkos	0.64	0.0002	1.6	-0.004*
Cide	0.75	0.002*	1.78	0
Sinop	0.63	0.003*	1.49	0.003*
Bafra	0.65	0.003*	1.53	0.005*
Çarşamba	0.65	0.003*	1.54	0.005*
Sochi	0.56	0.004*	1.38	0.007*

4.2.9 Relation of Shoreline Changes with Long-Term Variations of Atmospheric Parameters

Up to now, the variations of several atmospheric properties (winds, waves, SSTs, precipitation, and evaporation) over the Black Sea Basin in the last decades have been investigated and the trends of each parameter were presented. Along with these, the shoreline changes along the coasts of the Black Sea were also evaluated. This section, it is aimed to search for a relationship between the long-term variations of three atmospheric parameters which are winds, waves, and SSTs with shoreline changes.

For this purpose, in the 271 shoreline zones which and the annual shoreline changes were investigated, the trend values of each of three atmospheric parameters and shoreline position were calculated. For all shoreline zones, significant trends of each parameter were examined; a relation between these values and shoreline change trends was checked out. To figure out this, shoreline changes in the regions and long-term trends of particular atmospheric parameters were plotted for the regions where the trends are significant among 271 shoreline zones near the Black Sea. These scatter plots are shown in Figures 4.50-55.

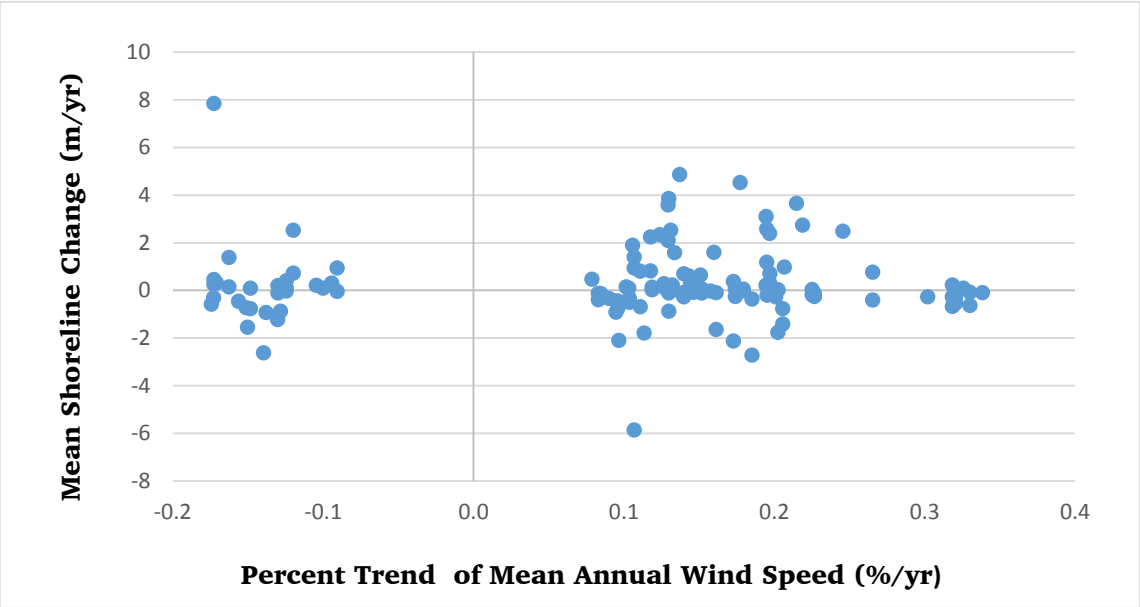


Figure 4.50 Mean annual shoreline changes vs mean annual wind speed trends scatter graph in 130 points where the trends are significant

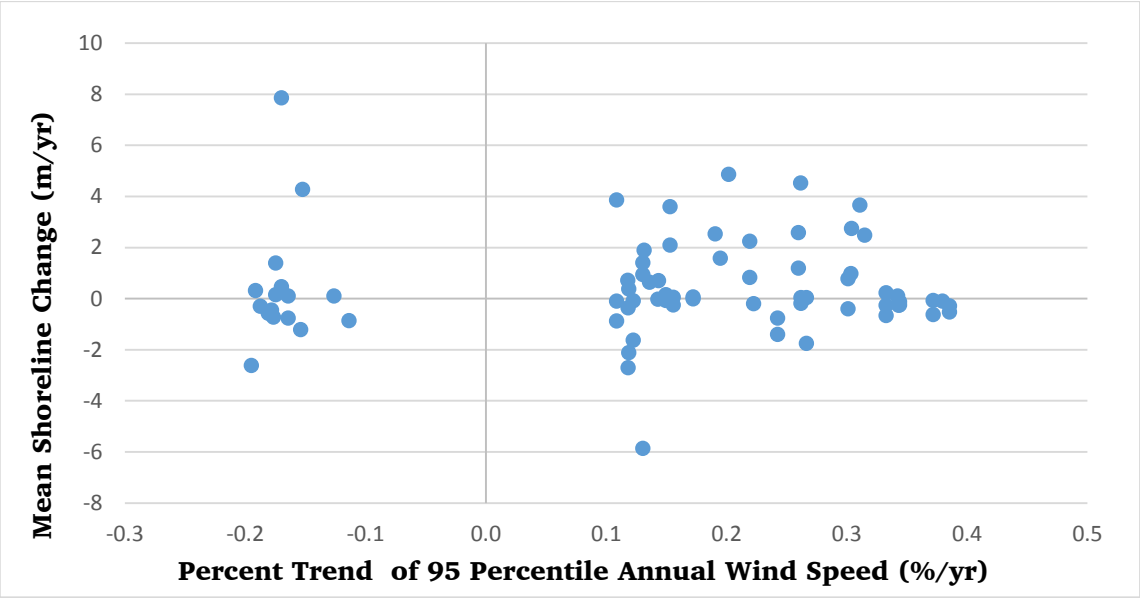


Figure 4.51 Mean annual shoreline changes vs 95th percentile annual wind speed trends in 75 Points where the trends are at least 90% significant

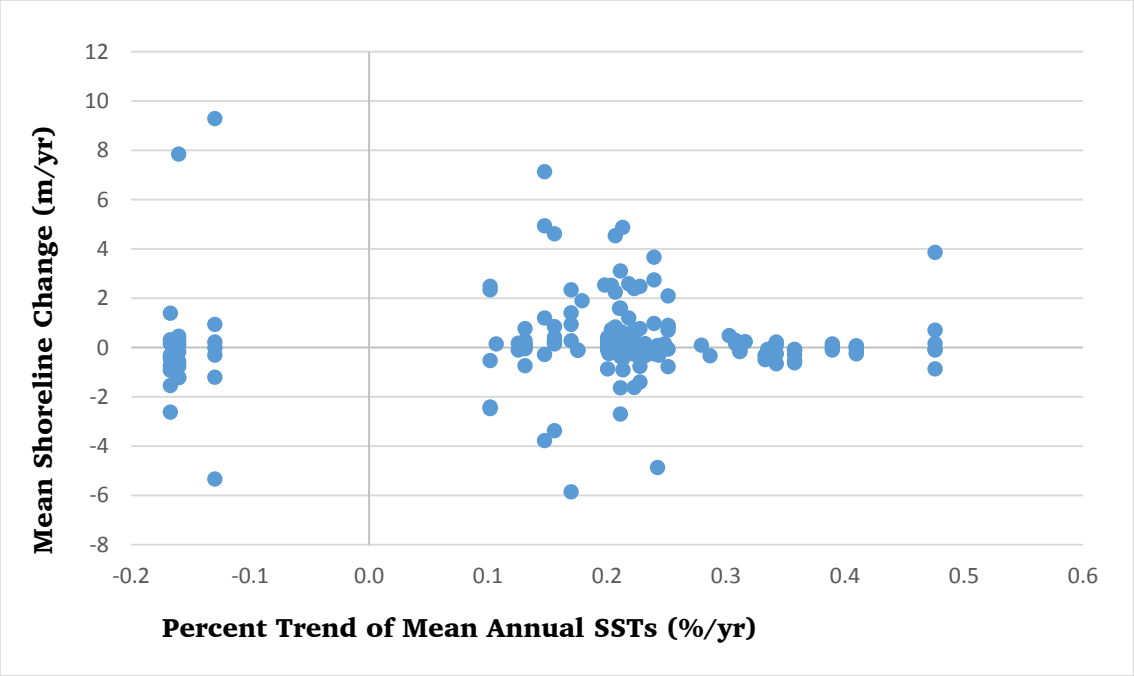


Figure 4.52 Mean annual shoreline changes vs mean annual SST trends in 174 points where the trends are at least 90% significant

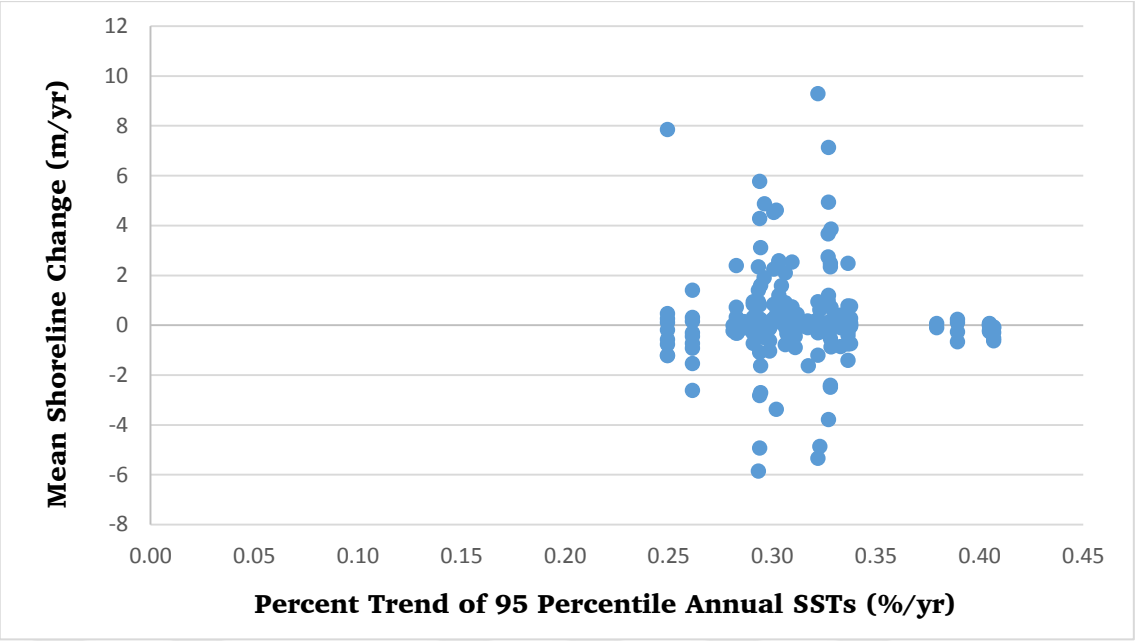


Figure 4.53 Mean annual shoreline changes vs 95th percentile annual SST trends in 198 points where the trends are at least 90% significant

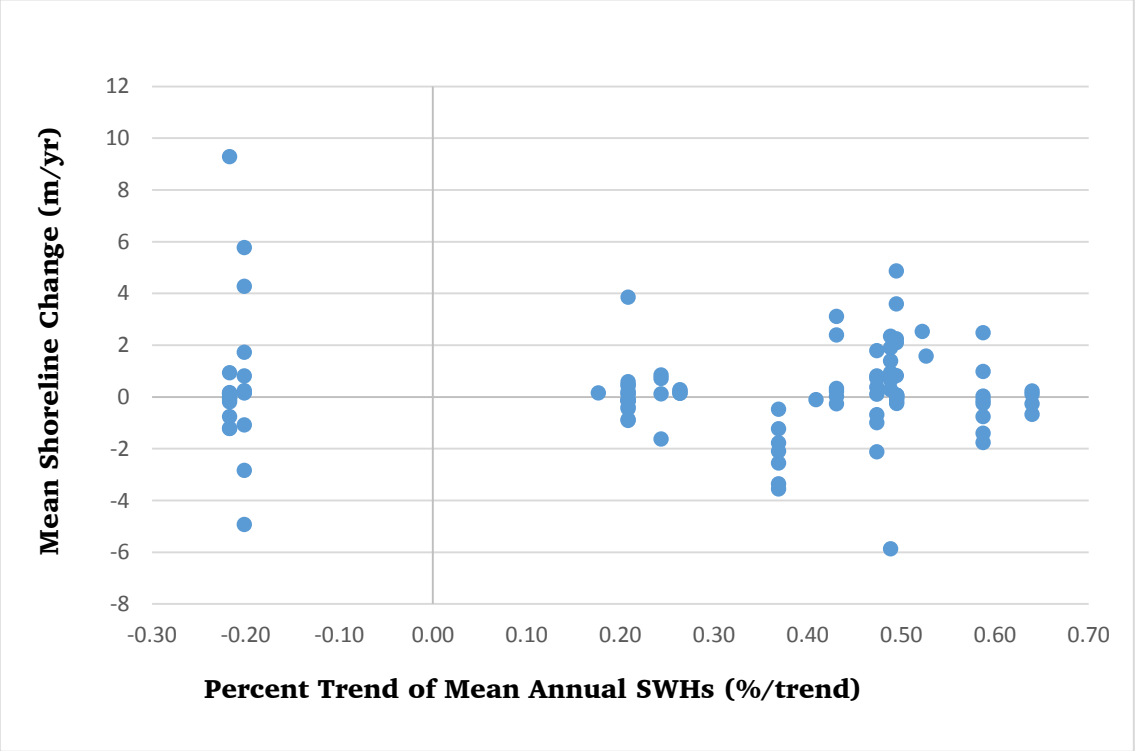


Figure 4.54 Mean annual shoreline changes vs mean annual SWH trends in 103 Points where the trends are at least 90% significant

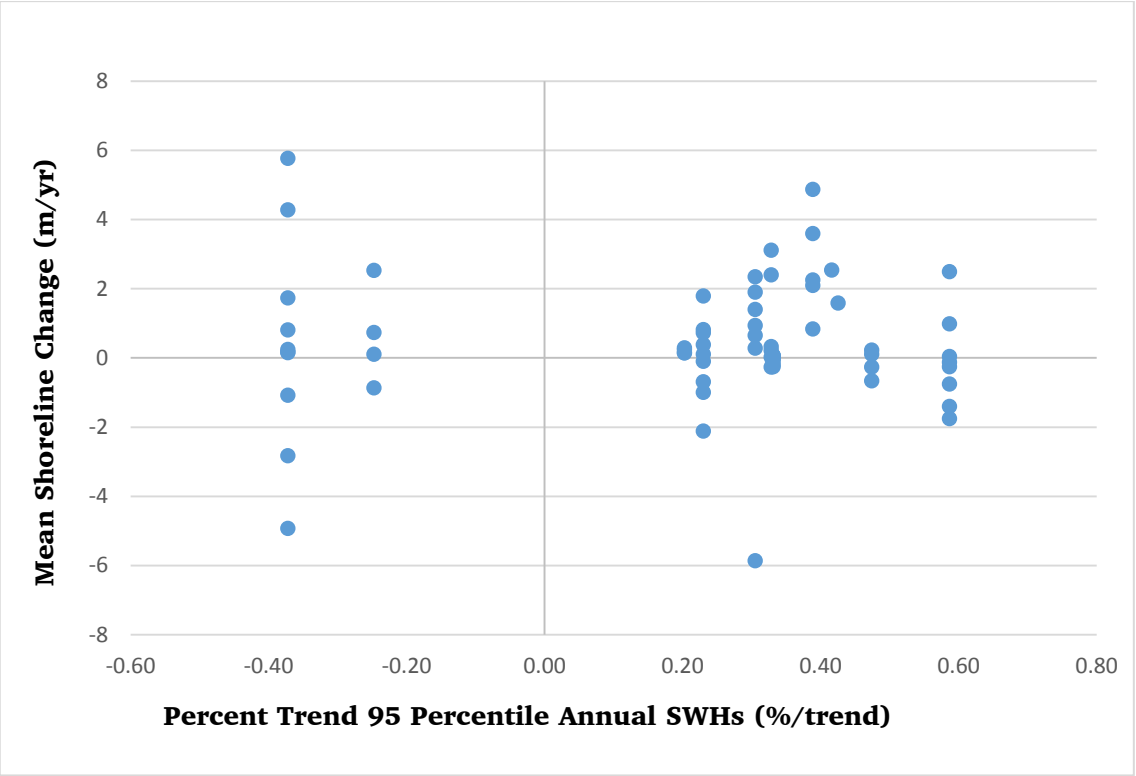


Figure 4.55 Mean annual shoreline changes vs mean annual SWH trends in 68 points where the trends are at least 90% significant

By considering the relationship between the shoreline change trends with the trends of wind, wave, and SST trends, it is not possible to define a mathematical connection among the scatter plots. This can be a result of several factors.

Firstly, the Total number of transection points is 15718 constituting 271 shoreline zones around the Black Sea. 271 shoreline zones are chosen due to shoreline geometry by detecting successive shoreline strips, which consist of an average of 58 transection points. Investigating each transection point separately may lead to better approximations for the relationship between shoreline change and atmospheric variations.

Besides, the shoreline changes depend on not only atmospheric conditions but also anthropogenic activities, shoreline direction, morphology, sediment properties, etc. Here, the necessity of studying in a finer resolution comes out, to investigate the interrelation of any parameter with long-term shoreline change.

Accordingly, to provide a clearer connection between shoreline changes and atmospheric forcing; the seven shoreline regions (Danube Delta, Terkos Lake, Cide, Sinop Peninsula, Bafra Delta, Çarşamba Delta, and Sochi) which were investigated for their shoreline change trends were evaluated. Long-term annual time series of mean and 95th percentile wind speeds, SWHs, and SSTs were constructed, and the Pearson correlation coefficients of each were calculated regarding the annual shoreline position trends. As an interpretation for the Pearson correlation coefficients (r), the r values which are between 0.5 and 1 or -0.5 and -1 are considered meaningful (Dancey and Reidy, 2004).

When considering the transection points in the Danube Region, it is possible to say that the annual shoreline positions do not represent moderate correlations with the annual time series of mean and 95th percentile wind speeds and SWHs. Mean and 95th percentile annual SSTs seem correlated with annual shoreline positions. In the transaction points, 1-10, where we see positive shoreline change trends (deposition), the correlation values between the shoreline positions and mean SSTs reach up to 0.73. This is also similar to 95th percentile annual SSTs and in these points, the correlation coefficient values reach up to 0.65. The correlation coefficient values for all transection points are shown in Table 4.15.

Table 4.15 Pearson correlation coefficients (r) between annual atmospheric parameters and shoreline positions for Danube. Green and yellow colors indicate strong and moderate correlations, respectively

Transection #	Mean Winds	95P Winds	Mean SWH	95P SWH	Mean SST	95P SST	Transection #	Mean Winds	95P Winds	Mean SWH	95P SWH	Mean SST	95P SST
1	0.02	-0.02	0.16	-0.16	0.63	0.56	**33**	0.28	0.20	0.45	0.26	0.15	0.14
2	0.10	0.04	0.18	-0.10	0.61	0.54	**34**	0.29	0.22	0.46	0.27	0.16	0.16
3	0.08	-0.05	0.18	-0.15	0.68	0.58	**35**	0.28	0.19	0.43	0.25	0.14	0.12
4	0.11	0.01	0.25	-0.05	0.70	0.63	**36**	0.27	0.18	0.40	0.24	0.09	0.04
5	0.08	-0.02	0.22	-0.08	0.73	0.64	**37**	-0.08	-0.18	-0.23	-0.19	-0.13	**-0.46**
6	0.15	0.05	0.29	-0.04	0.72	0.63	**38**	-0.10	-0.20	-0.26	-0.21	-0.23	**-0.50**
7	0.12	0.02	0.25	-0.05	0.72	0.65	**39**	-0.09	-0.20	-0.24	-0.18	-0.22	**-0.50**
8	0.14	0.02	0.24	-0.05	0.67	0.58	**40**	-0.14	-0.23	-0.25	-0.20	-0.11	**-0.41**
9	0.14	-0.01	0.19	-0.12	0.68	0.57	**41**	-0.12	-0.21	-0.22	-0.21	0.00	**-0.34**
10	0.13	0.00	0.18	-0.12	0.65	0.50	**42**	0.13	0.06	0.30	0.09	0.43	0.23
11	0.08	-0.05	0.01	-0.28	0.52	0.25	**43**	0.12	0.03	0.24	0.05	0.40	0.13
12	-0.05	-0.16	-0.08	**-0.33**	0.45	0.23	**44**	0.17	0.06	0.27	0.08	0.32	0.06
13	-0.20	**-0.32**	-0.25	**-0.42**	0.31	-0.06	**45**	0.06	-0.03	0.14	-0.02	0.39	0.11
14	-0.30	-0.28	**-0.31**	**-0.42**	0.39	0.10	**46**	0.08	-0.07	0.10	-0.08	0.40	0.20
15	-0.20	-0.27	-0.25	**-0.36**	0.35	0.01	**47**	0.07	-0.07	0.10	-0.08	0.38	0.19
16	0.04	-0.14	-0.07	-0.25	0.37	0.11	**48**	0.06	-0.10	0.01	-0.12	0.22	0.08
17	-0.03	-0.08	0.00	-0.20	0.52	0.15	**49**	0.02	-0.13	0.00	-0.14	0.34	0.07
18	-0.04	-0.15	-0.05	-0.22	0.30	-0.06	**50**	0.08	-0.05	0.02	-0.01	-0.14	**-0.42**
19	-0.04	-0.16	-0.07	-0.21	0.19	-0.20	**51**	-0.04	-0.11	-0.02	-0.11	0.31	-0.01
20	-0.10	-0.26	-0.23	-0.29	0.07	-0.27	**52**	-0.04	-0.12	-0.04	-0.11	0.23	-0.10
21	0.01	-0.18	-0.18	-0.19	-0.10	**-0.43**	**53**	-0.02	0.05	-0.08	-0.05	0.16	0.05
22	-0.03	-0.17	-0.20	-0.18	-0.09	**-0.39**	**54**	-0.28	-0.13	-0.23	**-0.31**	0.27	0.06
23	0.00	-0.14	-0.15	-0.18	-0.03	**-0.38**	**55**	-0.02	-0.05	-0.03	-0.26	0.34	0.34
24	0.01	-0.14	-0.16	-0.18	-0.11	**-0.44**	**56**	0.11	-0.03	-0.09	-0.10	-0.12	-0.15
25	0.04	0.10	0.03	-0.06	0.03	-0.26	**57**	-0.13	0.00	-0.17	0.00	**-0.51**	**-0.39**
26	0.06	0.13	0.02	-0.05	-0.01	-0.29	**58**	-0.13	0.00	-0.18	-0.01	**-0.47**	**-0.42**
27	0.02	-0.16	-0.19	-0.18	-0.17	**-0.48**	**59**	0.01	0.00	-0.18	-0.02	**-0.55**	**-0.64**
28	0.06	-0.11	-0.14	-0.12	-0.19	**-0.49**	**60**	**-0.41**	-0.26	**-0.53**	-0.28	**-0.46**	**-0.50**
29	0.01	-0.14	-0.18	-0.14	-0.23	**-0.52**							
30	-0.02	-0.17	-0.23	-0.17	-0.30	**-0.55**							
31	0.30	0.21	0.46	0.27	0.14	0.13	**Min**	**-0.41**	**-0.32**	**-0.53**	**-0.42**	**-0.55**	**-0.64**
32	0.28	0.20	0.45	0.26	0.16	0.14	**Max**	0.30	0.22	0.46	0.27	0.73	0.65

Table 4.16 Pearson correlation coefficients (r) between annual atmospheric parameters and shoreline positions for Terkos. Green and yellow colors indicate strong and moderate correlations, respectively

Transection #	Mean Winds	95P Winds	Mean SWH	95P SWH	Mean SST	95P SST	Transection #	Mean Winds	95P Winds	Mean SWH	95P SWH	Mean SST	95P SST
1	0.20	0.11	0.01	-0.06	-0.30	-0.42	**37**	-0.08	-0.06	-0.01	-0.15	0.61	0.57
2	0.22	-0.23	0.08	-0.19	-0.22	-0.25	**38**	0.16	0.21	0.11	0.04	0.14	0.04
3	0.20	-0.18	0.06	-0.34	0.04	-0.23	**39**	-0.31	-0.14	-0.14	-0.14	0.71	0.78
4	0.11	-0.09	0.13	-0.03	-0.27	-0.42	**40**	-0.18	-0.12	-0.16	-0.24	0.52	0.60
5	-0.03	-0.18	-0.12	-0.09	0.21	-0.06	**41**	0.04	0.07	-0.01	0.09	0.17	0.01
6	0.11	0.15	0.00	0.00	-0.21	-0.32	**42**	0.27	0.26	0.17	0.08	-0.13	-0.21
7	0.25	0.26	0.14	0.08	-0.09	-0.20	**43**	0.28	0.28	0.18	0.09	-0.06	-0.16
8	0.22	0.25	0.11	0.06	-0.05	-0.18	**44**	0.10	0.05	0.15	0.07	0.09	0.08
9	0.19	0.24	0.12	0.06	0.02	-0.12	**45**	-0.11	0.02	0.09	-0.06	0.62	0.65
10	0.21	0.24	0.12	0.08	0.07	-0.08	**46**	0.00	0.04	0.27	0.03	0.41	0.38
11	0.17	0.18	0.05	0.05	0.02	-0.14	**47**	0.11	0.18	0.09	0.00	0.17	0.12
12	0.26	0.23	0.08	0.12	-0.11	-0.23	**48**	0.14	0.20	0.11	0.03	0.10	0.04
13	0.27	0.25	0.14	0.16	-0.13	-0.28	**49**	0.21	0.23	0.13	0.05	0.03	-0.08
14	0.27	0.19	0.09	0.12	-0.21	-0.39	**50**	0.11	0.20	0.08	0.03	0.20	0.13
15	0.19	0.17	-0.05	-0.07	-0.11	-0.11	**51**	0.14	0.16	0.07	0.00	0.05	0.00
16	-0.23	-0.37	-0.35	-0.40	-0.32	-0.35	**52**	0.15	0.19	0.12	0.02	0.11	0.06
17	0.04	0.11	0.00	0.14	-0.28	-0.25	**53**	0.11	0.15	0.11	0.00	0.10	-0.01
18	0.19	0.19	0.04	-0.02	-0.02	-0.18	**54**	0.21	0.23	0.16	0.04	0.07	-0.08
19	0.04	-0.14	-0.19	-0.24	-0.18	-0.33	**55**	0.23	0.24	0.16	0.05	-0.01	-0.09
20	-0.21	-0.40	-0.29	-0.40	-0.04	-0.24	**56**	-0.26	-0.21	-0.05	-0.10	-0.14	-0.04
21	-0.02	-0.12	0.01	0.02	-0.08	-0.34	**57**	0.23	0.24	0.14	0.06	-0.02	-0.13
22	0.14	0.22	-0.01	0.32	-0.07	-0.18	**58**	0.23	0.24	0.14	0.05	-0.01	-0.11
23	0.05	0.12	-0.09	0.19	0.11	0.03	**59**	0.21	0.29	0.14	0.13	0.18	0.12
24	0.26	0.22	0.02	0.30	-0.45	-0.52	**60**	0.12	0.18	0.30	0.37	-0.18	-0.08
25	0.25	0.24	0.09	0.32	-0.39	-0.54	**61**	-0.22	-0.08	-0.16	-0.21	0.63	0.45
26	0.22	0.03	0.00	0.10	-0.62	-0.73	**62**	0.07	0.11	-0.01	-0.12	0.21	0.08
27	-0.22	-0.33	-0.28	-0.50	0.46	0.42	**63**	-0.07	-0.21	0.07	-0.12	0.00	-0.07
28	-0.31	-0.19	-0.13	-0.15	0.47	0.58	**64**	-0.04	0.05	0.04	0.00	-0.12	-0.13
29	-0.24	-0.08	-0.07	-0.14	0.68	0.80	**65**	-0.02	0.01	0.04	-0.08	0.17	0.20
30	-0.19	-0.04	-0.12	-0.17	0.58	0.76	**66**	0.00	-0.04	0.08	-0.12	0.02	0.17
31	-0.17	-0.07	-0.05	-0.11	0.70	0.75	**67**	-0.15	0.02	-0.13	-0.19	0.78	0.64
32	0.21	0.22	0.12	0.02	0.08	-0.02	**68**	0.22	0.23	0.11	0.02	0.05	-0.06
33	0.11	0.13	-0.02	-0.05	0.16	0.14	**69**	0.21	0.23	0.12	0.04	0.03	-0.08
34	0.24	0.26	0.19	0.07	-0.01	-0.07							
35	0.20	0.22	0.12	0.02	0.07	-0.03	**Min**	-0.31	-0.40	-0.35	-0.50	-0.62	-0.73
36	0.18	0.18	0.11	-0.03	0.19	0.09	**Max**	0.28	0.29	0.30	0.37	0.78	0.80

Similarly, from Table 4.16, it is also possible to detect moderate correlations between the trends of annual values of atmospheric forcing and annual shoreline position for the Terkos. Only, for a few transection points, correlation coefficients exceeding 0.5 for mean and 95th percentile annual SSTs.

By considering the Pearson correlation coefficient values in Table 4.17, it is only possible to define moderate correlations between the trends of annual values of atmospheric forcing and annual shoreline position for the transection points in the Cide. Between SST and shoreline positions, strong correlations exist. Likewise, this situation is also prevailing in Sinop. The correlation coefficient values for Sinop are represented in Table 4.18.

Table 4.17 Pearson correlation coefficients (r) between annual atmospheric parameters and shoreline positions for Cide. Green and yellow colors indicate strong and moderate correlations, respectively

Transection #	Mean Winds	95P Winds	Mean SWH	95P SWH	Mean SST	95P SST	Transection #	Mean Winds	95P Winds	Mean SWH	95P SWH	Mean SST	95P SST
1	-0.15	**-0.32**	-0.19	-0.14	0.05	0.12	**35**	0.17	-0.07	0.19	0.06	-0.05	-0.04
2	0.25	0.43	0.13	0.22	0.20	0.07	**36**	0.03	0.03	0.00	-0.01	0.07	0.20
3	-0.12	0.07	-0.25	-0.30	0.14	-0.02	**37**	-0.03	-0.01	-0.09	-0.07	-0.02	-0.28
4	-0.18	**-0.36**	-0.19	-0.13	0.01	0.11	**38**	-0.15	-0.01	-0.13	0.04	**-0.32**	-0.15
5	-0.21	**-0.32**	**-0.35**	**-0.38**	0.07	-0.01	**39**	-0.03	-0.09	0.02	0.14	**-0.32**	-0.01
6	0.01	-0.18	-0.07	0.02	0.11	0.18	**40**	0.12	0.00	0.07	0.02	-0.23	**-0.31**
7	-0.06	-0.24	-0.11	-0.05	-0.05	0.04	**41**	0.28	0.17	0.18	0.08	-0.13	-0.22
8	0.15	-0.05	0.04	0.05	-0.11	0.00	**42**	0.25	0.32	0.15	0.20	0.10	0.02
9	-0.02	-0.15	-0.12	-0.05	0.28	0.26	**43**	0.30	0.28	0.14	0.10	0.35	0.20
10	0.22	0.15	0.13	-0.02	0.63	0.58	**44**	0.16	0.03	0.11	0.07	-0.25	**-0.37**
11	0.31	0.14	0.23	0.05	0.37	0.29	**45**	0.26	0.19	0.12	0.05	0.07	-0.02
12	0.21	0.06	0.07	-0.03	0.04	-0.09	**46**	0.13	0.08	0.03	0.04	-0.10	**-0.34**
13	0.18	0.04	0.00	-0.07	0.18	0.04	**47**	0.35	0.32	0.22	0.25	-0.06	-0.18
14	0.19	0.07	0.01	-0.11	0.24	0.11	**48**	0.20	0.18	0.05	0.10	-0.18	-0.05
15	0.30	0.08	0.16	0.22	0.18	0.24	**49**	0.18	0.14	0.18	0.19	**-0.53**	**-0.45**
16	0.01	0.06	-0.05	0.04	-0.13	-0.20	**50**	-0.11	0.10	-0.03	0.12	**-0.68**	**-0.48**
17	0.01	-0.03	0.03	0.11	-0.20	**-0.43**	**51**	0.04	-0.02	-0.04	0.03	-0.25	-0.07
18	-0.15	-0.28	-0.16	-0.05	-0.15	**-0.32**	**52**	**-0.30**	**-0.50**	**-0.35**	-0.17	**-0.32**	-0.24
19	-0.16	-0.28	-0.16	-0.05	-0.15	**-0.31**	**53**	-0.27	**-0.42**	-0.28	-0.04	**-0.52**	**-0.38**
20	-0.25	**-0.38**	-0.28	**-0.37**	-0.08	-0.23	**54**	0.13	-0.10	-0.01	0.27	**-0.33**	-0.16
21	-0.06	-0.21	-0.15	-0.17	0.20	0.24	**55**	0.06	-0.14	0.09	0.17	-0.29	-0.19
22	0.02	-0.02	-0.13	-0.24	0.28	0.23	**56**	-0.13	**-0.31**	-0.29	-0.17	-0.01	-0.03
23	0.26	0.18	0.09	0.08	0.11	-0.01	**57**	-0.20	**-0.36**	-0.21	0.00	**-0.43**	**-0.33**
24	0.17	0.03	0.04	0.08	-0.11	-0.14	**58**	-0.18	**-0.37**	-0.20	-0.01	-0.28	-0.23
25	0.17	0.08	0.00	0.05	0.24	0.22	**59**	-0.02	-0.05	-0.03	0.04	0.02	-0.08
26	0.32	0.29	0.12	0.07	0.28	0.17	**60**	-0.14	**-0.31**	-0.12	-0.14	**-0.43**	-0.23
27	0.08	0.03	-0.03	-0.05	-0.03	-0.18	**61**	-0.18	-0.11	-0.18	-0.12	**-0.33**	-0.22
28	0.27	0.25	0.13	0.11	0.10	0.02	**62**	0.11	0.00	0.10	0.05	0.04	0.23
29	-0.19	**-0.33**	-0.19	-0.09	**-0.34**	**-0.30**	**63**	0.49	0.28	0.35	0.19	0.05	0.01
30	0.17	0.16	0.04	0.11	0.00	-0.19	**64**	0.17	0.15	0.02	-0.16	0.30	0.20
31	0.50	0.44	0.31	0.24	0.30	0.26	**65**	0.24	0.10	0.20	0.14	**-0.36**	**-0.37**
32	0.41	0.38	0.23	0.14	0.31	0.24	**66**	-0.22	-0.29	-0.24	-0.11	**-0.42**	**-0.39**
33	0.39	0.30	0.28	0.30	-0.09	-0.09	**67**	0.15	0.04	0.12	0.17	**-0.54**	**-0.55**
34	0.15	-0.09	0.16	0.02	-0.09	-0.16	**68**	0.13	0.01	0.14	0.16	**-0.46**	**-0.38**

Table 4.17 Pearson correlation coefficients (r) between annual atmospheric parameters and shoreline positions for Cide. Green and yellow colors indicate strong and moderate correlations, respectively (Continued)

Transection #	Mean Winds	95P Winds	Mean SWH	95P SWH	Mean SST	95P SST	Transection #	Mean Winds	95P Winds	Mean SWH	95P SWH	Mean SST	95P SST
69	0.19	0.06	0.20	0.28	-0.42	-0.40	**103**	0.29	0.23	0.15	0.18	0.42	0.43
70	0.50	0.40	0.34	0.40	0.09	0.09	**104**	0.54	0.46	0.35	0.42	0.26	0.25
71	0.32	0.20	0.22	0.36	-0.28	-0.32	**105**	-0.12	-0.13	-0.16	0.03	-0.40	-0.33
72	0.33	0.20	0.17	0.33	-0.04	0.15	**106**	-0.14	-0.14	-0.19	0.01	-0.39	-0.32
73	0.52	0.40	0.40	0.51	0.18	0.17	**107**	-0.06	-0.09	-0.18	-0.07	-0.01	-0.15
74	0.46	0.32	0.30	0.38	0.16	0.15	**108**	-0.04	-0.06	-0.10	-0.10	0.22	0.26
75	0.11	0.15	0.20	0.08	-0.06	-0.25	**109**	-0.05	-0.02	0.08	0.26	-0.18	-0.15
76	0.10	0.02	0.07	0.13	-0.51	-0.44	**110**	-0.05	-0.14	-0.07	0.00	-0.13	0.03
77	0.03	-0.05	0.03	0.12	-0.54	-0.47	**111**	-0.08	-0.08	-0.06	-0.07	-0.28	-0.18
78	0.11	0.08	0.12	0.27	-0.58	-0.43	**112**	0.41	0.27	0.48	0.44	0.04	-0.11
79	0.23	0.20	0.15	0.21	-0.42	-0.42	**113**	0.06	-0.31	-0.04	-0.04	0.10	0.26
80	0.34	0.26	0.29	0.25	-0.47	-0.48	**114**	-0.05	-0.31	-0.18	-0.17	-0.14	-0.02
81	0.22	0.02	0.19	0.24	-0.28	-0.35	**115**	-0.07	-0.09	0.06	0.01	-0.47	-0.28
82	0.19	0.05	0.14	0.18	-0.39	-0.54	**116**	-0.08	-0.15	0.10	0.00	-0.50	-0.28
83	0.04	-0.10	-0.01	0.06	-0.46	-0.54	**117**	0.12	-0.09	0.18	0.16	-0.30	-0.43
84	-0.24	-0.31	-0.27	-0.19	-0.32	-0.50	**118**	0.51	0.40	0.34	0.39	0.13	0.14
85	0.15	-0.01	0.15	0.20	-0.21	-0.43	**119**	0.49	0.41	0.28	0.25	0.28	0.24
86	0.03	-0.18	0.07	0.06	-0.39	-0.53	**120**	0.13	-0.03	0.01	0.03	-0.18	-0.21
87	0.08	-0.09	0.07	0.17	-0.33	-0.46	**121**	0.09	-0.02	0.05	0.14	-0.30	-0.30
88	0.09	-0.03	0.05	0.26	-0.49	-0.48	**122**	0.12	-0.05	0.03	0.09	-0.41	-0.37
89	0.48	0.32	0.38	0.38	-0.10	-0.13	**123**	0.16	0.10	0.07	0.16	-0.34	-0.40
90	-0.14	-0.17	-0.19	0.01	-0.45	-0.35	**124**	0.21	0.30	0.17	0.26	-0.21	-0.28
91	-0.03	-0.09	-0.01	0.00	-0.19	0.08	**125**	0.28	0.29	0.26	0.29	-0.18	-0.37
92	0.44	0.25	0.43	0.35	-0.07	-0.01	**126**	0.10	-0.08	0.03	0.03	-0.25	-0.41
93	0.03	-0.06	0.07	0.06	-0.45	-0.19	**127**	0.14	0.07	0.07	0.18	-0.13	-0.31
94	0.01	-0.12	0.00	0.07	-0.47	-0.57	**128**	0.13	0.06	0.09	0.20	-0.16	-0.37
95	-0.02	-0.14	-0.02	0.06	-0.48	-0.57	**129**	0.14	0.06	0.08	0.15	-0.46	-0.43
96	0.13	-0.08	0.13	0.08	-0.41	-0.49	**130**	0.14	0.03	0.18	0.19	-0.47	-0.44
97	0.17	-0.07	0.16	0.06	-0.36	-0.44	**131**	0.15	0.12	0.09	0.17	-0.59	-0.53
98	0.11	-0.02	0.17	0.08	-0.49	-0.45	**132**	0.11	-0.06	0.08	0.05	-0.37	-0.52
99	0.40	0.32	0.33	0.36	-0.21	-0.03	**133**	-0.04	-0.11	0.07	0.01	-0.20	0.00
100	0.14	0.07	-0.03	-0.09	0.13	0.20							
101	0.05	-0.08	-0.16	-0.11	0.12	0.19	**Min**	-0.30	-0.50	-0.35	-0.38	-0.68	-0.57
102	-0.05	-0.11	-0.16	-0.17	0.44	0.50	**Max**	0.54	0.46	0.48	0.51	0.63	0.58

Table 4.18 Pearson correlation coefficients (r) between annual atmospheric parameters and shoreline positions for Sinop. Green and yellow colors indicate strong and moderate correlations, respectively

Transection #	Mean Winds	95P Winds	Mean SWH	95P SWH	Mean SST	95P SST	Transection #	Mean Winds	95P Winds	Mean SWH	95P SWH	Mean SST	95P SST
1	-0.30	-0.14	-0.09	**-0.33**	0.61	0.23	**47**	**-0.42**	**-0.33**	-0.26	-0.22	0.45	0.03
2	-0.24	-0.12	-0.15	**-0.40**	0.37	0.18	**48**	**-0.32**	-0.20	-0.17	-0.04	0.41	-0.05
3	**-0.33**	-0.26	**-0.36**	**-0.41**	0.03	-0.10	**49**	**-0.35**	-0.29	-0.24	-0.21	0.40	-0.03
4	**-0.36**	-0.22	-0.25	-0.25	0.36	-0.04	**50**	**-0.41**	-0.28	-0.25	-0.13	0.37	-0.06
5	**-0.42**	-0.25	**-0.34**	**-0.35**	0.48	0.05	**51**	**-0.37**	-0.23	**-0.38**	**-0.32**	0.38	-0.01
6	-0.24	-0.20	**-0.30**	-0.26	0.41	0.10	**52**	**-0.42**	**-0.30**	-0.26	-0.25	0.46	0.05
7	**-0.50**	**-0.51**	**-0.31**	**-0.43**	0.26	0.18	**53**	-0.23	-0.14	-0.19	-0.25	0.44	-0.03
8	**-0.40**	-0.29	-0.29	**-0.32**	0.53	0.08	**54**	-0.27	-0.26	-0.24	**-0.33**	0.25	-0.11
9	-0.19	-0.14	-0.29	-0.24	0.39	0.03	**55**	**-0.50**	**-0.45**	**-0.37**	**-0.34**	0.39	0.01
10	0.00	0.00	-0.03	0.14	0.22	0.17	**56**	-0.28	-0.25	-0.24	**-0.45**	0.45	0.20
11	-0.15	-0.25	-0.13	-0.02	-0.07	-0.01	**57**	-0.20	-0.11	-0.23	**-0.53**	0.52	0.24
12	0.13	0.01	-0.07	0.15	**-0.33**	-0.09	**58**	-0.19	-0.22	-0.23	**-0.38**	0.23	0.08
13	0.22	0.02	0.14	0.06	-0.10	0.25	**59**	**-0.41**	**-0.37**	-0.25	-0.20	0.33	0.00
14	-0.12	-0.29	-0.12	0.26	**-0.55**	**-0.36**	**60**	-0.24	-0.24	-0.20	-0.19	0.24	-0.02
15	0.02	0.11	-0.02	0.12	0.00	0.03	**61**	-0.10	-0.06	-0.20	-0.22	0.31	0.04
16	-0.01	-0.14	0.07	0.07	-0.03	0.21	**62**	-0.16	-0.12	-0.16	**-0.41**	0.51	0.33
17	0.07	0.10	-0.16	0.01	-0.12	0.12	**63**	-0.07	-0.06	-0.14	-0.29	0.19	0.06
18	-0.29	-0.24	-0.20	**-0.30**	-0.18	-0.11	**64**	-0.30	**-0.34**	-0.12	-0.06	0.29	0.05
19	**-0.33**	**-0.36**	-0.14	-0.23	0.28	0.25	**65**	**-0.38**	**-0.32**	-0.20	-0.12	0.29	0.01
20	-0.22	-0.17	-0.10	-0.03	0.38	0.37	**66**	-0.25	-0.28	-0.10	0.00	0.18	0.03
21	-0.17	-0.19	-0.22	**-0.32**	0.12	0.39	**67**	**-0.31**	**-0.31**	-0.15	-0.07	0.26	0.14
22	0.27	0.32	0.21	0.01	0.06	0.12	**68**	-0.26	-0.28	-0.13	-0.06	0.25	0.04
23	**-0.33**	**-0.46**	**-0.31**	**-0.39**	-0.04	0.18	**69**	-0.22	-0.24	-0.11	-0.06	0.13	-0.02
24	**-0.36**	**-0.36**	-0.30	**-0.44**	0.28	0.29	**70**	-0.13	-0.16	-0.16	-0.02	0.02	-0.13
25	-0.08	-0.17	0.03	-0.25	0.18	0.38	**71**	-0.21	-0.16	-0.25	**-0.37**	0.36	0.16
26	-0.23	**-0.32**	-0.04	**-0.34**	0.24	0.22	**72**	-0.25	-0.25	-0.20	-0.10	0.21	0.03
27	0.03	0.09	0.02	-0.11	0.05	0.08	**73**	-0.20	-0.26	-0.09	-0.01	0.12	-0.03
28	-0.01	-0.02	0.05	-0.11	0.13	0.31	**74**	**-0.36**	-0.26	-0.29	-0.12	0.03	-0.24
29	-0.09	-0.22	-0.10	-0.18	0.14	0.28	**75**	-0.16	-0.20	-0.13	-0.01	-0.03	-0.13
30	-0.08	-0.10	-0.10	-0.29	0.16	0.26	**76**	-0.10	-0.13	-0.13	0.10	-0.22	**-0.37**
31	-0.11	-0.07	-0.08	-0.15	0.27	0.40	**77**	-0.11	-0.13	-0.15	0.09	-0.17	-0.27
32	-0.12	-0.14	-0.05	-0.17	0.35	0.28	**78**	-0.17	-0.19	-0.15	-0.03	0.00	-0.13
33	-0.07	-0.10	-0.05	-0.16	0.24	0.37	**79**	-0.15	-0.25	-0.01	0.04	0.08	0.09
34	0.02	0.00	0.00	-0.06	0.15	0.29	**80**	-0.24	**-0.31**	-0.20	-0.09	0.11	0.07
35	**-0.34**	**-0.33**	-0.30	**-0.37**	0.34	0.21	**81**	-0.18	-0.18	-0.18	0.00	-0.06	-0.25
36	-0.14	-0.03	-0.06	-0.22	0.41	0.32	**82**	-0.18	-0.27	-0.17	-0.01	-0.20	**-0.34**
37	-0.03	0.09	-0.04	-0.29	0.48	0.45	**83**	-0.18	-0.23	-0.17	0.11	-0.17	-0.22
38	-0.06	-0.11	0.02	-0.14	0.21	0.20	**84**	-0.17	-0.18	-0.16	-0.11	0.08	0.01
39	-0.05	-0.10	0.03	-0.01	0.06	0.10	**85**	0.10	0.00	0.00	0.21	-0.26	-0.28
40	-0.14	-0.14	-0.19	0.02	0.03	-0.21	**86**	0.04	-0.05	-0.06	0.21	**-0.34**	**-0.34**
41	-0.10	-0.02	-0.22	**-0.33**	0.16	-0.13	**87**	-0.06	-0.09	-0.12	0.17	-0.24	**-0.34**
42	-0.05	0.03	-0.15	-0.05	0.17	-0.13	**88**	0.43	0.45	0.40	0.44	0.18	0.15
43	-0.12	-0.06	-0.12	**-0.35**	0.41	0.35	**89**	0.41	0.35	0.36	0.24	0.24	0.15
44	**-0.39**	-0.27	-0.26	-0.16	0.38	-0.08							
45	-0.28	-0.14	-0.21	-0.07	0.44	-0.01	**Min**	**-0.50**	**-0.51**	**-0.38**	**-0.53**	**-0.55**	**-0.37**
46	**-0.36**	-0.26	-0.20	-0.27	0.56	0.13	**Max**	0.43	0.45	0.40	0.44	0.61	0.45

The Pearson correlation coefficients for the transection points in Bafra are shown in Table 4.19. There is not a distinct accumulation of successive transection points where Pearson correlation coefficient values which is more than 0.5. Lastly, in the same vein, there aren't strong correlations between the trends of annual values of atmospheric forcing and annual shoreline position in the Bafra.

Table 4.19 Pearson correlation coefficients (r) between annual atmospheric parameters and shoreline positions for Bafra. Green and yellow colors indicate strong and moderate correlations, respectively

Transection #	Mean Winds	95P Winds	Mean SWH	95P SWH	Mean SST	95P SST	Transection #	Mean Winds	95P Winds	Mean SWH	95P SWH	Mean SST	95P SST
1	**-0.48**	-0.28	**-0.51**	**-0.40**	-0.22	-0.25	**36**	0.25	0.16	0.29	0.39	0.03	-0.09
2	**-0.35**	-0.27	**-0.34**	-0.20	-0.17	**-0.30**	**37**	0.17	0.03	0.16	0.22	**-0.37**	-0.29
3	**-0.34**	**-0.35**	**-0.31**	**-0.32**	0.26	-0.15	**38**	0.27	0.10	0.28	0.17	-0.18	**-0.31**
4	-0.09	-0.10	0.00	-0.08	**-0.33**	-0.27	**39**	0.46	0.41	0.50	0.49	0.25	0.16
5	-0.17	-0.01	-0.03	0.08	**-0.46**	**-0.30**	**40**	-0.16	-0.28	-0.11	0.11	0.01	-0.08
6	-0.12	-0.07	-0.04	-0.08	-0.10	0.06	**41**	0.08	0.00	0.17	0.26	0.14	0.04
7	**-0.35**	-0.26	-0.18	-0.10	**-0.43**	**-0.40**	**42**	0.18	0.12	0.27	0.27	0.17	0.10
8	0.09	0.13	0.29	0.24	0.05	0.06	**43**	0.27	0.26	0.34	0.23	0.24	0.22
9	-0.10	-0.02	0.08	0.09	0.00	-0.06	**44**	0.31	0.28	0.37	0.24	0.25	0.22
10	-0.27	-0.22	-0.09	-0.01	-0.17	-0.06	**45**	0.11	0.22	0.11	0.01	0.02	0.03
11	-0.24	-0.24	-0.16	-0.17	0.07	0.02	**46**	0.11	0.22	0.11	0.00	0.02	0.05
12	0.13	0.11	0.14	0.09	0.23	0.14	**47**	0.28	0.26	0.35	0.23	0.23	0.21
13	0.20	0.08	0.27	0.16	0.10	0.19	**48**	-0.04	-0.03	-0.04	-0.11	0.28	0.32
14	-0.04	-0.18	0.05	0.15	0.22	0.03	**49**	0.12	0.10	0.11	0.00	0.26	0.31
15	-0.19	**-0.31**	-0.12	0.12	0.07	-0.10	**50**	0.02	-0.01	0.04	-0.05	0.28	0.26
16	-0.17	-0.30	-0.11	0.13	0.03	-0.12	**51**	-0.04	0.01	-0.04	-0.08	0.10	0.21
17	0.03	-0.16	0.05	-0.01	0.50	0.15	**52**	-0.16	-0.05	-0.10	0.01	-0.07	0.04
18	0.12	-0.10	0.25	0.13	0.30	0.09	**53**	-0.12	-0.06	-0.11	0.00	0.00	0.11
19	-0.02	-0.12	0.21	0.14	0.23	0.23	**54**	0.08	0.18	0.06	-0.12	-0.22	-0.15
20	-0.21	**-0.31**	-0.15	-0.22	0.45	0.02	**55**	0.23	0.37	0.14	0.18	-0.08	0.07
21	0.09	-0.13	0.25	0.16	0.14	0.17	**56**	0.08	0.26	-0.04	-0.08	-0.14	-0.05
22	-0.17	-0.29	-0.09	0.13	0.04	-0.11	**57**	-0.03	0.06	-0.07	0.06	-0.01	0.10
23	-0.16	-0.29	-0.09	0.15	0.03	-0.11	**58**	-0.22	-0.12	-0.23	-0.09	-0.04	-0.01
24	-0.16	-0.27	-0.09	0.15	0.01	-0.10	**59**	-0.09	-0.02	-0.10	-0.04	-0.05	0.09
25	-0.14	-0.27	-0.08	0.16	0.04	-0.10	**60**	-0.09	-0.06	-0.07	-0.05	0.03	0.13
26	-0.17	**-0.30**	-0.10	0.12	0.03	-0.11	**61**	-0.08	-0.08	-0.06	-0.04	0.10	0.19
27	-0.14	-0.25	-0.08	0.12	0.03	-0.05	**62**	-0.01	-0.07	-0.06	0.01	0.20	0.25
28	-0.16	-0.29	-0.11	0.13	0.06	-0.09	**63**	-0.05	-0.02	-0.09	0.05	0.08	0.19
29	0.01	-0.21	0.06	0.13	0.33	0.20	**64**	0.32	0.26	0.41	0.38	0.32	0.39
30	-0.02	-0.19	0.06	0.14	0.26	0.13	**65**	**-0.40**	-0.16	**-0.34**	-0.21	**-0.36**	-0.21
31	0.07	0.14	0.01	0.10	0.04	-0.11	**66**	-0.29	-0.18	-0.29	-0.15	-0.24	-0.13
32	-0.01	-0.04	-0.03	0.15	0.01	-0.11							
33	0.19	0.08	0.19	0.27	-0.18	-0.19							
34	0.35	0.20	0.40	0.47	0.00	-0.15	**Min**	**-0.48**	**-0.35**	**-0.51**	**-0.40**	**-0.46**	**-0.40**
35	0.05	0.08	0.00	0.11	0.01	-0.05	**Max**	0.46	0.41	0.50	0.49	0.50	0.39

Table 4.20 Pearson correlation coefficients (r) between annual atmospheric parameters and shoreline positions for Çarşamba. Green and yellow colors indicate strong and moderate correlations, respectively

Transection #	Mean Winds	95P Winds	Mean SWH	95P SWH	Mean SST	95P SST	Transection #	Mean Winds	95P Winds	Mean SWH	95P SWH	Mean SST	95P SST
1	0.23	0.27	0.18	-0.17	0.11	0.20	**25**	0.00	-0.03	0.10	-0.09	0.05	0.21
2	-0.03	-0.01	-0.04	-0.03	-0.29	-0.17	**26**	**-0.41**	-0.20	**-0.53**	**-0.40**	0.01	-0.20
3	-0.08	-0.06	-0.05	0.02	-0.27	-0.09	**27**	0.48	0.33	0.48	0.19	0.44	0.53
4	-0.20	-0.15	-0.22	-0.02	**-0.44**	**-0.34**	**28**	**-0.39**	**-0.31**	**-0.37**	-0.28	**-0.33**	**-0.32**
5	**-0.33**	**-0.30**	**-0.31**	-0.02	**-0.60**	**-0.52**	**29**	**-0.48**	-0.26	**-0.45**	-0.16	**-0.71**	**-0.60**
6	-0.24	-0.18	-0.24	0.07	**-0.54**	**-0.50**	**30**	**-0.38**	-0.24	**-0.31**	0.02	**-0.60**	**-0.54**
7	0.07	0.07	-0.08	0.09	**-0.32**	**-0.45**	**31**	-0.30	-0.29	-0.17	-0.17	-0.20	-0.28
8	0.20	0.14	0.13	0.16	**-0.30**	**-0.33**	**32**	-0.08	-0.12	-0.06	-0.06	-0.03	-0.16
9	0.48	0.34	0.31	0.23	0.11	-0.05	**33**	**-0.58**	**-0.41**	**-0.56**	**-0.31**	**-0.57**	**-0.55**
10	0.48	0.29	0.37	0.10	0.25	0.20	**34**	**-0.53**	**-0.36**	**-0.55**	-0.29	**-0.52**	**-0.58**
11	0.41	0.17	0.29	0.07	0.26	0.25	**35**	**-0.63**	**-0.44**	**-0.66**	**-0.49**	**-0.30**	**-0.38**
12	0.53	0.37	0.46	0.09	0.59	0.51	**36**	**-0.47**	**-0.34**	**-0.53**	**-0.57**	0.13	0.03
13	0.54	0.44	0.44	0.03	0.66	0.49	**37**	**-0.59**	**-0.41**	**-0.57**	-0.29	**-0.56**	**-0.55**
14	0.53	0.40	0.47	0.09	0.55	0.36	**38**	-0.29	-0.15	-0.26	0.00	**-0.33**	**-0.42**
15	0.11	0.13	-0.08	-0.14	0.21	-0.03	**39**	**-0.64**	**-0.46**	**-0.58**	-0.29	**-0.59**	**-0.49**
16	0.27	0.15	0.17	-0.25	0.56	0.41	**40**	-0.08	-0.08	0.10	0.03	**-0.37**	-0.24
17	0.00	-0.02	-0.11	**-0.43**	0.51	0.40	**41**	-0.02	0.06	0.15	-0.05	-0.03	0.18
18	0.03	0.01	-0.08	**-0.41**	0.43	0.32	**42**	0.06	0.04	0.06	-0.14	0.00	-0.09
19	0.08	0.04	-0.04	-0.29	0.15	-0.02	**43**	0.39	0.30	0.43	0.04	0.49	0.38
20	-0.24	-0.18	**-0.39**	**-0.39**	-0.08	-0.29	**44**	0.28	0.18	0.28	-0.21	0.68	0.59
21	**-0.51**	**-0.37**	**-0.63**	**-0.47**	-0.09	-0.23							
22	**-0.47**	**-0.33**	**-0.58**	**-0.44**	0.04	-0.10							
23	**-0.36**	-0.28	**-0.46**	**-0.35**	0.21	0.07	**Min**	**-0.64**	**-0.46**	**-0.66**	**-0.57**	**-0.71**	**-0.60**
24	**-0.47**	**-0.35**	**-0.39**	-0.12	-0.29	-0.13	**Max**	0.54	0.44	0.48	0.23	0.68	0.59

After investigating the correlation coefficients for Çarşamba in Table 4.20, we see that there are several groups of successive transection points where moderate correlation between annual time series of mean and 95th percentile wind speeds and SWHs over 0.5 exist. Trends of mean wind speeds has positive correlations reaching 0.54 with the negative trends of shoreline position on the transection points 12-14. Similarly, the changes of shoreline positions in these transection points are positively correlated with the trends of mean and 95th percentile SSTs. On the contrary, we see negative correlations down to -0.64 between the same parameters in the shoreline points 33-37, where erosions have been evaluated. Additionally, on the points 33-37, there are also clear negative correlations between shoreline positions and mean or 95th percentile wave heights. The most distinct correlation values reach -0.66 and -0.57 respectively. Besides, the shoreline positions of these points also seem correlated with long-term variations of mean and 95th percentile SSTs.

In addition, after evaluating Table 4.21 there is no obvious existence of successive transection points where Pearson correlation coefficient values which is more than 0.5, for the Sochi.

Table 4.21 Pearson correlation coefficients (r) between annual atmospheric parameters and shoreline positions for Sochi. Green and yellow colors indicate strong and moderate correlations, respectively

Transection #	MEAN WINDS	95P WINDS	MEAN SWH	95P SWH	MEAN SST	95P SST	Transection #	MEAN WINDS	95P WINDS	MEAN SWH	95P SWH	MEAN SST	95P SST
1	**-0.31**	**-0.36**	-0.27	**-0.34**	**-0.53**	**-0.55**	**36**	-0.03	-0.15	0.01	0.05	**-0.42**	-0.16
2	-0.29	**-0.31**	-0.23	**-0.35**	**-0.46**	**-0.51**	**37**	0.30	0.20	0.32	0.30	-0.10	0.05
3	0.00	-0.06	0.11	-0.05	-0.18	-0.18	**38**	0.32	0.34	0.46	0.43	0.27	0.48
4	-0.26	-0.28	-0.23	**-0.32**	**-0.32**	**-0.39**	**39**	0.31	0.27	0.39	0.39	0.07	0.32
5	-0.16	-0.20	-0.16	-0.24	-0.27	**-0.35**	**40**	0.34	0.31	0.41	0.43	0.09	0.25
6	-0.14	-0.24	-0.21	**-0.36**	-0.29	**-0.36**	**41**	0.09	0.05	0.15	0.10	-0.28	-0.13
7	0.21	0.15	0.16	-0.01	0.35	0.28	**42**	0.05	-0.03	0.02	0.04	-0.05	-0.06
8	0.27	0.30	0.32	0.13	0.32	0.34	**43**	0.09	0.07	0.15	0.22	-0.10	0.03
9	0.36	0.40	0.40	0.22	0.30	0.36	**44**	0.28	0.23	0.35	0.39	0.00	0.10
10	0.46	0.44	0.38	0.29	0.51	0.51	**45**	0.21	0.15	0.33	0.42	-0.04	0.09
11	-0.04	-0.10	-0.13	-0.12	0.23	0.20	**46**	0.11	-0.03	0.19	0.20	0.05	0.17
12	0.05	0.17	0.14	0.13	0.17	0.28	**47**	0.28	0.15	0.20	0.15	0.43	0.37
13	0.17	0.14	0.12	0.05	0.02	0.05	**48**	0.33	0.25	0.32	0.31	0.15	0.23
14	-0.17	-0.17	-0.11	-0.15	**-0.44**	**-0.39**	**49**	0.55	0.60	0.62	0.65	0.49	0.60
15	0.00	0.12	0.08	0.03	-0.17	-0.07	**50**	0.17	0.26	0.22	0.25	-0.08	0.13
16	-0.01	0.01	0.01	0.07	-0.18	-0.12	**51**	0.13	0.10	0.03	0.04	-0.16	-0.10
17	0.14	0.13	0.09	0.08	0.14	0.13	**52**	-0.06	-0.02	-0.01	0.12	**-0.32**	-0.12
18	0.14	0.06	0.10	0.10	-0.01	0.04	**53**	0.14	0.14	0.14	0.18	-0.13	-0.13
19	0.38	0.23	0.27	0.30	0.20	0.22	**54**	0.26	0.28	0.27	0.29	-0.17	0.04
20	0.30	0.23	0.30	0.21	0.12	0.28	**55**	-0.26	-0.15	-0.19	-0.20	**-0.58**	**-0.49**
21	0.54	0.41	0.44	0.43	0.36	0.38	**56**	**-0.35**	-0.30	-0.29	-0.28	**-0.64**	**-0.50**
22	0.49	0.35	0.40	0.41	0.43	0.43	**57**	-0.13	0.03	-0.04	0.03	0.00	0.13
23	-0.18	-0.13	-0.04	-0.03	**-0.34**	-0.16	**58**	**-0.36**	-0.13	**-0.39**	-0.30	-0.05	0.01
24	0.07	0.06	0.07	0.12	-0.08	0.05	**59**	0.04	0.11	0.05	0.07	-0.29	-0.14
25	0.30	0.37	0.37	0.39	0.15	0.35	**60**	-0.26	-0.11	-0.17	-0.17	**-0.55**	**-0.40**
26	0.39	0.34	0.43	0.43	0.18	0.33	**61**	**-0.37**	-0.24	**-0.34**	**-0.30**	**-0.60**	**-0.48**
27	0.18	0.06	0.14	0.24	-0.30	-0.15	**62**	**-0.35**	-0.21	-0.29	-0.23	**-0.40**	-0.22
28	0.45	0.39	0.46	0.48	0.36	0.47	**63**	**-0.38**	-0.23	**-0.47**	**-0.43**	-0.23	-0.20
29	0.24	0.15	0.26	0.26	-0.03	0.13	**64**	**-0.35**	-0.23	**-0.40**	**-0.40**	**-0.35**	**-0.38**
30	-0.11	-0.09	-0.02	0.02	-0.30	-0.16	**65**	-0.07	0.05	-0.04	-0.08	**-0.38**	-0.30
31	-0.13	-0.15	-0.05	-0.04	**-0.33**	-0.18	**66**	**-0.38**	-0.21	**-0.39**	**-0.38**	**-0.42**	**-0.43**
32	0.03	0.00	0.03	0.07	0.07	0.15	**67**	**-0.34**	-0.20	**-0.36**	**-0.33**	**-0.32**	**-0.36**
33	-0.14	-0.05	0.02	0.09	-0.23	-0.11							
34	0.28	0.25	0.29	0.32	0.32	0.34	**Min**	**-0.38**	**-0.36**	**-0.47**	**-0.43**	**-0.64**	**-0.55**
35	0.32	0.12	0.22	0.16	-0.04	0.11	**Max**	0.55	0.60	0.62	0.65	0.51	0.60

4.3 Conclusion

To sum up; by considering the relationships between the shoreline change trends and variations of atmospheric parameters, which are wind speeds, wave heights, and SSTs; it is not to figure out obvious correlations on the study points on seven shoreline locations. Especially, trends in wind speeds and wave heights do not represent a connection with shoreline change trends. This situation can be explained for several reasons. Firstly, trends of wind speeds and wave heights do not involve any data regarding direction. Both winds and waves have directions; and by considering the orientations of shorelines, the effects of wind and waves on shorelines are expected to have direction-dependent.

On the other hand, the relationships between the shoreline change trends and long-term variations of SSTs represent more correlated relationships. As the change in temperatures is a major representative of climate change effects (Dye, 2013) and the shoreline change, width is a cumulative result of all climate change effects; this situation makes sense. In other words, it can be said that the variations in SSTs can be regarded as a better indicator of climate change and represent more correlations between any other climate change impacts.

Another reason for the lack of proper amount correlations between the shoreline change trends and variations of investigated atmospheric parameters is considered as the local characteristics of particular shoreline regions. These characteristics can be counted as the grain size of shoreline materials, the orientation of streams in the neighborhood, beach profiles, anthropogenic activities, etc. That is why; it is apprehensible not to find significant correlations between the shoreline change trends and variations of atmospheric parameters.

This study aimed to figure out the long-term variations of atmospheric parameters due to climate change and their impacts on shoreline changes with a large-scale perspective covering the Black Sea Basin. Here, the necessity for further analysis to find out the relationship between the long-term variations of atmospheric parameters and shoreline changes by considering hydrodynamic conditions in a local and detailed manner comes out.

The long-term variations of climate parameters (wind speed, significant wave height, sea surface temperature, precipitation) and shoreline change trends over the Black Sea are investigated. The relations of long-term variations of climate parameters and shoreline change trends were evaluated.

Long-term trends of wind speeds show considerable spatial and seasonal variability in the study area. In general, both $U10_m$ and $U10_{95}$ have been increasing over the eastern part of the Black Sea. This points out that the Black Sea is inhomogeneous in means of long-term trends in wind speeds. This inhomogeneity must be taken into account in site-specific studies instead of using basin-averaged quantities. ERA-I reanalysis data indicate that moderate and severe wind speeds are increasing over 36% and 28% of the Black Sea surface area, respectively, while they are decreasing over 4% and 2% of the surface area, respectively. ERA-I data indicates that annual $U10_m$ and $U10_{95}$ have statistically significant decreasing trends down to -0.17 %/yr and -0.20 %/yr in the Sea of Azov, while they have an increasing trend up to 0.35 %/yr and 0.38 %/yr in the eastern part, respectively. This result shows that severe wind speeds change at higher rates. Long-term trends of wind speeds are shown to have strong seasonality in the Black Sea. The monthly analysis revealed different magnitude increasing or decreasing trends in both monthly $U10_m$ and $U10_{95}$. ERA-I gives the highest increasing trends along the eastern coast with a rate of 0.81 %/yr in month March and along the western coast with a rate of 0.53 %/yr in month September for the monthly $U10_m$. For the severe wind conditions, the highest increasing trends are estimated southeastern coast with a rate of 0.68 %/yr for March and around the Crimean Peninsula with a rate of 0.42 %/yr for April. Analysis of correlation coefficients between well-known teleconnection indices and the wind speeds revealed that EA, EA/WR, NAO, PNA, POL, and SCA indices have influence inhomogeneously over the Black Sea. PNA has an influence almost all over the basin with statistically significant correlation coefficients over 0.4. NAO dominates over the western basin for $U10_m$ and a much wider area covering the southwestern, western and northern Black Sea with inverse correlation coefficients reaching over 0.4. Southern coasts are dominated by EA/WR and POL for both $U10_m$ and $U10_{95}$. Although general consistency is found

between ERA-I and CFSR, especially in means of the correlation coefficients, slight differences are observed in the spatial distribution and coverage area of each considered teleconnection index among the two reanalysis data.

Investigations of the long-term variation of annual averaged SWH show that the trends represent spatial variations over the Black Sea Basin. In the eastern regions of the Basin, there are increasing trends up to 0.8 %/yr, whereas the general characteristics of the trends in the western regions and the Sea of Azov are decreasing down to -0.4 %/yr. It can also be concluded that positive trends have greater values than negative ones. The 95th percentile annual SWHs represent positive trends and these trends are steeper and more significant than the trend of mean SWHs. In addition, the area with increasing or decreasing trends is larger for 95th percentile annual SWHs than to mean SWHs.

The spatial distributions of trends of annual averaged and 95th percentile wind speeds show significant consistency with the ones of SWHs over the Black Sea. Besides the monthly trends averaged and 95th percentile wind speeds are coherent with the monthly trends of averaged and 95th percentile monthly SWHs in the literature.

The influence of teleconnection indices on the trends of annual averaged and 95th percentile wind speeds show significant consistency with the ones of SWHs over the Black Sea. Besides these influences of teleconnection indices on the monthly trends averaged and 95th percentile wind speeds are coherent with the ones of averaged and 95th percentile monthly SWHs in the literature.

To define the long-term variations of the annual mean and 95th percentile SST were also examined. For mean SSTs, there are decreasing trends only on the Sea of Azov for SST down to -0.02 °C/yr. It is found that the SST has an increasing trend over the whole Black Sea basin. In the eastern regions, increasing trends are relatively higher and the values reach up to 0.07 °C/yr. The basin averaged increasing trend in SST is estimated to be 0.036 °C/yr over the Black Sea basin. For extreme SST values over the Black Sea, the minimum increasing trend of 95th

is 0.05 °C/yr, and the mean increasing trend is 0.08 °C/yr. On the basin of the Black Sea, the maximum increasing trend for 95th percentile SST is detected as 0.11 °C/yr.

As another atmospheric parameter, understanding the long-term variations of precipitation was also investigated over the Black Sea Basin by evaluating annual total precipitation and the annual number of days with precipitation. The minimum decreasing trends are seen on the southeastern coasts and the values reach down to -6.6 mm/yr, on the other hand, the maximum increase in annual total precipitation reaches 2.6 mm/yr on the western coasts. If we consider the mean annual total precipitation over the study area as 261 mm, the trends can be evaluated as small. Long-term trends of the annual number of days with precipitation are negative nearly all over the Black Sea Basin. The trend values can reach up to -1 day/yr. If we consider slight long-term variations of annual total precipitations and the negative trends in the annual number of days with precipitations together; it is possible to state that, in the study period, the amount of precipitation over the Black Sea did not change however the days which these precipitations occurred decreased. In other words, the same amount of precipitation started to be seen in less time over the Black Sea Basin. Extreme events are expected to increase in the future.

The investigations for the shoreline changes in the Black Sea stated that Deltas along the Black Sea are facing high erosional rates. In the selected shoreline segments in Danube Delta, Kızılırmak Delta and Yeşilırmak Delta, maximum erosion rates are -8.7 m/yr, 21.81 m/yr and 23.33 m/yr respectively. These values are seen in the transection points near the river mouths. The barrier between the Terkos Lake and the Black Sea is also under threat of erosion. Despite protection activities, the maximum erosion rate for the barrier is found to be -1.35 m/yr. As Terkos Lake is one of the most important freshwater resources in Istanbul, more efficient protection strategies should be held urgently. The maximum erosion rates reach up to -7.25 m/yr and -1.20 m/yr in Cide and Sinop. These trends led to moderately abraded morphology in these coastal zones. Possible effects of this

situation on the anthropogenic and the natural process should be evaluated well, and action plans should be prepared for the future.

Just like the common situation along the Russian coastline in the eastern Black Sea, there are hard coastal protection structures such as groynes, sea walls, revetments, or breakwaters in Sochi. However, in Sochi, despite the existence of hard coastal protection structures, the erosion is going on and the maximum shoreline change trend rates reach down to -0.75 m/yr.

The shoreline change and climate parameter time series indicated spatially inhomogeneous statistically significant correlations in the selected seven-shoreline sectors. The highest correlations are provided by the sea surface temperature among all others. This is considered to be a result of the fact that SST is an important indicator of climate change. Another possible reason for this relation is the fact that the increasing SSTs over the coastal regions of the Black Sea could trigger increasing storminess, which is a key factor for shoreline change mechanisms.

This study evaluates the general characteristics of shoreline changes and their relationship with the climate parameters for the Black Sea. Directional characteristics of the wind and wave parameters are not considered in this study. Relative direction of dominant wind and wave impact and the shoreline characteristics have an influence on the shoreline change and is recommended to be considered in further local studies. Further research is also recommended to include the long-term changes in hydrodynamic conditions and the circulations along the Black Sea coastline to better understand the impact of climate change on the local drivers of the shoreline change.

REFERENCES

Abuodha, P. A. O., & Woodroffe, C. D. (2010). Assessing vulnerability to sea-level rise using a coastal sensitivity index: A case study from southeast Australia. Journal of Coastal Conservation, 14 (3), 189-205, https://doi.org/10.1007/s11852-010-0097-0

Adger, W.N. (2006). Vulnerability. Global Environmental Change, 16, 268-281. http://dx.doi.org/10.1016/j.gloenvcha.2006.02.006

Akpinar, A., & Bingolbali, B. (2016). Long-term variations of wind and wave conditions in the coastal regions of the Black Sea. Natural Hazards, 84(1), 69-92. https://doi.org/10.1007/s11069-016-2407-9

Alexandrakis, G., & Poulos, S. E. (2014). An holistic approach to beach erosion vulnerability assessment. Scientific reports, 4, 6078. https://doi.org/10.1038/srep06078

Allenbach, K., Garonna I., Herold, C., Monioudi C., Giuliani G., Lehmann A., & Velegrakis A.F. (2014). Black Sea beaches vulnerability to sea level rise. Environmental Science & Policy. 46. https://doi.org/10.1016/j.envsci.2014.07.014

Aral, M. M., & Guan, J. (2016). Global Sea Surface Temperature and Sea Level Rise Estimation with Optimal Historical Time Lag Data. Water 2016, 8, 519. https://doi.org/10.3390/w8110519

Arkhipkin, V. S., Gippius, F. N., Koltermann, K. P., & Surkova, G. V. (2014). Wind waves in the Black Sea: results of a hindcast study. Nat. Hazards Earth Syst. Sci., 14, 2883–2897. https://doi.org/10.5194/nhess-14-2883-2014

Athanasatos, S., Michaelides, S., & Papadakis, M. (2014). Identification of weather trends for use as a component of risk management for port operations. Natural Hazards, 72:32-40. https://doi.org/10.1088/1755-1315/638/1/012040

Ataol, M., Kale, M.M., & Tekkanat, İ. (2019). Assessment of the changes in shoreline using digital shoreline analysis system: a case study of Kızılırmak Delta in northern Turkey from 1951 to 2017. Environmental Earth Sciences. 78. https://10.1007/s12665-019-8591-7.

Avşar N. B. (2019). Sea Level Changes in the Black Sea and its Impacts on the coastal Areas. Zonguldak Bülent Ecevit University Graduate School of Natural and Applied Sciences, Department of Geomatics Engineering, Doctor of Philosophy Thesis.

Aydoğan B., & Ayat B. (2018). Spatial variability of long-term trends of significant wave heights in the Black Sea. Applied Ocean Research, Volume 79, 2018, Pages 20-35, https://doi.org/10.1016/j.apor.2018.07.001

Aydoğan, B. (2017). Offshore wind power atlas of the Black Sea region. Journal of Renewable and Sustainable Energy, 9-013305. https://doi.org/10.1063/1.4976968

Barnston, A.G. & Livezey, R.E. (1987) Classifications, Seasonality, and Persistence of Low-Frequency Atmospheric Circulation Patterns. Monthly Weather Review, 115, 1083-1126. https://doi.org/10.1175/1520-0493(1987)115<1083:CSAPOL>2.0.CO;2

Baylan E., & Karadeniz N. (2006). Terkos Gölü (İstanbul) Örneğinde Doğal ve Kültürel Çevrenin Korunması ve Geliştirilmesi Üzerine Bir Araştırma. Tarim Bilimleri Dergisi 2006, 12 (2) 151-161 Ankara Üniversitesi Ziraat Fakültesi, https://doi.org/10.1501/Tarimbil_0000000471 1083-1126

Cakiroglu A.M., Cevher N.C., & Agirbas, E. (2017). The meteorological Investigation of Turkish coasts of the Black Sea. Journal of Anatolian Environmental & Animal Sciences, 2(3), 53-58, https://doi.org/10.35229/jaes.358566

Çarpar, T., Ayat, B., & Aydogan, B. (2019). Spatio-seasonal variations in long-term trends of offshore wind speeds over the Black Sea; an inter-comparison of two

reanalysis data. Pure Appl. Geophys. 177 3013-3037, https://doi.org/10.1007/s00024-019-02361-7

Climate Prediction Center (CPC). (2011). Northern hemisphere teleconnection patterns. http://www.cpc.ncep.noaa.gov/data/teledoc/telecontents.html

Cohen, J. (1988). Statistical power analysis for the behavioral sciences (2nd Ed.). Hillsdale, NJ: Lawrence Erlbaum Associates.

Croitoru, A.E., Chiotoroiu, B.C., Todorova, V.I., & Torica, V. (2013). Changes in Precipitation Extremes on the Black Sea Western Coast. Global and Planetary Change. 102. 10-19. https://doi.org/10.1016/j.gloplacha.2013.01.004

Dee, D.P., Uppala, S.M., Simmons, A.J., Berrisford, P., Poli, P., Kobayashi, S., Andrae, U., Balmaseda, M.A., Balsamo, G., Bauer, P., Bechtold, P., Beljaars, A.C.M., vandeBerg, L., Bidlot, J., Bormann, N., Delsol, C., Dragani, R., Fuentes, M., Geer, A.J., Haimberger, L., Healy, S.B., Hersbach, H., Hólm, E.V., Isaksen, L., Kållberg, P., Köhler, M., Matricardi, M., McNally, A.P., Monge-Sanz, B.M., Morcrette, J.J., Park, B.K., Peubey, C., Rosnay, P., Tavolato, C., Thépaut, J.N., & Vitart, F. (2011). The ERA-interim reanalysis: configuration and performance of the data assimilation system. Quarterly Journal of the Royal Meteorological Society, 137, 553-597. https://doi.org/10.1002/qj.828

Dancey, C. & Reidy, J. (2004). Statistics without Maths for Psychology: using SPSS for Windows. Prentice Hall, London.

Deser, C., Knutti, R., & Solomon, S. (2012). Communication of the role of natural variability in future North American climate. Nature Clim. Change 2, 775–779. https://doi.org/10.1038/nclimate1562

Divinsky, B.V. & Kosyan, R.D. (2015). Observed wave climate trends in the offshore Black Sea from 1990 to 2014. Oceanology 55, 837–843. https://doi.org/10.1134/S0001437015060041

Drapela, K., & Drapelova, I. (2011). Application of Mann-Kendall test and the Sen's slope estimates for trend detection in deposition data from Bílý Kříž

(Beskydy Mts., the Czech Republic) 1997–2010. Mendelova Univerzita v Brně, Beskydy, 4, 133-146.

Dye, S., Hughes, S. L., Tinker, J., Berry, D. I., Holliday, N. P., Kent, E. C., Kennington, K., Inall, M., Smyth, T., Nolan, G., Lyons, K., Andres, O., & Beszczynska-Möller, A. (2013). Impacts of climate change on temperature (air and sea). In MCCIP Science Review 2013 (pp. 1-12). Marine Climate Change Impacts Partnership. https://doi.org/10.14465/2013.arc01.001-012

Dyer, A. J. (1974). A review of flux-profile relationships. Boundary Layer Meteorology, 7, 363– 372.

EC (European Commission). (2021). A European Green Deal. https://ec.europa.eu/info/strategy/priorities-2019-2024/european-green-deal_en (accessed: March 8, 2022)

Edwards, A. L. (1976). The Correlation Coefficient. An Introduction to Linear Regression and Correlation. Chapter 4. San Francisco, CA: W. H. Freeman, pp. 33-46.

Efimov, V.V., & Anisimov, A.E. (2011). Climatic Parameters of Wind Field Variability in the Black Sea Region: Numerical Reanalysis of Regional Atmospheric Circulation, Izvestiya Atmospheric and Oceanic Physics 47 (3): 350–361, https://doi.org/10.1134/S0001433811030030

Efimov, V., Belokopytov, V., & Anisimov, A. (2012). Estimation of water balance components in the Black Sea. Russian Meteorology and Hydrology. 37. http://doi.org/10.3103/S1068373912110118

Fach, B. (2014). Modeling the Influence of Hydrodynamic Processes on Anchovy Distribution and Connectivity in the Black Sea. Turkish Journal of Fisheries and Aquatic Sciences. 14. 353-365. https://10.4194/1303-2712-v14_2_06

FEMA (2008). Coastal AE Zone and VE Zone Demographics Study and Primary Frontal Dune Study to Support the NFIP. Washington, DC: Federal Emergency Management Agency Technical Report, 98p.

Foo, S. A., & Asner, G. P. (2020). Sea surface temperature in coral reef restoration outcomes. Environmental Research Letters, 15(7). http://10.1088/1748-9326/ab7dfa

Franke, R. (1982). Scattered Data Interpolation: Tests of Some Method. Mathematics of Computation, 38(157), 181–200. https://doi.org/10.2307/2007474

Füssel, Hans-Martin. (2007). Vulnerability: A generally applicable conceptual framework for climate change research. Global Environmental Change. 17. 155-167. https://doi.org/10.1016/j.gloenvcha.2006.05.002

Ganea, D., Mereuta, E., & Rusu, L. (2018). Estimation of the Near Future Wind Power Potential in the Black Sea, Energies, 2018, 11, 3198 https://doi.org/10.3390/en11113198

Ganea, D., Mereuta, E., & Rusu, E. (2019). An Evaluation of the Wind and Wave Dynamics along the European Coasts. J. Mar. Sci. Eng. 2019, 7, 43. https://doi.org/10.3390/jmse7020043

Georgopoulou, E., Mirasgedis, S., & Sarafidis, Y. (2019). Climatic preferences for beach tourism: an empirical study on Greek islands, Theor. Appl. Climatol. 137, 667–691. https://doi.org/10.1007/s00704-018-2612-4

Gilbert, R.O. (1987). Statistical Methods for Environmental Pollution Monitoring, Van Nostrand Reinhold Company Inc.

Ginzburg, A. I., Kostianoy, A. G., & Sheremet, N. A. (2004). Seasonal and interannual variability of the Black Sea surface temperature as revealed from satellite data (1982–2000). J. Mar. Syst. 52, 33–50, http://dx.doi.org/10.1016/j.jmarsys.2004.05.002

Görmüş, T., Ayat, B., Aydoğan, B., & Tătui, F. (2021), Basin scale spatiotemporal analysis of shoreline change in the Black Sea, Estuarine. Coastal and Shelf Science, 252, , 107247, ISSN 0272-7714, https://doi.org/10.1016/j.ecss.2021.107247

Gornitz, V., & Seeber, L. (1990). Vertical crustal movements along the East Coast, North America, from historic and Late Holocene sea level data. Tectonophysics, 178, 127-150, https://doi.org/10.1016/0040-1951(90)90143-V

Gunnerson, C. G., & Özturgut, E. (1974). The Bosporus and the Black Sea Geology, Chemistry and Biology. Degens E T and Ross D A (Eds.), Volume 20, ISBN electronic: 978-162-98-1215-1, American Association of Petroleum Geologists, 99– 114. https://doi.org/10.1306/M20377

Hadi, S.J. & Tombul, M. (2018). Long-term spatiotemporal trend analysis of precipitation and temperature over Turkey. Met. Apps, 25: 445-455. https://doi.org/10.1002/met.1712

Hartmann, D. L., Klein Tank, A. M. G., Rusticucci, M., Alexander, L. V., Brönnimann, S., Charabi, Y. A. R., Dentener, F. J., Dlugokencky, E. J., Easterling, D. R., Kaplan, A., Soden, B. J., Thorne, P. W., Wild, M., & Zhai, P. (2013). Observations: Atmosphere and surface. In Climate Change 2013 the Physical Science Basis: Working Group I Contribution to the Fifth Assessment Report of the Intergovernmental Panel on Climate Change (Vol. 9781107057999, pp. 159-254). Cambridge University Press. https://doi.org/10.1017/CBO9781107415324.008

Hasanean, H.M. (2005). Variability of teleconnections between the Atlantic subtropical high and the Indian monsoon low and related impacts on summer temperature over Egypt. Atmospheric Science Letters, 6, 176-182. http://doi.org/10.1002/asl.113

Healy T.R. (2018). Coastal Wind Effects. In: Finkl C.W., Makowski C. (eds) Encyclopedia of Coastal Science. Encyclopedia of Earth Sciences Series. Springer, Cham. https://doi.org/10.1007/978-3-319-93806-6_91

Hersbach, H., Bell, B., Berrisford, P., Hirahara, S., Horányi,A., Muñoz-Sabater, J., Nicolas, J., Peubey, C., Radu, R., Schepers, D., Simmons, A., Soci, C., Abdalla, S., Abellan, X., Balsamo, G., Bechtold, P., Biavati, G., Bidlot, J., Bonavita, M., Chiara, G., Dahlgren, P., Dee, D., Diamantakis, M., Dragani, R., Flemming, J.,

Forbes, R., Fuentes, M., Geer, A., Haimberger, L., Healy, S., J. Hogan, R., Hólm, E., Janisková, M., Keeley, S., Laloyaux, P., Lopez, P., Lupu, C., Radnoti, G., Rosnay, P., Rozum, I., Vamborg, F., Villaume, S., & Thépaut, J.N., (2020). The ERA5 Global Reanalysis. Q. J. Roy. Meteor. Soc., 146 (730), pp. 1999-2049, https://doi.org/10.1002/qj.3803

Holtslag, A. A. M., & Bruin, H. A. R. (1988). Applied modeling of the nighttime surface energy balance over land, Journal of Applied Meteorology, 27, 689–704.

IPCC (2013). Climate Change 2013: The Physical Science Basis. Contribution of Working Group I to the Fifth Assessment Report of the Intergovernmental Panel on Climate Change [Stocker, T.F., D. Qin, G.-K. Plattner, M. Tignor, S.K. Allen, J. Boschung, A. Nauels, Y. Xia, V. Bex and P.M. Midgley (eds.)]. Cambridge University Press, Cambridge, United Kingdom and New York, NY, USA, 1535 pp.

IPCC. (2019). Climate Change and Land: an IPCC special report on climate change, desertification, land degradation, sustainable land management, food security, and greenhouse gas fluxes in terrestrial ecosystems [P.R. Shukla, J. Skea, E. Calvo Buendia, V. Masson-Delmotte, H.-O. Pörtner, D. C. Roberts, P. Zhai, R. Slade, S. Connors, R. van Diemen, M. Ferrat, E. Haughey, S. Luz, S. Neogi, M. Pathak, J. Petzold, J. Portugal Pereira, P. Vyas, E. Huntley, K. Kissick, M. Belkacemi, J. Malley, (eds.)]. In press.

Ivanov, V. & Belokopytov, V. (2013). Oceanography of the Black Sea. National Academy of Sciences of Ukraine, Marine Hydrophysical Institute, Sevastopol, 210 p.

Jiang, Y., Luo, Y. Zhao, Z., & Tao, S. (2010). Changes in wind speed over China during 1956–2004. Theoretical and Applied Climatology, 99, 421-430. https://doi.org/10.1007/s00704-009-0152-7

Kaya H., Ertek T.A., & Gazioğlu C. (2019). Geomorphological Features of Terkos Lake. International Journal of Environment and Geoinformatics (IJEGEO), 6(2), 192-205. DOI: 10.30897/ijegeo.569748

Kazmin, A.S, & Zatsepin, A.G. (2007). Long-term variability of surface temperature in the Black Sea, and its connection with the large-scale atmospheric forcing. Journal of Marine Systems, Volume 68, Issues 1–2, 2007, Pages 293-301, ISSN 0924-7963, https://doi.org/10.1016/j.jmarsys.2007.01.002

Kendall, M.G. (1938). A new measure of rank correlation. Biometrika, 30(1-2), 81-93.

Kendall, M.G. (1970). Rank Correlation Methods. 4th edition. London: Griffin.

Knutson, T.R., Zeng, F., & Wittenberg A.T. (2013). Multi-model assessment of regional surface temperature trends: CMIP3 and CMIP5 twentieth-century simulations. J. Clim. 26, 8709–8743, https://doi.org/10.1175/JCLI-D-12-00567.1

Kosyan, R., Kuklev, S., Khanukaev, B., & Kochergin, A. (2012). Problems of the coasts erosion in the North—Eastern Black Sea Region. Journal of Coastal Conservation, 16(3), 243–250. https://doi.org/10.1007/s11852-010-0115-2

Kostianoy, A. G. & Kosarev, A. N. (2008). The Black Sea Environment. Springer-Verlag Berlin Heidelberg, https://doi.org/10.1007/978-3-540-74292-0

Koulov, B. (2012). Sustainable Environmental Management of Marine Regions: The Black Sea Case Study. Geoadria, 17:1, 3-11.

Kubryakov, A., Stanichny, S., Shokurov, M., & Garmashov, A. (2019). Wind velocity and wind curl variability over the Black Sea from QuikScat and ASCAT satellite measurements. Remote Sensing of Environment, 224, 236-258. https://doi.org/10.1016/j.rse.2019.01.034

Lehmann, A., Guigoz Y., Ray N., Mancosu E., Abbaspour K.C., Freund E.R., & Allenbach K. (2017). A web platform for land use, climate, demography,

hydrology and beach erosion in the Black Sea catchment. Scientific Data. 4. 170087. https://doi.org/10.1038/sdata.2017.87.

Leon, J. V. (2006). Vulnerability: A Conceptual and Methodological Review. Source 4/2006. 4

Luijendijk, A., Hagenaars, G., Ranasinghe, R., Baart, F., Donchyts, G. & Aarninkof, S. (2018). The State of the World's Beaches. Sci Rep 8, 6641. https://doi.org/10.1038/s41598-018-24630-6

Maktav, D., Filiz, S., & Kabdasli, S. (2002). Monitoring coastal erosion at the Black Sea coasts in Turkey using satellite data: A case study at the Lake Terkos, North-west Istanbul. International Journal of Remote Sensing, 23(19), 4115- 4124, https://doi.org/10.1080/01431160110115979

Mann, H.B. (1945). Nonparametric tests against trend. Econometrica, 13(3), 245-259.

Masuda, D., Kai, S., & Yamamoto, N. (2014). The effect of lunar cycle, tidal condition and wind direction on the catches and profitability of Japanese common squid Todarodes pacificus jigging and trap-net fishing. Fisheries Science, 80(6), 1145-1157. https://doi.org/10.1007/s12562-014-0799-6

Mclaughlin, S. & Cooper, A. (2010). A Multi-scale coastal vulnerability index: A tool for coastal managers, Environmental Hazards, 9, 233-248, https://doi.org/10.3763/ehaz.2010.0052

Moore, D., Heilweck, & M., Petros, P. (2021). Saving the planet with appropriate biotechnology: 1. Diagnosing the problems. Mexican Journal of Biotechnology. 6. 1-30. https://doi.org/10.29267/mxjb.2021.6.1.1

Nardelli, B., Colella, S., Santoleri, R, Guarracino, & M., Kholod, A. (2010). A re-analysis of Black Sea surface temperature. Journal of Marine Systems. 79. 50-64. https://doi.org/10.1016/j.jmarsys.2009.07.001

National Geophysical Data Center, NOAA, https://www.ngdc.noaa.gov/, (accessed: March 8, 2022)

Nicolae. F., Bucur M., & Cotorcea A. (2018). Port performance evaluation. Case study: Ports in the Black Sea basin. IOP Conference Series: Earth and Environmental Science. 172. 012004. https://doi.org/10.1088/1755-1315/172/1/012004

NOAA (National Oceanic and Atmospheric Administration). (2021). Update to data originally published in: NOAA. 2009. Sea level variations of the United States 1854–2006. NOAA Technical Report, NOS CO-OPS 053. www.tidesandcurrents.noaa.gov/publications/Tech_rpt_53.pdf

Nogueira M. (2020). Inter-comparison of ERA-5, ERA-interim and GPCP rainfall over the last 40 years: process-based analysis of systematic and random differences. Journal of Hydrology, 583, 124632 https://doi.org/10.1016/j.jhydrol.2020.124632

Oğuz, T., Çokaçar, T., Rizzoli, P. M., & Ducklow H.W. (2003). Climatic warming and accompanying changes in the ecological regime of the Black Sea during 1990s. Global Biogeochemical Cycles - GLOBAL BIOGEOCHEM CYCLE. 17. 14-1. https://doi.org/10.1029/2003GB002031

Onea, F., & Rusu, E., (2014). Wind energy assessments along the Black Sea basin. Meteorological Applications. Vol. 21. 316-329. https://doi.org/10.1002/met.1337

Özsoy E., & Ünlüata Ü. (1997). Oceanography of the Black Sea: A review of some recent results, Earth-Science Reviews, 42(4), 231-272, ISSN 0012-8252, https://doi.org/10.1016/S0012-8252(97)81859-4

Öztürk, D., & Sesli, F.A. (2015). Shoreline change analysis of the Kızılırmak Lagoon Series. Ocean & Coastal Management, Volume 118, Part B, Pages 290-308, ISSN 0964-5691, https://doi.org/10.1016/j.ocecoaman.2015.03.009

Paola, C., Twilley R.R., Edmonds D.A., Kim W., Mohrig W., Parker, G., Viparelli, E., & Voller V.R. (2011). Natural Processes in Delta Restoration: Application to the Mississippi Delta, Annual review of marine science. 3. 67-91, https://doi.org/10.1146/annurev-marine-120709-142856

Potter, S. F., Di Marco, S. F., & Knap, A. H. (2019). Tropical cyclone heat potential and the rapid intensification of Hurricane Harvey in the Texas Bight. Journal of Geophys. Res. Oceans 124, 2440–2451. https://doi.org/10.1029/2018JC014776

Ramieri, E., Hartley, A., Barbanti, A., & Santos F. D. (2011). Methods for assessing coastal vulnerability to climate change. https://doi.org/10.13140/RG.2.1.1906.9840

Ross, D. A., & Degens, E. T. (1974). Recent Sediments of the Black Sea. The Black Sea Geology, Chemistry and Biology, Degens E T and Ross D A (Eds.), Volume 20, ISBN electronic: 978-162-98-1215-1, American Association of Petroleum Geologists, 183–199. https://doi.org/10.1306/M20377C21

Rusu L., Raileanu A.B., & Onea F. A. (2018). Comparative Analysis of the Wind and Wave Climate in the Black Sea along the Shipping Routes. Water, 10(7):924. https://doi.org/10.3390/w10070924

Rusu, L., Bernardino, M., & Guedes Soares, C. (2014). Wind and wave modelling in the Black Sea. Journal of Operational Oceanography, 7(1), 5-20. https://doi:10.1080/1755876X.2014.11020149

Saha, S., Moorthi, S., Pan, H., Wu, X., Wang, J., Nadiga, S., Tripp, P., Kistler, R., Woollen, J., Behringer, D., Liu, H., Stokes, D., Grumbine, R., Gayno, G., Wang, J., Hou, Y., Chuang, H., Juang, H. H., Sela, J., Iredell, M., Treadon, R., Kleist, D., Van Delst, P., Keyser, D., Derber, J., Ek, M., Meng, J., Wei, H., Yang, R., Lord, S., van den Dool, H., Kumar, A., Wang, W., Long, C., Chelliah, M., Xue, Y., Huang, B., Schemm, J., Ebisuzaki, W., Lin, R., Xie, P., Chen, M., Zhou, S., Higgins, W., Zou, C., Liu, Q., Chen, Y., Han, Y., Cucurull, L., Reynolds, R. W., Rutledge, G., & Goldberg, M. (2010). The NCEP Climate Forecast System Reanalysis. Bulletin of the American Meteorological Society, 91(8), 1015-1058. https://doi.org/10.1175/2010BAMS3001.1

Saha, S., Moorthi, S., Wu, X., Wang, J., Nadiga, S., Tripp, P., Behringer, D., Hou, Y., Chuang, H., Iredell, M., Ek, M., Meng, J., Yang, R., Mendez, M. P., van den

Dool, H., Zhang, Q., Wang, W., Chen, M., & Becker, E. (2014). The NCEP Climate Forecast System Version 2, Journal of Climate, 27(6), 2185-2208. http://doi.org/10.1175/JCLI-D-12-00823.1

Salmi, T., Maatta, A., Anttila, P., Ruoho-Airola, T., & Amnell, T. (2002). Detecting Trends of Annual Values of Atmospheric Pollutants by the Mann Kendall Test and Sen's Slope Estimates the Excel Template Application MAKESENS. Finnish Meteorological Institute, Publications on Air Quality, No. 31, Helsinki.

Schlitzer, R. (2018). Ocean Data View, https://odv.awi.de

Sen, P.K. (1968). Estimates of the Regression Coefficient Based on Kendall's Tau. Journal of the American Statistical Association, 63, 1379-1389.

Shepherd J.G., Brewer P.G., Oschlies A., & Watson A.J. (2017). Ocean ventilation and deoxygenation in a warming world: introduction and overview. Phil. Trans. R. Soc. A 375: 20170240. http://dx.doi.org/10.1098/rsta.2017.0240

Stanica, A., Dan, S., Jiménez, J.A., & Ungureanu, G.V. (2011). Dealing with erosion along the Danube Delta coast. The CONSCIENCE experience towards a sustainable coastline management, Ocean & Coastal Management, Volume 54, Issue 12, Pages 898-906, ISSN 0964-5691, https://doi.org/10.1016/j.ocecoaman.2011.06.006.

Sterl, A. & Caires, S. (2005). Climatology, variability and extrema of ocean waves: the Web-based KNMI/ERA-40 wave atlas. International Journal of Climatology, https://doi.org/10.1002/joc.1175

Stopa, J.S., & Cheung, K.F. (2014). Intercomparison of wind and wave data from the ECMWF Reanalysis Interim and the NCEP Climate Forecast System Reanalysis. Ocean Modelling, 75, 65-83. http://dx.doi.org/10.1016/j.ocemod.2013.12.006.

Surkova, G.V., Arkhipkin, V.S., & Kislov, A.V. (2013). Atmospheric circulation and storm events in the Black Sea and Caspian Sea. Cent. Eur. J. Geosci, 5(4), 548-559. http://dx.doi.org/10.2478/s13533-012-0150-7

Süzen, M., & Özhan, E. (2003). Monitoring shoreline changes at Yeşilırmak Delta by remote sensing and GIS. Proceedings of Sixth International Conference on The Mediterranean Coastal Environment, Volume 3, https://hdl.handle.net/11511/83495

Tatui, F., Pirvan, M., Popa, M., Aydoğan, B., Ayat, B., Görmüş, T., Korzinin, D., Vaidianu, N., Vespremeanu-Stroea, A., Zainescu, F., Kuznetsov, S., Preoteasa, L., Shtremel, M., & Saprykina, Y. (2019). The Black Sea coastline erosion: Index-based sensitivity assessment and management-related issues. Ocean & Coastal Management. 182. 104949. https://doi.org/10.1016/j.ocecoaman.2019.104949

The Guardian (2020). Treat coastal erosion as a natural catastrophe, UK ministers urged. https://www.theguardian.com/environment/2020/jan/19/ treat-coastal-erosion-as-natural-catastrophe-uk-ministers-urged-east-yorkshire (accessed: May. 26, 2022)

The Orange County Register (2019). Sea-level rise threatens Orange County's coast from top to bottom. https://www.ocregister.com/2019/09/13/sea-level-rise-threatens-orange-countys-coast-from-top-to-bottom (accessed: May. 26, 2022)

Torresan, S., Critto, A., Rizzi, J., & Marcomini, A. (2012). Assessment of coastal vulnerability to climate change hazards at the regional scale: the case study of the North Adriatic Sea. Nat. Hazards Earth Syst. Sci., 12, 2347–2368, https://doi.org/10.5194/nhess-12-2347-2012

Troccoli, A., Muller, K., Coppin, P., Davy, R., Russell, C., & Hirsch, A.L. (2012). Long-Term Wind Speed Trends over Australia. Journal of Climate, 25, 170-183. https://doi.org/10.1175/2011JCLI4198.1

Tuik.gov.tr. (2022). The Turkish Statistical Institute Website. (accessed: June. 5, 2022)

Tuller, S.E. (2004). Measured WS Trends on the West Coast of Canada. International Journal of Climatology, 24: 1359-1374, https://doi.org/10.1002/joc.1073

Valchev, N., Belberov, Z., & Palazov, A. (2010). Hindcasting and assessment of the western Black sea wind and wave climate. Journal of environmental protection and ecology. 11. 1001-1012.

Valchev, N., Trifonova, E., & Andreeva, N. (2012). Past and recent trends in the western Black Sea storminess. Natural Hazards and Earth System Sciences, 12, 961–977. https://doi.org/10.5194/nhess-12-961-2012

Velea, L., Bojariu, R., & Cica, R. (2014). Occurrence of Extreme Winds over the Black Sea during January under Present and Near Future Climate. Turkish Journal of Fisheries and Aquatic Sciences, 14, 973-979. https://doi.org/10.4194/1303-2712-v14_4_17

Vespremeanu E., & Golumbeanu M. (2018). Black Sea Coastal Population. In: The Black Sea. Springer Geography. Springer, Cham. https://doi.org/10.1007/978-3-319-70855-3_9

Vespremeanu-Stroe, A., Tatui, F., Constantinescu, S., & Zainescu, F. (2017). Danube Delta Coastline Evolution (1856–2010). In: Radoane, M., Vespremeanu-Stroe, A. (eds) Landform Dynamics and Evolution in Romania. Springer Geography. Springer, Cham. https://doi.org/10.1007/978-3-319-32589-7_23Wallace, J. M., Gutzler, D. S. (1981). Teleconnections in the geopotential height field during the Northern hemisphere winter. Monthly Weather Review, 109, 784-812.

Wang, D.W., & Hwang, P.A. (2001). An operational method for separating wind sea and swell from ocean wave spectra. Journal of Atmospheric and Oceanic Technology, 18,2052-2062. https://doi.org/10.1175/15200426(2001)018

Weisse, R., & Gunther, H. (2007). Wave climate and long-term changes for the Southern North Sea obtained from a high-resolution hindcast 1958–2002. Ocean Dynamics, 57, 161–172. https://doi.org/10.1007/s10236-006-0094-x

Worldometers.info. (2022). (accessed: June. 5, 2022)

Young, I.R., Zieger, S., & Babain, A. (2011). Global trends in wind speed and wave height. Science, 332(6028), 451-455. https://doi.org/10.1126/science.1197219

Zainescu, F., Tatui, F., & Valchev, N., Vespremeanu-Stroe, A. (2017). Storm climate on the Danube delta coast: evidence of recent storminess change and links with large-scale teleconnection patterns. Natural Hazards, 87,599–621. https://doi.org/10.1007/s11069-017-2783-9

Zecchetto, S., & de Biasio, F. (2007). Sea Surface Winds over the Mediterranean Basin from Satellite Data (2000–04): Meso- and Local-Scale Features on Annual and Seasonal Time Scales. Journal of Applied Meteorology and Climatology, 46, 814-827, http://dx.doi.org/10.1175/JAM2498.1

Zeng, X., R. E. & Dickinson, Y. H. (1998). Effect of surface sublayer on surface skin temperature and fluxes. Journal of Climate, 11, 537–550.

Zhang, D., Cronin, M.F., Wen, C., Xue, Y., Kumar, A., & McClurg, D. (2016). Assessing surface heat fluxes in atmospheric reanalysis with a decade of data from the NOAA Kuroshio Extension Observatory. Journal of Geophysical Research: Oceans, 121, 6874–6890. https://doi:10.1002/2016JC011905

PUBLICATIONS FROM THE THESIS

Papers

1. Çarpar, T., Ayat, B., Aydoğan, B. (2019). Spatio-seasonal variations in long-term trends of offshore wind speeds over the Black Sea; an inter-comparison of two reanalysis data, Pure Appl. Geophys. 177 3013e3037, https://doi.org/10.1007/s00024-019-02361-7